Geological Survey of Japan Open-File Report, No. 609

Coordinating Committee for Geoscience Programmes in East and Southeast Asia (CCOP)

PROCEEDINGS OF THE THEMATIC SESSION

"GEOHAZARDS: IMPACTS AND CHALLENGES FOR SOCIETY DEVELOPMENT IN ASIAN COUNTRIES"

49TH CCOP ANNUAL SESSION
22-23 OCTOBER 2013, SENDAI, JAPAN

Geological Survey of Japan (GSJ),
National Institute of Advanced Industrial Science and Technology (AIST)

Proceedings of the Thematic Session, 49th CCOP Annual Session, 22-23 October 2013, Sendai, Japan

Published as Geological Survey of Japan Open-File Report, No. 609, by Geological Survey of Japan (GSJ), National Institute of Advanced Industrial Science and Technology.
October 1, 2014

Editors:
Anthony J. Reedman, United Kingdom
Adichat Surinkum, CCOP Technical Secretariat
Nguyen Thi Minh Ngoc, CCOP Technical Secretariat
Toshihiro Uchida, Geological Survey of Japan, AIST

Photo on the front cover:
A view of Sendai City (courtesy of the City of Sendai)

Geological Survey of Japan Open-File Report, No. 609

Coordinating Committee for Geoscience Programmes in East and Southeast Asia (CCOP)

Proceedings of the Thematic Session

"Geohazards: Impacts and Challenges for Society Development in Asian Countries"

49th CCOP Annual Session
22-23 October 2013, Sendai, Japan

Geological Survey of Japan (GSJ),
National Institute of Advanced Industrial Science and Technology (AIST)

Preface

The Thematic Session held at the 49th CCOP Annual Session on 22-23 October 2013 in Sendai, Japan, focused on geological hazards, which include geological disasters caused by earthquakes, tsunami, volcanic eruptions, landslides, ground subsidence, flooding, etc.

The Asian region has experienced very severe geological hazards in the past decade: for example, devastating earthquakes in Sumatra, Indonesia (2004), Sichuan, China (2008) and Tohoku, Japan (2011) and huge floods in Bangkok, Thailand (2011). In almost all Asian countries, landslides, both large and small, have caused extensive economic damage and social disruption. In particular, extreme weathers, such as huge typhoons or very strong rains, which are probably due to the global warming phenomena, are frequently causing severe landslides and floods in Asian countries in recent years. In the case of the Great Tohoku Earthquake in March 2011, many seismologists in Japan thought that several M8-class earthquakes might be expected in the region but not an M9-class earthquake. We now understand that our knowledge concerning geohazards is still limited. Extreme geological phenomena are matters of the natural system of the globe, however, such disasters can devastate the human society, partly due to our failure to prepare for those hazards.

Understanding risks posed by such unexpected geohazards and sharing this information among people in Asian countries is now becoming very important. This is why the organizer set the theme "Geohazards: Impacts and Challenges for Society Development in Asian Countries" for the Thematic Session in 2013.

Thirty-five papers from 8 countries and one international organization were submitted to the Thematic Session. Thirty-two papers were actually presented in Sendai, by either oral or poster presentation. Among those presented papers, the editors have accepted 24 full manuscripts for publication on the Proceedings of the Thematic Session.

These manuscripts are divided into the following six groups.

- ✓ Policy for Mitigating Geohazards
- ✓ Earthquakes and Tsunami
- ✓ Volcanic Eruptions
- ✓ Flooding and Erosion
- ✓ Land Subsidence
- ✓ Landslides

We believe that the Thematic Session successfully provided a venue for exchanging updated information on geohazards in Asia and for discussing our future tasks among CCOP countries and cooperating organizations. We also hope the papers in this Proceedings will provide further useful information to engineers, researchers and governmental officials in the CCOP countries for their activities related to the mitigation of geological hazards.

October 1, 2014

Dr. Adichat Surinkum
Director
CCOP Technical Secretariat

Table of Contents

Land subsidence

Landslides

Activities of the Geological Society of Japan in support of reconstruction after the 2011 Tohoku earthquake disaster

Hideo Takagi

Director of Social Outreach and Geopark Affairs, the Geological Society of Japan,
Department of Earth Sciences, Waseda University
hideo@waseda.jp

Abstract

This paper introduces the activities of the Geological Society of Japan (JGS) in support of reconstruction after the 2011 Tohoku earthquake disaster which were undertaken on behalf of the Social Contribution Committee of the JGS. The JGS asked its members to submit proposals in support of the disaster recovery, and six out of nine research proposals in 2011 and one of two in 2012 were adopted and supported by funds from the Society. The seven projects can be categorized under three research areas: 1) recovery of specimens from museums destroyed by the tsunami, 2) development of methods of decontamination to deal with the radioactive materials spread by the Fukushima Daiichi nuclear power plant accident, and 3) surveys to recognize and quantify liquefaction caused by the Tohoku Earthquake. The results of these studies were reported in poster presentations given at the JGS annual meetings and in newsletter articles published in 2012 and 2013. This report also introduces briefly the geopark activity that has been promoted by the JGS and its importance for local education in earth sciences, including disaster prevention and mitigation in Sanriku, the eastern Tohoku coastal area.

Keywords: earthquake disaster, tsunami, liquefaction, Fukushima Daiichi nuclear disaster, recovery of museum specimens, Tohoku, geopark, Geological Society of Japan

1. Introduction

A mega-earthquake measuring Mw 9.0 took place on March 11, 2011 off the Pacific coast of Tohoku, northeastern Japan and is known as the Tohoku Earthquake or Great East Japan Earthquake. Fault slip between the oceanic and continental plates triggered a huge tsunami, which devastated cities along the coastline in Iwate, Miyagi and Fukushima prefectures. The devastating explosion of the Fukushima Daiichi nuclear power plant was also triggered by the tsunami, and the consequent spread of radioactive materials is a major ongoing problem in Japan.

Within the three months after the Tohoku Earthquake, the Geological Society of Japan (JGS) released several statements to Japanese society.

- March 2011: *On the mega-earthquake that attacked northeastern Japan (JGS president)*
- April 2011: *Statements concerning the Tohoku earthquake disaster on the basis of geology (JGS president)*
- May 2011: *Report on the Tohoku earthquake and tsunami disaster (JGS Working Group for the Tohoku Earthquake)*

The JGS then asked its members to submit proposals in support of the disaster recovery, and six out of nine research proposals in 2011 and one of two in 2012 were adopted and supported by funds from the Society. The results of these studies were reported in poster presentations

given at the JGS annual meetings (2012 in Osaka and 2013 in Sendai) and in newsletter articles published in 2012 and 2013. Most of the activities were also reported in the newsletter or the Journal of the Geological Society of Japan. The seven research projects are briefly described below.

The JGS is also active in promoting geoparks and particularly their role in local geoscience education. Such public education in earth sciences is important for disaster prevention and mitigation in the eastern Tohoku coastal area (Sanriku area) and is also briefly introduced below.

2. Research projects of the JGS members

2.1 Recovery of specimens ("rescue" projects) from museums totally destroyed by the tsunami

(1) Recovery of specimens from the Rikuzentakata City Museum, Iwate Prefecture
by Masayuki Ohishi (Iwate Prefectural Museum)

The Rikuzentakata City Museum (RCM) has a history of more than 50 years, and houses more than 150,000 objects covering the fields of archeology, history, folklore, entomology, zoology, botany, and geology. The tsunami on 11 March 2011 severely damaged the RCM and other museums along the coast of Iwate Prefecture. The "rescue" activity began in early April for cultural objects and natural history specimens such as shells, insects, and plants. The geological specimens, for which there were less concerns about rapid deterioration, were brought from the RCM to a recently closed elementary school in the geographically higher area of Rikuzentakata City in early May. In August and October, a total of thirty three geologists and paleontologists from 24 institutions were engaged in recovering those geological specimens.

During the "rescue" activity two issues came to our attention. First, unlike cultural properties, natural history collections have no legal protection in Japan. However, we believe it is vital to ensure the integrity of important natural history specimens. To achieve this goal we must ensure that the significance of collections in natural history museums is better understood by the Japanese public. Secondly, a good network of curators is necessary to organize an effective "rescue" activity. In addition to the personal network of curators, in order to help participating individuals, it is also desirable for a system to be developed that facilitates cooperation between institutions.

The geological specimens in the museums help the public to understand not only local geological history but also the history and evolution of the Earth system. The destruction wreaked by the earthquakes and tsunamis on 11 March 2011 highlights the importance of these specimens and the need for them to be better known to the public so that communities throughout Japan are better prepared for future natural disasters.

(2) Recovery of specimens from the Utatsu Ichthyosaur Museum, Miyagi Prefecture
by Masayuki Ehiro (Tohoku University Museum)

The staff of the Tohoku University Museum joined a "rescue" project for the tsunami-damaged cultural facilities along the eastern coast of Miyagi Prefecture, and participated in salvaging, caring for and curating the fossil collections exhibited in the Utatsu Ichthyosaur Museum (Fig. 2). To explain the significance of these "rescued" collections, we are also helping with the organization of a traveling exhibition of these collections holding events in various places throughout Japan including disaster areas.

Fig. 1. Rikuzentakata City Museum destroyed by the tsunami (left) and "rescued" specimens being sorted by curators from many museums in Japan (right).

Fig. 2. Rescue of large specimen from the Utatsu Ichthyosaur Museum damaged by the tsunami (left) and an exhibition of rescued specimens in the Sendai Science Museum (right).

2.2 Development of the decontamination method of radioactive materials spread by the Fukushima Daiichi nuclear power plant accident

(1) Concentration of radioactive cesium in native *Eleocharis acicularis* in the paddy fields of Fukushima Prefecture, northern Japan

by Masayuki Sakakibara[1)], Yuki Kubota[2)] and Yasushi Sato[1)]

[1)]Graduate School of Science and Engineering, Ehime University, [2)]Nature Environment Support Co., Ltd.)

Soil contamination with radiogenic Cs has a long-term radiological impact because it is commonly transferred through the food chain to human beings. Remediation of soil contaminated with radiogenic Cs remains one of the most important problems after the Fukushima Daiichi nuclear disaster.

In this study the distribution of the native aquatic plant *Eleocharis acicularis* and its effectiveness in absorbing radiogenic Cs in the paddy soils in Fukushima Prefecture was investigated (Fig. 3). Results indicated that the native *Eleocharis acicularis* has absorbed up to 6,710 Bq/kg in wet weight. *Eleocharis acicularis* therefore shows great potential for use in the phytoremediation of soil and water contaminated by radiogenic Cs at nuclear disaster areas such as Chernobyl and Fukushima.

Fig. 3. Testing applicability of phytoextraction by *Eleocharis acicularis* of soil contaminated with ^{137}Cs in paddy field, Fukushima Prefecture

(2) Decontamination of radioactive cesium from environmental water using rice chaff
by Masanori Takahashi (Syoken Technical Inc.)

Many practical methods including the use of bacteria have been proposed to assist in the decontamination of radioactive cesium from environmental water. This issue is particularly serious in a region up to 24 km from the Fukushima Daiichi Nuclear Plant. Water purification methods have been proposed using bacterium+zeolite, or +vermiculite and rice chaff as filters. Our comparative study showed the effectiveness of using rice chaff (Fig. 4, left) in the decontamination of radioactive cesium from environmental water, and therefore we have developed a water purification system that incorporates the use of rice-chaff (Fig. 4, right).

(3) Investigation of radiation levels in Iidate Village, near the Fukushima Daiichi Nuclear Power Plant, Japan
by Shoichi Uesuna, Yoshiaki Aikou, Atsushi Kagawa, Kazuya Kimura, Takashi Kusuda, Kyoichi Satou, Hisashi Nirei, Taro Fuse, Kunio Furuno, Toshihisa Masuda, Yutaka Kasahara, Yoshiyuki Tamura and Hideki Okano (Investigation Team of Space Radiation Dose in Fukushima)

The Tohoku Earthquake caused a nuclear accident in the Fukushima Daiichi Nuclear Power Plant resulting in the release of a large amount of radioactive materials. Radioactive contamination has spread beyond the surrounding areas, across the Tohoku Region and even into the Kanto Region. Although decontamination efforts are under way by central and local governments, only standardized methods are used as prescribed in the Soil Contamination Countermeasures Act without conducting detailed studies of the distribution of radioactive materials.

The radioactive materials were spread by natural agencies and are therefore distributed differently depending on topographical and geological conditions. Air radiation levels were measured at one meter above the ground (Fig. 5, left). The measurement of air radiation levels is an important part of identifying the distribution of radioactive materials and a vital first step in tackling pollution by radioactive materials. In highly contaminated areas, the results of radioactivity measurements in the air 1 m above the ground showed significant differences with measurements conducted on the ground surface. The latter values were higher than those measured 1 m above the ground, clearly indicating that surface measurement can tell the existence of radioactive materials in more detail because the levels of the materials on the ground surface are affected by the surface geological conditions, vegetation and microtopography. While air radiation levels are measured in all directions, the measurement

on the ground surface can show the distribution of the materials in more detail since radiation levels on the ground surface are dominated by radioactive materials that settled on the ground.

Fig. 4. Rice chaff (concentration of more than 30,000 Bq/kg radioactivity) after the test of decontamination of radioactive cesium (left), and a contaminated water purification system using rice-chaff named SEMJ-system (right).

Fig. 5. Radiation dose measurements (left) from ground surface to 1.0 m height, and (right) at several depths below the ground surface, in which the radiation detector was capped by a lead box to shield from air radiation.

An inexpensive, quick, practical and reproducible method is required for the wide-area contamination survey of radioactive materials. The greatest challenge is to understand to what depth the materials have moved below the ground surface. The Fukushima air radiation level survey team measured radiation levels on the ground surface, at one meter above the ground, and below the ground surface. For the below-ground measurement, the team took the measurement while excavating the ground and using lead or other materials to shield the instrument from lateral radiation (Fig. 5, right). Our method of investigation for air radiation levels is based on the method for geo-stratigraphic investigation, and is designed to measure and analyze air radiation levels in a relative manner while under the influence of the surrounding environment.

2.3 Surveys to recognize and quantify liquefaction caused by the Tohoku Earthquake

(1) Liquefaction damage at reclaimed residential land in the inland area of the Kanto district, central Japan.
by Atsushi Urabe (NHDR, Niigata University)

Serious liquefaction damage that occurred in the downstream region of the Tone River was caused by the 2011 Tohoku Earthquake. The Hinode area, Itako City, Ibaraki Pref. is one of the areas most seriously affected by liquefaction (Fig. 6). This damaged area was on reclaimed land filled by dredged sediment. Drilling surveys revealed that the stratum of this area consists of lowland sediment and dredged sandy sediment. Judging from the sedimentary facies and grain size, liquefaction occurred in the area underlain by a thick layer (thickness of about 2 to 4 m) of dredged sand.

Fig. 6. Liquefaction-damaged district, Hinode, Itako City, including lateral spreading damage of a road (right).

(2) Differentiating between damage caused by quake-motion and damage caused by the tsunami during the 2011 Tohoku Earthquake.
by Takayuki Kawabe (Yamagata Univ.), Tsunemasa Shiki (JILES) and Osamu Kazaoka (RIEGC)

Damage to surficial geology and deformation of the surface commonly occur by liquefaction of sandy beds and/or compaction of muddy or peaty beds caused by strong motion of large earthquakes. However, such phenomena have not been clearly recognized along the coast area of the Sendai Plain due to the severity of the damage caused by the large tsunami, which affected the area soon after the Tohoku Earthquake. Recognition of the surficial geological damage is vital for reconstruction of the damaged area.

Figure 7a and 7b show the topographic map made from GSI 5 m DEM data of 2009 and 2012, and Fig. 7c shows the difference between the data of 2009 and 2012. Depression of surface topography is generally seen along the lowland between dunelands. Three reasons for this depression can be considered. The first one is due to general tectonic subsidence as a direct result of the earthquake; the value of this subsidence is estimated to be about 43 cm based on the change in elevation of the runway of Sendai Airport (Fig. 7c). The second reason is surface erosion by rapid flow (of upper flow regime) of the tsunami currents (Fig. 8). The third reason is local subsidence by deformation of the surficial geology, liquefaction and/or compaction (Fig. 8).

Detailed surveys of the surficial geology should be carried out and taken into account when designing and reconstructing buildings or embankments. Such information can help

minimizing the potential structural damage caused by the next earthquake.

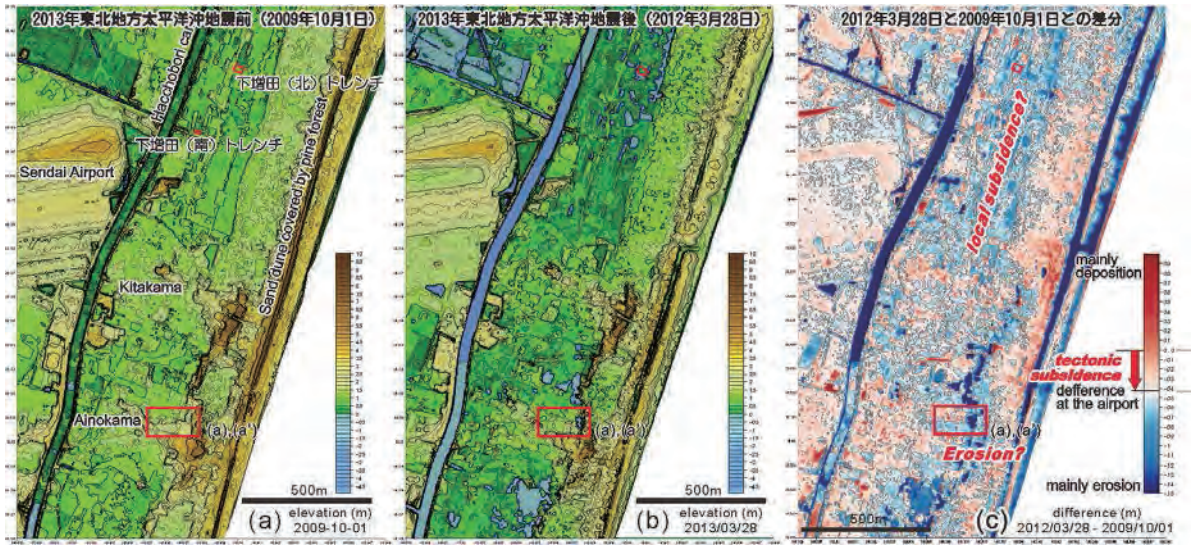

Fig. 7. Topographic map of the coastal area east of Sendai Airport, Sendai Plain drawn from the GSI DEM data of 2009 (a) and 2012 (b), and the difference between the data of 2009 and 2012 (c).

Fig. 8. Deformation of the base of houses caused by local liquefaction and/or compaction of surficial geology.

3. Geopark activity for local education in disaster prevention and mitigation

The JGS have been promoting geopark activities since 2005, and 32 geoparks including 6 members of Global Geoparks Network have been established in Japan since 2008. In cooperation with the Japan Geoparks Committee (JGC), JGS support for geopark activity has played an effective role in promoting local geoscientific education relevant to disaster prevention and mitigation. The *Sanriku Geopark*, including the coastal area of Tohoku which was severely damaged by the tsunami, has just be certified as a member of Japan Geoparks Network on 24 Sept. 2013 by JGC. The contribution that the geopark activity can make to local education for disaster prevention and mitigation will be particularly important in this area. One of the ways to prevent memories fading with time is to preserve some of the erosion scars and other effects (Fig. 9) of the tsunami disaster as geosites.

Fig. 9. Taro Kanko (sightseeing) Hotel destroyed by Tsunami preserved as one of the geosites for disaster prevention education in the *Sanriku Geopark*.

4. Conclusion

The JGS has supported various activities including improved public education immediately after the Tohoku earthquake and disasters, and some of the major activities are introduced in this paper. Even though, the reconstruction of the affected areas is half the battle, after more than two years the JGS would like to continue to help the reconstruction of the eastern Tohoku (Sanriku) region through outreach and academic activities.

JAMSTEC's contribution for the next generation of earthquake/tsunami hazard research

Shin'ichi Kuramoto

Center for Deep Earth Exploration
Japan Agency for Marine-Earth Science and Technology, JAPAN
e-mail: s.kuramoto@jamstec.go.jp

Abstract

An improved understanding of repeated earthquake-related/tsunami hazards is one of the highest priorities for science in Japan. Japan has promoted various kinds of earthquake research based on dense seismometer and GPS networks, geodesy, geochemical, geophysical and geological investigations. However most of the research targets are located on land, not in the ocean where large earthquakes and related tsunamis are currently occurring. JAMSTEC (Japan Agency for Marine-Earth Science and Technology) is working to understand the so-called "seismogenic zone" along plate subduction margins by employing direct sampling and borehole observations, submarine cable network observations (DONET), submersible dives, AUV/ROV surveys and using other ordinal marine survey tools. The deep sea drilling vessel *Chikyu* was introduced for such research in 2005, and has already conducted 9 research expeditions under the IODP framework off the Kii peninsula, Nankai accretionary margin, where the Philippine Sea plate is subducting beneath the Eurasian plate at the rate of 4-5 cm/yr. The Nankai Trough is one of the most surveyed subduction margins in the world and its earthquake recurrence time is estimated based on much historical literature recording more than 1000 years of history. The last event, the Tonankai Earthquake, occurred in 1944 but the next event may already be under preparation. One of the main reasons to drill at Nankai is that the up-dip limit of the seismogenic zone is the shallowest in the world and may be possible to reach by current deep sea drilling technology. *Chikyu* also drilled off Tohoku where a large slip may have happened during the March 11 Tohoku-oki Earthquake (Mw 9.0). Approximately 2 years after the earthquake occurred, *Chikyu* drilled into the deformation zone and cut core samples. Also, a string of thermistors in the borehole to measure the frictional heat that may be generated by fault slip during the earthquake was successfully installed. This presentation will introduce recent research highlights of JAMSTEC using *Chikyu* and other state-of-the-art technologies for better understanding of earthquake/tsunami, mitigating earthquake hazards and improving our knowledge of marine earth sciences.

Keywords: JAMSTEC, *Chikyu*, IODP, DONET, earthquake, tsunami, scientific drilling

1. Introduction

JAMSTEC was established in 1971 as the Japan Marine Science and Technology Center and in 2004 became the Japan Agency for Marine-Earth Science and Technology, an independent administrative institution. JAMSTEC covers various marine-earth science fields, including geo-hazard research, using research ships, ROVs, AUVs and a drilling vessel. Since 2007, JAMSTEC introduced the scientific drilling vessel *Chikyu* (means the Earth in Japanese, Fig. 1) for scientific drilling under the IODP (Integrated Ocean Drilling Program) framework: Japan and U.S.A. are co-leading this program and 26 countries are participating. *Chikyu* is a key facility to lead a new science and contribute to understanding the mechanism of seismogenesis. Two target areas are currently under investigation at the Nankai Trough and the Japan Trench subduction margins.

Fig. 1. Scientific drilling vessel *Chikyu* (http://www.jamstec.go.jp/chikyu/eng/index.html).

2. Nankai and Tohoku Seismogenic Zone Drilling by *Chikyu*

The first drilling target of *Chikyu* was the Nankai trough subduction margin where the Philippine Sea plate is subducting beneath the SW Honshu Arc at 4-5 cm/yr (Fig. 2).

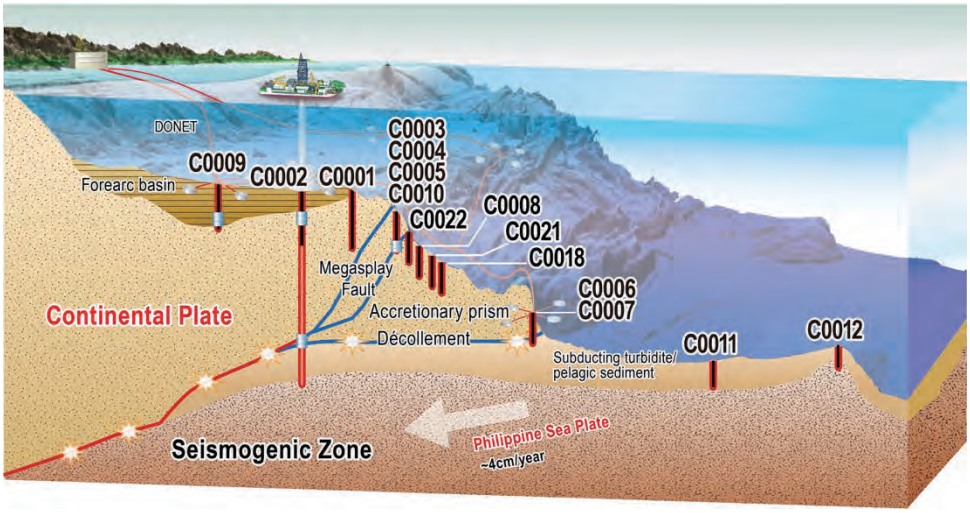

Fig. 2. Schematic diagram of the Nankai subduction margin and drilling sites of *Chikyu*.

This margin is well documented and understood. The recurrence time of M8 class large earthquakes is 1000 years or more. One of the unique features of this margin is that the shallowest up-dip boundary of a seismogenic zone has been identified. It may be possible to reach by ocean drilling and to return samples from depth. One of the prominent scientific results is the discovery of the frictional heating even at the very shallow part of the splay fault (an out-of-sequence fault) and at the toe of décollement as detected by the study of vitrinite reflectance. This is a quite new finding, suggesting that the décollement may slip with high speed during an earthquake which causes shaking and tsunami waves. Especially, the toe region was previously believed to be an aseismic zone. After the Tohoku-oki earthquake in

2011, we confirmed that the same things that occurred in Tohoku also happened in Nankai in the past.

Chikyu drilled off the Tohoku seismogenic zone after the Tohoku-oki earthquake in 2012 (Fig. 3). The target area was estimated to be a large slip, about 50m horizontally, near the trench axis of the Japan Trench. The water depth was approximately 7,000m and drilling penetrated about 900m below the seafloor and successfully cut cores from the plate boundary between the subducting pacific plate and the North American plate. The borehole was used for long-term monitoring of temperature. Fifty five thermistors were installed in the borehole and continuous measurement was conducted for about nine months and the data retrieved in April 2013. A thermal anomaly was detected and this may suggest that the fault slipped during the M9 earthquake.

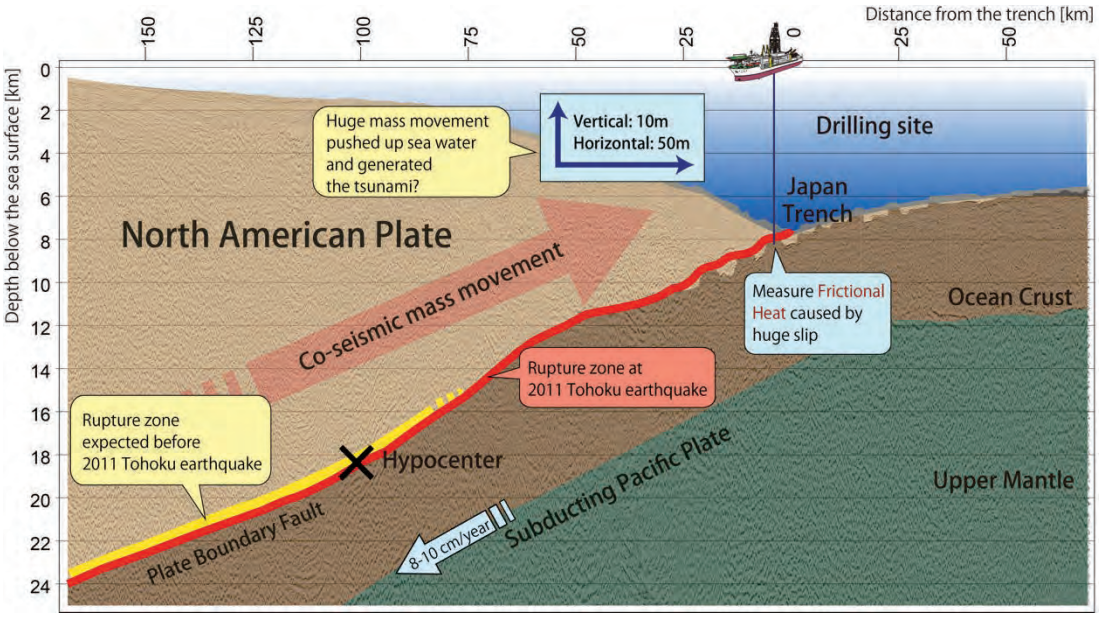

Fig. 3. Schematic section of the Off Tohoku subduction margin at the Japan Trench. Huge slip was measured at the toe of subduction margin caused by the Mw 9.0 earthquake on 11 March, 2011.

3. Seismogenic Zone Real-time Observation

DONET (Dense Oceanfloor Network system for Earthquake and Tsunamis) is a submarine cabled real-time seafloor observation infrastructure which was designed to realize precise earthquake and tsunami monitoring on the seafloor during a long period of time (Fig. 4). The density of observatories is comparable to the earthquake observatory network on land and the tsunami monitoring is an unprecedented capability. The main purpose of DONET is to monitor the hypocentral region of the Tonankai earthquake that is predicted to occur with a probability of more than 70% within the next 30 years according to the report published by the Earthquake Research Committee. DONET consists of an approximately 300km length of backbone cable system, 5 science nodes, and 20 observatories. Its installation at 20 stations in Kumanonada started in 2006 and was completed in July 2011. In August 2011, the seismic data started to be provided to the Japan Meteorological Agency and the National Research Institute for Earth Science and Disaster Prevention, where the data will be used for earthquake early warning. In 2012, one borehole observatory was connected to the DONET and came under operation.

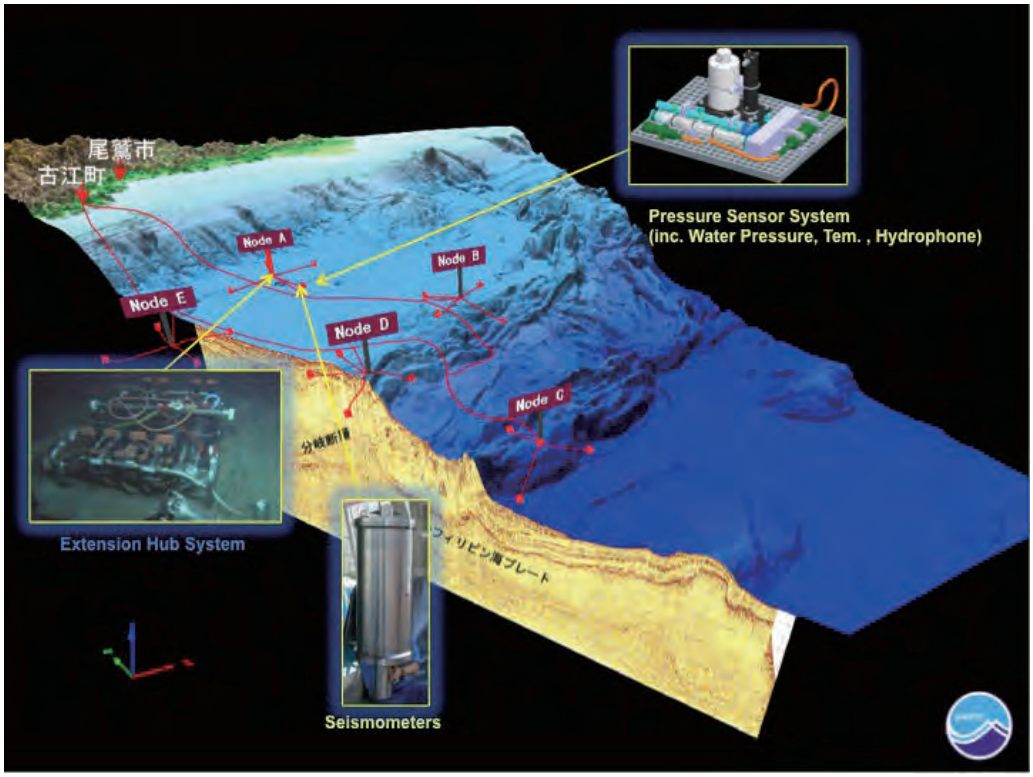

Fig. 4. Schematic diagram of DONET at the Nankai subduction margin.

4. Conclusions

A sample return technology from the seismogenic zone is opening a new insight into the slip behavior of large earthquakes. Nankai and Tohoku scientific drilling results clearly show that a high-speed rupture occurred near the trench axis. This causes us to re-consider the earthquake mechanism and disaster mitigation plan. Also, real-time monitoring is underway in the Nankai Trough. This is the only way to understand the process of earthquake preparation. The data are being carefully monitored and this presents an advantage for disaster prevention in the future. JAMSTEC is contributing to implement Chikyu and other state-of-the-art equipment to enhance geohazard research. This involves doing research close to the seismogenic targets, and observing, measuring, and obtaining materials to carry out more precise research in laboratories. This way should continue to open new horizons.

Activity of ICHARM and reconstruction of Tohni-Hongo area in Kamaishi City

Nario Yasuda

ICHARM

Abstract

Floods, droughts and windstorms were the most frequent disaster events in the past century, accounting for more than 88 percent of the most hazardous one-thousand disasters between 1900 and 2009. The recorded number of water-related disasters, especially floods and windstorms, shows an upward trend from 1980 to 2013. Under these circumstances, the International Centre for Water Hazard and Risk Management (ICHARM), a UNESCO Category II centre, was established as a part of the Public Works Research Institute (PWRI) on 6 March 2006 under the auspices of UNESCO. The Mission of ICHARM is to be the world centre of excellence to provide and assist implementation of best practicable strategies to localities, nations, regions and the globe to manage water-related disasters including floods, droughts, landslides, debris flows, storm surges, tsunami and water contamination.

The Tohni-Hongo Area, Kamaishi City has suffered damage caused by tsunami repeatedly in the past. In this area, the dead and a missing persons are 90.2% by population ratio for the tsunami in 1896 (Meiji Sanriku Tsunami) and 53.5% in 1933 (Showa Sanriku Tsunami), respectively. The past tsunami brought serious damage to this area. Among 165 households, 57 households suffered damage with the tsunami of the East Japan Great Earthquake. However, the ratio of the dead and missing persons is very low at 0.6%. In this area, it is just going to form the disaster victims' transfer plan and future city planning as the tsunami disaster management. We are studying the earthquake disaster recovery of this area, and expecting to obtain lessons for similar areas in the future.

Keywords: water-related hazard, risk management, tsunami, Tohoku

1. Mission and Principles of ICHARM

The International Centre for Water Hazard and Risk Management (ICHARM), a UNESCO Category II Centre, was established as a part of the Public Works Research Institute (PWRI) on 6 March 2006 under the auspices of UNESCO.

The mission of ICHARM is to be the world centre of excellence to provide and assist implementation of the best practicable strategies to localities, nations, regions and the globe to manage the risk of water-related disasters including floods, droughts, landslides, debris flows, storm surges, tsunami and water contamination.

The guiding principles of ICHARM are as follows:

1) To be need-driven, rather than supply-driven, and responsive to respective local realities.
2) To prescribe tailored strategies to realize integrated risk management under the multifaceted, social, economic institutional and cultural conditions as well as technological availability.
3) To produce policy-effective information and raise public awareness to promote societal action.
4) To promote research development and capacity building jointly to bring science where most needed.

5) To work in alliance with all the related organizations of the world to mutually complement resources and expertise and create synergy in implementation.
6) To serve as a global think-tank in water hazard and risk management and play a central role in its strategic promotion.

2. Commitment of ICHARM

Through the integration of its the three-pillars, ICHARM will promote the development and dissemination of "Capacity Development" and "Advanced Technology" to implement "Local Practices" (Fig. 1).

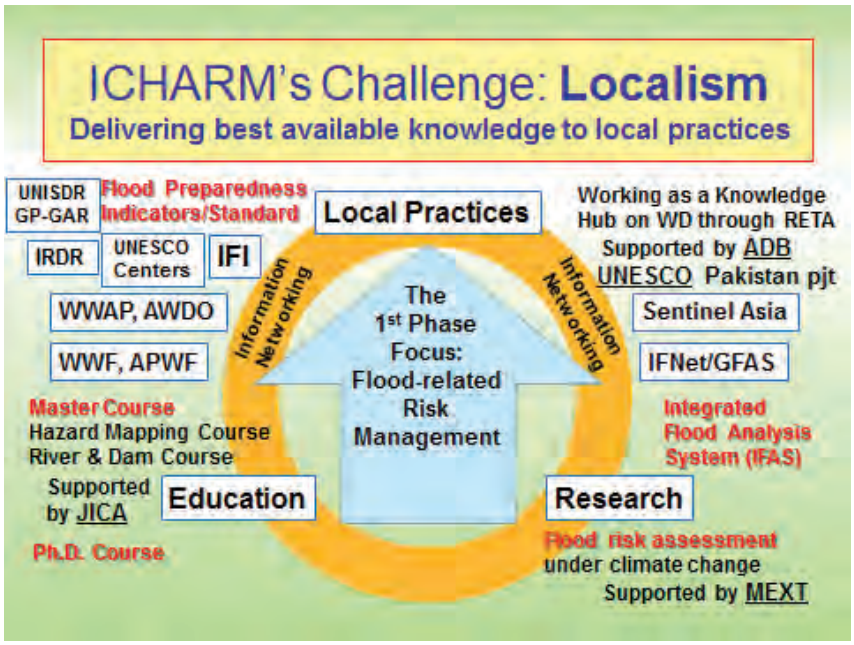

Fig. 1. ICHARM's Commitment

2.1 Research activity

2.1.1 Flood analysis systems developed by ICHARM

(1) Development and dissemination of IFAS

The Integrated Flood Analysis System (IFAS) is designed to help create a runoff analysis model easily by using topographic and land-use data which cover almost the entire globe and are available free of charge via the Internet (Fig. 2). With IFAS alone, users can conduct a series of tasks necessary for runoff analysis including data acquisition, model creation, rainfall-runoff analysis and result display. With an additional module named Auto-IFAS, the system is capable of executing automatic functions such as downloading satellite rainfall information, loading ground rainfall information, performing runoff calculations, issuing a warning, etc. With these automatic functions, users can build a real-time flood forecasting and warning system though the functions are minimal as a device for such a purpose. IFAS with this additional module is very useful even in areas with limited Internet access. It can perform calculation while collecting data regularly according to a predetermined time schedule. In this way, the network and the computer can avoid being overloaded with information processing, which thus enables fast runoff calculation and quick flood forecasting and warning.

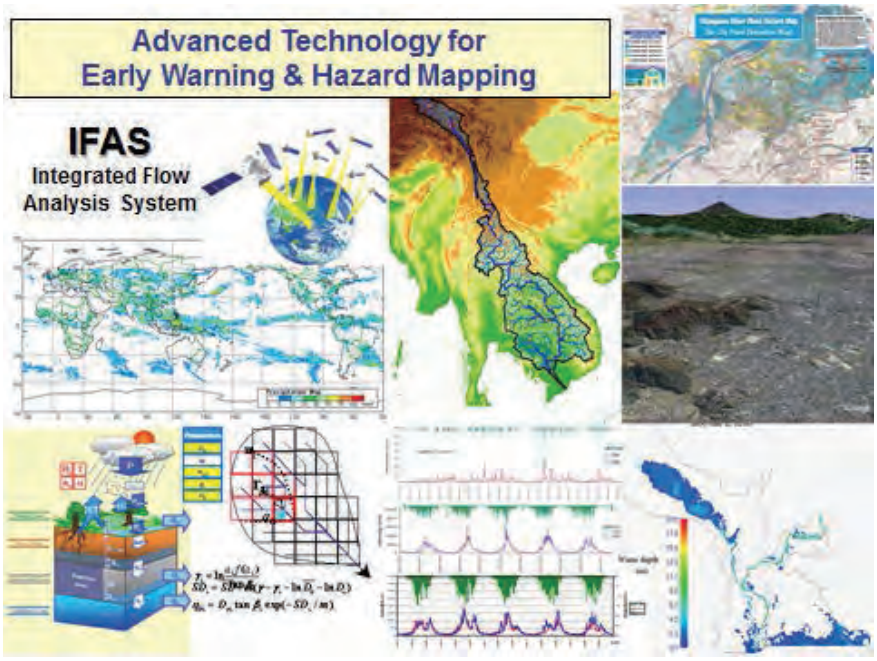

Fig. 2. Integrated Flood Analysis System (IFAS).

(2) RRI Model (Rainfall Runoff Inundation Model)

Conventional flood prediction models, which mainly focus on rainfall-runoff processes in mountainous areas, have difficulties in simulating floods on low-lying areas with large-scale inundations, such as the 2010 Pakistan and 2011 Thailand floods. In addition, although it is important to quickly simulate a large-scale behavior of floodwaters in global-scale flood risk assessment and large-scale flood prediction, conventional models are not capable of quickly estimating river discharge and flooding from rainfall information. They can only predict river discharge.

To overcome this disadvantage, ICHARM has been developing a new numerical model called the Rainfall-Runoff-Inundation (RRI) model (Fig. 3). The model simulates various hydrologic processes including rainfall-runoff, stream-flow propagation, and inundation over floodplains in an integrated manner.

By using the RRI model, we can assess future flood risks for different regions under different climate conditions, for example, based on climate-change prediction information. The model may also be applied to large-scale flood prediction on a near real-time basis by using satellite-based topography, land-use and rainfall information in a similar manner to the IFAS procedure.

2.1.2 Research on Risk Assessment from Flood Analysis

Risk assessment is generally conducted through a series of analyses on possible hazards, vulnerability to and countermeasures for the hazards. ICHARM carries out risk assessment, based on one of the most important institute principles: localism. We start the process with thorough local investigation in each target basin to understand its physical, social and economic conditions, while also using advanced hydrological and hydraulic modeling technology. We then assess the impact of socioeconomic risk on a basin and propose effective counter-measures to cope with such risk (UNISDR, 2009) (Fig. 4).

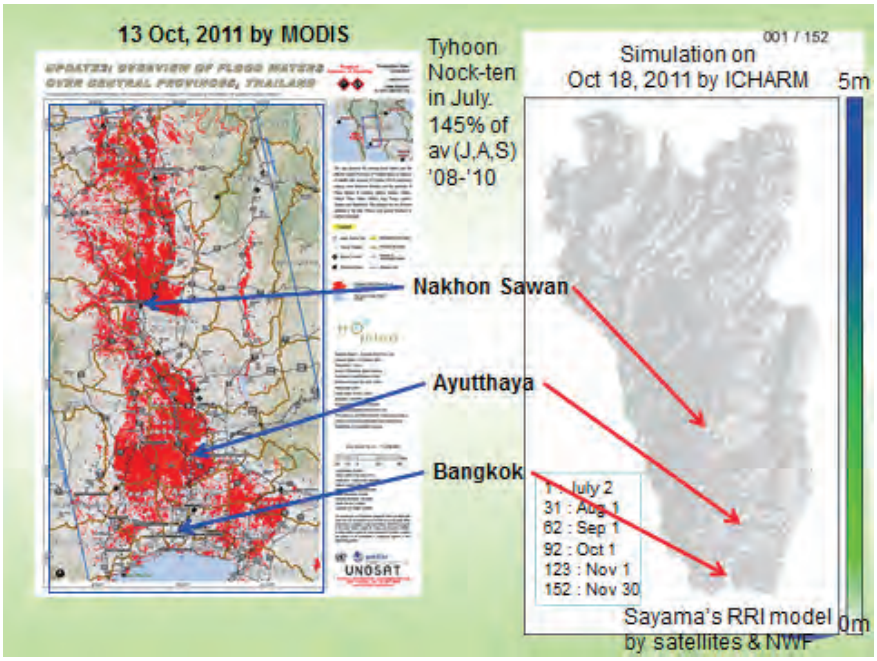

Fig. 3. Rain run-off inundation model.

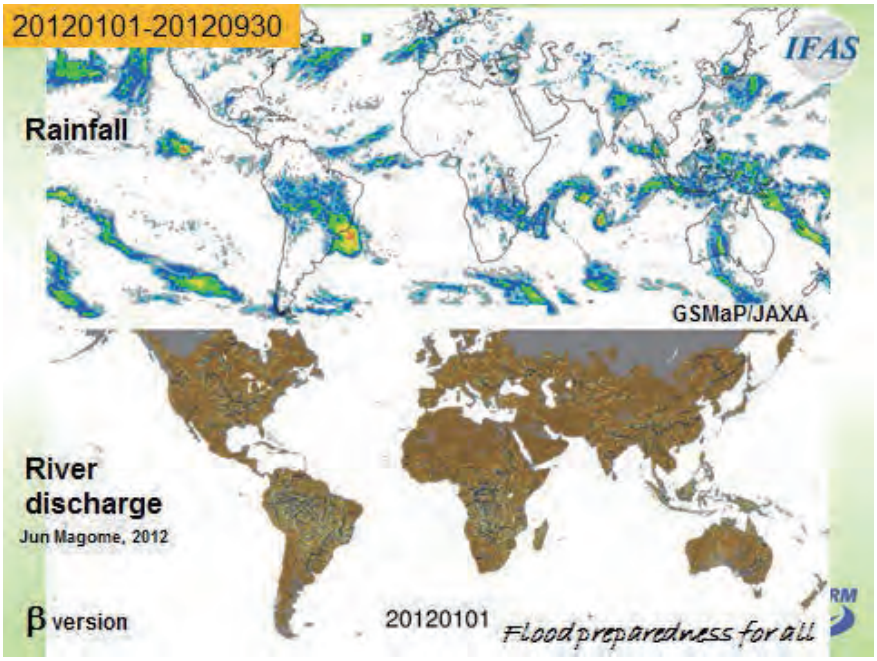

Fig. 4. Risk Assessment from Flood analysis.

2.1.3 Sousei Project

In the Innovative Program of Climate Change Projection for the 21st Century (Kakushin Project), which ended March 2011, ICHARM specifically focused on flood disaster risk and simulated its changes under climate change by using a high-resolution GCM in order to propose a methodology to obtain information for the development of climate change adaptation measures. In April 2012, a new research project, "Program for Generation of Climate Change Risk Information (Sousei Project)", started to expand the previous project. The new project focuses on the impact assessment of uncertainties inherent to climate change

projection and on the improvement of individual component technologies such as socio-economic impact assessment. ICHARM is working on the quantitative projection of how flood and drought risks may change around the world as global warming progresses in consideration with projection uncertainties. This will eventually lead to the development of a methodology for socio-economic impact assessment, which will include methods for the global- and basin-scale assessment of flood and drought hazards as well as for the assessment of social vulnerability to those hazards. Coupled with multiple scenarios of the fifth-generation CMIP and GCM-based climate projections, the methods will make such assessments viable by improving previously-developed technologies for bias correction, global flood runoff analysis and inundation hazard analysis.

2.1.4 Basin-scale water/material cycle model (WEP model)

The Water and Energy Transfer Processes (WEP) model was originally developed as a basin-scale water cycle model. Responding to the recent need for the management of nutrient load and runoff in closed water bodies, ICHARM has been further improving the WEP model into a basin-scale water/material cycle model by adding the function of simulating the behavior of nitrogen and phosphorus in both dissolved and particulate forms.

2.1.5 Automated measurement system for river discharge during flooding

ICHARM is developing and disseminating a next-generation discharge measurement system that ensures highly reliable measurements while requiring less labor and cost. The system under development is unique in that automated measurement using fixed current meters such as non-contact current meters (radio current meters) is combined with an acoustic Doppler current profiler (ADCP) for accuracy control. Through observational experiments, the system has been proven applicable even to severe flow regimes, typically seen in Japanese steep rivers. We are further exploring methods to observe river bed fluctuations by use of this advanced automated system.

2.2 Local practices (Implementation science)

2.2.1 Water-related Disaster Mitigation Project with ADB

In June 2008, ICHARM was officially acknowledged as a Knowledge Hub with particular focus on disaster risk reduction and flood management. As a Knowledge Hub, ICHARM is expected to promote local application of high value-added know-how and research results in order to realize water security in the Asia-Pacific region under the framework of the Asia-Pacific Water Forum (APWF).

As the framework of the Knowledge Hub duties, ICHARM has started a technical assistance project with ADB, “Capacity Development Technical Assistance for Supporting Investments in Water-Related Disaster Management (TA7276-REG),” since November 2009 (Fig. 5). This project aims to help reduce flood disaster vulnerability in target countries through knowledge sharing and capacity development. The project comprises country-specific activities and regional standard activities and has been implemented in Bangladesh, Indonesia, the lower Mekong area (in Cambodia), and the Philippines. In Indonesia, training has been provided for local experts to learn the practical use of IFAS and to enhance the disaster management system through the demonstration of community-based disaster management drills. In Bangladesh, a proposal for an improved flood forecasting and early warning system has been made in workshops with various stake-holders. In the lower Mekong area, flood vulnerability indices have been in development along with training concerning the indices and their use. In the Philippines, flood risk assessment training with IFAS was organized for the management

of the Pampanga and Cagayan Rivers, in which IFAS has been implemented. Flood risk indices are also being developed for the case study countries.

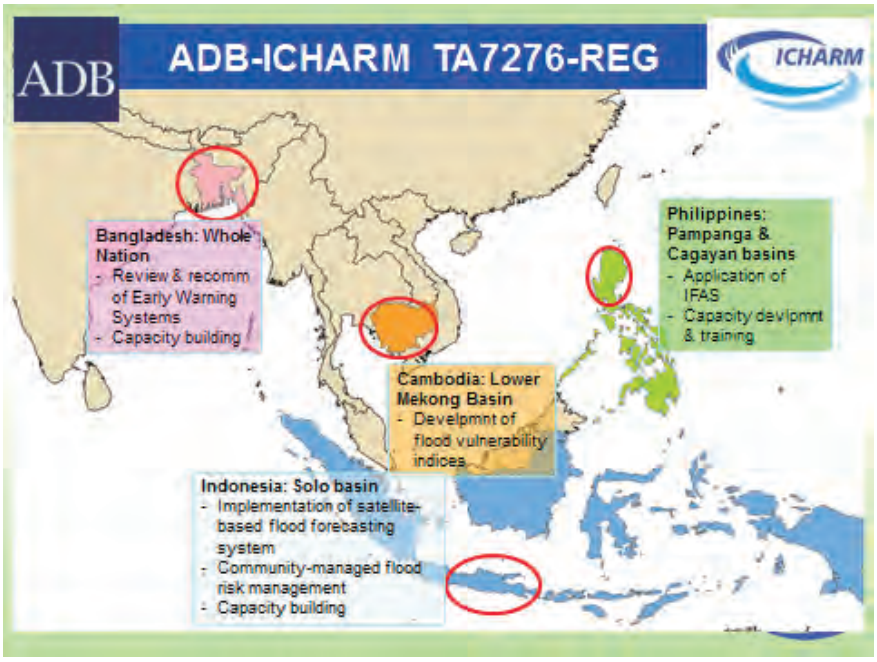

Fig. 5. Water-related disaster mitigation projects with ADB.

2.2.2 UNESCO Pakistan Project

In late July 2010, the monsoon brought a record rainfall over northern Pakistan and caused the worst flood in the past 80 years. As a part of the restoration effort from this flood disaster, in July 2011 UNESCO started a project called “Strategic Strengthening of Flood Warning and Management Capacity of Pakistan”. This comprehensive project consists of three components, and ICHARM has been assigned to two of these components: technical assistance and capacity development. In the first component, ICHARM assists Pakistan in the development and implementation of “Indus-IFAS” and the production of flood hazard maps (Fig. 6). Indus-IFAS is specifically designed to fit the conditions and needs of the Indus River basin by combining IFAS and the RRI model. In the other component, ICHARM has provided the opportunity to participate in its M.Sc. program and short-term training programs for government administrators such as the Pakistan Meteorological Department, the Pakistan Space and Upper Atmosphere Research Commission and other agencies.

2.3 Training Programs for Organizational Capacity Development

To cope with major water-related disasters like floods, it is important to empower not only individuals but also organizations involved in disaster management because there is a limit to what each individual can do. Being well aware of that fact, ICHARM provides training programs that help improve both individual problem-solving capacity and organizational coping capacity in disaster management (Fig. 7).

2.3.1 Short-term training program

Participants gain knowledge and learn technologies relevant to water-related disaster risk management for a period of several days or weeks. Training courses are typically conducted in cooperation with the Japan International Cooperation Agency (JICA). We started “Capacity

Development for Flood Risk Management with IFAS" from FY2012.

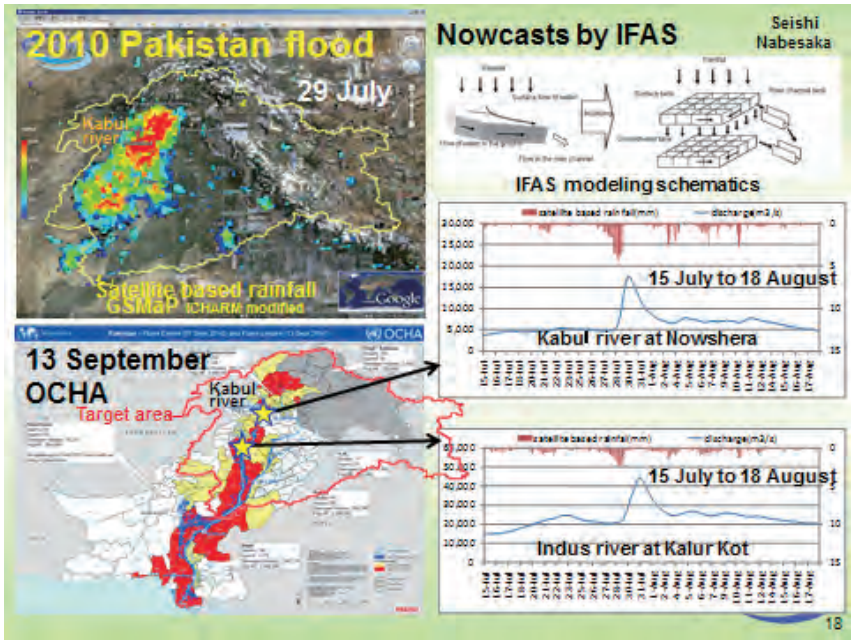

Fig. 6. UNESCO Pakistan Project.

Fig. 7. Training program for Organizational Capacity Development.

2.3.2 M.Sc. program

The one-year M.Sc. program, "Water-related Disaster Management Course of Disaster Management Policy Program," has been provided jointly with JICA and GRIPS since 2007. The program is mainly designed for administrators in flood management in developing countries. Students attend lectures, practices and field trips in the first half and work on a master's thesis in the latter half. As of September 2012, a total of 60 students graduated with a

master's degree in disaster management.

2.3.3 Ph.D. program

A Ph.D. program, "Disaster Management Program," has been provided since 2010 in collaboration with GRIPS. As of November 2012, five students from Japan, the Netherlands, Nepal, Bangladesh and Guatemala have enrolled in the program.

2.3.4 Follow-up activities

Post-training seminars and other workshops and meetings are occasionally organized mainly to support ex-trainees' activities in their countries.

2.4. Other Activities

2.4.1 ICFM5

ICHARM organized the 5th International Conference on Flood Management (ICFM5) in Tokyo on 27-29 September 2011. More than 450 people from 41 countries participated. Under its main theme, "Floods: From Risk to Opportunity," the participants had productive discussions on five topic areas including flood risk management. The conference finally adopted the ICFM5 declaration based on the discussion results of each topic-area (http://www.ifi-home.info/icfm-icharm/icfm5.html). ICFM6 is planned to be held in Brazil in 2014.

2.4.2 International Flood Initiative (IFI)

IFI is a framework to promote collaboration in flood management among international organizations such as UNESCO, WMO, UNU and UNISDR. IFI focuses on research, information networking, education and training, community empowerment, and technical assistance in various areas including integrated flood management (Fig. 8). ICHARM is currently serving as its secretariat.

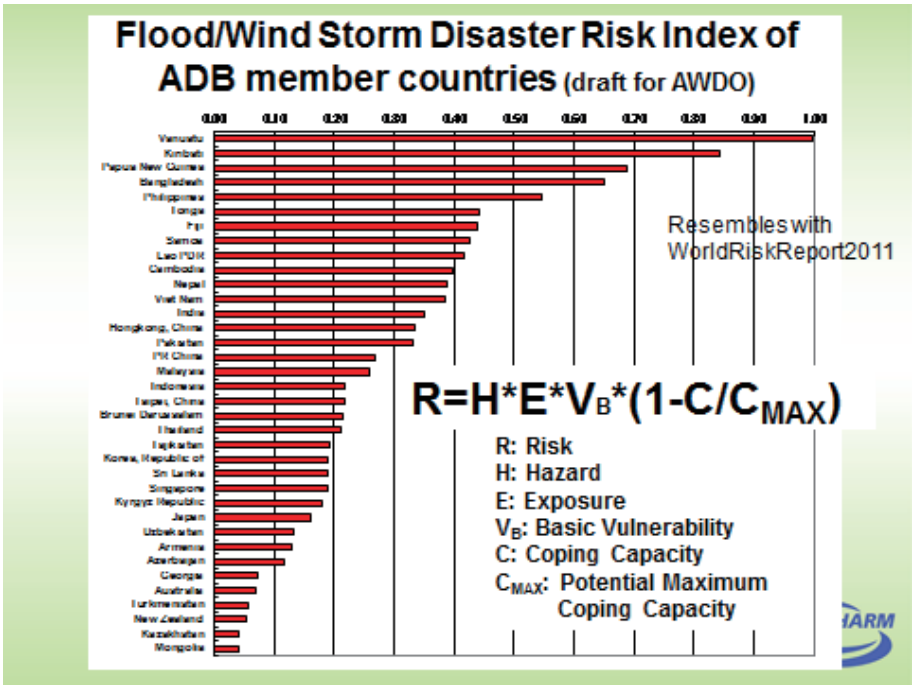

Fig. 8. International Flood Initiative of Risk Index.

3. Reconstruction of Tohni-Hongo Area in Kamaishi City

3.1 Tsunami Disaster Management

Before the Great East Japan Earthquake on March 11, 2011, tsunami disaster management was about: a) the estimation of the design tsunami from past events; b) the reduction of tsunami damage by seawalls, breakwaters, and tide-water control forests; c) relocation to higher ground and construction of embankment (by heightening), refugee shelters and refugee roads; and d) implementation of tsunami warning systems and disaster prevention drills. After the 3.11 earthquake, the focus of tsunami disaster management has shifted to: a) how to cope with tsunami force over the design magnitude; b) verification of effectiveness of tsunami disaster management in evacuation of residents; and c) development of tsunami- resilient communities.

3.2 Tohni-Hongo Area, Kamaishi City

The coastal Tohni-Hongo area, a part of Kamaishi City in Iwate Prefecture, has repeatedly suffered from tsunamis (Fig. 9). In relatively recent years, during the Meiji Sanriku Tsunami of 1896, 90.2% of the total population in this area were either dead or missing. During the Showa Sanriku Tsunami of 1933, the percentage was 53.5% (Fig. 10). These numbers tell us how devastating past tsunami damages were in this area.

After the 1933 tsunami disaster, Tohni-Hongo residents relocated to higher ground far from their fishing grounds as part of the reconstruction effort. However, when the seawall was extended and heightened to further protect the area after the Chile Tsunami in 1966, residents started coming back to live in their old settlement near the sea, which had been repeatedly flooded in past tsunami events.

When the Great East Japan Earthquake occurred in 2011, 57 out of 165 Tohni-Hongo households suffered damage from huge tsunamis triggered by the quake (Fig. 11). This time, however, the percentage of the dead or missing was extremely low at 0.6%.

Fig. 9. Location of Tohni-Hongo area.

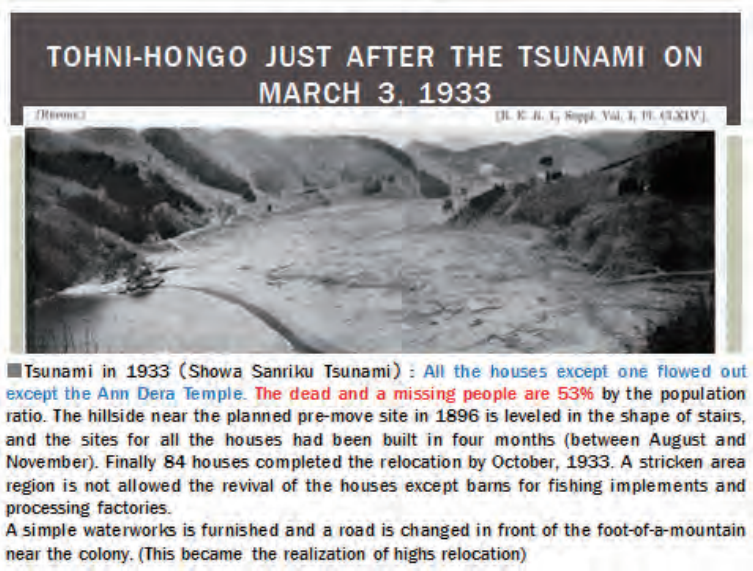

Fig. 10. Tohni-Hongo area just after the 1933 Showa Sanriku Tsunami.

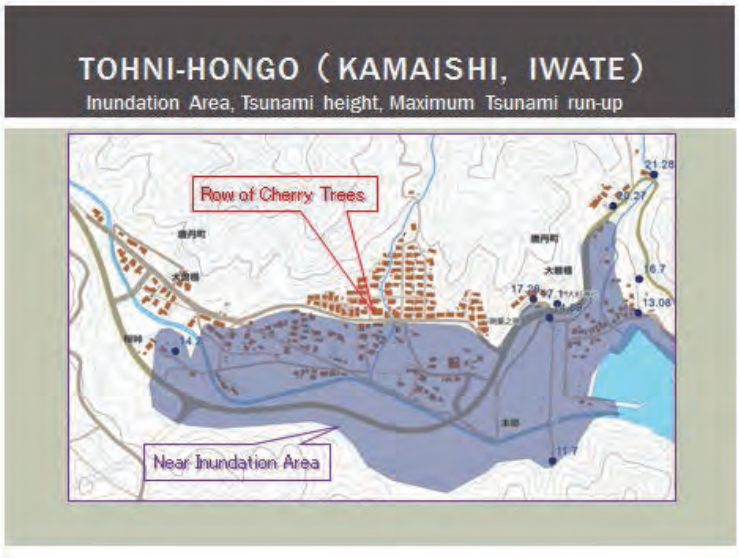

Fig. 11. Inundation of tsunami at Tohni-Hongo.

The Tohni-Hongo area is currently working on a disaster victims' relocation plan and future city planning as part of tsunami disaster management. To design practical reconstruction plans, it is important to clearly understand the behavior of the tsunami that hit the Tohni-Hongo area just after the earthquake. An investigation team visited Tohni-Hongo residents, including those who experienced the tsunami, and interviewed them about how the tsunami behaved when it hit the coast of Tohni-Hongo. Based on the interview results, we were finally able to accurately reproduce the movement of the tsunami in the Tohni-Hongo area. During the visit, the team also learned a great deal about the resident's knowledge, thoughts and understanding of the tsunami itself and tsunami countermeasures.

The following are the main questions asked in the interview:

a) Did you think a tsunami would come after the earthquake? Why?
b) What do you think about effect of the seawall against a tsunami?
c) What did you do during and just after the earthquake?

3.3 Reconstruction Plan of the Tohni-Hongo Area

A draft reconstruction plan was drawn up by Tohni-Hongo residents three months after the earthquake. A relocation place was selected among several proposed sites after intensive discussion between the residents and the municipal government of Kamaishi (Fig. 12). They also decided to heighten the embankment-type seawall roughly for an additional 3 meters in crest elevation from 11.8m to 14.5m. The selected relocation site is considered to be safe from tsunamis comparable to the one they experienced on March 11, 2011. However, residents are still advised to evacuate the relocation site in the event of an unexpectedly huge tsunami.

3.4 Issues in the planning of the reconstruction program

a) Shortage of flat land (i.e. difficulty of land acquisition)
b) Ambiguity of land ownership in the Sanriku district
c) Shortage of engineers for community design (especially concerning large-scale public works)
d) Unavailability of proper construction materials (resulting from frequent changes of specifications due to rising unit prices)
e) Lack of cooperation between governmental bodies (duplication of reconstruction works)

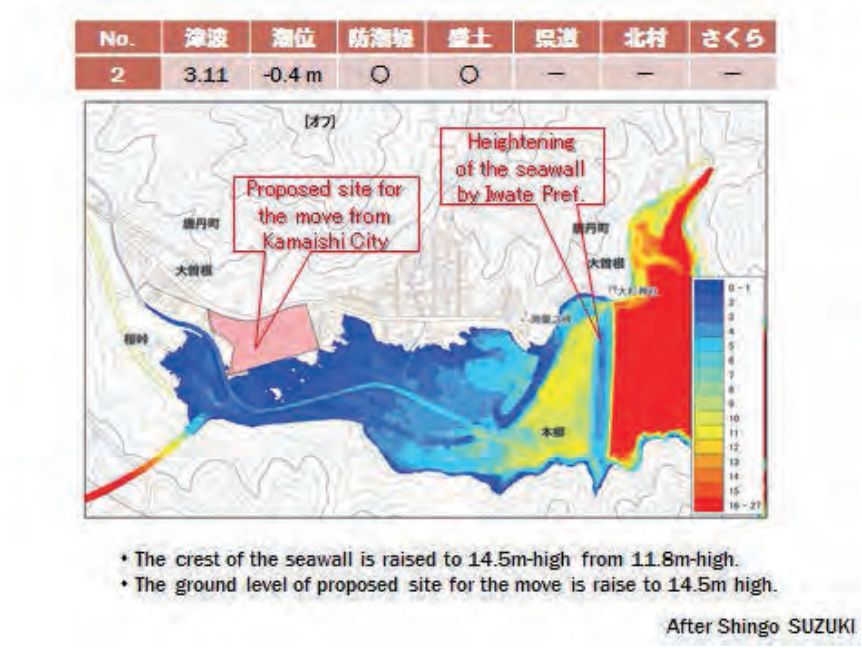

Fig. 12. Reconstruction plan in Tohni-Hongo.

References

UNISDR, 2009, “Terminology on Disaster Risk Reduction”

Activities undertaken by Tohoku University for reconstruction after the Great East Japan Earthquake

Hiroshi Nishi

The Center for Academic Resources and Archives, Tohoku University Museum, Tohoku University
hnishi@m.tohoku.ac.jp

Abstract

After the Great East Japan Earthquake disaster in March 11, 2011, Tohoku University commenced rescue and reconstruction activities together with scientific research related to the earthquake and subsequent tsunami. The University promoted and conducted eight initial projects, together with other member's projects within "Reconstruction Action 100."

Keywords: The Great East Japan Earthquake, reconstruction activities, Tohoku University

1. Situation just after the Great East Japan Earthquake

The Great East Japan Earthquake and the subsequent tsunami caused extensive damage in the Tohoku districts including Miyagi Prefecture. After ensuring the safety of students and members, the University started the rescue activities with hospital support and volunteer reconstruction work in the damaged area, together with research for earthquake and tsunami damage. Several buildings in the campus area were damaged, and severe damage occurred in the Aobayama campus. Constructions around the coast, such as boat and yacht houses and the science field center, were totally destroyed by the tsunami. All public schedules were cancelled until the end of April.

In addition, the consequences of the Fukushima Nuclear explosion started to become increasingly influential from March 11 through March 15, 2011. Serious radioactive pollution was a concern together with the earthquake damage noted above in the Universities vicinity because of its only 100 km distance from the Fukushima Nuclear Plants. Fortunately, the Onagawa Nuclear Plant, which is situated in Miyagi Prefecture, was not damaged by the earthquake or tsunami. Radiation monitoring was started in the campus area and the highest values, over 0.15 μSv/h, were recorded between March 11 and 27, however declined to normal level (0.08 μSv/h) after this period. Logistic support, particularly fuel supplies, had not recovered within one to two weeks after the disaster.

2. Contribution of Tohoku University

In spite of all the disruption, Tohoku University quickly started emergency rescue activity in various divisions. For example, Tohoku University hospital supported medical activity including the supply of medicine and medical materials to the disaster area. The radiation monitoring started with atmospheric measurement on campus (4 posts) and other areas (7 posts), followed by food, water and soil in Fukushima City. A robot system was provided to the Fukushima Nuclear Power Plant for inside survey of the nuclear reactor building. Many volunteer activities by members and students of Tohoku University were conducted for reconstruction in the damaged areas. Tohoku University specialists reported the disaster situations of the tsunami, earthquake, and subsequent radioactive pollution from the academic

point of view. In addition, after 25 March, the Tohoku University Museum started restoration activity of scientific collections in damaged museums around the coastline after. This activity expanded to involve others in the scientific community, such as the Paleontological Society of Japan, and continues at the present time.

3. Reconstruction Projects of the Tohoku University

In April 2011, Tohoku University established the Institute for Disaster Reconstruction and Regeneration Research as an organization to be engaged in research, education and societal contributions, and to communicate the results of its activities to the public. Tohoku University have proposed eight projects, and also promoted eight "Institute-initiated projects," and promoted and supported "Reconstruction Action 100^{+}" through flexible operation and participation by the entire university (Fig. 1). Tohoku University will continue to pursue these efforts for the rebirth of Japan.

4. Conclusions

Geological hazards such as earthquakes, volcanic activities and landslides are important social concerns all over the world. Because countries in Asian region have similar geological and geographical backgrounds, we believe that our experiences in dealing with geological hazards can contribute to the prediction and prevention of these hazards in many Asian countries. To accomplish the goal to reduce natural hazards in the region, it is essential to build a global cooperation system covering all Asian countries.

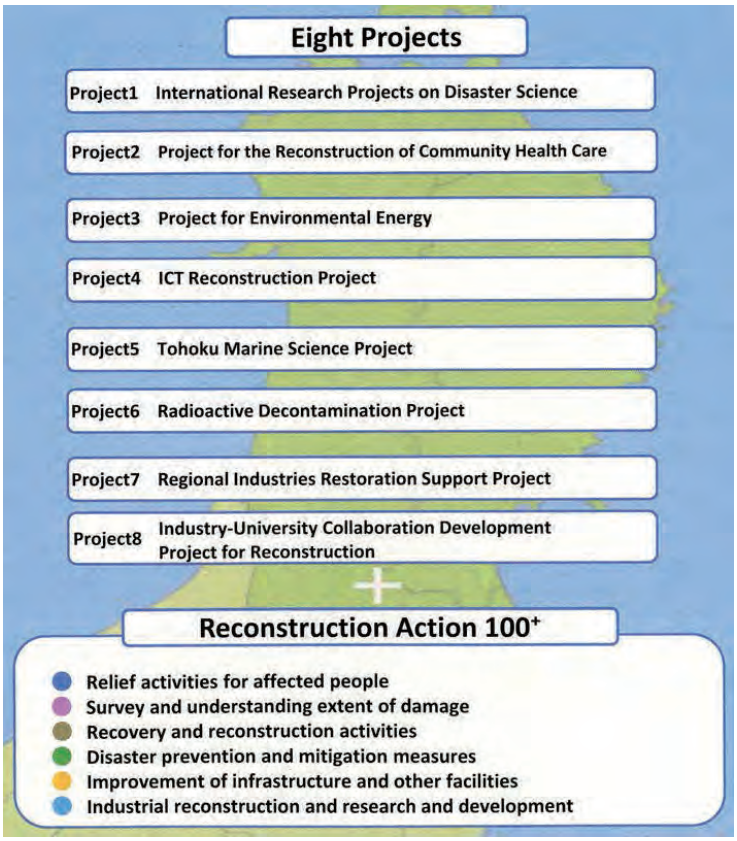

Fig. 1. Eight projects of the Tohoku University action (Tohoku University, 2013).

References

Tohoku University, 2013, Tohoku University Reconstruction Action, Vol. 2.

A free geohazard information service for Europe: the PanGeo Project

Luca Demicheli[1], Claire Roberts[2], Luke Bateson[3], Stuart Marsh[3], and Patrick Wall[1]
[1]EuroGeoSurveys, the Geological Surveys of Europe
e-mail: luca.demicheli@eurogeosurvey.org
[2]CGG NPA [Project Coordinator], United Kingdom
e-mail: claire.roberts@cgg.com
[3]British Geological Survey, United Kingdom

Abstract

PanGeo is a 3-year Collaborative Project of the European Commission that started in February 2011. During the project, PanGeo will provide free online geohazard information for 52 of the largest towns in Europe, mapping geohazards that could potentially affect up to 13% of the EU population. It is hoped that more towns will be added over time.

PanGeo provides information describing the stability of the ground on which we live, work and play. Ground instability can be dangerous and costly, yet information on ground stability has, to date, been difficult to obtain. PanGeo provides free access to ground instability geohazard information for many of Europe's largest cities. Users of the PanGeo service include local authorities, civil protection agencies, geological surveys, insurers and businesses providing environmental and land reporting services and the general public.

PanGeo provides a 'ground stability layer' which describes the spatial location and extent of geohazards for all the towns mapped. Each polygon within the ground stability layer is linked to a full interpretation made by that country's National Geological Survey. PanGeo data is created by combining satellite measurements of ground and building movement, and geological information already held by National Geological Surveys. The European Commission's Urban Atlas land use data also provides insights into what types of urban land use are affected by geohazards described in the ground stability layer.

PanGeo is supporting 'Copernicus', a European initiative designed to support EU environmental policy. Copernicus is based upon data from Earth observation satellites, but includes any other data available relevant to the service. Copernicus addresses six thematic areas: land, marine, atmosphere, climate change, emergency management and security. These support a wide range of applications, including environment protection, management of urban areas, regional and local planning, agriculture, forestry, fisheries, health, transport, climate change, sustainable development, civil protection and tourism.

Keywords: geohazards, ground stability, Europe, free online data, Copernicus

1. Introduction

PanGeo is a 3-year collaborative European project that started on the 1st February 2011 with the objectives of enabling free and open access to geohazard information in support of Copernicus. This will be achieved by providing an INSPIRE-compliant, free, online geohazard information service for 52 of the largest towns in Europe covering approximately 13% of the population, down to a mapping scale of 1:10,000.

The geohazard information is served in a standard format by the 27 EU national Geological Surveys via a modified version of the 'shared access' infrastructure as devised for the project One-Geology Europe. The information (a new ground stability data-layer and accompanying

interpretation) has been made by each Survey. These products are compiled from integrations of:

- Satellite Persistent Scatterer InSAR processing, providing measurements of terrain-motion. Half of these are existing datasets coming from the ESA GMES Service Element project Terrafirma,
- Geological and geohazard information already held by national Geological Surveys, together with their expertise,
- The polygonal landcover and landuse data contained within the GMES Land Theme's Urban Atlas.

2. The PanGeo portal and its uses

The PanGeo service can be accessed via the PanGeo website (www.pangeoproject.eu). A user can view the data on the PanGeo portal, built on One Geology Europe infrastructure, or via Google Earth. Upon user enquiry, the portal retrieves information on individual town ground stability layer polygons and automatically integrates it with the Urban Atlas dataset. The products can be downloaded and integrated into a user's own system. Clicking on polygons will hyperlink to interpretative reports. User input to design is facilitated by the 27 National Geological Surveys contracted into the project and a core group of Local Authority representatives.

It is trusted that sustainability of PanGeo will be achieved by attracting a proportion of the remaining 253 Urban Atlas towns to procure the PanGeo service for their towns. The service that will already be provided in their country will form the basis of the required promotional activity.

The key users of PanGeo are:

- Local Authority planners and regulators who are concerned with managing development risk,
- National geological surveys and geoscience institutes who collect and disseminate geohazard data for public benefit,
- Policy-makers concerned with assessing and comparing European geological risk, much as the Urban Atlas data is used to compare the landcover/use status of European towns,
- The public.

The provision of an open-access, standardised information service on geohazards will enable policy-makers, regulators, and the public to:

- Systematically assess geohazards in each of the 52 towns involved,
- Gain understanding of the geohazards themselves,
- Know who to talk to for more information,
- Statistically analyse and cross-compare geohazard phenomena across EU countries,
- Gain a better understanding of the socio-economic costs involved,
- Make more informed decisions, e.g. on civil defence and planning controls,
- Have confidence that the information provided is robust and reliable.

3. The PanGeo Team

The PanGeo team comprises 13 ‘core’ partners, as well as all 27 EU National Geological Surveys. Core Team partners are: Fugro NPA Ltd (UK - Project Coordinator), British Geological Survey (UK), Landmark Information Group (UK), TNO (NL), SIRS (FR), Institute of Geomatics (ES), BRGM (FR), EuroGeoSurveys (BE), AB Consulting Ltd (UK), European Federation of Geologists (BE), Tele-Rilevamento Europa (IT), Altamira Information (ES), Gamma Remote Sensing (CH).

Monitoring systems and adaptation activities along the Korean coast

Seong-Pil Kim[1] and Se Won Chang[2]

[1]Petroleum and Marine Geology Division, Korea Institute of Geoscience and Mineral Resources, Republic of Korea
[2]International School for Geoscience Resources, Korea Institute of Geoscience and Mineral Resources, Republic of Korea
e-mail: spkim@kigam.re.kr

Abstract

As a country with a high ratio of shoreline length to land area, the Republic of Korea (hereafter, Korea) has been experiencing various kinds of coastal geohazards, either chronically or sporadically. Adjoining a back-arc basin (the Ulleung Basin) in the east and an epicontinental sea (the Yellow Sea) in the west, Korea has three (east, west and south) unique coasts showing conspicuously different aspects. The eastern coast is an uplifted coast which has gently curved and relatively smooth shorelines without a large river system. Most of the backshore areas have been artificially changed so as to lose their original appearances, whereas nearshore areas are still remained untouched. The west coast is a submerged coast with many bays and muddy tidal flats interconnected with rivers and channels. Under macrotidal regime (up to 9 m) most of the coastal low lands have been extensively reclaimed since the late 1800s, the most representative example of which is the Saemangeum Dyke. The south coast is a typical ria-type coast with many archipelagos, wide bays and peninsulas. Most of the islands are large and have adequate water resources to accommodate a number of local people. In this document several distinct aspects of the Korean coasts will be summarized and various coastal monitoring systems and adaption activities will be introduced with some illustrative examples.

Keywords: coast, Korea, monitoring, adaptation, geohazard

1. Aspects of Korean Coasts

Korea is surrounded by three different types of coasts in the east, west and south respectively (Fig. 1). The east coast comprises the western margin of a back-arc basin (the Ulleung Basin) which was opened during the late Tertiary Period. The overall view of this shoreline gives a gently-curved and smooth appearance with a narrow coastal land area. The tidal range is less than 2 m, decreasing northwards. Neither large river systems nor distinct muddy tidal flats exist. With a closer look, however, many sedimentary environments such as sandy or gravelly beaches, lagoon-and-spit complexes, and rocky cliffs could be recognized decorating the coastal area. At some locations remnants of raised marine terraces and ridge complexes are found. The wind system affecting the east coast is dominated by the northeasterly and the easterly directions (KMA, 2013a). Major current systems are the North Korean Cold Current flowing southwards and a branch of the Kuroshio Warm Current affecting the southern offshore area..

The west coast of Korea is located on the mid-eastern part of the Yellow Sea. The shoreline is very rugged and irregular in appearance. As the Yellow Sea is a part of an epicontinental sea, the water depth is generally shallow (less than 50 m in average, ca. 154 m in maximum) and the adjacent onshore areas are low in altitude (less than 10 m above mean sea level). The tidal range is more than 4 m (up to 9 m near Incheon) so that a number of large muddy tidal flats, estuaries, bars, bays, islands and supratidal beaches are found.

Dunes formed by monsoonal wind are another characteristic coastal environments. Most of them are difficult to recognize due to strong civil works or windbreak plantation except the Sinduri coastal sand dune preservation zone, which still shows the original form. The dominant wind is the westerly with local bias towards the SW or NW (KMA, 2013a). A coastal boundary current is reportedly flowing northward in the offshore while the tidal current generally shows ebb-dominance in the nearshore and transports suspended material to the south.

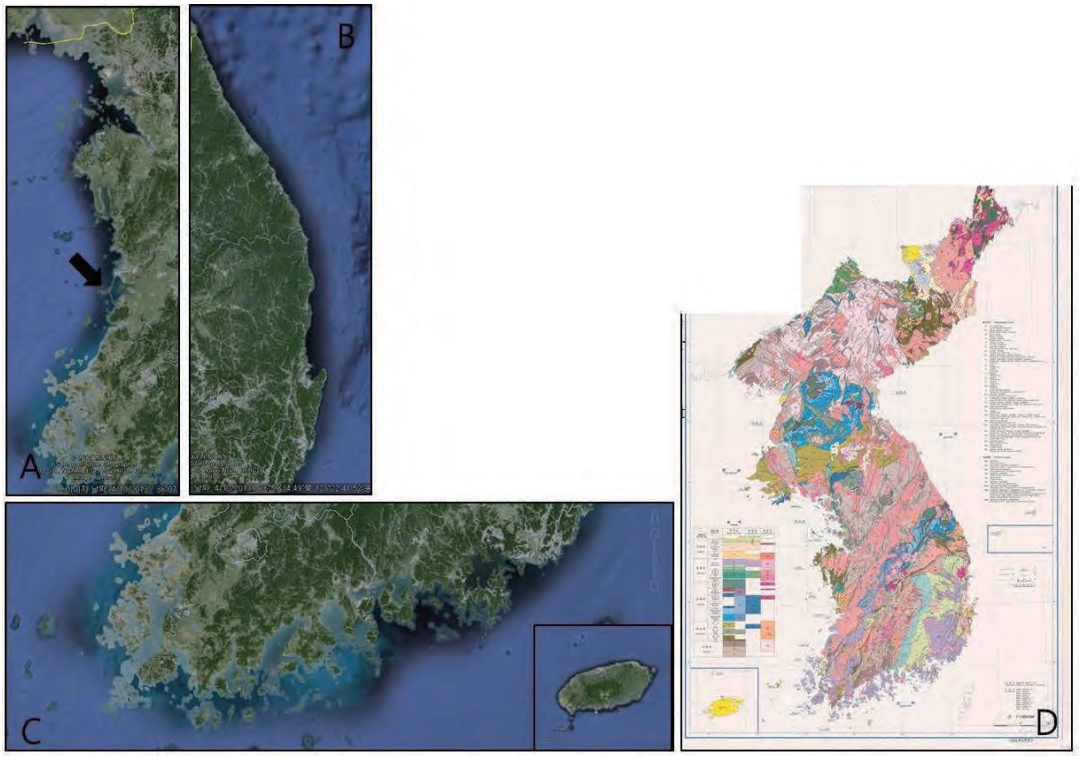

Fig. 1. Overview of the Korean coasts. (A) The west coast looks irregular with abundant islands, bays and estuaries. Muddy tidal flats are well-developed due to large tidal range so that they are easily found in many embayed areas where reclamation would be made actively. Note the 34-km-long Saemangeum Dyke in the middle part of the west coast (black arrow in A) which is visible even in the satellite images. (B) The east coast shows monotonous and gently curved shorelines composed mainly of long beaches, spits and rocky cliffs. (C) The south coast has a typical ria-type character with abundant islands, bars, and peninsulas. In the southern offshore, the biggest volcanic island in Korea, Jeju Island (inset) is located. Despite its complex appearance there are not many tidal flats in the south coast. Tidal range of the south coast is smaller than the western counterpart and no significant river input exist along the southern coast except in the eastern margin. The age of the basement rocks in its eastern part is generally younger than those in the less weathered western part (D).

The south coast adjoins the northeastern part of the East China Sea, where the northern branch of the Kuroshio Warm Current is passing from the East China Sea toward the East Sea. Except the volcanogenic Jeju Island the shoreline has a typical ria-type morphology comprised of a number of archipelagos, bays, and peninsulas. The tidal range is between 2 to 4 m and increases eastwards. Most of the bay areas are very shallow and flat while straits and passages among islands are very narrow and deep.

Unlike the west coast the spatial extents of tidal flats or beaches are limited because of relatively small tidal range, lack of river supply, and steep basement rocks. In the eastern end

of the coast the biggest river delta in Korea, the Nakdong River delta, is developed near Busan Metropolitan City. Although artificially controlled these days, large amounts of suspended materials are fed into the coastal area.

It is reported that a water front has formed between the coastal water and the Kuroshio Current so that suspended materials fed by the rivers in the coast are transported along the coast and finally form longitudinally-elongated mud deposits along the southeastern corner of the Korean peninsula. The dominant wind system is the southerly with local bias to the SE or SW (KMA, 2013a).

Fig. 2. Pictures showing typical geomorphological features in the east coast of Korea: (A) a sand beach in Naksan, (B) a gravel beach in Jeongja, (C) Hajodae sea cliff, (D) Cheongchoho lagoon in Sokcho.

2. Major coastal geohazards

The term geohazards is commonly used for those hazardous phenomena driven by geological events. According to the generally accepted criteria (UNESCO, 2013) they include earthquakes, volcanic activities, landslides, tsunamis, floods, wind-blown dust, meteorite impacts and hazardous geological materials. Considering recent global events, those phenomena usually occur catastrophically sometimes inducing pandemic influences (e.g., the tsunamis in Banda Ache, Indonesia in 2004 and in Tohoku, Japan in 2011).

On the other hand slow and continuous phenomena such as soil creep, ground subsidence, sea water intrusion, erosion or siltation have been also reported frequently. They are relatively small in scale so that they would not be easily detected in a short time period. But, once accumulated, the resultant impacts are fairly comparable to those catastrophic ones. The

statistics on damages of human life and economy which were resulted from natural disasters in Korea are shown in Fig. 4.

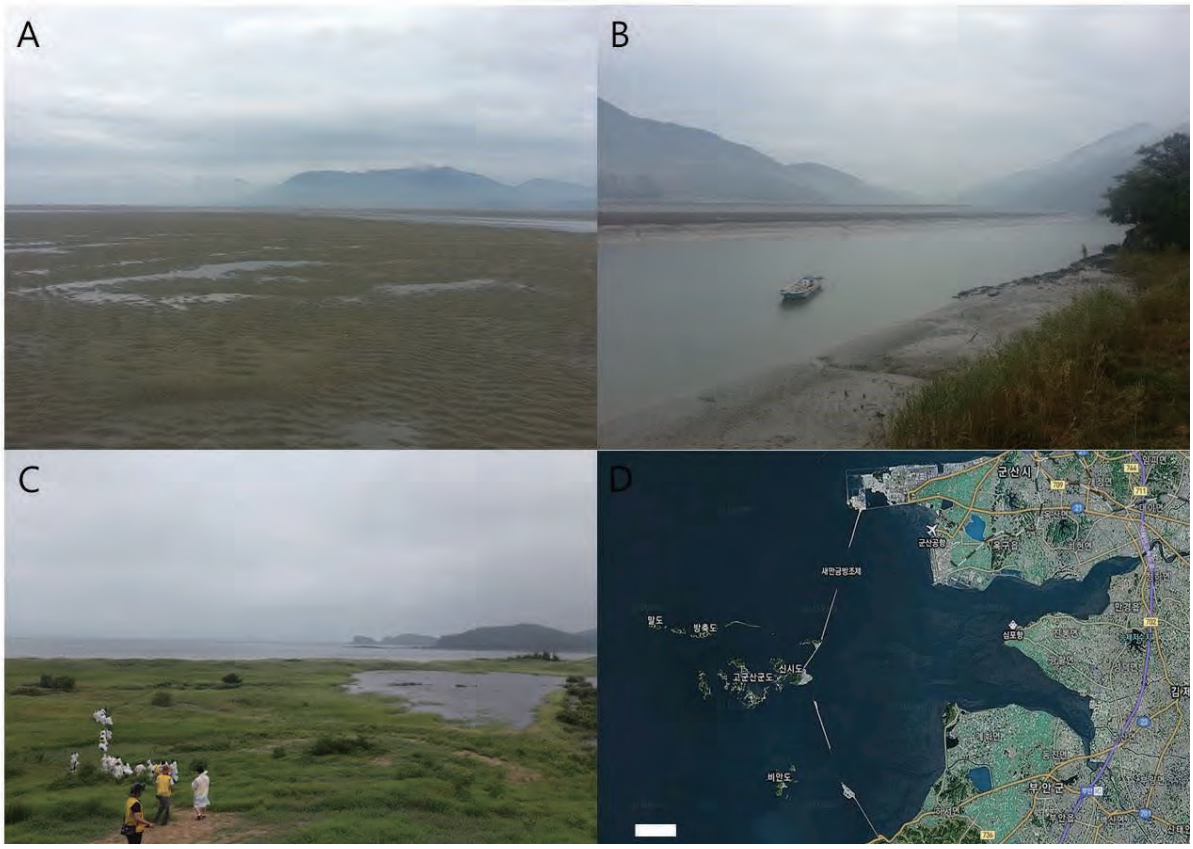

Fig. 3. Pictures showing the typical geomorphological features in the west coast of Korea: A sandy or muddy intertidal flat (A), a tide-dominant river mouth estuary (B) in the Gomso bay, (C) grass-covered sand dunes in the Sinduri Sand Dune Preservation Zone, (D) the Saemangeum Dyke (arrow bar is 8 km; an aerial photograph before completion; image source from DAUM).

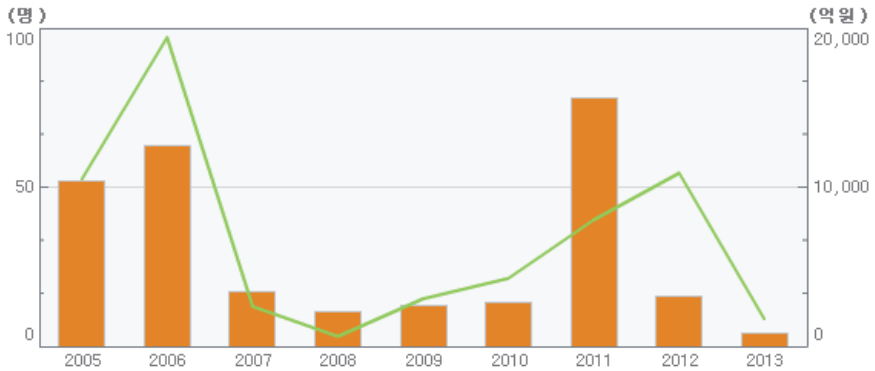

Fig. 4. Statistics on the casualties (orange bar and left axis) and property loss (green line and right axis in $*10^5$ USD) induced by natural disasters in Korea (Statistics Korea, 2013).

Taking the recurrence frequency and the scale of impact into account, Korea doesn't seem so much vulnerable to catastrophic geohazards as compared to many other countries. Especially earthquakes, which are one of the main geohazards in the other Asian region, broke out in

small magnitude (mostly less than M5) leaving no directly-induced damage so far. However, records of tsunamis induced by submarine earthquakes could be found with notable several casualties and property losses in 1983 and 1993.

Meanwhile, gradual processes such as shoreline retreat, coastal erosion and siltation are reportedly to be the origins of major hazardous phenomena in Korea which frequently induce societal issues. Pollution, despite its anthropogenic origin, always stimulates the public especially in highly industrialized areas. Nowadays, without doubt, global sea level rise has become a key factor which aggravates the negative impacts of these hazardous agents.

Table 1 is the summary of the major coastal geohazards in Korea. Shoreline retreat seemingly prevails all over the country due to global sea level rise. Most of the beaches are being narrowed unless they are continuously nourished or protected with strong seawalls and dykes. Due to the strong protective measures the exact speed of retreat would not be easily detected in short periods.

Table 1. Major types of coastal geohazards recognized in several locations and their possible causes with driving agents.

Coast	Major Types	Examples	Possible Causes	Major Agents
East	Shoreline retreat Erosion/Siltation Flood Pollution	Most beaches Gangneung, Uljin, Gori Gangneung, Imwon Lagoons and estuaries	Sea level rise Port/Seawall construction Earthquake/Storm Chemical/Heavy Industry	Wave/Current Wave/Current Surge(Tsunami) Drainage
West	Shoreline retreat Erosion/Siltation Flood Pollution	Most Beaches/Cliffs Buan, Gomso, Mokpo Younggwang, Mokpo Dyked rivers/Lakes	Sea level rise/Lithology Dyke construction Storm/Morphology(?) Dyke construction	Wave Wave/Tide Surge/Tide/Wave Drainage/Circulation
South	Flood	Changwon, Busan	Storm	Surge/Tide

Coastal erosion (or siltation) is common and became a chronic problem in recent years. The origin could be either natural or artificial and the east coast seems relatively more vulnerable to this issue than the other coasts. Despite the general status the surrounding areas of the Saemangeum and Youngsan dykes, because of their scale, have had great changes in hydrodynamic condition, which are being monitored for more than thirty years by the government and scientists.

As Korea is bordering a back-arc basin, deeply-rooted earthquakes occur frequently. According to numerical models (Ha et al., 2007; An et al., 2010) tsunamis could bring serious damage to the east coast of Korea especially when the epicenters are located in the northwestern offshore of Japan. The 1983 and 1993 tsunami records in Gangneung and Imwon clearly seem to reflect this possibility (Statistics Korea, 2013).

From late summer to autumn, two or three typhoons on average have a direct or indirect influence on the Korean coasts (mainly southern) every year. Combined with high tides, storm-driven surges and flooding occur in the coastal areas (Kang et al., 2011). Although these kinds of hazards are driven meteorologically, local geological and geomorphological features would become essential keys to reinforce their impact.

Pollution generally originates from modern industrialization of the country. Despite its

anthropogenic origin the behavior of pollutants will be closely related with the seafloor geology and the reservoir physiography. Combined with the fisheries and tourist industries this issue becomes one of the major items subject to strict hazard monitoring in certain areas.

3. Monitoring systems and adaptation activities

Several monitoring programs are under operation in Korea for the purpose of geohazard protection (or mitigation) and human adaptation. Precise shoreline measurement, earthquake monitoring, and periodic water quality assessment would be representative examples being operated nationwide in order to systematically monitor geological status and check their potential to become hazardous agents. Tsunami (or surge) early warning systems, seawall construction and coastal set-back could be nominated as typical adaptation examples.

In the central government the Ministry of Oceans and Fisheries (MOF) and the Ministry of Environment (ME) have main authorities to conduct programs or projects on coastal researches and monitoring works. Major operating agencies are Korea Institute of Ocean Science and Technology (KIOST), Korea Hydrography and Oceanography Administration (KHOA), Korea Meteorological Agency (KMA) and Korea Institute of Geoscience and Mineral Resources (KIGAM) (KHOA, 2013; KIGAM, 2013; MOF, 2013).

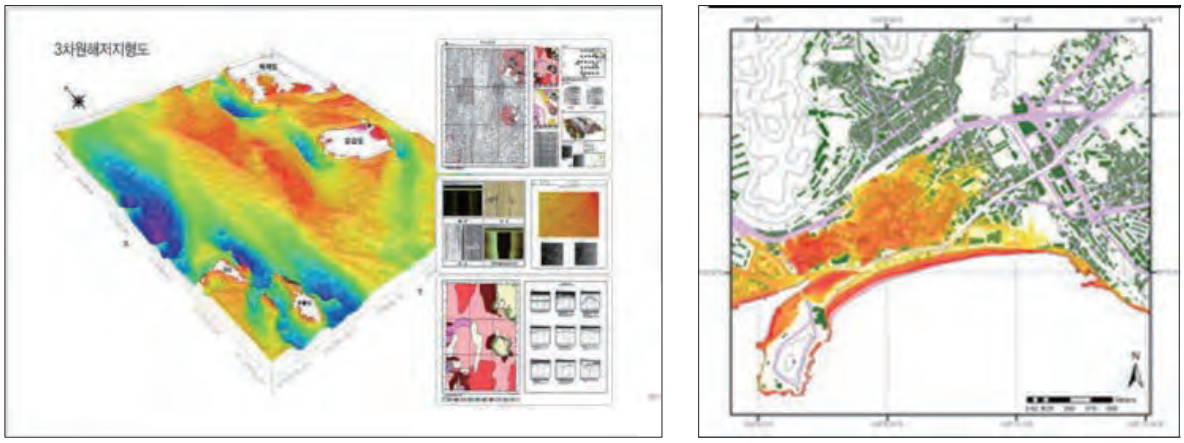

Fig. 5. Examples of a shoreline monitoring result conducted by a government agency (KHOA, 2013; left) and a forecast result of the flood-vulnerable zone in the east coast based on precise elevation measurement using LiDAR system (Han and Kim, 2011; right).

Owing to the recent development of information technology, most of the systems are operated in real-time so that the warning can be issued mush earlier (KIGAM, 2013). Increasing usage of mobile networks greatly helps to propagate warnings and alerts to the public living in the related areas (NDMI, 2013). Recently the integration of remote control and mobile network technologies allows the public to see video images of the major beaches in real-time through their mobile phones.

Fig. 6. The earthquake and earthquake-generated tsunami monitoring network in Korea which is jointly operated by KMA and KIGAM in Korea (KMA, 2013b). Both agencies are jointly monitoring natural or artificial movements of the earth crust, which are announced by KMA.

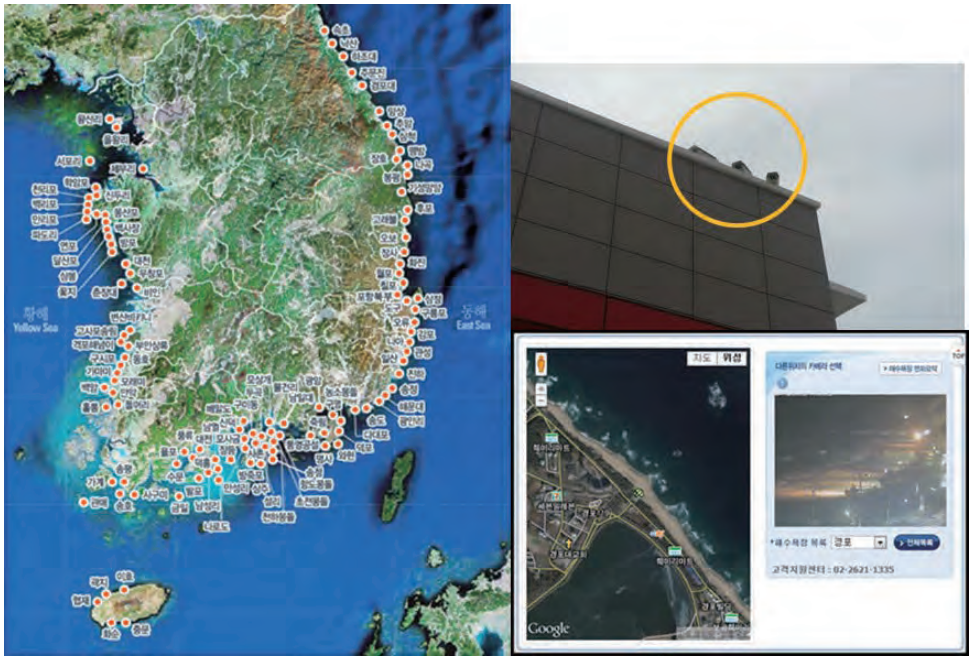

Fig. 7. Beaches being monitored in Korea (left) and the video camera (in the circle in upper right) and web service window (lower right). An example of the Gyeongpodae beach in Gangwon-do.

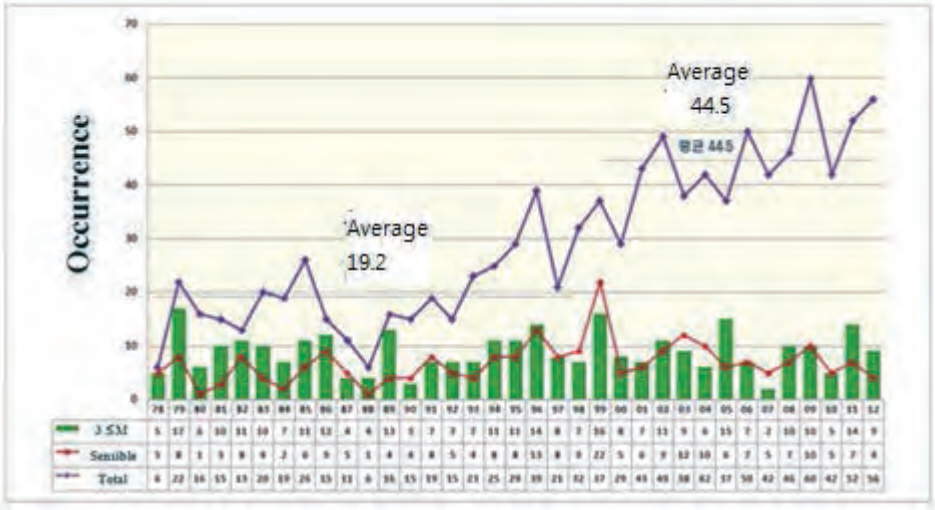

Fig. 8. Statistics on earthquake magnitude (green), sensible (red) and total occurrences (blue) in and around the Korean peninsula. Note the total number of occurrence is increasing (KMA, 2013b).

4. Conclusions

There are three different types of coasts in Korea: the uplifted gently curved east, the submerged irregular west, and the typical ria-type south. Based on the past records Korea seems to have relatively few catastrophic geohazards. However, some recent data (Fig. 8) and researches (e.g., Oh, 2007) imply that Korea could be confronted with those kinds of unexpected geohazards, especially with earthquakes and tsunamis.

Long-term gradual sea level rise induced by global warming is expected to aggravate negative influences of various hazardous situations. Shoreline retreat, hydrodynamic disequilibrium and storm-driven tsunamis would be notable examples. Multidisciplinary approaches together with precise monitoring will therefore become more important for coastal management.

Recently there seems to be a considerable change in the Korean government's policy on coastal zone management. The first period of integrated coastal zone management plans were completed. Conceptual migration seems to be made from simple to integrated management based on information technology, which again calls for systematic environmental monitoring.

References

An, S.-H., Ha, T., and Cho, Y. S., 2010, Generation of Tsunami Hazard Map, *Journal of Korean Society of Hazard Mitigation*, **10**(4), 127-133. (in Korean with English Abstract)

Ha, T.-M., Cho, Y.-S., Choi, M.-K., and Jeong, W.-C., 2007, Run-up heights of Tsunami along the eastern coast of the Korean Peninsula, *Journal of Coastal Research Special Issue*, **50**, 348-352.

Han, J.G. and Kim, S.-P., 2011, Inundation Vulnerability Zone Mapping of Urban Coastal Area using High Spatial Resolution Data (Airborne LiDAR) and GIS Spatial Analysis. Journal of Coastal Research, Spec. Issue, 64, 1681-1684.

Kang, J. W., Kim, Y. S., Cho, H. Y., Shim, J.-S., 2011, Characteristics of Nearshore Surge-Intensity, *Journal of Korean Coastal and Ocean Engineering Society*, **23**(6), 458-465. (in Korean)

KHOA, 2013, *http://www.coast.kr/CoastIn/BeachCamera.aspx* (October 20, 2013)

KIGAM, 2013, *http://www.kigam.re.kr/Contents/ContentsEngView.asp?strPageID=P258* (October 20, 2013).

KMA, 2013a, Climatological Normals of Korea (1981~2010), Korea Meteorological Administration, Publication Number 11-1360000-000077-14, 188p.

KMA, 2013b, *http://web.kma.go.kr/eng/weather/earthquake/intro.jsp* (accessed on October 20, 2013).
MOF, 2013, *http://www.coast.kr/portal/html/eng/about/cmis_01.asp* (accessed on October 20, 2013).
NDMI, 2013, *http://eng.ndmi.go.kr/depart/analysis/task/task.jsp* (accessed on October 20, 2013).
Oh, J. H., 2007, Prospect of Natural Disaster in Korea with Global Warming, *Journal of safety and crisis management*, **3**(2), 82-94. (in Korean)
Statistics Korea, 2013, *http://www.index.go.kr/egams/stts/jsp/potal/stts/PO_STTS_IdxMain.jsp?bbs=INDX_001&clas_div=C&idx_cd=1397&rootKey=1.48.0* (accessed on October 20, 2013).
UNESCO, 2013, Geohazards: mitigating the risks, *http://www.unesco.org/new/en/natural-sciences/environment/earth-sciences/international-geoscience-programme/igcp-projects/geohazards/* (accessed on October 19, 2013).

Asia-Pacific Region Global Earthquake and Volcanic Eruption Risk Management (G-EVER) activities

Shinji Takarada, Joel Bandibas, and G-EVER Promotion Team

Geological Survey of Japan, AIST, Japan
e-mail: s-takarada@aist.go.jp

Abstract

The First Workshop of Asia-Pacific Region Global Earthquake and Volcanic Eruption Risk Management (G-EVER1) was held in Tsukuba, Japan from February 22 to 24, 2012. The workshop focused on the formulation of strategies to reduce disaster risks caused by earthquakes, tsunamis and volcanic eruptions worldwide. The G-EVER1 accord was approved by the participants during the workshop and 10 recommendations were made that focus on: enhancing collaboration, sharing of resources, and making information about the risks of earthquakes and volcanic eruptions freely available and understandable. The G-EVER Consortium among the Asia-Pacific geohazard research institutes was established in 2012. Likewise, the G-EVER Promotion Team in GSJ was started in Nov. 2012. The G-EVER Hub website was setup to promote the exchange of information and knowledge about volcanic and seismic hazards among the Asia-Pacific countries. Establishing or endorsing data interchange and standards for analytical methods for geohazard institutes of the world are important in promoting data sharing and comparative analyses. Several G-EVER Working Groups and projects were proposed such as the Next-generation volcanic hazard assessment Working Group and the Asia-Pacific region earthquake and volcanic hazard mapping project. The assessment system as developed is based on volcanic eruption scenario datasets, volcanic eruption database, and numerical simulations. The next-generation real-time hazard assessment system has been implemented with a user-friendly interface, making the risk assessment system easily usable and accessible online. The Asia-Pacific region earthquake and volcanic hazard mapping project aims to make a sophisticated online information system that provides past and recent earthquake and volcanic hazards information, risk assessment tools for earthquake and volcanic eruption hazards and links to global earthquake and volcanic eruption databases. The hazard mapping project plans to create the system with the cooperation of Asia-Pacific countries.

Keywords: G-EVER, Asia-Pacific, earthquake, volcanic eruption, hazard, risk assessment

1. Introduction

The Asia-Pacific Region Global Earthquake and Volcanic Eruption Risk Management (G-EVER) Consortium formed amongst geohazard research institutes in the Asia-Pacific region was established in 2012. G-EVER aims to formulate strategies to reduce the risks caused by the occurrence of earthquakes, tsunamis and volcanic eruptions worldwide (Takarada, 2013a).

2. G-EVER Activities

The First Workshop on Asia-Pacific Region Global Earthquake and Volcanic Eruption Risk Management (G-EVER1) was held in Tsukuba, Japan from February 22 to 24, 2012 (Fig. 1). During the workshop, the G-EVER1 accord was approved by the participants and consisted of 10 recommendations as follows:

1. Establish a consortium of Asia-Pacific geohazard research institutes, with the goal of enhancing collaboration, sharing resources, and making information about risk from earthquakes and volcanic eruptions freely available and understandable.
2. Promote the use of hazard information in decision-making by citizens, governments, and businesses, so that our science supports mitigation actions.
3. Develop a website hub for the consortium in English and major Asian languages, which would link to websites of allied global efforts, such as VHub, GEM Nexus, and the International Seismological Centre (ISC).
4. Establish or endorse data interchange standards and standardized analytical methods for geohazard institutes of the world to promote data sharing and comparative analyses.
5. Actively participate in related global risk reduction efforts, such as the Integrated Research on Disaster Risk (IRDR) Program, Global Earthquake Model (GEM), Global Volcanic Model (GVM) and their component databases like World Organization of Volcano Observatories Database (WOVOdat) and GEM Faulted Earth.
6. Promote "the borderless world of science" with trans-border hazard maps built using common data sets, together with more uniform and advanced methods and software than has been possible in the past.
7. Promote exchange visits among researchers of the consortium, and encourage opportunities for graduate study in geohazards.
8. Encourage the formation of working groups for broad, multi-disciplinary, and unifying themes.
9. Promote best practice training on interaction with the media, outreach to citizens and school children on hazard preparedness, and interaction between volcanologists and Volcanic Ash Advisory Centres in the region.
10. Convene a G-EVER workshop every 2 years in Asia-Pacific countries in conjunction with major regional events (such as AOGS, WPGM and AGU meetings).

Fig. 1. The First Workshop of Asia-Pacific Region Global Earthquake and Volcanic Eruption Risk Management (G-EVER1) at AIST, Tsukuba, February 22-24, 2012.

The G-EVER Promotion Team of GSJ was formed in November 2012. The G-EVER Hub website (Fig. 2; http://g-ever.org) was setup to promote the exchange of information and knowledge about volcanic and seismic hazards among the Asia-Pacific countries. Establishing

or endorsing standards on data sharing and analytical methods is important when promoting data and analyses results sharing. The major activities of G-EVER include participation in global risk reduction efforts such as the Integrated Research on Disaster Risk (IRDR) Program, Global Earthquake Model (GEM) and Global Volcanic Model (GVM).

Fig. 2. G-EVER Hub site (http://g-ever.org)

A G-EVER international conference is planned to be held every 2 years in the Asia-Pacific region. On the other hand, a one to two days G-EVER international symposium will be held annually. The 1st G-EVER International Symposium was held in Tsukuba, Japan on March 11, 2013. The 2nd G-EVER Symposium and IUGS&SCJ International Workshop was held in Sendai, Tohoku Japan on October 19-20, 2013.

Several G-EVER Working Groups (WG) and projects were proposed such as: (1) Risk mitigation of large-scale earthquakes WG, (2) Risk mitigation of large-scale volcanic eruptions WG, (3) Next-generation volcanic hazard assessment WG, and (4) Asia-Pacific region earthquake and volcanic hazard mapping project.

3. Next-generation volcanic hazard assessment system

The next-generation volcano hazard assessment WG is developing a useful system for volcanic eruption prediction, risk assessment, and evacuation strategy at various eruption stages. The assessment system is based on volcanic eruption history datasets, volcanic eruption database and numerical simulations (Fig. 3; Takarada, 2013b). Volcanic eruption histories including precursor phenomena leading to major eruptions are important in predicting future volcanic eruptions. A high quality volcanic eruption database, which contains compilations of eruption dates, volumes, and styles, is important for the next-generation volcano hazard assessment system. Formulating international standards on how to estimate the volume of volcanic materials is important in order to make a high quality volcanic eruption database. GIS based spatial distribution database of volcanic materials (e.g. Tephra and pyroclastic flow distributions) is important for accurate area and volume estimations and risk assessment.

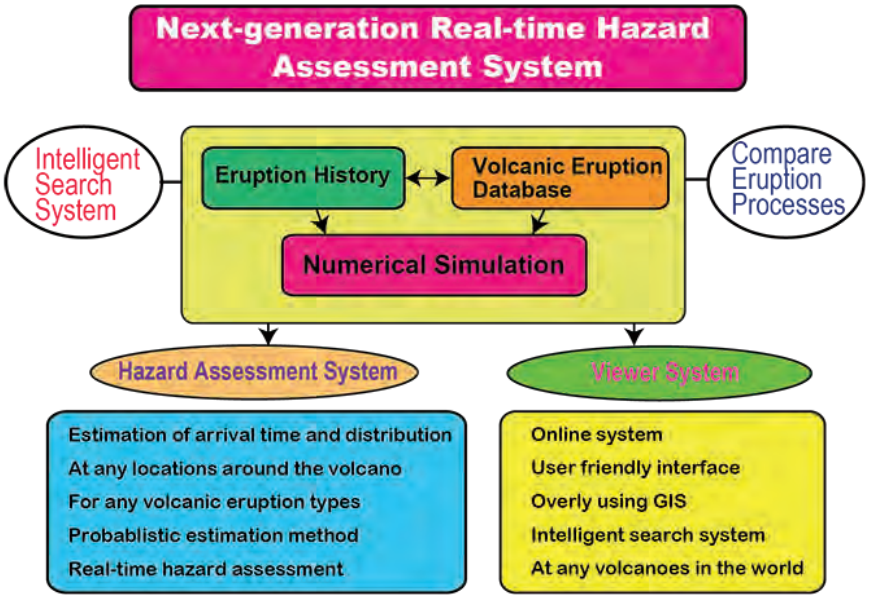

Fig. 3. Conceptual diagram of the next-generation real-time volcanic hazard assessment system

The volcanic eruption database is developed as based on past eruption results, which only represent a subset of possible future scenarios. Therefore, numerical simulations with controlled parameters are needed for more precise volcanic eruption predictions. The "best-fit" parameters of the past major eruptions in the world have to be estimated and the simulation results database should then be made.

The use of the next-generation system should enable the visualization of past volcanic eruptions datasets such as distributions, eruption volumes and eruption rates, on maps and diagrams using timeline and GIS software. Similar volcanic eruptions types should be easily identifiable from the eruption database. Using the volcano hazard assessment system, prediction of the time and the area that would be affected by volcanic eruptions at any location near the volcano should be possible using numerical simulations. The system could then be used to estimate volcanic hazard risks by overlaying the distributions of volcanic deposits on major roads, houses and evacuation areas using a GIS enabled systems. The next-generation real-time hazard assessment system will be implemented with a user-friendly interface, making the risk assessment system readily usable and accessible online.

A preliminary version of the next-generation volcanic hazard assessment system, that can run energy cone simulations at any volcano in the world, using ASTER Global DEM, and the links to major volcanic databases, such as Smithsonian, VOGRIPA and Quaternary volcanoes, was made available since June 2013 (Figs. 4 and 5). A previous GEO Grid volcanic gravity simulation system covers only 14 major volcanoes in the world. On the other hand, almost all volcanoes in the world can be evaluated using this volcanic hazard assessment system. Currently, the system covers more than 3200 Quaternary volcanoes worldwide. Links to major volcanic databases in the world are useful in order to examine eruption history in detail. Using Google and Bing maps as base maps provides more information for hazard evaluations.

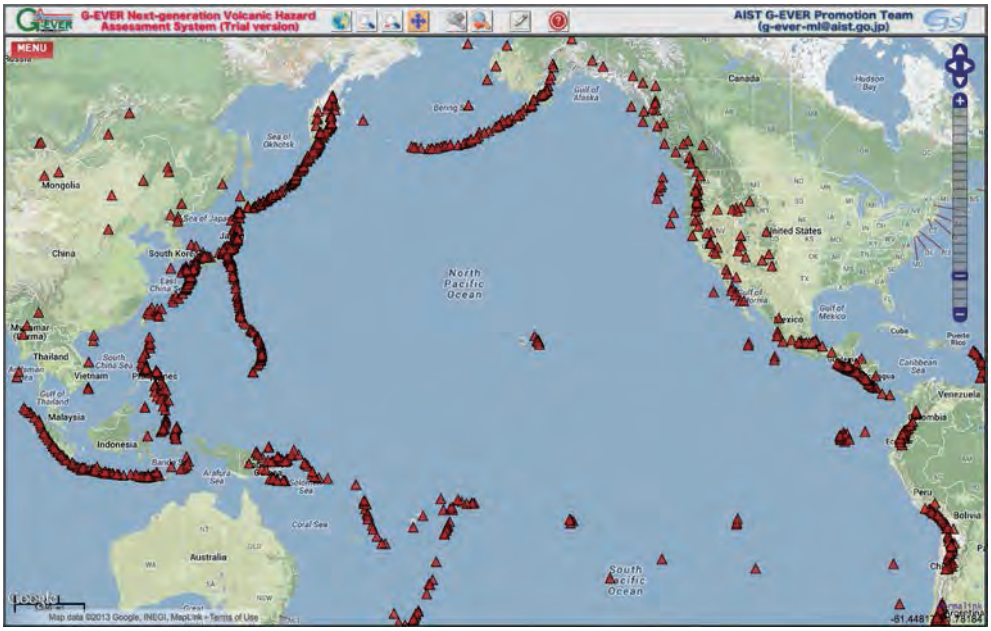

Fig. 4. G-EVER next-generation volcanic hazard assessment system (trial version). http://volcano.g-ever1.org/vhazard/HazardAssessment/

4. Asia-Pacific region earthquake and volcanic hazard mapping project

The Asia-Pacific region earthquake and volcanic hazard mapping project aims to make an advanced online information system that provides past and recent earthquake and volcanic eruption information (e.g. age, location, scale, affected areas and fatalities) and risk assessment tools for earthquake and volcanic eruption hazards. A printed map version will also be published as the new version of the Eastern Asia Geological Hazard Map of the Commission for the Geological Map of the World (CGMW). The online hazard mapping system provides useful information about earthquake and volcanic hazards in an interactive and user-friendly interface (Fig. 6). Past and recent large-scale earthquakes (>M6) and volcanic eruptions (>VEI 5), tsunami inundation areas, distribution of active faults, and major landslides will be shown on the map. Links to major earthquakes and volcanic eruptions databases will be available in the system. The earthquake and volcanic eruption hazard mapping project will be implemented with the cooperation of major research institutes and organizations in the Asia-Pacific region such as PHIVOLCS, CVGHM, GNS Science, EOS, USGS and CCOP.

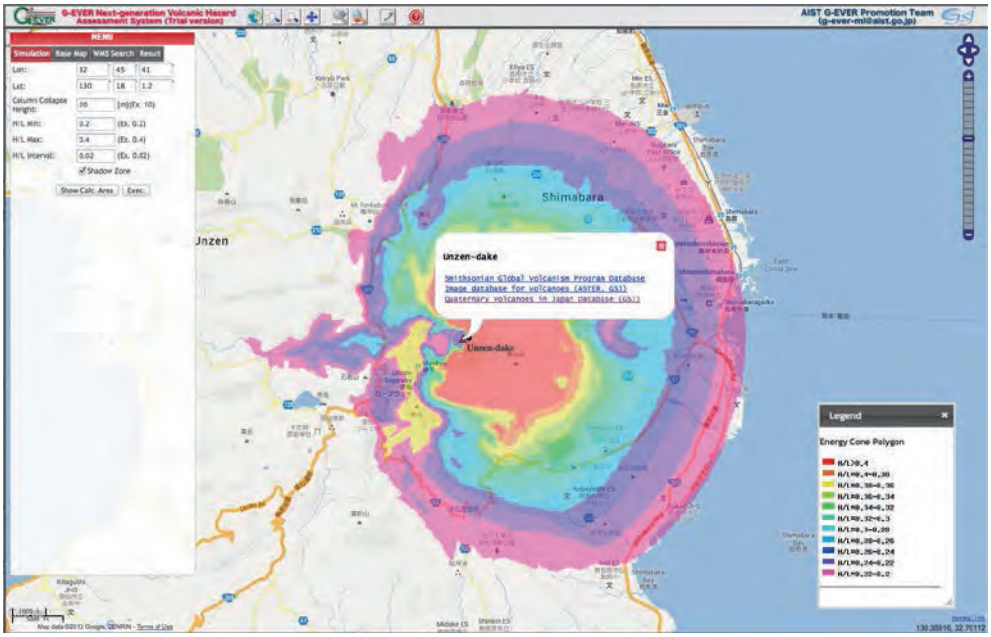

Fig. 5. An energy-cone simulation result at Unzen Volcano, western Japan, using G-EVER next-generation volcanic hazard assessment system. Almost all volcanoes in the world can be evaluated with this system because of the wide coverage of ASTER Global DEM.

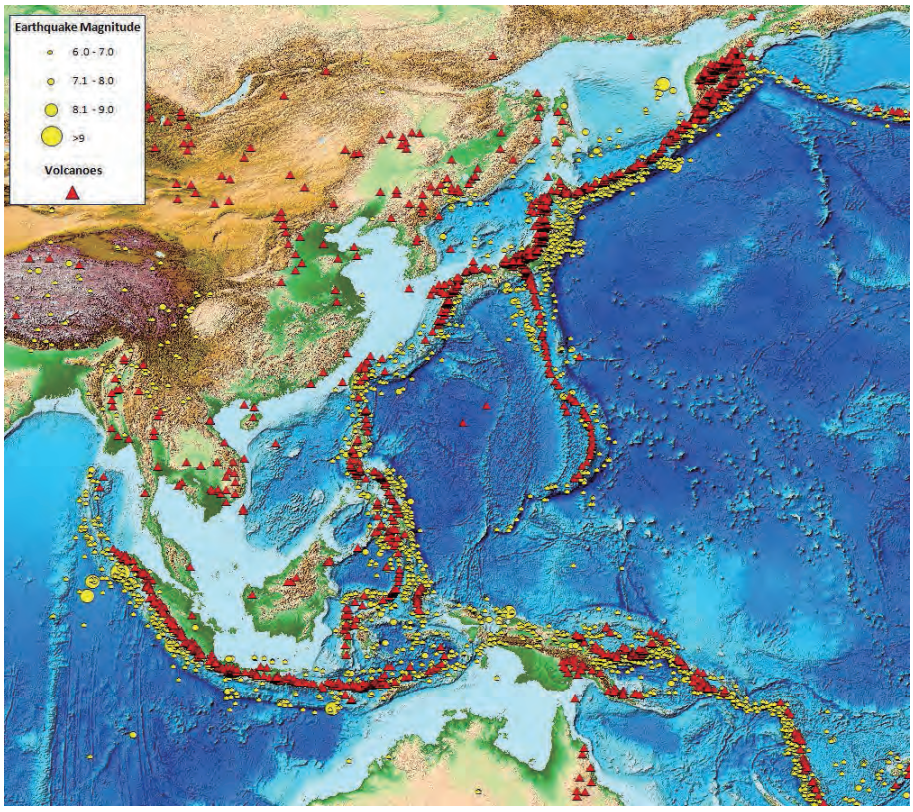

Fig. 6. Preliminary version of Asia-Pacific region earthquake and volcanic hazard assessment system. Distribution of epicenters of large-scale earthquakes (M>6) since 1971 (USGS) and Quaternary volcanoes (Smithsonian, VOGRIPA and Japanese Quaternary volcanoes databases) are shown. Etopo1 (NOAA) is used as a topographic map. Detailed information is available on clicking on each volcano or earthquake epicenter.

References

Takarada, S., 2013a, Asia-Pacific Region Global Earthquake and Volcanic Eruption Risk Management (G-EVER) Consortium: the new hazard mitigation activities, *IAVCEI 2013 abstract*, Kagoshima, 4A1_4H-O4.

Takarada, S., 2013b, The next-generation real-time volcanic hazard assessment system in G-EVER, *IAVCEI 2013 abstract*, Kagoshima, 4P1_4D-O21.

Tsunami risk assessment of Padang City, West Sumatra

Agus Solihin, Cipta Muhamad Firmansyah, and Imam Santosa

Center for Volcanology and Geological Hazard Mitigation, Geological Agency,
Ministry of Energy and Mineral Resources, Indonesia
Jl. Diponegoro No. 57, Bandung 40122

Abstract

Tectonic earthquakes along subduction zones and the presence of active faults in West Sumatra may have the potential to trigger tsunamis which can result in tremendous waves inundating the marine shoreline. An earthquake derived from a reverse fault and of magnitude greater than 7 on the Richter scale has the potential to be tsunamigenic. Seismic data indicate that the west coast of the island of Sumatra, including the capital city of Padang, is an area with frequent earthquakes. For example, a huge earthquake that occurred in October 2009 resulted in more than 1,000 casualties (Dian Oktiari et al., 2010). The city of Padang, especially its southern part, has a long coastal border and is a marine tourism area with many hotels, lodgings and attractive places of entertainment for residents living in the vicinity.

The goal of tsunami risk assessment is to provide information on regions that have high levels of tsunami risk to the surrounding environment such as man, residential areas, infrastructure, property and others. Tsunami risk assessment is the examination of the risk posed to people and the natural or built environment as a result of a damaging tsunami occurrence. Humans have a long and often tragic history of building large civilizations in close proximity to the coast. As long as people continue to settle in the coast, we should continue to develop technological tools to aid us in understanding the tsunami risks we face and advance our ability to mitigate them.

Risk assessment is based on the threat posed by a hazard, vulnerability and capacity elements. The formula for calculating the risk assessment is: $\text{Risk of Disaster (R)} = \frac{\text{Hazard (H)} \times \text{Vunerability (V)}}{\text{Capacity (C)}}$. This research method uses both quantitative and qualitative research techniques. A hundred and fifty people representative respondents of different backgrounds, sexes, education, occupations and locations were interviewed and asked for vulnerability analysis.

Fatalities can be reduced if, associated with a well monitoring system, including early warning and land use planning, a culture of prevention is socialized within all levels of the society and also the preservation of local wisdom. The result of tsunami risk assessment indicates that sub-districts of Bugis, Teluk Kabung and North Padang are in a high risk zone, whereas the eastern part of Air Pacah and West Padang sub-districts are in very low risk zone.

Keywords: Tsunami, earthquake, risk, mitigation

1. Introduction

Padang city is located on the West Coast of Sumatra, directly adjacent to the Indian Ocean and close to the zone of active collision of two tectonic plates, making Padang city potentially vulnerable to earthquakes and a resulting tsunami hazard. Generally, faulting along subduction zones indicates reversed faulting and if a resulting earthquake has a magnitude equal to or greater than 7 on the Richter scale, it has the potential to generate tsunami waves.

Padang city, especially in the south, has a long coastal border and as a marine tourist area visited by many tourists, has many hotels, lodging houses and entertainment facilities which

are attractive to residents living in the vicinity. Seismic data show that the west of the island of Sumatra, including the city of Padang, is an area with frequent earthquakes with a wide spread of epicenters.

Tsunami may be very destructive and cause many losses. The Nias tsunami of March 28, 2005, that hit the area of Singkil, Meulaboh and Sibolga, resulted in more than 620 fatalities and more than 2,030 people injured. The geographic location of the study (Fig. 1) is administratively included in the region of Padang, West Sumatra (Supartoyo et al., 2006).

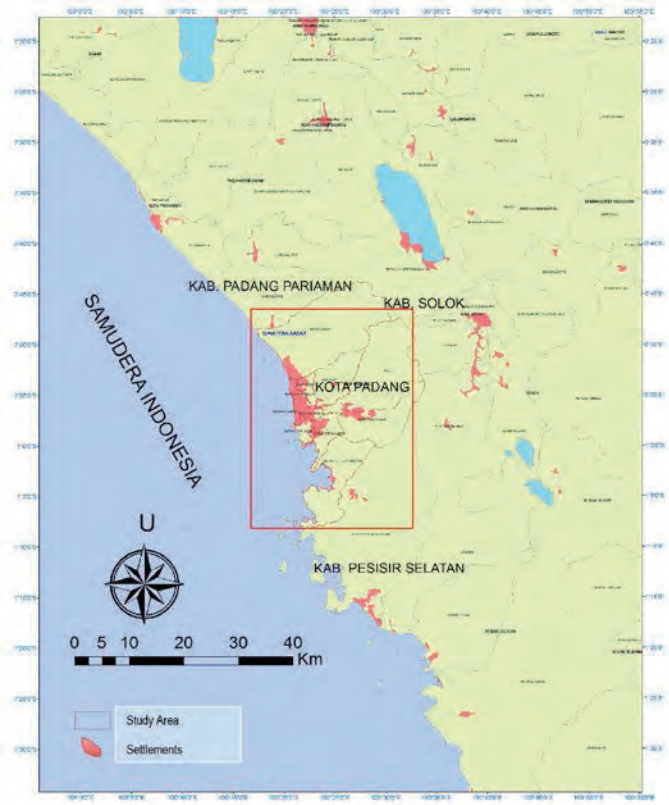

Fig. 1. Location of study area at Padang City, West Sumatra Province.

2. Overview

2.1 Earthquake and tsunami

Geographic conditions of Padang, a coastal city flanked by two large rivers, show a high level of vulnerability to tsunami waves. Seismic data shows that the area along the west coast of Sumatra Island, including the city of Padang, has frequent earthquakes (Fig. 2). Plate movement on the fault along the southwestern Sumatra coast to Java can be fairly significant.

Based on the tsunami hazard map of Padang (Yudichara et al., 2008) the study area is divided into three tsunami prone regions: high tsunami disaster prone areas, medium tsunami disaster prone areas, and low tsunami disaster prone area. Each of these disaster-prone areas has its own characteristics.

An event can be classified as a disaster if it resulted in at least one of the following three events:

- Loss of human life,
- Damage to property and the environment, or
- Loss of human life and property and environmental damage.

So it can be concluded that, if there is one incident which did not result in any of the three items above, the incident cannot be categorized as a disaster, but we categorize the incident as a hazard.

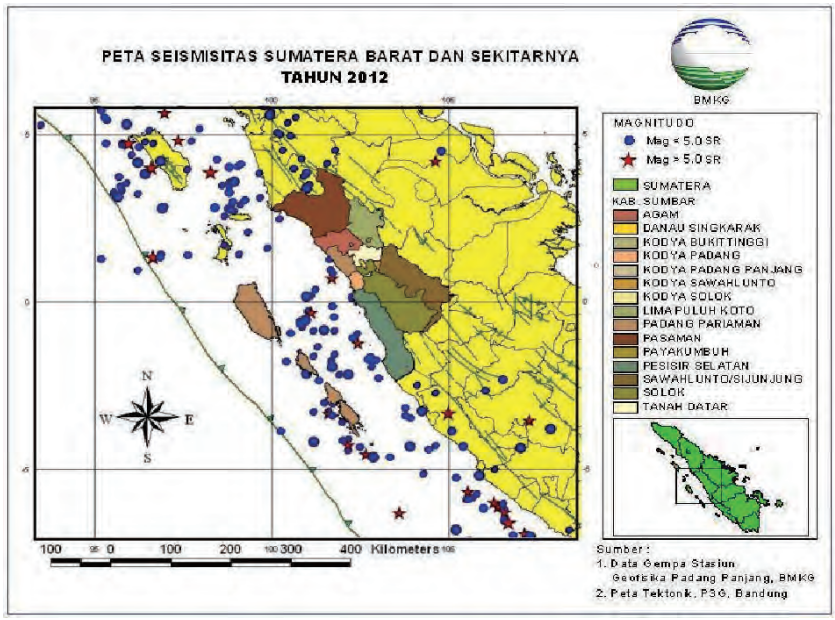

Fig. 2. Seismicity map of West Sumatra.

Fig. 3. Tsunami vulnerability zone map of Padang.

2.2 Analysis of Disaster Risk

From the translation of the above definition of a disaster, we can construct the following formula:

$$\text{Risk of Disaster (R)} = \frac{\text{Hazard (H)} \times \text{Vunerability (V)}}{\text{Capacity (C)}} \quad (1)$$

Analysis of Disaster Risk is strongly influenced by the nature of the hazard, vulnerability and capacity. Hazard (H) is an event that has the potential to either cause damage to, or loss of human life, or environmental damage. Vulnerability (V) is conditions or characteristics of the biological, geographical, social, economic, political, cultural and technological society in a region for a certain period of time which reduces the ability of the community to prevent, mitigate, and prepare to manage the impacts of a hazard. Capacity (C) is resource mastery and ability of the community to maintain and prepare, prevent, overcome, mitigate and to recover from a disaster.

3. Results of tsunami risk analysis

As seen above, risk is the potential loss caused by the threat of a hazard (tsunami) or disaster and can be mitigated by the ability of the public to cope the hazard or disaster.

In Equation (1), Hazard (H) will take account of the nature of the area as follows:

- High risk zone
- Medium risk zone
- Low risk zone
- Very low risk zone

Vulnerability (V) will be affected by:

- Population density
- Infrastructure
- Land use

And, Capacity (C) will vary with:

- Quality of buildings
- Local knowledge of disaster
- Existing Institutions
- Infrastructure

Determining the value of risk, as shown in Equation (1), is the combination of three elements (hazard, vulnerability and capacity), each of which has a weight value totaling 100 and the distribution of the weighted value of each element is given in Table 1.

Hazard Element (H)

Based on the Tsunami hazard map of Padang (Yudichara et al., 2008), the study area is divided into three types of tsunami prone areas, namely: high, medium and low tsunami disaster prone areas (Table 2, Fig. 4). Each of these disaster-prone areas has its own characteristics.

Vulnerability Element (V)

The parameters included in the Vulnerability Element (V) divided into three levels are shown in Table 3.

Table 1. The weight value distribution of each element in making the tsunami risk map.

ELEMENT OF HAZARD					
No	**Subelement Type**	**Indicator**	**Relative Weight Value**	**Sub element (%)**	**Element (%)**
H1	Tsunami Hazard	High	100	100	100
H2		Medium	60		
H3		Low	30		
ELEMENT OF VULNERABILITY					
V1	Population density (people/ha)	High (>60 people/ha)	60	60	100
V2		Medium (15-60 people/ha)	30		
V3		Low (<15 people/ha)	10		
V4	Facilities / Infrastructure	Vital Strategic Building (Chemical industry, Nuclear, Power, Oil & Gas, Airports, Ports, Terminals, Government Buildings, Installation of Water, telecommunications networks, hospitals, apartments)	15	30	
V5		General Building (Markets, Malls, Amusement Places, Travel Places, Plant, hotels, Schools, harbour)	10		
V6		Highways / railroads / Bridge	5		
V7	Landuse	Settlements	5	10	
V8		Paddy field	2		
V9		Garden/field	2		
V10		Forest	1		
ELEMENT OF CAPASITY					
C1	Preparedness	High	40	40	100
C2		Medium	25		
C3		Low	5		
C4	Early Warning System	Well Function	20	20	
C5		Poorly	10		
C6		None	1		
C7	Institutional	Well Function	20	20	
C8		Poorly	10		
C9		None	1		
C10	Mitigation Infrastructure	Adequate	20	20	
C11		Insufficient	10		
C12		None	1		

Table 2. The weight value of Hazard Element

Hazard Element (H)	Weight value
High Tsunami Prone Areas	100
Medium Tsunami Prone Areas	60
Low Tsunami Prone Areas	30

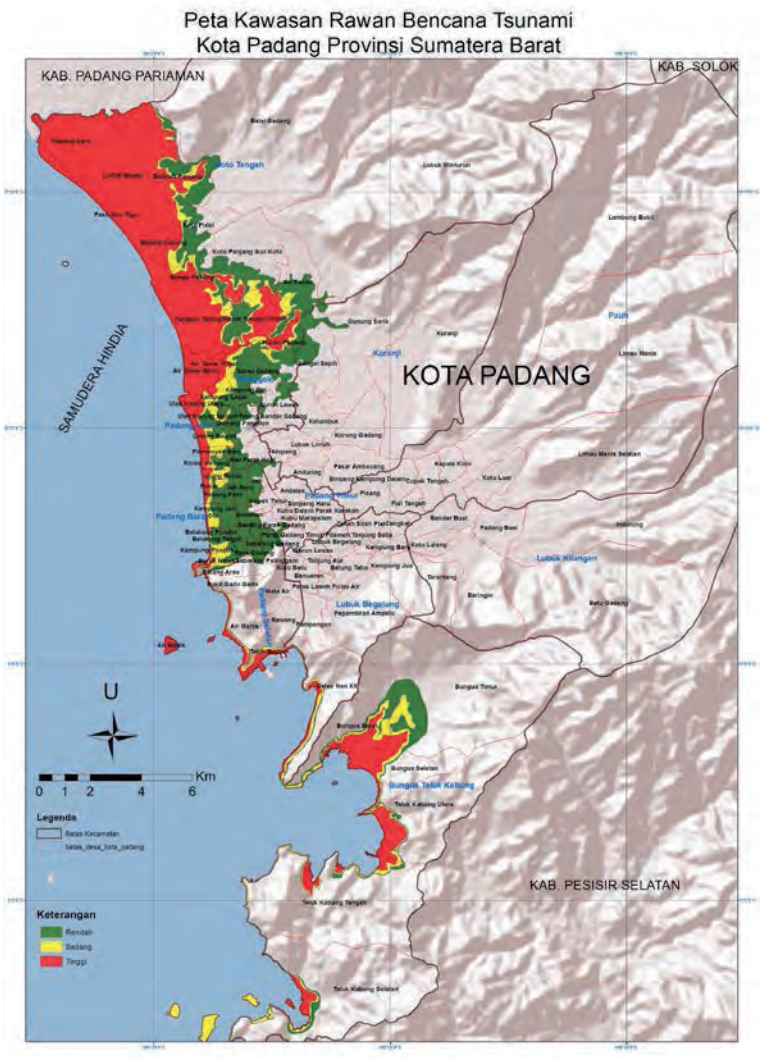

Fig. 4. Map of tsunami prone areas of this study.

Table 3. Parameter and weight value of Vulnerability Element

ELEMENT OF VULNERABILITY					
V1	Population density (people/ha) (souce : BPS)	High (>60 people/ha)	60	60	100
V2		Medium (15-60 people/ha)	30		
V3		Low (<15 people/ha)	10		
V4	Facilities / Infrastructure	Vital Strategic Building (Chemical industry, Nuclear, Power, Oil & Gas, Airports, Ports, Terminals, Government Buildings, Installation of Water, telecommunications networks, hospitals, apartments)	15	30	
V5		General Building (Markets, Malls, Amusement Places, Travel Places, Plant, hotels, Schools, harbour)	10		
V6		Highways / railroads / Bridge	5		
V7	Landuse	Settlements	5	10	
V8		Paddy field	2		
V9		Garden/field	2		
V10		Vital Strategic Building (Chemical industry, Nuclear, Power, Oil & Gas, Airports, Ports, Terminals, Government Buildings, Installation of Water, telecommunications networks, hospitals, apartments)	1		

Population Density

Population density is the number people per unit of territory. To calculate the population density, total population can be divided by population area. Based on data from the Padang City Central Bureau of Statistics (2010), the population density of each district is determined and classified as shown below:

$$\text{Population Density} = \frac{\text{Population}}{\text{Area}} \quad (2)$$

High : >60 people/ hectare
Moderate : 15 – 60 people/ hectare
Low : <15 people/ hectare

Infrastructure

Based on data from the Padang Central Bureau of Statistics and field observations, the following is the calculation of the weight value of each parameter of infrastructure.

Padang infrastructure data can be seen in Fig. 5, where the mass concentration of activity in coastal areas. There are government buildings, social and economic activities in the area.

Critical object is a very important object such as public facilities which serve the people, the power supply company (PLN, hydropower, power plant), drinking water company (PDAM), and banks. In the event of a disaster, the vital objects must survive.

Land Use

Land usage includes residential, mixed plantations, rice fields, marshes, beaches and attractions. Additionally electric utilities, telephone and water supply exist in the district.

Settlements spread out almost evenly distributed, generally elongated parallel to the road along the coast. Around the coast there are many tourist attractions, restaurants and hotels. In addition there are places such as harbor fishing boats and fish markets.

Each land-use parameter then aggregated to obtain a total weight value of each land-use parameters.

The results of all parameters are displayed in the form of maps, namely map of population density, map of land use, and map of infrastructure. Then all of the maps are overlaid to be a map of vulnerability (Fig. 5).

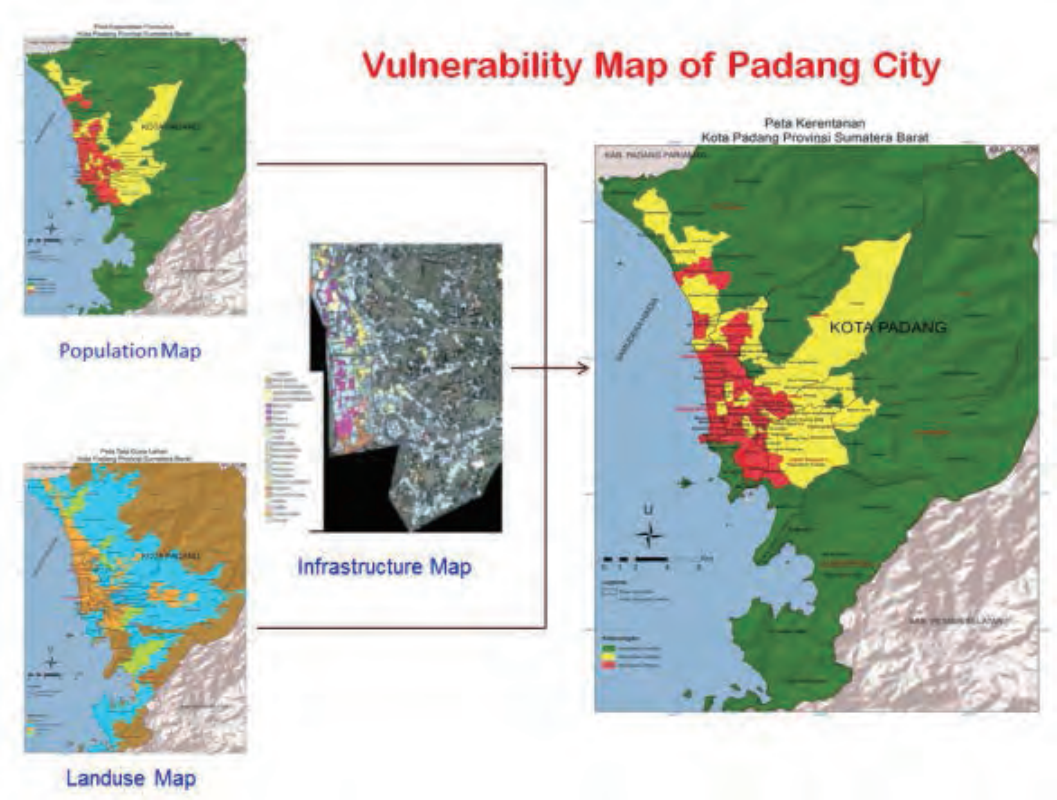

Fig. 5. Vulnerability map of Padang City resulted by overlaying a map of population density, land use and infrastructure.

Capacity Element (C)

Capacity is resource mastery, and the strength of the ways that allows a community to maintain and prepare, prevent, tacke, mitigate and recover quickly from the disaster. The parameters included in the Element Capacity (C) are divided into four (Table 4).

Capacity assessment was done by distributing a questionnaire form to the public and institutions in each area. From the results obtained from the questionnaires, a Weight Value calculation of each element of capacity (C) for each was obtained and displayed in the form of a capacity Map (Fig. 6).

Table 4. Parameter values and weights of the Capacity Element.

ELEMENT CAPASITY					
C1	Preparedness	High	40	40	100
C2		Medium	25		
C3		Low	5		
C4	Early Warning System	Well Function	20	20	
C5		Poorly	10		
C6		None	1		
C7	Institutional	Well Function	20	20	
C8		Poorly	10		
C9		None	1		
C10	Mitigation Infrastructure	Adequate	20	20	
C11		Insufficient	10		
C12		None	1		

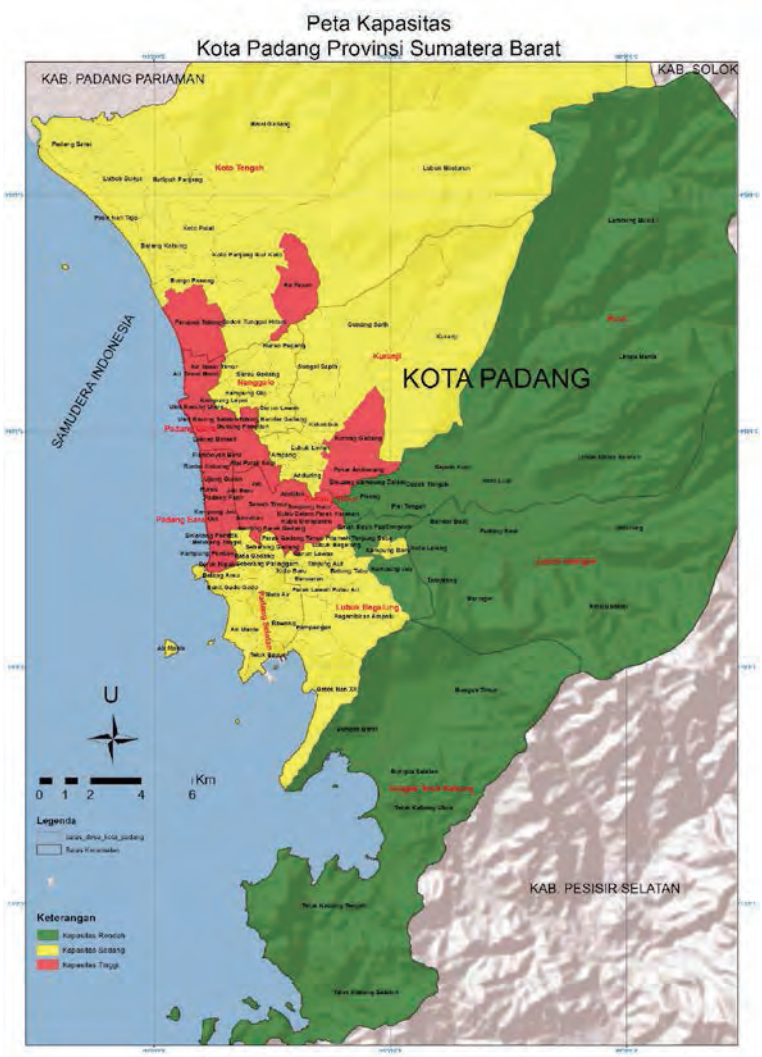

Fig. 6. Map of Capacity Element of Padang City.

Result of Risk Analysis

From the result of weighting of all elements (element of hazard, vulnerability and capacity), the value of risk for each sub-district can be calculated by using Equation (1) and we can obtain a Tsunami Risk Map (Fig. 7).

Padang City is divided into four risk zones, as follows:

1. High risk zone
   Zones where the tsunami wave can result in the destruction of wooden buildings, brick buildings, concrete buildings and coastal forests.
2. Medium risk zone
   Zones where Tsunami waves can cause damage to only partly to buildings of wood.
3. Low risk zone
   Zones where tsunami waves do not cause damage to buildings, leaving only a thin trace of fine sand sediments.
4. Very low risk zone
   Zones not directly affected by the tsunami.

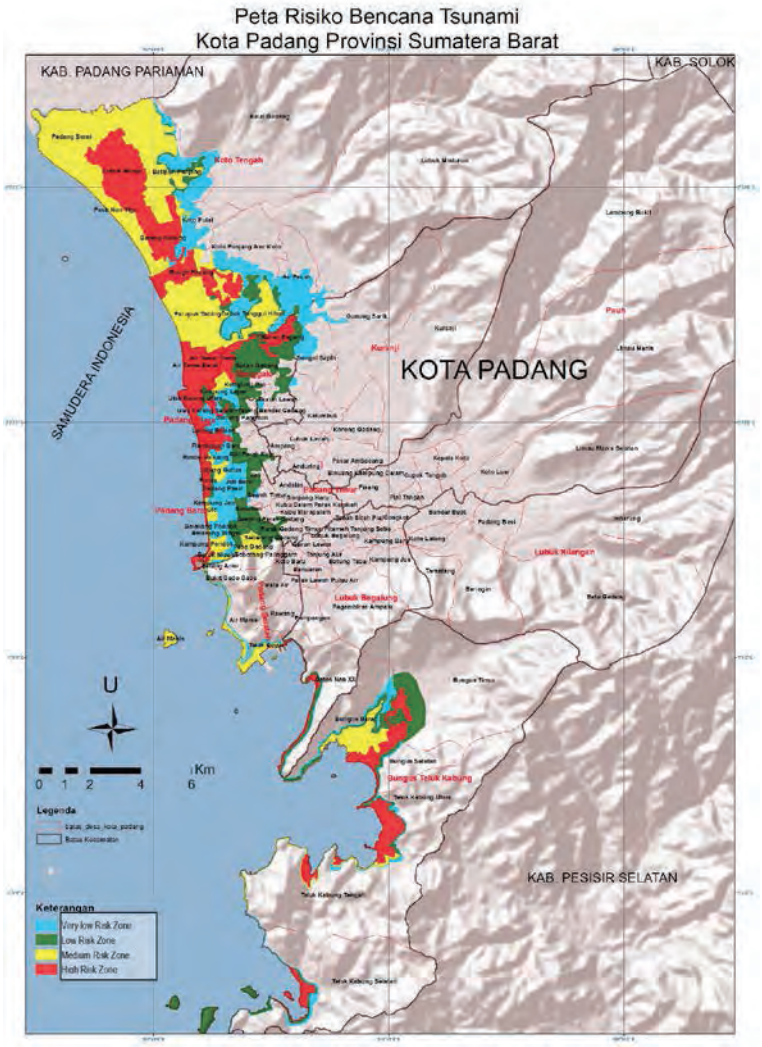

Fig. 7. Tsunami risk map of Padang City.

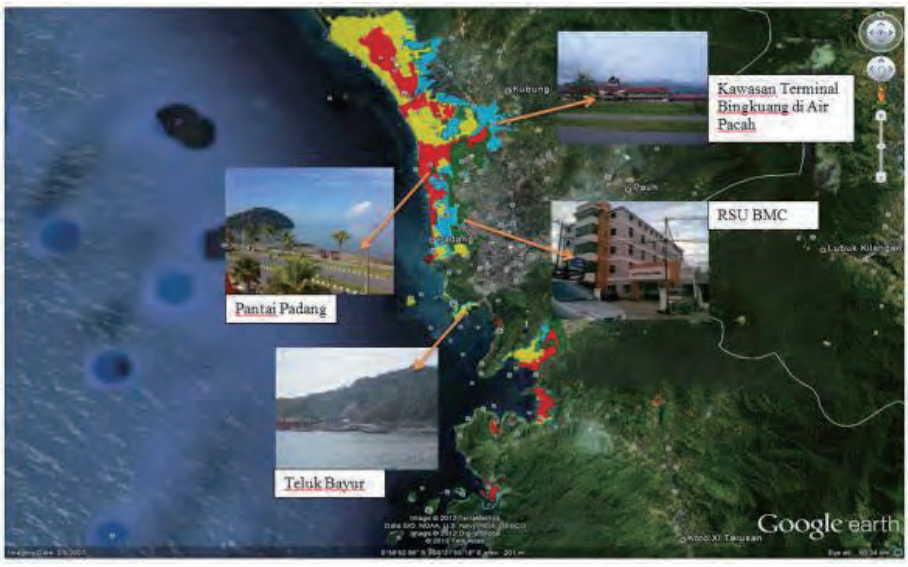

Fig. 8. Risk map overlaid on a satellite image (GoogleEarth^{TM}).

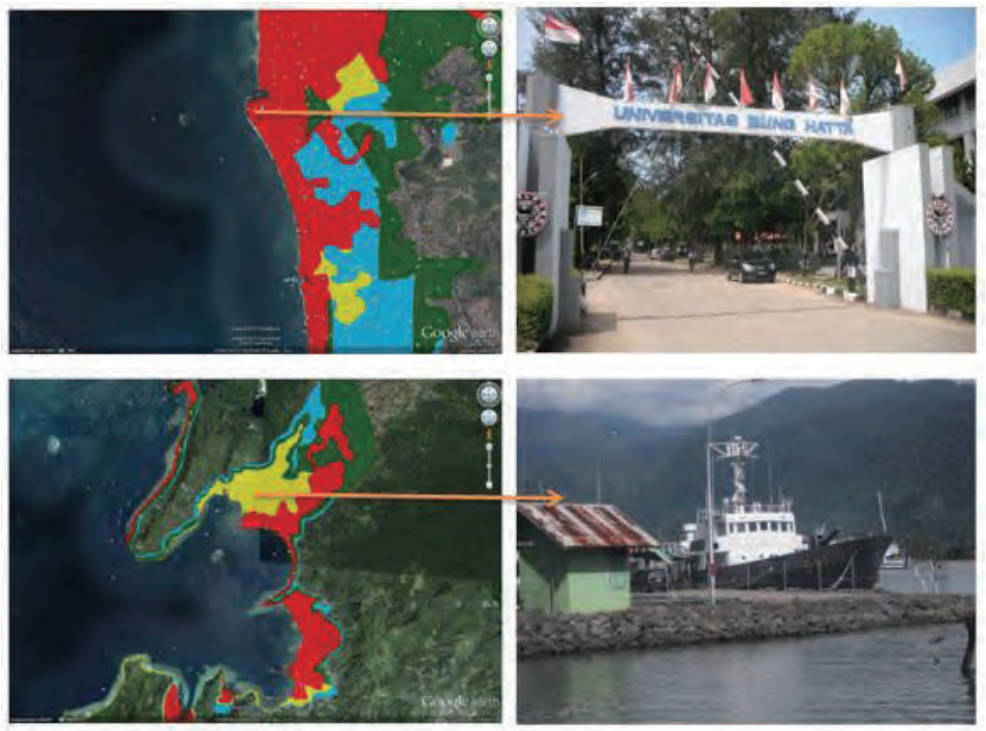

Fig. 9. Risk map overlaid on a satellite image (GoogleEarth™), Bung Hatta University (top) and Teluk Bayur harbour (bottom) that are in the high risk zone.

4. Conclusions and recommendations

Tsunami risk in the city of Padang, as in most areas of the villages in the Bungus Teluk Kabung sub-district, will be high if the Capacity Element (C) in the the area is at low level. This shows that increasing the level of capacity to be larger relative to the hazard (H) and vulnerability elements (V) is an important factor to reduce the risk of earthquake disaster. The level of tsunami hazard factors in a region cannot be reduced, therefore the level of vulnerability factors must be reduced and the level of capacity factors should be improved.

Dissemination of information and tsunami disaster knowledge should be actively spread (socialized) within all levels of the community and local government in the Tsunami Prone Regions in order to increase the capacity of the community.

References

Padang City Central Bureau of Statistics, 2010, Kota Padang Dalam Angka 2010.

Supartoyo, Putranto E.T., and Surono, 2006, *Destructive Earthquake Catalog In Indonesia 1629-2006 (Third Edition)*, Center for Volcanology and Geological Hazard Mitigation.

Yudichara et al., 2008, *Tsunami hazard map of Padang City*, Center for Volcanology and Geological Hazard Mitigation.

Dian Oktiari et al., 2010, *Model of The Geospatial Potential Tsunami Vulnerability of Padang City*, Journal of Meteorology and Geophysics, Vol. II, No. 2, (p. 136 – 141), BMKG.

Earthquake hazard map of Papua, Indonesia

Sri Hidayati[1], Athanasius Cipta[1,2], Amalfi Omang[1], Rahayu Robiana[1], and Jonathan Griffin[3]

[1]Geological Agency of Indonesia
[2]Australian National University
[3]Geosicence Australia

Abstract

Indonesia occupies an area of pronounced tectonic activity where three of the world's major tectonic plates are in collision rendering it a country very prone to earthquakes. The northern part of Papua Island, for example, has experienced destructive earthquakes in the past with several destructive earthquakes occurring in the region during the last decade including the Nabire earthquake in 2004 and Serui earthquake in 2010 which resulted in casualties and damage to buildings and other parts of the local infrastructure. This is an area likely to be vulnerable in the future therefore the availability of an earthquake hazard map of Papua is required so that the earthquake mitigation efforts receive more emphasis prior to any future disaster.

An appropriate hazard map has been created using the PSHA (*Probability Seismic Hazard Assessment*) method and developed using an EQRM (*Earthquake Risk Model*) computer program. This method requires inputs of earthquake sources (active faults, subduction zones and diffuse earthquakes), site classes, return period and GMPE (*Ground Motion Prediction Equation*) for each earthquake zone. For the Papua hazard map, the earthquake source is classified into 19 zones for both active faults and subduction, and 9 zones for diffuse earthquakes.

The result is a PSHA map for 0.2 second spectral acceleration. The map represents the 10% probability of exceedance in 50 years (475 years return period). The Papua seismic hazard map is based on the estimated intensity, which was obtained by converting the acceleration level on 0.2 second RSA (*Response Spectral Acceleration*). The hazard levels are divided into four classifications, they are very low (MMI < V), low (VII > MMI ≥ V), moderate (VIII > MMI ≥ VII), and high (MMI ≥ VIII), respectively.

Keywords: Papua, PSHA, seismic hazard map

1. Introduction

Indonesia is located in a tectonically active area at the point convergence of three major plates (Pacific, Eurasia and Australia) creating a complex network of plate boundaries (Bird, 2003). This situation (Fig. 1) makes Indonesia an area of pronounced tectonic activity that is prone to earthquakes. Papua is one of the areas which have experienced many earthquakes since it is located at northern limit of the Australian Plate. Tectonic activity in this region cannot be separated from the formation of Melanesia Orogenesis (Simanjuntak, 2004), which produced oblique subduction, reactivation of the Sorong Fault, active faulting in land, formation of troughs in northern Papua and formation of a 6000 m high mountains range.

The collision of these plates forms a trough, with depths ranging from 4500-7000 meters, known as a subduction. This is where most of Papua's earthquakes originated. Some earthquakes generated tsunamis, as occurred in Biak in 1996. Faults formed by the Melanesia orogenesis generally trend in west - east, northwest - southeast, north - south and southwest -

northeast directions. The destructive earthquakes that have occurred in Papua were mostly caused by active inland faults, such as the Sorong Fault, Ransiki Fault, Tarera-Aiduna Fault, Asmat Fault, and Jayawijaya Mountains range fault.

Based on previous experience such as Nabire earthquake in 2004 and Serui earthquake in 2010, most of the casualties and losses due to earthquakes are caused by collapsed and damaged infrastructure. The damage to structures due to earthquakes can be minimised by anticipating seismic loads from ground shaking in the design stage. Consequently, in designing earthquake resistant structures, determination of ground motion parameters is very important. The availability of an earthquake hazard map of Papua is therefore needed in order to emphasise earthquake mitigation efforts prior to any future disaster. This paper will discuss the development of such an earthquake hazard map of Papua using the PSHA method.

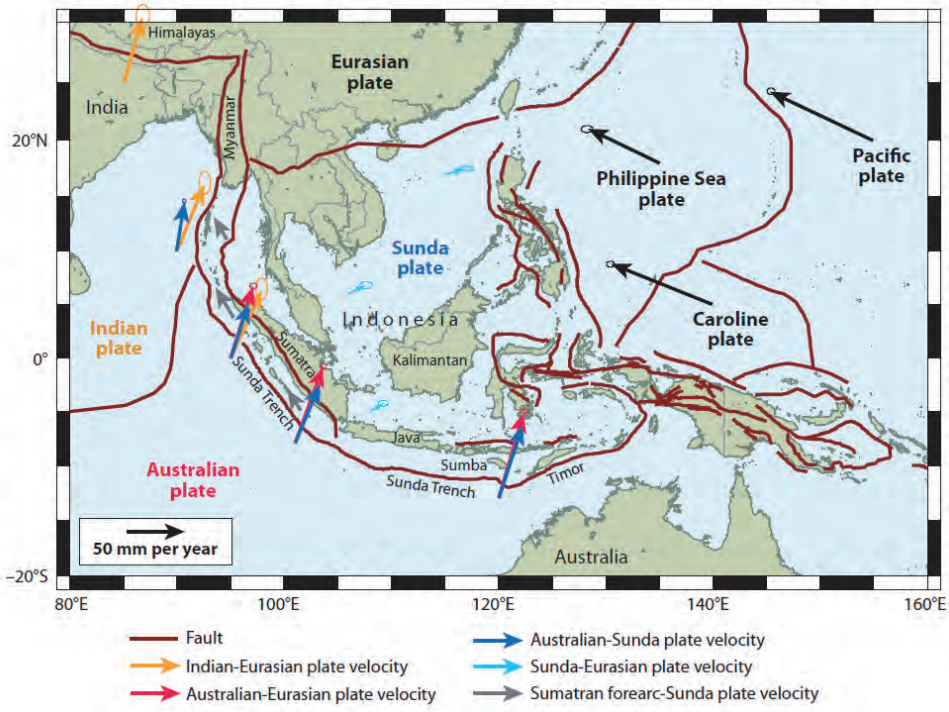

Fig. 1. Tectonic setting of Indonesia which located at the point convergence of four major plates (Indian, Australian, Eurasia, and Pacific plate, and three minor plates (Sunda, Caroline, and Philippine Sea plates) (McCaffrey, 2009).

2. Methods

Seismic hazard analyses involve the quantitative estimation of ground-shaking hazards at a particular site. Seismic hazards may be analyzed deterministically, as when a particular earthquake scenario is assumed, or probabilistically, in which many possible earthquakes of various magnitudes, locations, and probabilities of occurrence are explicitly considered (Kramer, 1996).

The Probabilistic Seismic Hazard Analysis (PSHA) used in this study can be described as a procedure of four steps (Reiter, 1990), as illustrated in Fig. 2 (Kramer, 1996).

1) Identification and characterisation of earthquake sources.

2) A recurrence relationship, which specifies the average rate at which an earthquake of some magnitude will be exceeded, is used to characterize the seismicity (or activity) of

each source zone.

3) The ground motion produced by any given earthquake must be determined with the use of predictive relationships.

4) The uncertainties in earthquake location, earthquake size, and ground motion parameter prediction are combined to obtain the probability that the ground motion parameter will be exceeded during a particular time period.

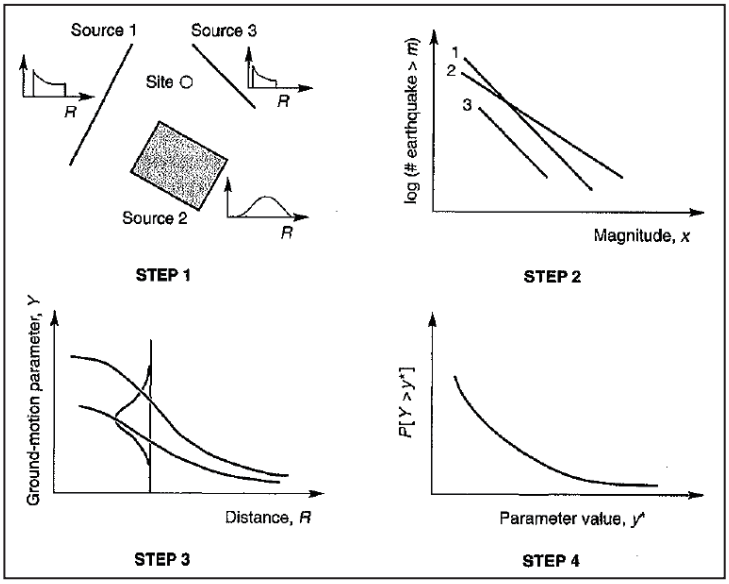

Fig. 2. Four steps of a probabilistic seismic hazard analysis (Kramer, 1996).

As for the source model input to PSHA, seismo-tectonics, active fault maps, and earthquake catalogue of Papua are required. Earthquake recurrence relationship requires earthquake catalogue and active fault slip rates. Ground motion prediction equations (GMPEs) and site amplification maps are required for estimation of attenuation relationship. The ground motion parameters can be represented by: 1) peak ground acceleration (PGA), 2) response spectra, and 3) acceleration time histories (Irsyam et al., 2010). Ground motion is represented by site amplification. Site amplification is often classified in terms of shear-wave velocity in the top most 30m (Vs_{30}), according to the US National Earthquake Hazard Reduction Program (NEHRP) system. Meanwhile, seismic hazard calculation requires PSHA software, and in this case we use EQRM (Earthquake Risk Model).

3. Analysis

3.1 Site amplification input

The Vs_{30} is estimated based on consideration of geomorphology, slope and distance from Tertiary or pre-Tertiary mountains (Matsuoka et al., 2006). The classification of geomorphology and coefficients for this method are shown in Table 1. Geomorphological and geological maps were used along with SRTM topography data to classify Papua's geomorphology using Matsuoka's scheme (Fig. 3) and then calculate Vs_{30}.

Table 1. Geomorphology classification

SLOPE(deg)	**ELEV** (m)	**LITHOLOGY**	**GEOMORPHIC UNIT** (Matsuoka et al., 2006)	**NOTES**
>15	>700	Tertiary rock	Tertiary mountain	
		Pre-Tertiary rock	Pre-Tertiary mountain	
	<700	Pre-Quaternary and Quaternary soft to hard rock	Hill	
		pyroclastic flow deposits	Volcanic hill	
5-15		Colluvium, talus, debris deposits	Mountain footslope	
		Quaternary volcanic rocks and deposits	Volcanic footslope	Located around skirt of volcano
plain to very steep		Moderately dense – dense gravel in mountain. Loose sandy soil – very soft cohesive soil in plain	Valley bottom lowland	long and narrow lowland formed between river to extremely steep slopes of mountain, hill, volcano or terrace.
		Coarse sediment materials	Alluvial fan	Semicone-like form, formed at boundary between mountains and lowland
		Very soft cohesive soil, contain peat or humus	Back marsh	Swampy Formed behind natural levees, surrounded by hill, mountain or terrace
		Very loose sandy soil Occasionally covered with soft cohesive soil	Abandoned river channel	Swampy Depression Elongate shape
		Fluvial sandy soil (delta) Submarine deposits (coastal lowland)	Delta and coastal lowland	Delta: flat lowland, formed at the river mouth Coastal lowland: flat lowland form along shoreline
> 5		dense sand and gravel, occasionally boulder	Marine sand and gravel bars	Form along shoreline
Volcano		Quaternary volcanic rocks and deposits	Volcano	
		Hard to soft rock	Rocky strath terrace	Flat surface, step-like shape
		Sand gravelly oil	Gravelly terrace	Flat surface, step-like shape
		Stiff volcanic ash	Terrace covered by volcanic ash soil	Flat surface, step-like shape
5-15		Aeolian sand	Sand dune	Wavy topography Form along shoreline
		Loose sand overlying very soft cohesive soil.	Reclaimed land	Former bottom flat of sea, lake, lagoon
		Very loose to loose sandy soil	Filled land	Former water body
		Loose sandy soil	Natural levee	natural barrier parallel to river/coast, sand bar, flood plain

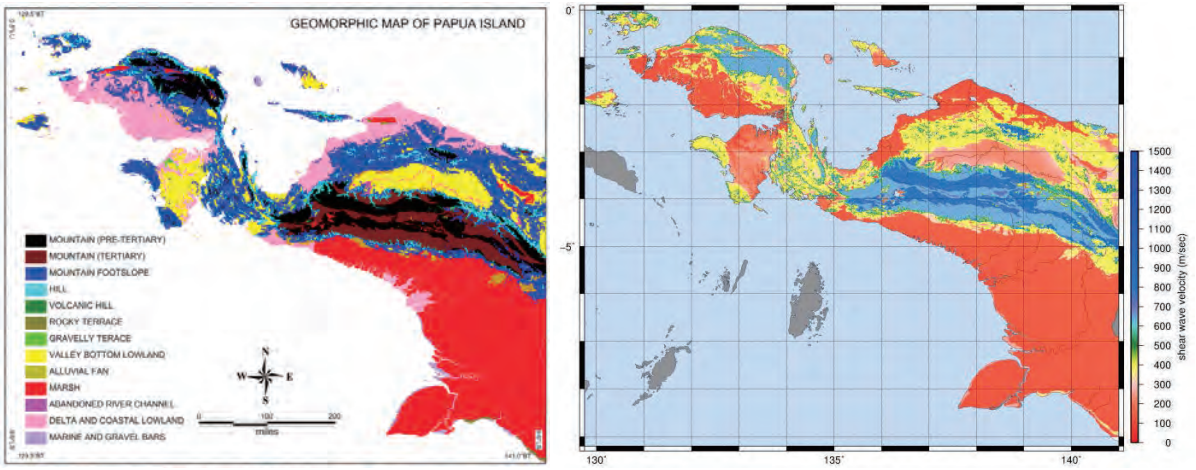

Fig. 3. Geomorphology of Papua using Matsuoka's (2006) classification (left) and Vs_{30} values for Papua derived from Matsuoka's (2006) method, higher Vs_{30} is indicated by blue band and lower Vs_{30} is indicated by red band (right).

Papua Island can be divided into 13 geomorphic units of which marsh comprises about 40% of the total area. This kind of geomorphic unit forms in basins with poor drainage and it can be assumed that such areas are composed of fine - very fine grained sediment including clay. Marsh is predominantly found in the southern part of Papua Island which borders the Central Mountains in the north. The delta and coastal lowland unit covers about 10% of Papua, spreads the north coast of Papua Province and south coast of Bird's Head, West Papua Province. Valley bottom lowland occupies about 8% of Papua, in the north of the Central Mountains. In all these three geomorphic units soft Quaternary sediments, which are highly vulnerable to shaking, predominate.

Pre-Tertiary and Tertiary mountains make up about 10% of Papua area, particularly in the Central Mountains and the north-eastern part of Bird's Head. These mountains separate marsh composed of soft sediments in the southern part of island from the northern part which is topographically wavy and composed by various type of geomorphic units (Fig. 3). Geomorphic units represent physical properties of rock and Vs_{30} can be estimated based on a geomorphic approach. There is some parallelism between the geomorphic map and the Vs_{30} map; the higher Vs_{30} is correlated with both Tertiary and pre-Tertiary mountains, medium Vs_{30} is correlated to footslope (mountain and volcanic) and hills while lower Vs_{30} is correlated to lowland areas (valley, delta and coastal).

3.2 Source input

Sources may be of three types:

- *Sources zones* are defined by a geographic polygon and a minimum and maximum depth; synthetic ruptures occur randomly within this zone with random selection of strike and dip within a range of values specified by the user.
- *Fault sources* are defined as rectangular planes defined by the up-dip surface projection of the fault trace. Ruptures occur randomly on the plane and strike and dip are controlled by the geometry of plane.
- *Intraslab sources* are defined using the same functionality as fault sources, except now the plane defines the geometry of the dipping slab and individual synthetic events are allowed to rupture at some angle out of the plane (out-of-dip rupture). This allows for

realistic simulation of the variety of earthquake focal mechanisms that occur within subducting slabs. Out-of-dip rupture can also be used to simulate uncertainty in the dip for fault sources.

Catalogue and background crustal source zones

The ISC catalogue was downloaded and declustered using the Seisan software package (Ottemöller, 2011). The catalogue was separated into shallow crustal (depth <= 35 km), intraslab (depth > 35 km) and megathrust events and was complete for events of magnitudes greater than 4.8 and 5.0 for shallow crustal and intraslab earthquakes respectively. Gutenberg-Richter *b* values were calculated for crustal and instraslab events and used for all crustal and intraslab source zones, respectively. Activity rates (λm_0) above a minimum magnitude of catalogue completeness m_0 were calculated based on the average annual number of events above m_0 within each source zone. Crustal earthquakes within 10 km of mapped active faults were assumed to occur on these faults, allowing for hypocentre location errors (Husen and Hardebeck, 2010), and therefore excluded from the background zone analysis.

To accommodate diffuse earthquakes, we also considered 9 source zones as follows:

- *Bird's Head* is a minor tectonic plate incorporating the Bird's Head Peninsula at the western end of the island of Papua. The plate is separating from the Australian Plate and the small Maoke Plate along a divergent boundary to the southeast. Convergent boundaries exist along the north between the Bird's Head and the Caroline Plate, the Philippine Sea Plate, and the Halmahera Plate to the northwest. A transform boundary exists between the Bird's Head and the Molucca Sea Collision Zone to the southwest. Another convergent boundary exists between the Bird's Head and the Banda Sea Plate to the south (Bird, 2003). The East Seram and West Seram Faults are the borders from Bird’s Head to the Banda Zone in the south. A relatively active and long strike-slip fault, named the Sorong Fault (East to West trend) crosses this zone. This zone is less active than neighboring zones such as Banda and Moluccas Sea, however, shallow earthquakes (depth < 35 km) have occurred more frequently than medium or deep earthquakes.
- *Maoke* is a small tectonic plate located in western New Guinea underlying the Sudirman Range from which the highest mountain on the island - Puncak Jaya rises. To its east is a convergent boundary with the Woodlark Plate. To the south lies a transform boundary with the Australian Plate and the Bird's Head Plate lies to the west (Bird, 2003).
- *Molucca Sea*. Seismicity within the Molucca Sea Zone is active to depths of approximately 260 km to the east and 400 km to the west. The tectonic setting of this region is unique in that it is the only global example of an active arc-arc collision consuming an oceanic basin via subduction in two directions (USGS, 2009).
- *Sunda* is the tectonic plate on which the majority of Southeast Asia is located.[1] It was formerly considered a part of the Eurasian Plate, but GPS measurements have confirmed its independent movement at 10 mm/yr eastward relative to Eurasia. The eastern, southern, and western boundaries of the Sunda Plate are tectonically complex and seismically active. Only the northern boundary is relatively quiescent (Socquet et al., 2006).
- *Timor* is a microplate in Southeast Asia carrying the island of Timor and surrounding islands. The Australian Plate is subducting under the southern edge of the plate, while a small divergent boundary is located on the eastern edge. Another convergent boundary exists with the Banda Sea Plate to the north, and to the west is a transform boundary.

(Bird, 2003).

- *Woodlark* is a small tectonic plate located in the eastern half of the island of New Guinea. The Caroline plate subducts along its northern border while the Maoke Plate converges on the west, the Australian plate converges on the south, and on the east an undefined compressive zone which may be a transform fault marks the boundary with the adjoining Solomon Sea Plate (Bird, 2003).
- *The Australia Zone*. The sources here are the least active among other sources considered in PSHA modeling of Papua. The Indo-Australian Plate is a major tectonic plate that includes the continent of Australia and extends northwest to the Indian subcontinent. The eastern part is moving northward at the rate of 5.6 cm per year while the western part is moving only at the rate of 3.7 cm per year due to impediment by the Himalayas. This differential movement is resulting in the compression of the plate near its center at Sumatra and a potential division into Indian and Australian Plates.
- *The Banda Arc* is a double island arc formed by the collision of the Australian continent with the Malay Archipelago. The northern margin of the Australian continent is presently colliding with the volcanic islands of the Banda Arc which stand on oceanic crust of the Banda Sea. Since at least 38 Ma ago oceanic lithosphere or highly attenuated continental lithosphere of the Australian plate subducted northwards beneath the Banda Sea at about 75 mm a~ with local or periodic incorporation of small terrains, continental crustal blocks or oceanic plateau, in the accretionary complex (Hamilton, 1979). The volcanoes of the Banda Arc between Flores and Damar have been inactive for the past 3 Ma. Damar volcano and the arc volcanoes to the east-northeast of the survey area remain active.
- *Gunung Api* is an unusual volcano because its edifice was constructed on the back-arc oceanic crust of the Banda Sea approximately 400 km above the Wadati-Benioff zone. It has been active in historic times, with Portuguese sailors reporting eruptions in 1800 (Snyder et al., 1996). It is clearly shown that the Banda Zone, both inner and outer, are the most active sources zone where earthquakes frequently happened down to 300 km depth (Fig. 4).

Fault sources

The initial reference fault model was that used for the 2009 revision of Indonesia's national seismic hazard map (Irsyam et al., 2010). However, several of the fault sources were modified to take into account new data regarding fault location, geometry and earthquake recurrence.

For PSHA modeling purposes, 1 subduction zone, slab source and 18 crustal faults have been defined. The *North Papua Subduction Zone* spreads south-eastward from north of Biak to North of Wewak in Papua New Guinea. The ~650 km long slab is visible to a depth of about 300 km and subducts with a dip angle that varies from ~30^{o} at 136^{o} E to ~10^{o} at 143^{o} E (Okal, 1999). The largest recorded earthquake on the NGT in the last century was the Mw = 8.2 Biak thrust event on 17 February, 1996, occurring on a section of the trench that had had a marked absence of recorded seismicity. The combined slip caused by the 1996 Biak earthquake and the 1979 Mw =7.5 earthquake that occurred on the Yapen Fault amounted to 14 m in an azimuth of 253^{o}, nearly parallel to the azimuth of convergence (248^{o}) of the two major plates (Henry and Das, 2002). Given that the total convergence rate is 111 mm/yr (DeMets et al., 1994), this represents 130 years of convergent motion, assuming that all the convergence is accommodated on only these two tectonic structures. Since this is not likely to be the case, the relative motion accommodated during these two events may represent the convergence of considerably more than 130 years (Tregoning and Gorbatov, 2004).

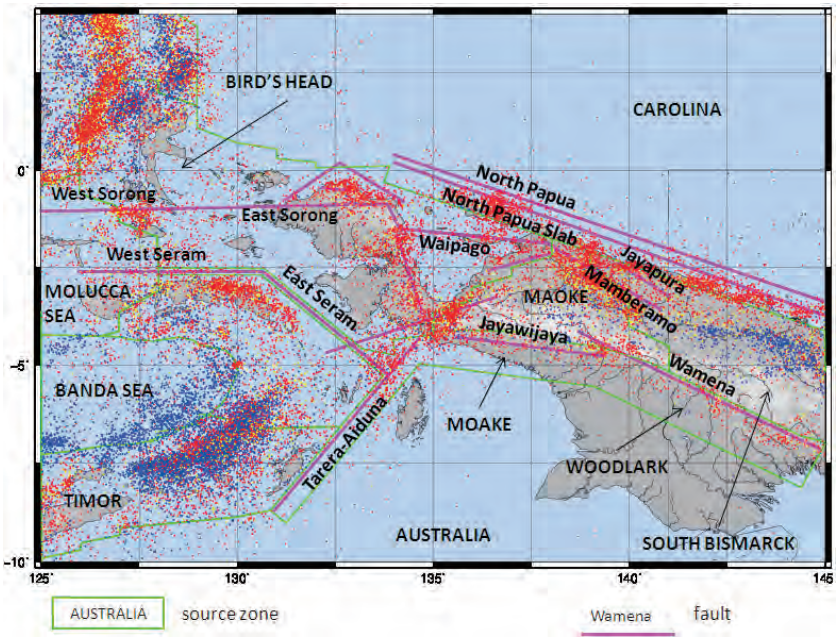

Fig. 4. Source zones, fault sources and intraslab source used in this PSHA modeling. The green polyline indicates source zone border, red line indicates fault (include subduction) and intraslab trace.

The Sorong fault offsets streams by only 300 m or so (Dow and Sukamto, 1984) and its eastern end is truncated by the NW-trending Ransiki fault. This part of the fault system is displaced 40 km to the north relative to the Yapen fault. Nevertheless, Dow and Sukamto (1984) suggest that there has been at least 370km of left-lateral slip on the Sorong-Yapen fault since the Middle Miocene. Hamilton (1979) suggested that the broad strand of the fault mapped by Visser and Hermes (1962) extending ENE from the town of Sorong is probably an old melange belt rather that a young shear zone (Puntodewo et al., 1994).

Earthquakes of M ≥ 7 in this century are located near the north coast of Bird's Head rather than near the mapped trace of the Sorong fault (Everingham, 1974). The mechanisms of these earthquakes are unknown and they may have occurred either on the Koor fault or at the Manokwari trough (Puntodewo et al., 1994).

The Yapen fault is active seismically, producing occasional large left-lateral strike-slip earthquakes (Fig. 3). The Yapen fault probably forms the strait between Biak and Yapen islands and may comprise more than one strand (Hamilton, 1979). To the east, the fault comes back onto land, but is not distinct and either merges with the Mamberambo thrust belt or extends out to the New Guinea trough (Puntodewo et al., 1994).

Tarera-Aiduna is visible as a linear feature on a radar image (Hamilton, 1979) and forms a topographically sharp southern boundary of Bird's Head. Its slip rate is estimated at 20 mm/yr (Puntodewo et al., 1994).

Manokwari and the New Guinea troughs are two linear but disconnected seafloor depressions running parallel to the north coast of Irian Jaya. The active Manokwari trough is dominated by strike-slip motion in its western part and compression in its eastern part. The western end of the Manokwari trough accommodates subduction of the Philippine Sea plate (Puntodewo et al., 1994).

Briefly, sources parameters are shown in Table 2.

Table 2. Sources parameters used in PSHA modeling of Papua.

No.	Name	Type		Mmax (Mw)	Slip-rate (mm)	Area (km^2)	a value	b value
1.	North Papua	interface	subduction	8.2	70.0	-	-	-
2.	East Sorong	strike slip	crustal	7.6	17.0	-	-	-
3.	West Sorong	strike slip	crustal	7.9	8.5	-	-	-
4.	Yapen	strike slip	crustal	7.7	4.6	-	-	-
5.	Tarera-Aiduna	strike slip	crustal	7.8	20.0	-	-	-
6.	Wamena	strike slip	crustal	6.6	5.1	-	-	-
7.	Mamberamo	thrust	crustal	7.9	2.2	-	-	-
8.	Jayawijaya	strike slip	crustal	7.5	10.0	-	-	-
9.	Waipago	thrust	crustal	6.5	5.0	-	-	-
10.	West Seram	interface	subduction	8.5	40.0	-	-	-
11.	East Seram	interface	subduction	8.5	40.0	-	-	-
12.	Jayapura	thrust	crustal	7.0	2.0	-	-	-
13.	East Manokwari	trough	crustal	8.0	6.0	-	-	-
14.	West Manokwari	trough	crustal	8.0	6.0	-	-	-
15.	Koor	trough	crustal	6.5	1.5	-	-	-
16.	Wandamen	strike slip	crustal	7.6	4.2	-	-	-
17.	Ransiki	strike slip	crustal	7.6	9.0	-	-	-
18.	Aru	trough	crustal	8.0	12.0	-	-	-
19.	North Papua	intraslab	crustal	7.2	-	-	-	-
20.	Bird's head	zone	crustal	7.6	-	476800	4.20	0.95
21.	Inner Banda	zone	crustal	7.5	-	149100	3.55	0.92
22.	Moake	zone	crustal	7.3	-	106300	3.34	0.94
23.	Moluccas Sea	zone	crustal	7.5	-	114200	5.66	1.02
24.	outer Banda	zone	crustal	7.5	-	180700	6.02	1.07
25.	Sunda	zone	crustal	7.5	-	160500	5.23	1.00
26.	Timor	zone	crustal	7.5	-	192700	5.62	1.03
27.	Woodlark	zone	crustal	7.5	-	159600	4.08	0.89
28.	Australia	zone	crustal	7.5	-	1924000	6.37	0.99

4. Results

Probabilistic seismic hazard results are shown for annual probabilities of exceedance of 0.01, 0.002 and 0.001 (equivalent to return periods of 100, 500 and 1000 years) produced for response spectral acceleration (RSA) of 0.2 and 1.0 s and peak ground acceleration (PGA). These are shown in Fig. 5. It is clearly shown that in shorter return periods (100 years), only areas close to an active fault has the probability to be struck by ground shaking with PGA of 0.6 g. Areas close to active faults are also possible to suffer from acceleration of 0.6 g, while on 2 s of RSA they are possible to suffer from acceleration of 1.0 g.

In longer return periods (500 and 1000 years), a fault zone area has the possibility to experience shaking with PGA reaching 1.0 g, moreover at 2 s of RSA this area is possible to suffer from ground shaking of 2.5 g or even more. However, the southern part of the island, which is located on the Australian Plate, is much safer than other parts of Papua. This area is possible to experience ground shaking with acceleration of 0.3 g - 0.5 g (500 years at 0.2

RSA) or 0.5 g - 0.7 g (1000 years at 0.2 RSA). This area spreads south of the Central Mountains, far away from seismic source. Even though the area is composed of soft sediment, the seismic waves from a seismic source in the north would attenuate before reaching this area (Fig. 5).

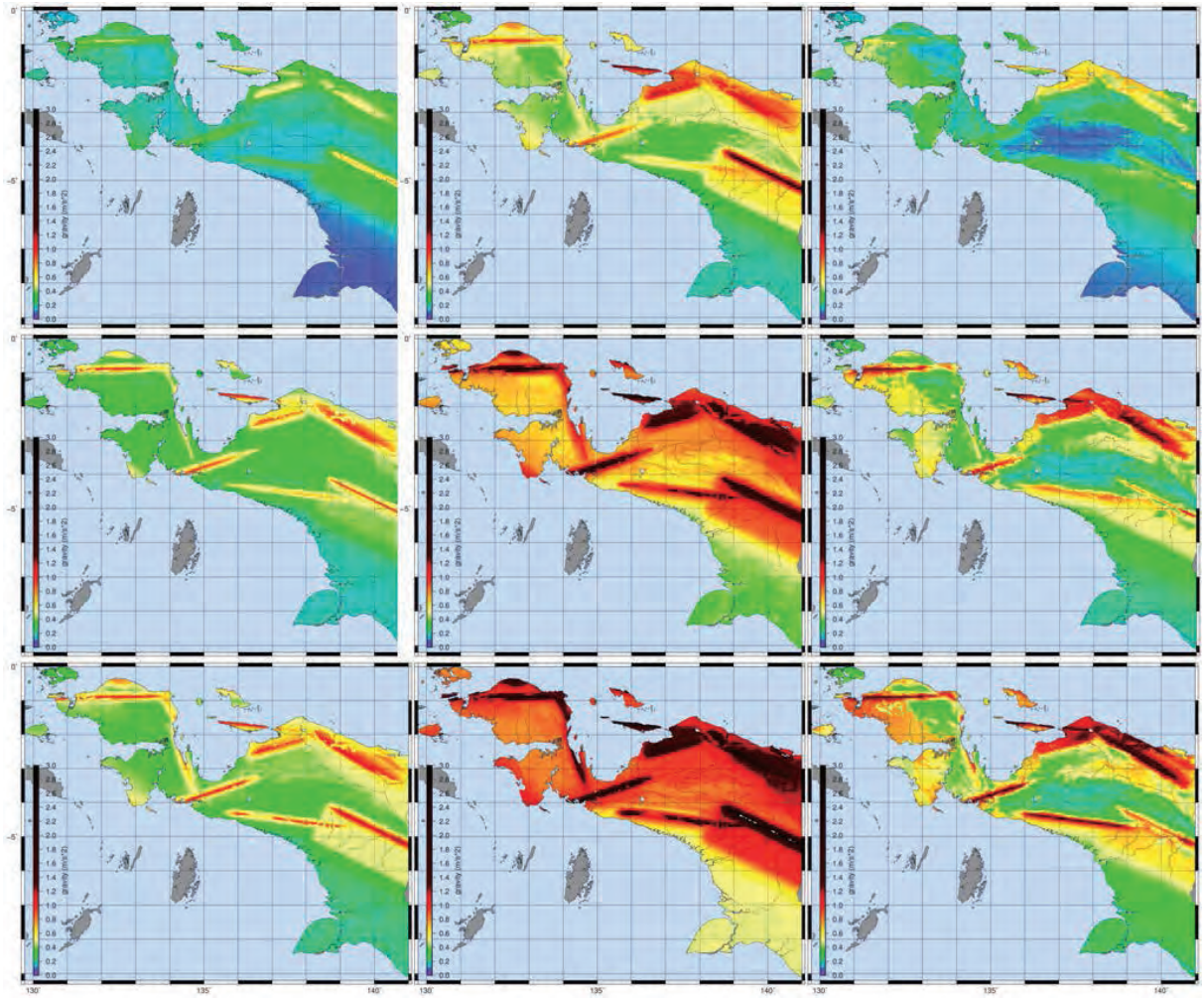

Fig. 5. Result of PSHA, first row shown ground acceleration for 100 years return period on 0.0, 0.2 and 1.0 s response spectra respectively, second row and third row shown ground acceleration for 500 and 1000 years return period.

The Pre-Tertiary and Tertiary mountains, in the central mountains, composed of hard rocks show that site class plays an important role in the level of hazard. The Central Mountains, the area sandwiched between the Mamberamo and Jayawijaya Faults in the south and the Jayapura and Mamberamo Faults in the north, experiences relatively low ground shaking. However on the opposite side, the valley in the north of the Central Mountains, the area that is also sandwiched by those for faults, experiences higher ground shaking (Fig. 5).

Acceleration results from modeling will be converted to MMI using formula introduced by Atkinson and Kaka (2007). The purpose of converting is to simplify the zonation and provide a simple map for the general public with regard to earthquake hazards (Fig. 6). The intensity map indicates that areas along north coast of Papua Province are classified as high earthquake intensity areas. The high earthquake intensity in this area in regard to site class and distance from earthquake zone. This area is the frontal area of a subduction zone and is composed of relatively soft sediment along the coast. Other high intensity areas are fault zone and areas

close to fault traces. In this case, site class is not the dominant factor for the level of hazard. The Central Mountains, in the north of the Jayawijaya and Wamena Faults, is classified as low intensity zone and the southeastern tip of Papua is also classified as low intensity zone. Hard rock is the main cause of the low hazard level in the Central Montains while in the southeastern tip, distance from the seismic source lowers the level of intensity.

Along the northern shore of Papua is categorized as a high intensity area through 2 reasons: this area is close to earthquake source and composed of soft sediment. The Central Mountains area is unique with regards to site class phenomena. The area is classified as a low intensity area even though it is close to earthquake source. The Central Mountains area is composed of old hard rock that acts as a pathway for seismic waves to go through. On the opposite side, the area composed by marsh deposits in the south of Central Mountains is classified as an area of medium intensity even though this area is far away from a seismic source. In this case, the soft sediment amplifies seismic waves that propagate inside.

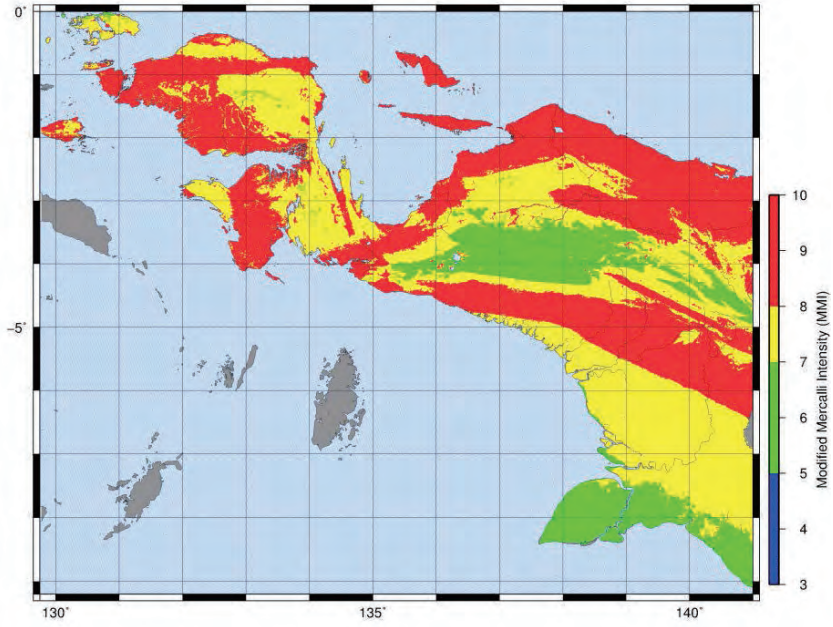

Fig. 6. Earthquake intensity map of Papua Island. MMI is converted from acceleration at 0.2 s of RSA in 500 years return period.

5. Conclusions

The Papua seismic hazard map was created based on the estimated intensity, which was obtained by converting the acceleration level on 0.2 second RSA (Response Spectral Acceleration) using 10% probability of exceedance in 50 years (475 years return period). The hazard level was divided into four classifications: they are very low (MMI < V), low (VII > MMI ≥ V), moderate (VIII > MMI ≥ VII), and high (MMI ≥ VIII), respectively.

Within 500 years, Papua Island has the possibility to experience ground shaking up to 3.0 g (0.2 s of RSA), especially in the areas close to active crustal faults. There are 3 factors contributing to hazard level, such as, distance to fault, site class and return period. It is clear on the map that areas close to faults may suffer from high ground shaking, means high intensity (MMI). Seismic wave could reach close to the area before being attenuated by distance, though it is understandable that all areas along fault zones have high earthquake intensity.

References

Atkinson, G. M. and Kaka, S. I. 2007. Relationships between Felt Intensity and Instrumental Ground Motion in the Central United States and California, Bulletin of the Seismological Society of America, Vol. 97, No. 2, pp. 497–510, doi: 10.1785/0120060154.

Bird, P., 2003. An updated digital model of plate boundaries. Geochemistry, Geophysics, Geosystems, 4 (3), 1027. doi: 10.1029/2001GC000252.

DeMets, C., R. G. Gordon, D. F. Argus and S. Stein, 1994. Effect of recent revisions to the geomagnetic reversal time scale on estimates of current plate motions, Geophysical Research Letters, vol. 21, No. 20.

Dow, D.B and R. Sukamto, 1984. Western Irian Jaya: the end-product of oblique plate convergence in the Late Tertiary. Tectonophysics, 106, 109 - 139.

Everingham, L.B., 1974. Large earthquake in the New Guinea-Solomon Islands area, 1873-1972. Tectonophysics, 23, 323-338.

Hamilton, W,. 1979. Tectonics of the Indonesian Region, U. S. Geol. Surv. Prof. Paper, 1078, 345p.

Henry, C. and S. Das, 2002. The Mw 8.2, 17 February 1996 Biak, Indonesia, earthquake: Rupture history, aftershocks, and fault plane properties, Journal of Geophysical Research, vol. 107, no. B11, 2312

Husen, S., and J.L. Hardebeck, 2010, Earthquake location accuracy, Community Online Resource for Statistical Seismicity Analysis, doi:10.5078/corssa-55815573.

Irsyam, M., Sengara, I.W., Asrurifak, M., Ridwan, M., Aldiamar, F., Widiyantoro, S., Triyoso, W., Natawijaya, D.H., Kertapati, E., Meilano, I., and Suhardjono., 2010. Summary: Development of Seismic Hazard Maps of Indonesia for Revision of Seismic Hazard Map in SNI 03-1726-2002, research report submitted to the Ministry of Public Works by Team for Revision of Seismic Hazard Maps of Indonesia.

Kramer, S.L., 1996. Geotechnical Earthquake Engineering, Prentice-Hall, New Jersey

Matsuoka, M., K. Wakamatsu, K. Fujimoto and S. Midorikawa, 2006. Average Shear-Wave Velocity Mapping Using Japan Engineering Geomorphologic Classification Map, Structural Eng./Earthquake Eng., JSCE, Vol.23, No.1, 57-68.

McCaffrey, R., 2009, The tectonic framework of the Sumatran subduction zone, Annual Reviews of Earth and Planetary Sciences, 37, 345-366.

Okal, E., 1990, Historical Seismicity and Seismotectonic Context of the Great 1979 Yapen and 1996 Biak, Irian Jaya Earthquakes, Pure Appl. Geophys. 154, 633–675

Ottemoller, Voss and Havskov, 2011, SEISAN Earthquake Analysis Software for Windows, Solaris, Linux and MacOS.

Puntodewo S.S.O., R. McCaffrey, E. Calais, Y. Bock, J. Rais, C. Subarya, R. Poewariardi, C. Stevens, J. Genrich, Fauzi, P. Zwick, S. Wdowinski, 1994. GPS measurements of crustal deformation within the Pacific-Australia plate boundary zone in Irian Jaya, Indonesia, Tectonophysics, 237, 141-153.

Reiter, L., 1990, Earthquake Hazard Analysis: Issues and Insights, Columbia University Press, New York.

Simandjuntak,T.O., 2004. Tektonika. Bandung. Pusat Penelitiandan Pengembangan Geologi Bandung.

Snyder, D.B., H. Prasetyo, D.J. Blundell, C.J. Pigram, A.J. Barber, A. Richardson and S. Tjokosaproetro, 1996. A dual doubly vergent orogen in the Banda arc continent-arc collision zone as observed on deep seismic reflection profiles. Tectonics, 15, 34-53.

Socquet, A., W. Simons, C. Vigny, R. McCaffrey, C. Subarya, D. Sarsito, B. Ambrosius, W. Spakman, 2006. Microblock rotations and fault coupling in SE Asia triple junction (Sulawesi, Indonesia) from GPS and earthquake slip vector data. Journal of Geophysical Research, Vol. 111, doi: 10.1029/2005JB003963.

Tregoning, P. and A. Gorbatov, 2004. Evidence for Active Subduction at the New Guinea Trench, Geophysical Research Letters, vol. 31, L13608, Doi:10.1029/2004GL020190.

USGS, 2009, http://earthquake.usgs.gov/earthquakes/eqarchives/poster/2009/20090211.php

Visser, W. and Hermes, J., 1962: Geological Results of the Exploration for Oil in the Netherlands New Guinea: Kononklijk Nederlands Geologisch Mijnbouk - undig. Genoolschap Verhandelirgen, Geologische Serie, 256p.

Renewal of Active Fault Database of Japan

Toshikazu Yoshioka and Fujika Miyamoto

Geological Survey of Japan, AIST
e-mail: yoshioka-t@aist.go.jp

Abstract

An updated Active Fault Database of Japan is available to the public on the Internet. Major updating and renewal involved 1) the addition of about 10 behavioral segments and modification of fault parameters and traces of about 20 behavioral segments, 2) revision of the index map of "Search for behavioral segments" such that the Seamless Digital Geological Map of Japan can be overlain on the map.

Keywords: active fault, database, Internet, Japan

1. Introduction

The Active Fault and Earthquake Research Center, GSJ/AIST constructed an active fault database, open to the public on the internet since 2005, in order to make a probabilistic evaluation of future faulting events and earthquake occurrences on major active faults in Japan. The database consists of three sub-databases: 1) sub-database on individual sites, which includes long-term slip data and paleoseismicity data with error range and reliability, 2) sub-database on details of paleoseismicity, which includes the excavated geological units and faulting event horizons with age-control, 3) sub-database on characteristics of behavioral segments, which includes the fault-length, long-term slip-rate, recurrence intervals, most-recent-event, slip per event and best-estimate of cascade earthquake.

2. Evaluation of behavioral segments

This database contains information of active faults in Japan, sorted by the concept of "behavioral segments" (McCalpin, 1996). Each fault is subdivided into about 550 behavioral segments based on surface trace geometry and rupture history revealed by paleoseismic studies. Behavioral segments can be searched on the Google Maps. One can select a single behavioral segment directly or search segments in a rectangle area on the map. The result of the search is shown on a fixed map or the Google Maps with information of geologic and paleoseismic parameters including slip rate, slip per event, recurrence interval, and calculated rupture probability in the future. Behavioral segments can be searched also by name or combination of fault parameters. All those data are compiled from journal articles, theses, and other documents. A revised edition is currently being developed. About 10 behavioral segments and modified fault parameters and traces of about 20 behavioral segments have been added in this revision.

3. User friendly interface

An effort to make this database to be more easily accessible is in progress. The index page for the search of behavioral segments is shown using Google Maps. One can select a behavioral segment directly on this map, or search by location, name, length, slip-rate, and so on. One

can also overlay the Seamless Digital Geological Map of Japan on this index map in order to understand the relationship between the distribution of active faults and other aspects of the geology.

4. Visit our website

The Active Fault Database of Japan is open to public on the Internet. It can be accessed without any registration. Please visit our website. The new URL is as follows:

https://gbank.gsj.jp/activefault/index_e_gmap.html

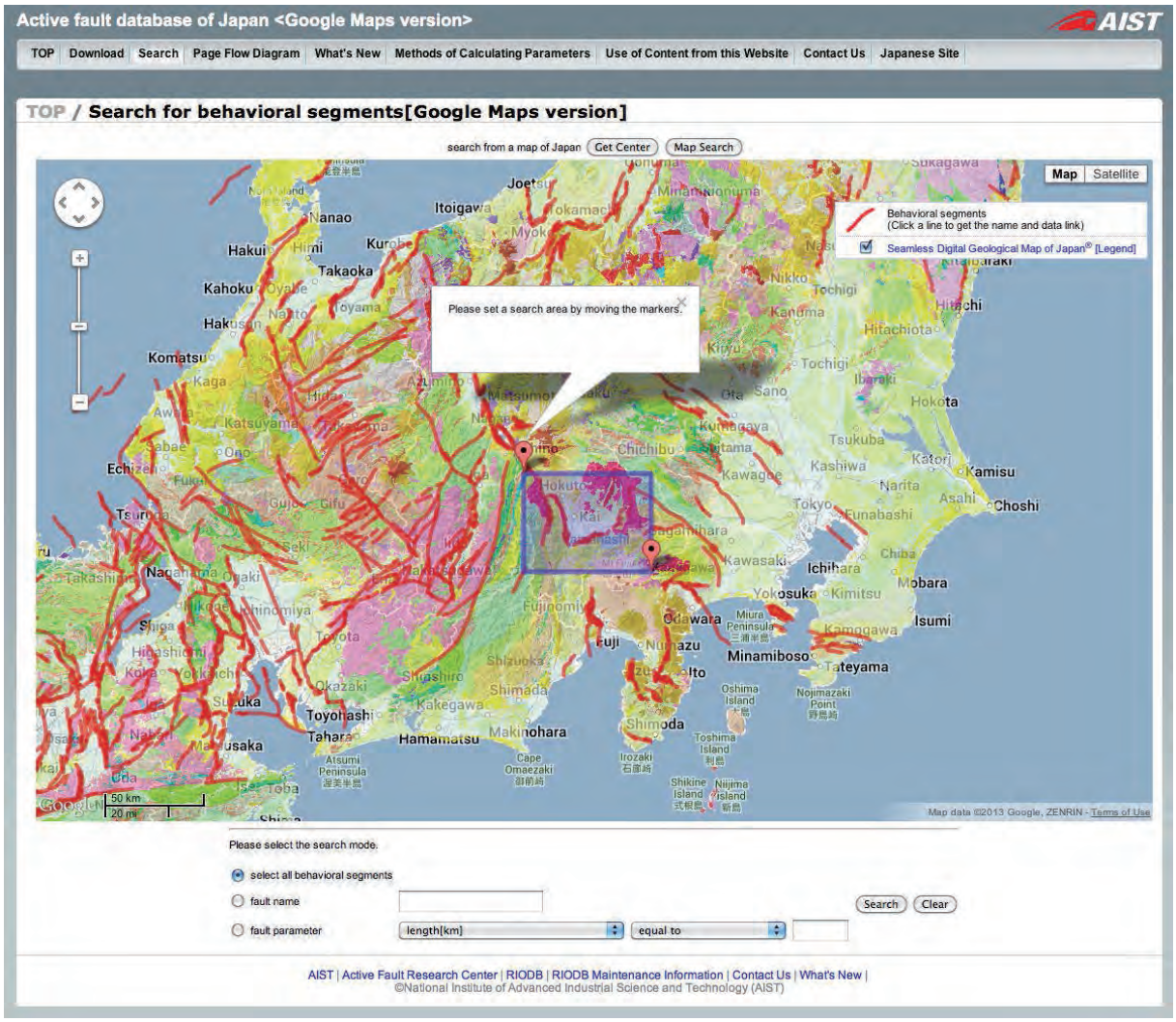

Fig. 1. Screen view of "Search for behavioral segments" with overlain Seamless Digital Geological Map of Japan.

References

McCalpin, J. P., 1996. Application of paleoseismic data to seismic hazard assessment and neotectonic research. McCalpin ed. "Paleoseismology", Academic Press, 439-493.

Seismotectonics of the Palu-Koro active fault and analysis of the disappearance of megalith cultures from central Sulawesi Island

Asdani Soehaimi[1] and Dicky Muslim[2]

[1]Geological Agency, Ministry of Energy and Mineral Resources, Indonesia
[2]Faculty of Geology, University of Padjadjaran, Indonesia

Abstract

Sulawesi Island, especially the Central Sulawesi region along the Palu-Koro and Matano active faults, is one of the earthquake prone regions of the eastern part of the Indonesian Island Arc. Based on the morphological structure, fault kinematics, historical destructive earthquake epicentres and lithologic boundaries, the active fault zone can be divided into 13 seismotectonic segments. The determination of maximum earthquake magnitude along this active fault zone is 7 Mw and the maximum peak ground acceleration is 0.6 g, and the maximum intensity estimated is IX of MMI scale.

Palu City, as the capital of Central Sulawesi Province, is located at the center of the main seismic source zone of the Palu-Koro active fault. It is one of the most earthquake prone areas, which must be protected from the potential seismic activity in the near future. The determination of geoseismological conditions and potential earthquake risk of this city is a priority for mitigation purposes. Seismic hazard microzonation is one solution for seismic risk mitigation.

The analysis of the disappearance of megalithic cultures in Central Sulawesi presents a previous portrait of the threat to life sustainability in this region.

1. Introduction

Sulawesi Island is located in the eastern part of the Indonesian archipelago. Historically this island has frequently been struck by destructive earthquakes, generated by tectonic activity along subduction and active fault zones. The maximum intensity of earthquakes in and around this region is IX on the MMI Scale (Fig. 1).

The Geological Agency of Indonesia, as a technical institution under the Ministry of Energy and Mineral Resources, executes research and services in the areas of geological resources, volcanology, geological hazard mitigation, and environmental geology. The vision of the institution is to make use of geological knowledge for protecting human life and for the greater welfare of the people. This is consistent with the preamble to the basic laws of the 1945 constitution of Indonesia which said that the State Government of Indonesia should protect all the Indonesian people and the entire homeland of Indonesia and promote general welfare, foster the intellectual life of the nation, and participate in the establishment of a world order based on independence, peace and social justice. To carry out this mandate the Government of the Republic of Indonesia has issued several state laws such as Law No. 32 of 2009 on Environmental Protection and Management, Laws No. 24 of 2007 on Disaster Management and No. 26 of 2007 on Spatial Planning and Government, Regulation No. 26 of 2008 concerning Spatial Planning on a National scale including clause No. 52, verse No. 5, which mentioned those regions located on an active fault zone are all relevant.

In order to implement the above functions under the laws mentioned above, the Geological Survey Institute under the Geological Agency in 2012 carried out mapping and research on active fault microzonation in Central Sulawesi. The result of this activity can be used by

central and local government for establishing and improving regional and local spatial planning in order to mitigate earthquake risk in this region.

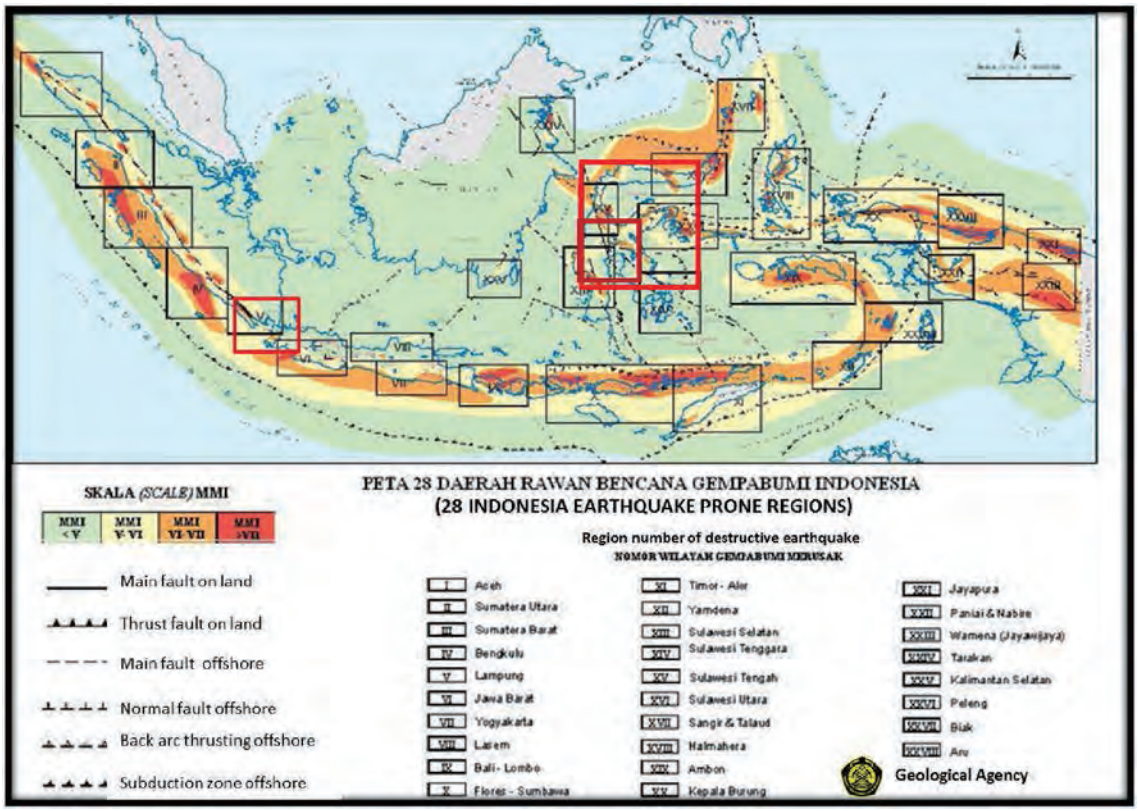

Fig. 1. Map of 28 earthquake hazard prone areas in Indonesia (GRDC, 2004).

2. Geotectonics of Sulawesi

Geotectonically, Sulawesi Island and surrounding areas lie in part of the eastern Indonesia tectonic collision zone between three active plates: the Pacific and India-Australia Oceanic Plates and the Eurasian Continental Plate. This collision zone displays special features in Central Sulawesi, where the the Micro Oceanic Plate of India-Australia (Banggai-Sula) is subducted from the east beneath the Continental Plate of Eurasia in the eastern part of Kalimantan Island. This dynamic tectonic behavior results in Sulawesi Island being influenced by several active faults with a special character in the active seismicity of the region. The geotectonic map of Sulawesi Island and surrounding areas is shown in Fig. 2.

3. Sulawesi seismic source zone

The seismicity of Sulawesi Island is controlled by tens of shallow seismic sources namely Walanai active fault, Palu-Koro active fault, Poso active fault, Matano-Tolo Bay active fault, Batui active fault, Balantak active fault, Lawanopo and Lasolo active fault, Uekuli active fault, Minahasa subduction and Gorontalo active fault, Sorong active fault, South Buton Island active fault and Mamuju-Lariang active fault (Kertapati, 2005) as shown in Fig. 3. All of these shallow seismic source zones were generated from deep up to shallow. This indicates that the seismic source zones in this region represent the reactivation of the active fault zones progressing from deep levels consisting of old formations to shallow younger formations near the surface.

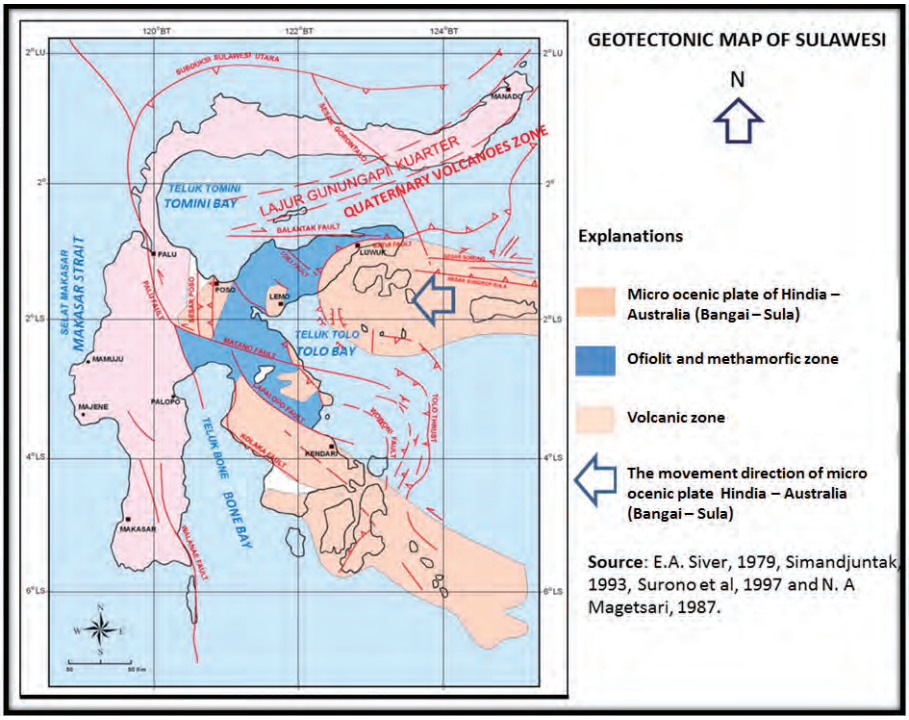

Fig. 2. Geotectonic map of Sulawesi.

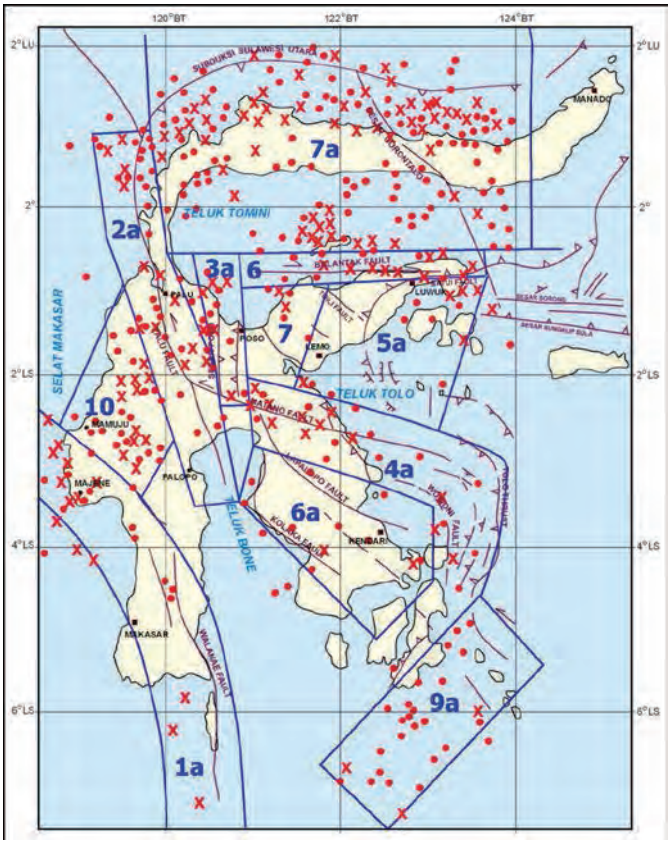

Fig. 3. Sulawesi shallow seismic source zones (Kertapati, 2005).

4. Seismotectonic of Central Sulawesi

The seismogenesis of Central Sulawesi is expressed by the seismotectonics of the Palu-Koro

active fault. This active fault is one of the large trans-current faults in Sulawesi, which displays the character of a single strike slip fault zone in its southern part and bifurcation with a normal fault component in the northern part (Palu Bay). Seismotectonic studies along this fault zone (morphotectonic, kinematic, history of destructive earthquake epicentres and stratigraphy/lithology and focal mechanism) indicate that the active fault can be divided into the following 13 seismotectonic segments (Fig. 4).

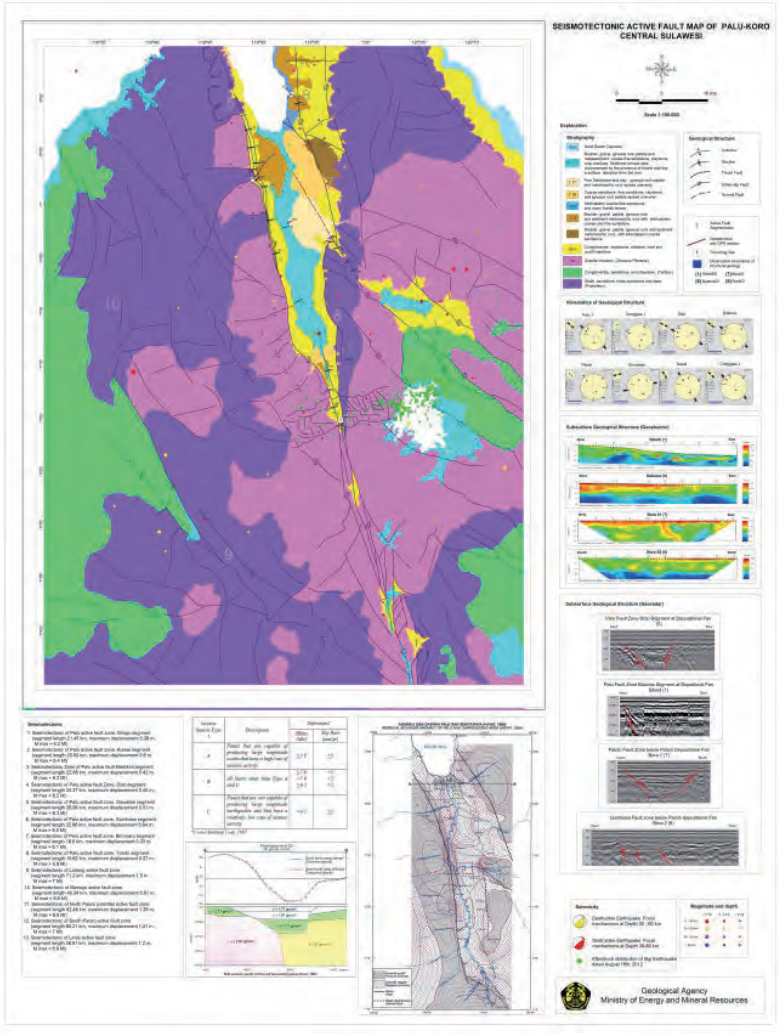

Fig. 4. Seismotectonic maps of Palu-Koro active fault.

1) Gimpu seismotectonic segment of the Palu active fault with length of fault segment 21.45 km, maximum displacement 0.2 m and maximum magnitude 6.2 Mw.

2) Kulawi seismotectonic segment of the Palu active fault with length of fault segment 20.93 km, maximum displacement 0.2 m and maximum magnitude 6.4 Mw.

3) Mantikole seismotectonic segment of the Palu active fault with length of fault segment 22,88 km, maximum displacement 0.21 m and maximum magnitude 6.2 Mw.

4) Dolo seismotectonic segment of the Palu active fault with, length of fault segment 24.37 km, maximum displacement 0.22 m and maximum 6.2 Mw.

5) Gawalise seismotectonic segment of the Palu active fault with length of fault segment 26.96 km, maximum displacement 0.23 m and maximum magnitude 6.3 Mw.

6) Gumbasa seismotectonic segment of the Palu active fault, with length of fault segment 32.88 km, maximum displacement 0.26 m and maximum magnitude 6.5 Mw.

7) Biromanu seismotectonic segment of the Palu active fault, length of fault segment 18.6 km, maximum displacement 0.18 m and maximum magnitude 6.1 Mw.

8) Tonodo seismotectonicsegment of the Palu active fault, length of fault segment 15.62 km, maximum displacement 0.16 m and maximum magnitude 5.9 Mw.

9) Seismotectonic segment of the Lariang active fault, length of fault 71.25 km, maximum displacement 0.34 m and maximum magnitude 7 Mw.

10) Seismotectonic segment of Mamuju active fault, length of fault 40.34 km, maximum displacement 0.28 m and maximum magnitude 6.6 Mw.

11) Seismotectonic segment of North Palolo active fault, length of fault 62.48 km, maximum displacement 0.32 m and maximum magnitude 6.9 Mw.

12) Seismotectonic segment of South Palolo active fault, length of fault 65.21 km, maximum displacement 0.33 m and maximum magnitude 7 Mw.

13) Seismotectonic segment of Lindu active fault, length of fault 56.61 km, maximum displacement 0.32 m and maximum magnitude 6.9 Mw.

5. Seismic hazard assessment

The potential seismic hazard of Sulawesi and surrounding areas was analysed by probabilistic seismic hazard assessment (PSHA) using the USGS PSHA software (Harmsen, 2007). Sulawesi Island, which is located at 118^0E-127^0E and 7^0S-5^0N, was divided into 10,800 grid areas, with a grid size of 0.1^0 x 0.1^0 in latitude and longitude. This analysis gives the peak ground acceleration (PGA) at a period of 1 second with the probability greater than 2 % in the next 50 years (Pasau, pers. comm.). The result of analysis indicates that the Palu-Koro potential seismic hazard region is located in the zone of 0.5 to 0.6 g (Fig. 5).

6. Megalithic culture of Central Sulawesi

Remains of the megalithic culture of Central Sulawesi were found in the Lore-Lindu National Park at the high land of Napu. The megalithic complex of Pokekea, Lempe and Beriri is located in the valley of Doda-Beriri covering an area of 215 km^2 at an elevation of 1,215 meters above sea level. This valley is covered by the alluvial plain along the river of Uwei Torire. The megalithic remains in this area consist of large water jars (tempayan besar) with lids and statues of men and women made of granite and metamorphic rocks.

The water jars were found surrounding a small dry lake (Telaga). This lake was a kind of small pond along the intermittently flowing river of Uwei Torire. At several places the lids were found on two sides of water jars (east and west directions). These lids were fallen due to heavy ground shaking by an earthquake in the south, where the Lindu Lake is located along the Palu-Koro and Matano active fault seismic source zone.

Topographic and satellite image (DEM and InSAR) analysis and field checking show that the megalithic complex of Doda-Beriri is located in areas of ancient giant landslides and extensive flooding. The environment of the Doda-Beriri valley is shown in Fig. 6.

Based on field investigation, it can be concluded that the disappearance of the megalithic community in the Doda-Beriri complex might have been caused by frequent strong earthquakes, ground shaking, giant landslides, flooding and drought.

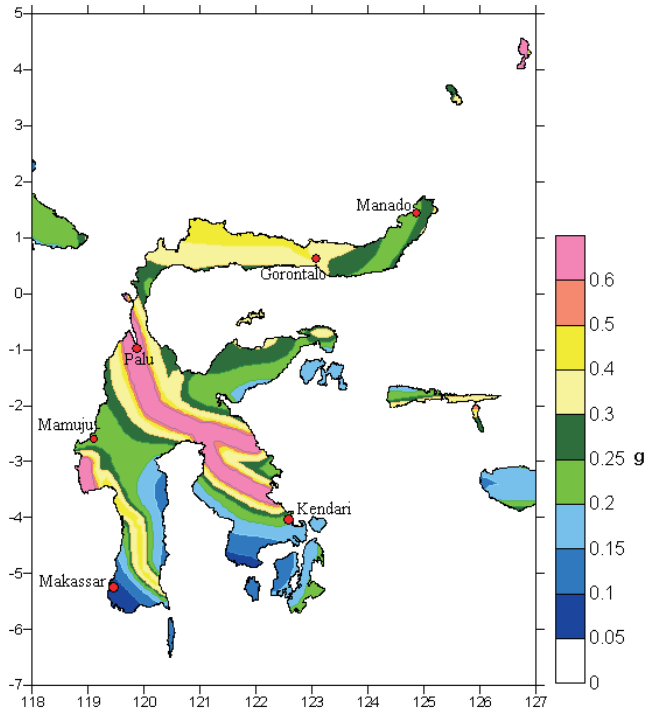

Fig. 5. Probabilistic seismic hazard map of Central Sulawesi; probability exceeded 10 % and 2 % in 50 years at the peak ground acceleration (PGA) in period of 1 second (Pasau, pers. comm.).

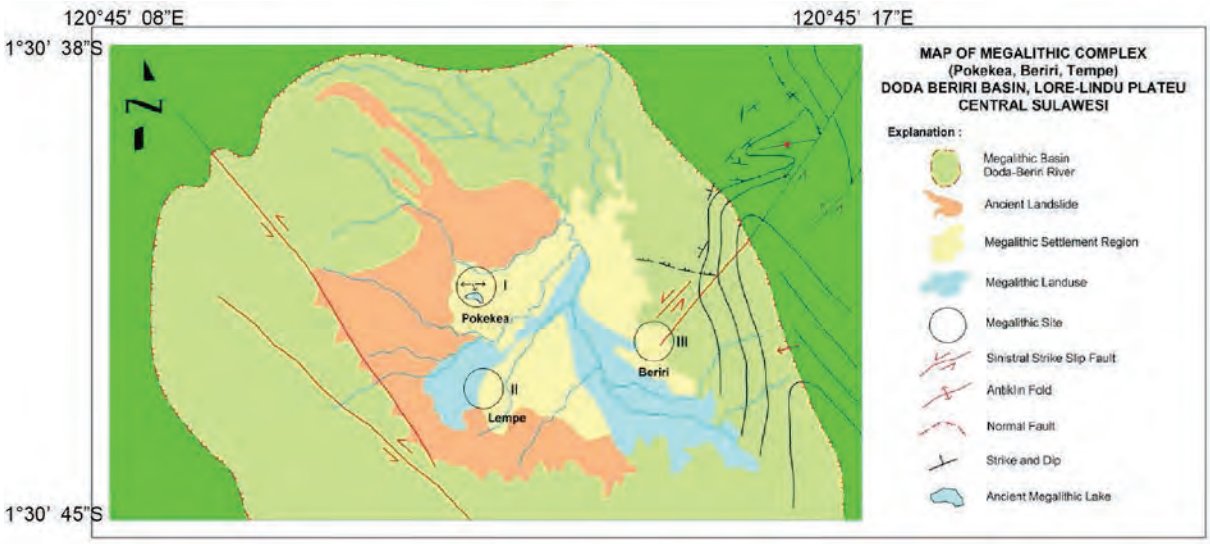

Fig. 6. The environmental geology of Pokekea-Beriri-Lempe basin.

7. Conclusions

Sulawesi Island is one of the earthquake prone regions in eastern part of the Indonesia Island Arc, especially the area along the active faults of Palu-Koro and Matano. The maximum magnitude along this active fault zone is 7 Mw, and the maximum peak ground acceleration 0.65 g and estimated maximum intensity of IX MMI Scale. Palu City, as the capital city of Central Sulawesi Province which is located at the center of the main seismic source zone of the Palu-Koro active fault, is one of the most earthquake prone areas and must be protected

from potential seismic risk in the near future. The possibility of the reasons for the disappearance of the megalithic community in Central Sulawesi presents a portrait of past natural hazards and the challenge of maintaining sustainable communities in the future.

Acknowledgements

This paper has been written through secondary and primary data which were collected by A. Soehaimi, Marjiono, J. H. Setiawan, Kamawan, Akbar Cita, Yayan Sopian, Sukahar Eka, Moch.Wahyudiono, Robby Setianegara and Neng Sri Mulayati. The authors would like to thank and express their appreciation to all members of the Seismotectonic and Active Fault Team of the Geological Survey Institute of Indonesia.

References

Geological Research and Development Centre (GRDC), 2004, Atlas Geology and Potency of Mineral and Energy Resources, GRDC, Bandung, p. 18.

Harmsen, S., 2007, USGS Software for Probabilistic Seismic Hazard Analysis (PSHA), Draft Document ,USGS.

Kertapati, E., 2005, Aktifitas Gempabumi di Indonesia, Pusat Suvei Geologi, pp 25 - 29.

The fluid geochemistry of Lusi mud volcano, East Java, Indonesia

Akhmad Zaennudin, Hanik Humaida, and Euis Sutaningsih

Geological Agency of Indonesia
Jl. Diponegoro No. 57, Bandung, Indonesia
e-mail: zen@vsi.esdm.go.id

Abstract

The Lusi mud volcano in Sidoarjo East Java, Indonesia has been erupting mud and water since May 29, 2006. At the peak of its activity it discharged greater than180,000 cubic meters of material per day. This destroyed thousands of homes, displaced tens of thousands of people, and covered an 840 ha area of farms, factories, rice fields, settlements, and infrastructure. The erupting fluid is a mixture of water, mud, and fragments of sand, shale, andesite, tuff, other rock material and minerals. It is at near-boiling temperatures accompanied by venting of primarily water vapor, CO_2, and CH_4. Lusi mud volcano exhibits variations in flow rate and pulsating activity. This mud volcano has been erupting for more than six years and is still extruding between 40,000–60,000 cubic meters per day of mud which contained from 63% up to 85% of water in June 2012. It has caused deformation by cracking of the surface and damage to buildings in an area of up to 3.5 km in diameter. Bubbles and gas outbursts occur especially in areas to the south and west of the main crater. The characteristics of the geochemistry of fluids and of gas bubbles at the main crater and the dikes show different features. Water composition at the main crater has a higher sodium and chlorine content and is at a higher temperature as compared to the chemical composition of normal temperature water from bubbles and gas outbursts elsewhere which has lower sodium and chlorine content, perhaps reflecting different water sources. Stable isotopes of deuterium and oxygen of the waters of the main crater and bubble outbursts are different. The isotopes of high temperature water of the main crater reflect interactions with cooling igneous rock, while isotopes from bubbles and gas outbursts indicate meteoric water.

1. Introduction

Outburst of hot mud as at Lusi is a natural phenomenon commonly called a mud volcano. Such an eruption of water, mud, clay, and other fragments may build a volcano like hill as high as 25 m (Davies et al., 2007). The mud volcano of Lusi is still growing following the first eruption on May 29, 2006 that was located only 200 m to southwest of the exploration petroleum well of Banjarpanji-1. On June 2, 2006 the second and the third mud extrusions occurred about 500 and 800 m to the northeast of the Banjarpanji-1 well, respectively (Lapindo, 2006), but these second and the third extrusions ceased on June 5, 2006. The first extrusion site, however, is still active to the present day, producing between 50,000 to 60,000 cubic meters of material per day.

The Lusi mud volcano is located at Porong, Sidoarjo District, East Java Province, which is only 10 km to the south of Sidoarjo town, 30 km to the south of Surabaya city and 20 km to the northeast of a Quaternary volcanic complex (Fig. 1) (Zaennudin et al., 2010).

Due to the huge volume of the extrusion, the deposit caused damage to an the area up to 2.5–3 km in diameter and totaling about 840 ha around Lusi comprising rice fields, farm buildings, settlements, schools, factories and other infrastructure. In order to manage and protect a wider area around Lusi from the mud, the Indonesian government contracted a dike around the Lusi mud volcano (Fig. 2).

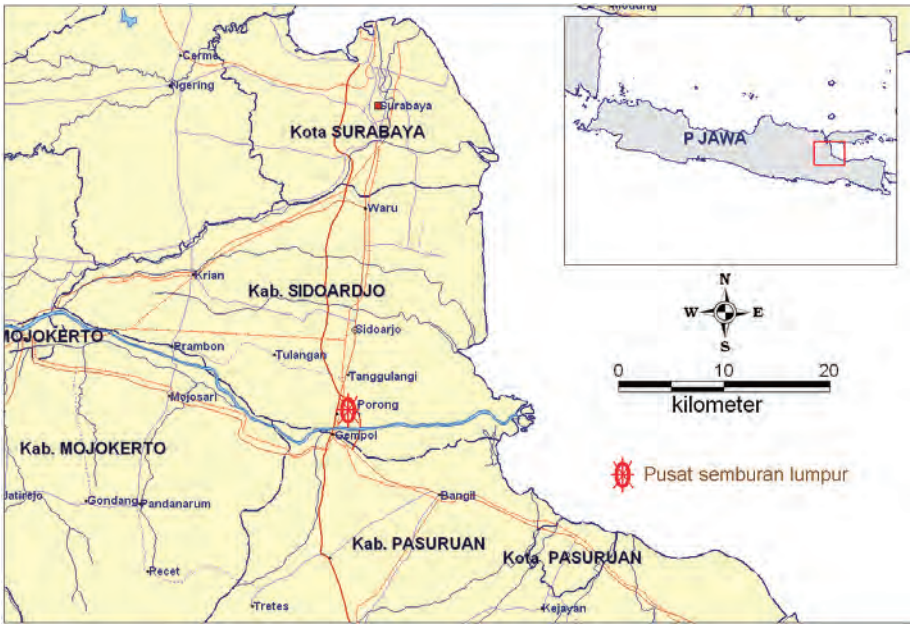

Fig. 1. Location of mud volcano of Lusi, 10 km to the south of Siodarjo, East Java.

A huge volume of material has been erupted, amounting to about 150,000 up to 180,000 m^3 per day at the peak extrusion period and subsequently up to about 50,000-60,000 m^3 per day (Zaennudin et al., 2010). The mud extrusion is still a big problem for the area surrounding Lusi due to the collapse of the dikes that controlled the spreading mud deposit. It has caused damage up to 2.5 to 3 km from the eruption point with the worst area found up to 700 m from the eruption, especially in the western area. Various areas are separated by dikes as high as 9 m from the surrounding areas in order to control the mud distribution. The mud deposit is attempting to flow to the Madura Strait through the Porong River.

Fig. 2. Dikes constructed to control mud flow of Lusi, looking to the south. Steam dominates the mud volcano, rising as high as 100–150 m from the main crater which is extruding mud, water, gases, and a mixture rock fragments.

Upward movement of mud to intrude and break through the overlying capping layers requires a lot of energy, perhaps sourced from hydrostatic pressure of the sedimentary rocks or from the energy of a geothermal system that is found in this area and which drives high pressure gases that consist of steam, hydrocarbon and other gases. The erupted mud at the Lusi mud volcano consisted mainly of hot water (up to 70%) mixed with 30% of solid material in the middle of 2006 until 2008. In early 2009 until 2011 it was dominated by solid material (up to 60%) and water accounted for about 40% (Fig. 3), but from early 2012 until June 2012 its composition changed again with water comprising 63–85%. The fragments contained in the mud are dominated by shale and silt beside andesite and tuff. The fragments generally vary in size from about 0.5 cm up to 2 cm and are sub rounded to rounded.

Fig. 3. Mud of Lusi composed mostly of water with fragments of shale, silt, andesite, tuff, and various minerals. The temperature of the mud is nearly at boiling temperature. A: Sampling hot mud of Lusi from the crater. B: Temperature (^{o}C) of hot mud. C: Dried mud. D: Mud washed by rain.

The Lusi mud outburst has been active for seven years, and it cannot be predicted when it will cease. The extrusion is driven by high pressure steam and gases from a depth of more than 2,800 m, the depth of the Banjarpanji-1 oil exploration borehole (Aziz, 2007; Kadar et al., 2007; Zaennudin et al., 2010). Lusi is located only 20 km to the northeast of the active Quaternary Volcanic Complex of Arjuno-Welirang and the hot mud of Lusi might be influenced by the volcanic processes of the volcanic complex.

Some water and gas samples from the main crater at Lusi and from bubbles around the Lusi area were analysed in order to clarify their chemical composition. The water samples that are found in these outbursts were also dated.

Lusi mud volcano eruption caused cracking and damage in areas around the mud volcano with outbursts of water and appearance of bubbles. The gases from the main crater of Lusi are mostly composed of steam with hydrocarbon gases and differ in composition from the gases of the outbursts and bubbles around the western and southern areas. In the latter areas thermogenic hydrocarbon gases predominate.

The Lusi mud volcano appears to be structurally controlled by the Quaternary fault of Watukosek which trends in a northeasterly direction from the Penanggungan volcano to Madura Island in the north. In the same direction several other mud volcanoes, such as Pulungan, Gunung Anyar, Kalang Anyar, are found around Surabaya and Sidoarjo. Also the Geger mud volcano is found in Madura Island. Based on the similar hot water content of these mud volcanoes, all might be the result of similar processes.

2. Methods

This study was conducted by observing phenomena in the field, taking temperature measurements, gas and water sampling, and laboratory analysis of the samples. Sampling of fluids (a mixture of water and mud) and gases was carried out near the main outbursts and from some points within and outside the levee embankment. Gas samples were collected in vacuum bottles for compositions to be analysed using gas chromatography. Fluid samples were collected and stored in polyethylene bottles.

Samples of water for isotopic analysis were taken in 20 cc vials which were sealed to prevent evaporation before analysis. The content of the water ions was measured by UV-VIS (ultra violet-visible) spectrometry and AAS (atomic absorption spectroscopy). The stable isotope ratios of $\delta^{18}O$ and $\delta^{2}H$ were measured with an isotope ratio mass spectrometer using the elemental analyzer for pyrolysing water at high temperature to produce CO_2 gas for analysing $\delta^{18}O$ and H_2 for analysing $\delta^{2}H$ respectively.

3. Fluid chemistry of Lusi Mud Volcano

In August 2013, the measured amount of mud being extruded was still 50,000–64,000 cubic meters per day and concentration of fragments inside the liquid was between 3.23 up to 33.87% of included fragments. It appeared less viscous than in June 2012 (Table 1). Based on the visual monitoring of the main crater activity the steam plume of the extrusion was higher whilst two, and often three, eruption points occurred at the same time in an almost west–east alignment. The most active of these was at the centre of the crater where the released steam and gas mixture rose to a height of 100 m and was white in color.

The volume of the Lusi mudflow is sufficient to threaten collapse of the containing dykes due to the pressure of mud on the dikes and subsidence in the weak zone areas up to 2.5–3 km in diameter. The latter condition has caused ground cracking resulting in several outbursts of gases and bubbles in the western and southern areas (Fig. 4). These gas outbursts are followed by water effusion either in the main crater or in the western areas of Lusi.

The water of the outbursts and that from main crater have different characteristics which reflect the water sources. The composition of liquid from the main crater is dominated by hot water with some hydrocarbon liquid (Fig. 5). In contrast the water from outbursts and bubbles around the western and southern areas of Lusi display normal temperatures and hydrocarbon liquids are absent. Also these outbursts occurred only during a few months or days and then ceased, whereas the main crater of Lusi still extrudes hot mud after nearly eight years. The chemical composition of samples from Lusi and its vicinity collected at a succession of different times are presented in Tables 2 to 6 below.

Table 1. Mud extrusion of Lusi in June 2012 and August 2013.

No.	Location	Fragments in mud,June 2012 (%)	Fragments in mud, August 2013 (%)	Temp (^{o}C)	Coordinates	Volume (m^3/day)
1	Point 25	45.00	33.87	46.1	S: 07^{o} 31' 52,5" E: 112^{o} 42' 29,5"	21,684.36
2	Point 25 east	-	3.23	45.6	S: 07^{o} 31' 52,8" E: 112^{o} 42' 37,0"	1,112.97
3	Point 68	-	10.48	42.5	S: 07^{o} 31' 14,8" E: 112^{o} 42' 50,7"	7,045.87
4	Point 68 west	7.37	7.34	45.4	S: 07^{o} 31' 15,1" E: 112^{o} 42' 46,0"	6,372.23
5	Point 43	14.53	8.87	39	S: 07^{o} 31' 50,6" E: 112^{o} 43' 01,0"	22,534.46
6	Point 43 west	-	-	35.3	S: 07^{o} 31' 30,7" E: 112^{o} 43' 04,7"	1,209.30
7	Point 70	-	3.55	35.3	S: 07^{o} 31' 03,8" E: 112^{o} 42' 32,3"	13,142.54
8	Point 21	-	11.94	45.8	S: 07^{o} 31' 32,4" E: 112^{o} 42' 22,1"	12,687.43
	Total Volume					85,789.16
	Total Volume assuming about 75% on the surface of stream					**64,341.87**

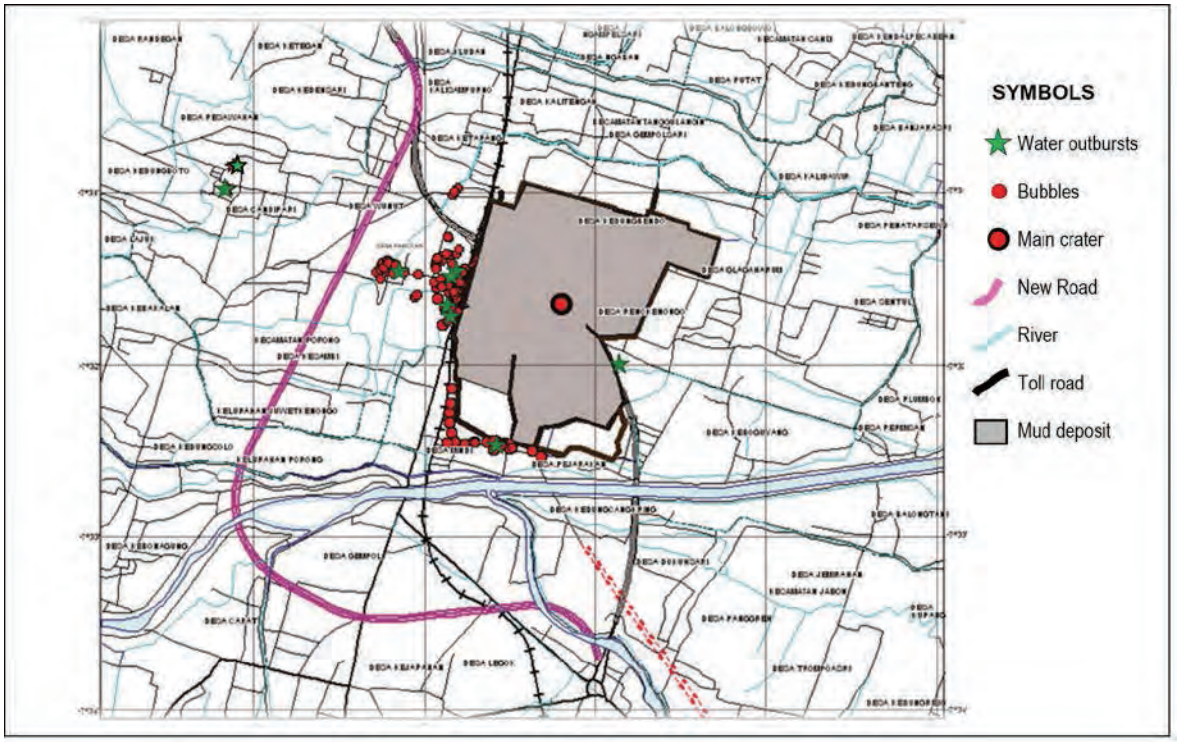

Fig. 4. Distribution of water, gas outbursts, bubbles, and mud volcano deposits of Lusi.

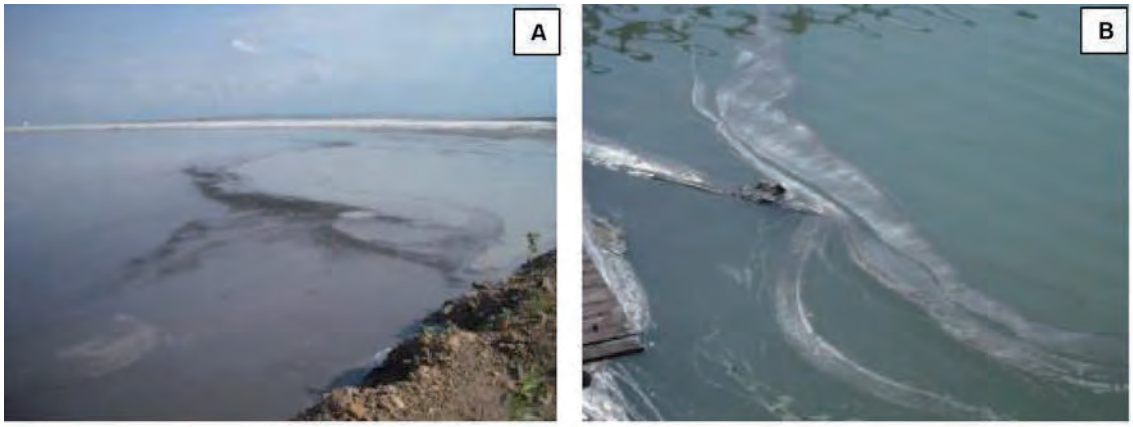

Fig. 5. A surface film of liquid hydrocarbon on water of the Lusi pond.

Table 2. Chemical composition of main crater water, bubbles around the Lusi, and hot spring of Welirang volcano measured in May 2007.

	Lusi(crater)	Lusi (crater)	Well (Besuki)	Bubbles (Mindi)	Well (Mindi)	Hot Spring Mt. Welirang
SiO_2	56.99	30.50	58.60	17.52	51.12	79.20
Al	3.47	0.21	-	-	-	-
Fe	0.27	0.47	391.0	0.31	0.07	-
Ca	1,085.00	1,205.00	0.60	5.87	15.87	94.60
Mg	140.00	135.50	101.20	97.30	10.10	33,50
Na	6,615.00	7,355.00	627.00	1,579.00	672.00	110.90
K	106.70	106.3	19.40	28.13	29.89	18,90
Mn	0,27	0.34	8.30	5.84	0.03	0.40
NH_3	77.09	69.72	9.56	7.25	8.06	0.60
Cl	14,170.18	14,001.20	8.29	3,701.47	563.26	241.40
SO_4	1.10	392.52	96.70	3.84	26.53	54.40
HCO_3	116.90	29.20	1.66	-	1.66	1.66
H_2S	639.30	663.80	372.83	225.64	845.32	377.70
B	-	-	-	-	-	-
pH lab.	7.7	7.35	7.3	6.9	7.8	6.6

Table 3. Chemical composition of main crater water, bubbles, and wells around the Lusi measured in February 2008.

	Crater Lusi	Well West Siring	Well Pamotan	Bubbles Lion Steel	Bubbles Candi Jaya	Bubbles Siring Barat
SiO_2	18.78	49.75	40.36	64.04	62.67	6.,14
Al	0.34	0.00	0.00	0.00	0.00	0.00
Fe	0.50	0.07	0.02	0.05	0.04	0.04
Ca	976.00	315.80	69.50	178.70	111.80	62.50
Mg	141.20	76.40	25.70	56.60	40.00	18.70
Na	7,562.00	141.90	353.00	502.50	269.20	109.20

K	135.80	22.34	28.65	22.83	18.93	12.43
Mn	0.40	8.34	0.00	2.03	0.00	0.38
NH_3	55.82	3.26	0.99	1.11	1.43	0.96
Cl	13,373.86	902.41	416.14	782.86	475.85	165.85
SO_4	210.94	4.63	45.27	65.53	16.88	1.75
HCO_3	714.20	358.53	469.83	591.16	323.26	295.72
H_2S	12.52	3.34	3.34	3.34	13.36	3.36
B	69.10	2.27	2.10	1.14	1.14	2.19
F	1.99	0.12	0.26	0.20	0.13	0.08
pH	7.72	7.20	6.80	6.29	7.05	7.21

Table 4. Chemical composition of main crater water, bubbles, and wells around the Lusi measured in August 2009.

	Lusi	Bubbles Siring (1)	Bubbles Siring (2)	Bubbles Siring (3)	Well Pamotan	Well Pamotan
SiO_2	14.02	38.84	65.76	61.31	42.32	68.05
Al	0.00	0.00	0.00	0.00	0.00	0.00
Fe	0.39	0.08	0.15	0.22	0.00	0.00
Ca	299.50	220.20	84.60	177.90	86.70	10820
Mg	8.10	57.50	56.90	114.60	34.70	44.50
Na	5,402.00	237.10	208.00	914.00	160.80	192.50
K	90.98	25.41	19.13	45.27	15.90	18.06
Mn	0.13	5.43	2.44	5.63	3.53	1.65
NH_3	56,25	4.75	3.44	9.06	3.75	2.75
Cl	7,496.86	270.35	171.97	1,463.45	358.02	266.68
SO_4	375.00	8.13	1.88	37.50	1.25	6.65
HCO_3	1,047.20	983.25	907.05	702.20	211.02	568.87
H_2S	0.00	2.80	2.10	2.10	0.00	2.10
B	7.38	0.00	0.00	0.00	0.10	0.14
pH lab	7.14	8.23	7.04	6.76	7.16	7.00

Table 5. Chemical composition of main crater water, bubbles around Lusi, and oil seepage well measured in February 2010.

	Lion Mesh	Lion Mesh	Bubbles 25	River (Krupuk)	Crater LUSI	Oil Seepage
SiO_2	78,42	50,80	8,43	49,47	46,62	58,43
Al	-	-	-	-	-	-
Fe	0,17	3,96	-	-	0,55	-
Ca	631,80	405,50	312,70	108,84	1.088,50	205,20
Mg	359,00	157,10	76,90	18,60	148,80	33,60
Na	3.580,00	1.420,00	1.256,00	115,90	8.575,00	167,80
K	133,40	37,64	44,13	9,29	198,40	12,65
Mn	25,97	2,80	-	0,66	0,30	0,92
NH_3	19,23	5,13	5,09	5,89	110,26	2,24
Cl	6.396,65	2.776,77	2.423,14	226,80	14,298.00	128,04

SO_4	185,19	27,16	351,85	8,64	130,86	171,47
HCO_3	878,62	706,47	285,83	286,57	440,05	701,86
H_2S	11,18	6,78	6,78	0,68	13,55	1,68
B	-	-	-	-	-	-
pH lab.	7,19	1,04	7,58	7,10	7,12	7,65

Table 6. Chemical composition of main crater water, bubbles around Lusi, and hot spring of Penanggungan volcano measured in June 2011.

	Well Ketapang	Bubbles Jatirejo	LUSI 25	LUSI North	LUSI 43-1	LUSI 43-2	LUSI 43-3	Hot Spring Penanggungan
SiO_2	53,15	90,71	51,31	67,51	47,06	46,63	49,35	107,78
Al	0	0	0	0	0	0	0	0
Fe	0.00	1.25	0.84	0.60	0.45	0.50	0.45	0.12
Ca	175.00	603.00	1287.5	992,00	896.50	869.00	890.75	67.95
Mg	43.35	406.00	200.00	138.85	115.60	112.30	111.70	23.7
Na	258.00	4,650.00	16,180.00	13,830.00	11,005.00	9,575.00	10,325.00	521.25
K	35.72	207.50	330.80	265.90	224.00	205.7	232.10	56.89
Mn	6.90	5.38	0.49	0.38	0.37	0.45	0.41	0.1
Li	0.00	0.12	3.14	2.67	2.47	2.41	2.39	0.62
NH_3	8.24	161.76	238.23	264.70	264.70	350.00	257.14	4.7
Cl	534.00	8,348.00	25,842.00	19,370.00	15,938.00	16,122.00	14,736.00	697.99
SO_4	8.44	41.77	35.63	153.29	102.41	119.74	124.12	0.00
HCO_3	548.40	2407.99	370.16	537.23	494.58	625.72	594.93	479.84
H_2S	1.27	6.33	0.63	2.53	5.06	3.79	5.06	0.00
B	0.00	0.00	113.71	64.19	54.66	54.86	59.19	13.63
pH lab.	6.84	6.95	7.40	7.37	7.04	7.72	7.62	7.36

There are differences in the chemical composition of water from the main crater and that from outbursts around Lusi. The Lusi crater water has high chlorine (Cl) and sodium (Na) content reflecting its origin at depth. The waters that are derived from the main crater and outbursts close to the main crater are mostly greater than 40,000 years old and are at high temperatures, whereas water from bubbles and outbursts around Lusi are younger and display normal temperatures.

Isotopes of deuterium and oxygen of the main crater water and water from outbursts surrounding Lusi were sampled periodically. There are some significant differences; isotopes of deuterium and oxygen of main crater water was derived from depth and was influenced by static magma during the magma cooling process. On the other hand, Isotopes of deuterium and oxygen from outbursts and bubbles mostly indicate derivation from shallow depths of formation and ages between recent up to 35,000 years BP.

Based on the ages of samples taken over time, water of the main crater that flowed radially away from the eruption point to a lower area was changed to become younger with time. This might be due to weaker pressure and contamination by young subsurface water, but the isotopes of deuterium and oxygen still indicate influence by deep water sources which reflect igneous rocks.

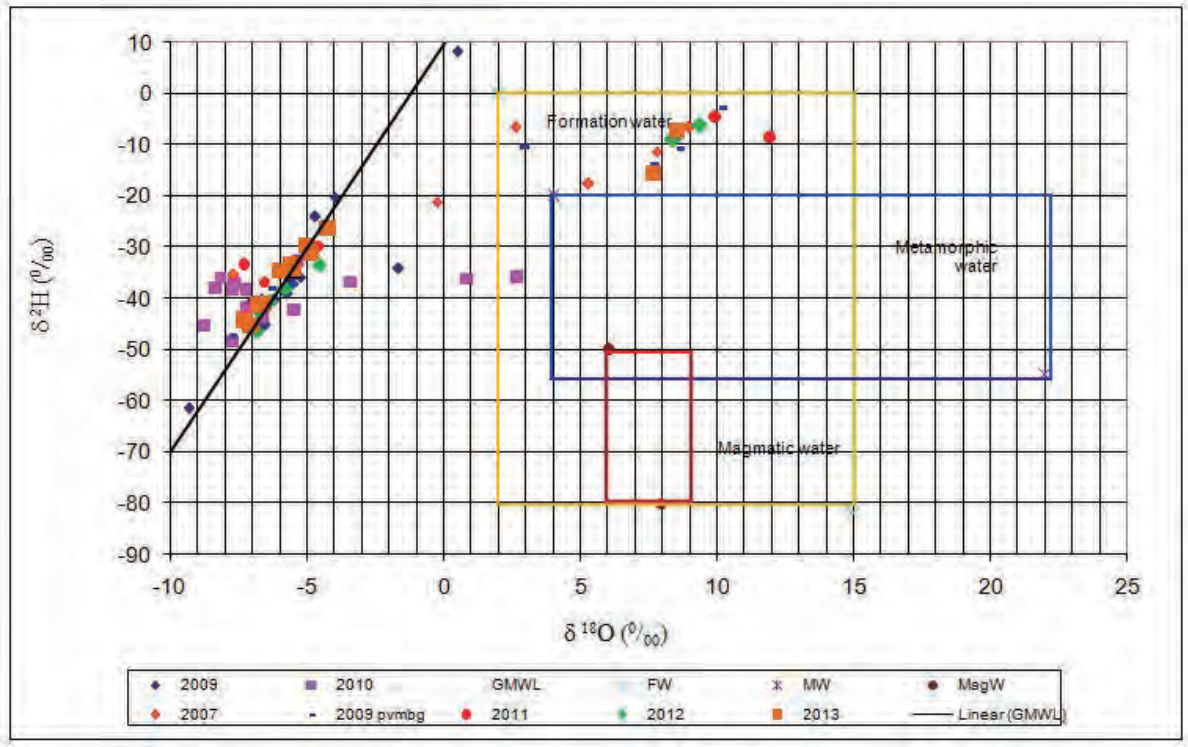

Fig. 7. Isotopes of deuterium and oxygen of water from Lusi and its surroundings which were collected periodically.

Mud extrusion from the main crater of Lusi is driven by hydrocarbon gases and steam at temperatures near to boiling point, whereas the extrusion of water in bubbles and outbursts around Lusi were triggered by hydrocarbon gases at normal temperatures. The hydrocarbon gases are thermogenic gases that are found in both areas and might be derived from depth and have reached the surface through the fractured area of the Watukosek fault zone but arrived at different locations and are in a different condition.

4. Conclusions

Liquids of the Lusi crater and those of outbursts and bubbles that are found in around Lusi differ in chemical composition and origin. Liquids of Lusi main crater are comprised of formation water from depth which was influenced by heating from cooling igneous rocks and were mixed with hydrocarbon liquid, whereas the water in outbursts and bubbles around Lusi are at normal temperatures and have younger ages and no hydrocarbon liquid. They are derived from different places through different processes. Liquid of the main crater at Lusi was derived from depth and was influenced by hydrothermal processes and the liquid of outbursts and bubbles around Lusi are derived from shallow formations which were contaminated with meteoric water.

Acknowledgments

The authors acknowledge Dr. R. Sukhyar, the Chief of Indonesian Geological Agency and Dr. Surono, the Chief of Centre for Volcanology and Geological Hazard Mitigation for their support of our work in Lusi. Special thanks are due to Prof. Hardi Prasetyo and M. Soffian of Sidoarjo Mud Mitigation Agency and Indra Badri, Andiani, Taat Setiawan, and Tatang Padmawidjaja of the Geological Agency of Indonesia for discussion and constructive

criticism during writing.

References

Aziz, F., 2007. What Happened with LUSI, Abstract on Geo Seminar, Pusat Survei Geologi.

Davies, R. J., Swarbrick, R. E., Evans, R. J., and Huuse, M., 2007. Birth of a mud volcano: East Java, 29 May 2006. GSA: vol. 17, no. 2, doi: 10.1130/GSATO1702A.1.

Kadar, A. P., Kadar, K., and Aziz, F., 2007. Pleistocene Stratigraphy of Banjatpanji-1 Well and the Surrounding Area. Abstract in International Geological Workshop on Sidoarjo Mud Volcano.

Lapindo, 2006. Banjarpanji "Mud volcano in the making", subsurface study. Geological Workshop of Mud Volcano, August 2006.

Zaennudin, A., Badri, I., Padmawidjaja, T., Humaida, H., and Sutaningsih, N.E., 2010. Fenomena Geologi Semburan Lumpur Sidoarjo. Badan Geologi.

Hazard mitigation of a caldera-forming eruption: From past experience in Indonesia to modern society

Akira Takada[1], Ryuta Furukawa[1], Kiyoshi Toshida[2], Supriyati D. Andreastuti[3], Nugraha Kartadinata[3]

[1]Geological Survey of Japan, AIST
[2]Central Research Institute of Electric Power Industry, Japan
[3]Center of Volcanology and Geological Hazard Mitigation, Indonesia
e-mail: a-takada@aist.go.jp

Abstract

A caldera-forming eruption can cause huge direct damage through widespread pyroclastic flows, ash fall, and tsunami as well as global impacts such as climate change. Indonesia has suffered twice during the last 200 years, and three times within 1,000 years. This paper tried to evaluate the potential for future caldera-forming eruptions using the eruptive histories of Indonesian volcanoes. Precursor events to a caldera-forming eruption were compiled for this purpose. We proposed various problems to modern society for hazard mitigation, using observations on past caldera-forming eruptions in Indonesia.

Keywords: caldera-forming eruption, large-volume eruption, precursor, eruptive history, volcanic hazard mitigation, Indonesian volcanoes

1. Introduction

A caldera-forming eruption, with an erupted volume of 10-1000 km^3 may cause very substantial direct damage through as widespread pyroclastic flows, ash fall, and even tsunami, as well as indirect global impacts such as climate change (Fig. 1). The recovery time is more than 10 years for climate, food and human health, and as much as 100-1000 years for land use. The Japanese people have forgotten such a caldera-forming eruption, because the last one occurred 7,000 years ago. Indonesia, however, has suffered such an eruption twice during the last 200 years, and three times within the last 1,000 years (Fig. 2). We all can learn valuable lessons from Indonesia's experience.

2. Evaluation of potential for a caldera-forming eruption

Here an evolutionary model for a caldera-forming eruption in Indonesia (Fig. 3) is proposed. The long-term evolution into a caldera-forming eruption in Indonesia was studied by Takada et al. (2000), Matsumoto and Takada (2000), and Toshida et al. (2012). This study differentiates between volcanoes evolving into caldera formation from those without caldera formation. The former volcanoes became quiet with only a few explosive eruptions during the last 10,000-5,000 years before the first caldera-forming episode (Takada et al., 2012, 2013). Some volcanoes experienced multiple caldera formation. Furukawa et al. (2012) studied a multiple caldera forming cycle in Bali. According to the model, the candidate evolving into a caldera-forming eruption is a volcano that is dormant following a large stratocone building episode. We must, however, distinguish between a target volcano that is accumulating magma from one that is terminating its activity. Moreover, some volcanoes are decreasing their potential for eruption by continuous degassing.

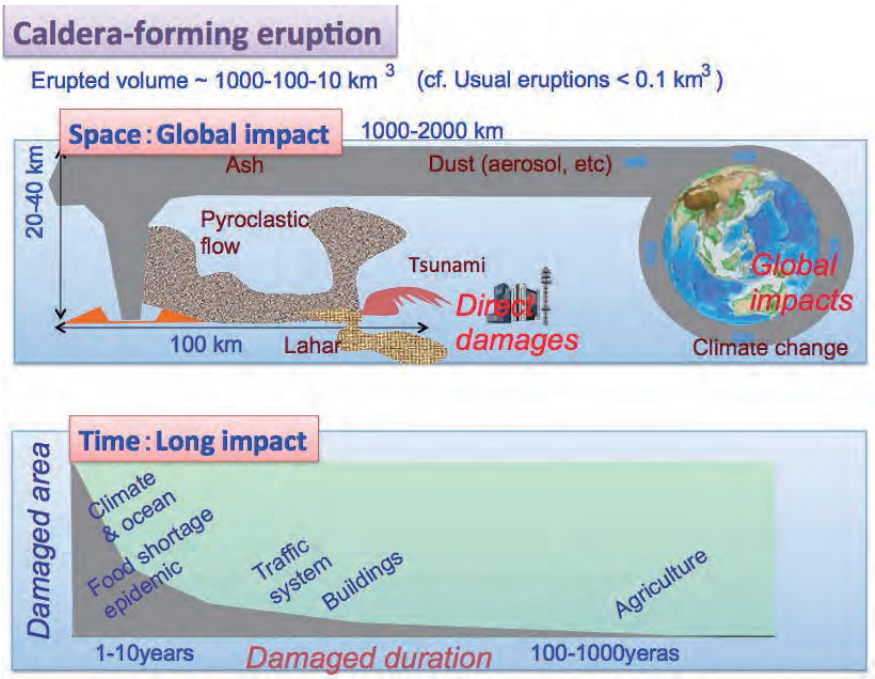

Fig. 1. Caldera-forming eruptions.

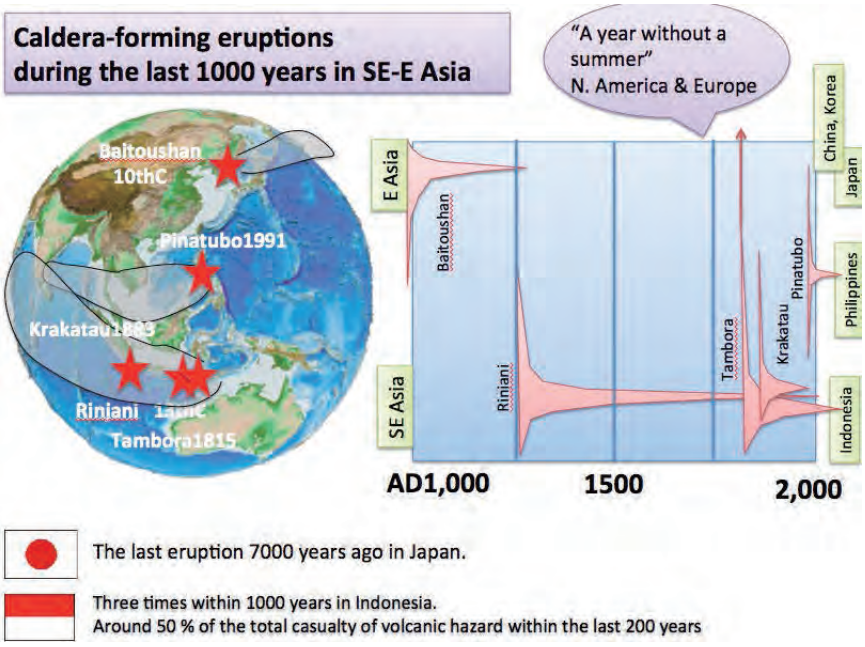

Fig. 2. Caldera-forming eruptions during the last 1000 years in East and Southeast Asia.

3. Precursor events

During the last a few months, we may have distinguished geologically short-term processes in the progressive activity towards the climax of an eruption in the cases of the Tambora 1815 eruption and Krakatau 1883 eruption (Takada, 2010; Takada et al., 2012, 2013) (Fig. 4). If a volcano reaches the stage just before its climax at the present time, we can recognize unusual geophysical signs from various monitoring systems. However, the problem is to evaluate or

predict when the volcano will reach a climactic condition, and how great a volume will be erupted. The evacuation plan depends on these latter factors.

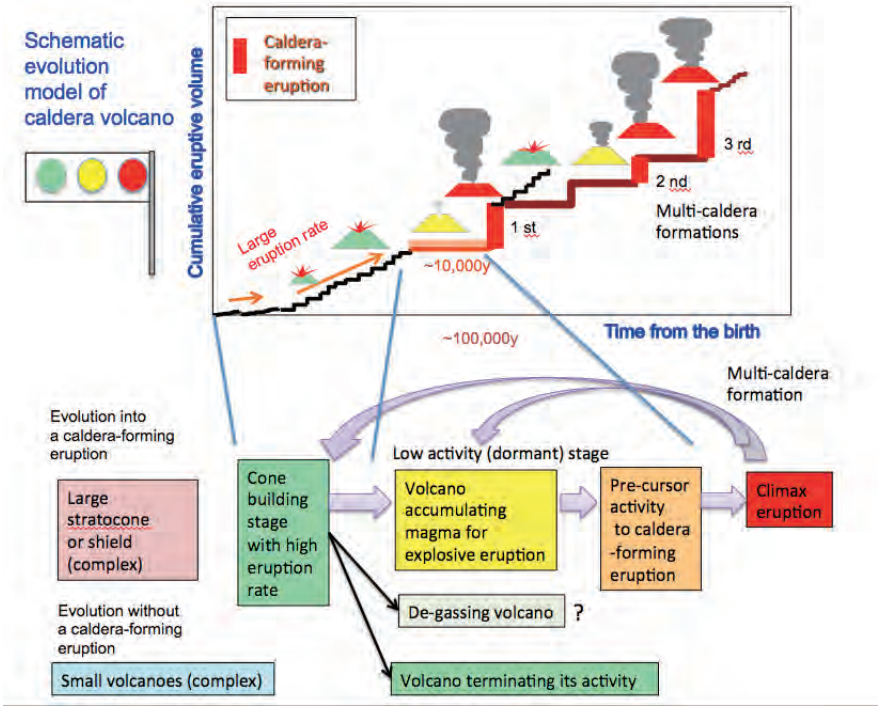

Fig. 3. Schematic model for the long-term evolution into a caldera-forming eruption.

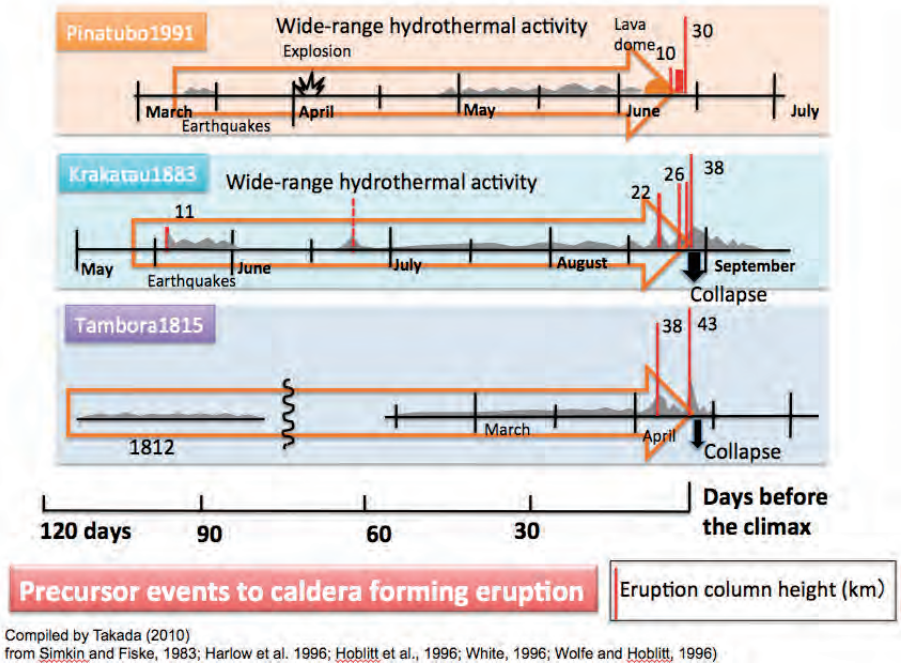

Fig. 4. Precursor events to caldera-forming eruption.

4. Linkage of disaster in the short-term (<10 years)

A caldera-forming eruption can cause a wide range of linked disasters (Fig. 5). Any

evacuation plan depends on factors such as the secondary, and the tertiary linked effects as well as the direct damage. Important considerations are the followings:

(1) The population on the earth has increased abruptly. For example, the modern population in Sumbawa is 0.9 million, compared with 0.1 million at the time of the Tambora 1815 eruption. Other areas in Asian countries are the same case as those above. (Fig. 6).

(2) Recently human society has developed with high technology, compared with the age of the caldera-forming eruptions in the 19th century. The larger the eruptive volume becomes, the wider the linkage is spread to cause traffic damage, energy plant damage, and various shortages, such as food, water and medicine, which connect with each other. For example, damage to the traffic system in an island country may close it to outside rescue due to volcanic ash-fall closing airports and tsunami causing coastal damage including ports or harbors.

(3) Climate change may increase the possibility of epidemics and food shortage. The aftermath of the Tambora 1815 eruption was “the year without a summer” (Stommel and Stommel, 1983).

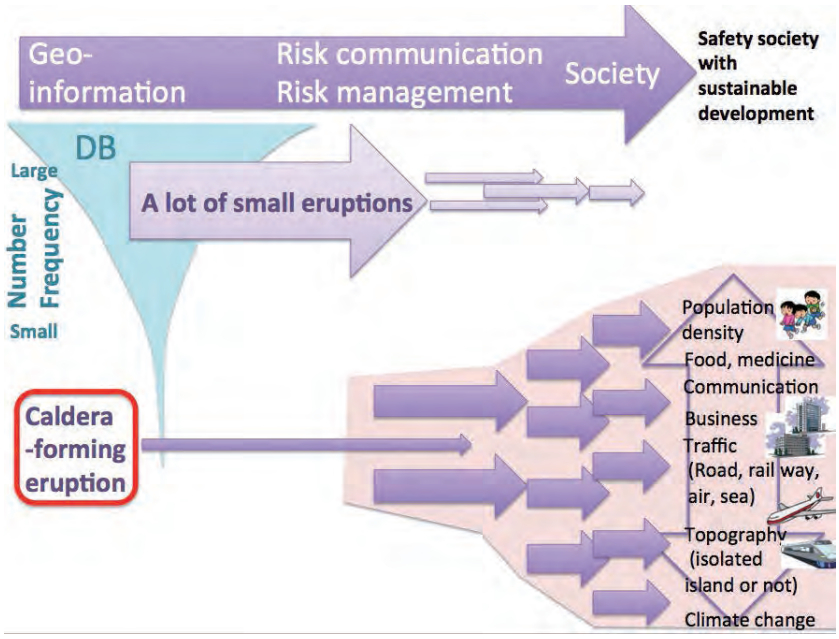

Fig. 5. Caldera-forming eruption will occur at a low frequency. However, a caldera-forming eruption causes a wide range of linked disasters. The problem remains how to convert past experience into modern societal conditions, and to evaluate a high order linkage system with vulnerability.

5. Long-term damage (> 10 years)

The damage in the area near the volcanoes that experienced caldera-forming eruptions can continues for a long time. For example, the accumulation of volcanic ash will cause lahars, block drainage (sewers) in a city, and result in air pollution. Thick pyroclastic flow deposits remain for a long time without erosion, and prevent agricultural development. The case of the Tambora 1815 eruption, 200 years ago, and that of Rinjani in the 13th Century, 700 years ago, are examples.

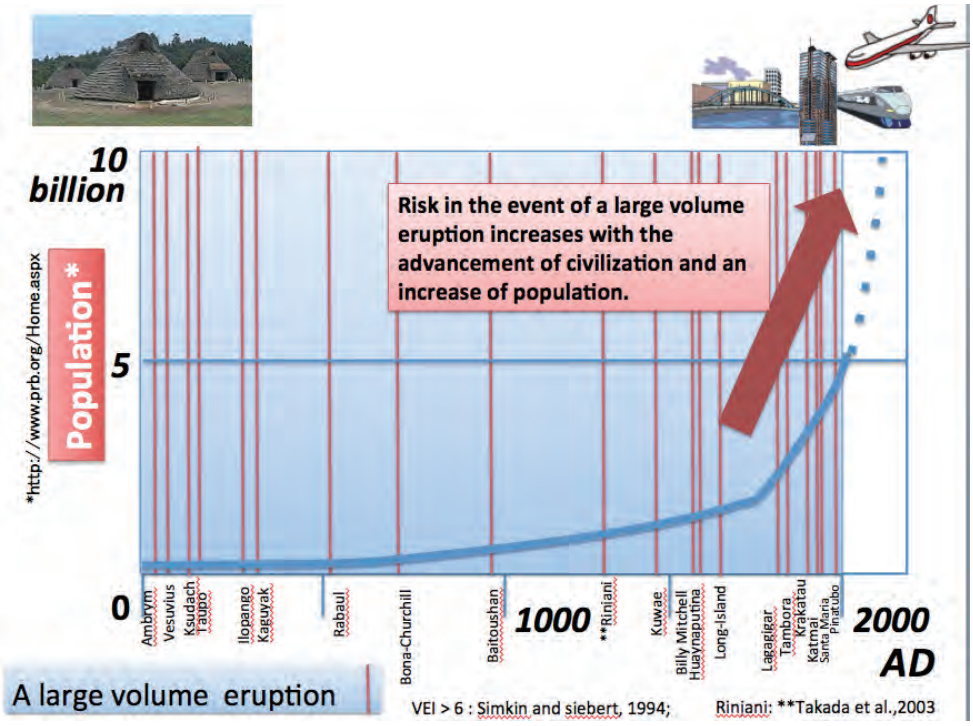

Fig. 6. Risk in the event of a large volume eruption increases with the advancement of civilization and an increase of population.

6. Conclusions

(1) A long-term evolutionary model of a caldera-forming eruption was proposed and potential evaluation for a caldera-forming eruption in Indonesia was attempted with the model.

(2) Precursor events of a caldera-forming eruption were identified up from three historical cases.

(3) Application of past experiences to modern societal conditions and development of a high order linkage system with vulnerability remains to be solved because the risks increase with the growth of infrastructural complexity and population.

(4) The eruptions of Tambora in 1815 and Rinjani in the 13th Century were presented as cases to show long-term damage in their vicinities after the caldera-forming eruption.

References

Furukawa, R., Takada, A., Toshida, K., Andreastuti, S., Kadarsetia, E., Kartadinata, N., Heriwaseso, A., Pramboda, O., Wahyudi, Y., and Firmansyah, N., 2012, Explosive eruptions associated with Batur and Bratan calderas, Bali, Indonesia, *G-EVER1 Abstracts Volume, Open-File Report of GSJ*, **557**, 114-115.

Matsumoto, A., and Takada, A., 2000, K-Ar age determination of lavas around Tmbora volcano, Indonesia, *Report of International Research and Development Cooperation ITIT Projects. Research on Volcanic Hazard Assessment in Asia. AIST, METI*, 83-87.

Stommel, H., and Stommel, E., 1983, Volcano Weather. *Seven Seas Press, Newport RI*, 177p.

Takada, A., 2010, Caldera-forming eruptions and characteristics of caldera volcanoes in the Sunda Arc, Indonesia. *J. Geol. Soc. Jpn*, **110**, 473-483 (in Japanese with English abstract).

Takada, A., Yamamoto, T., Kartadinata, N., Budianto, A., Munandar, A., Matsumoto, A., Suto, S., and Venuti, M. C., 2000, Eruptive history and magma plumbing system of Tambora volcano, Indonesia, *Report of International Research and Development Cooperation ITIT Projects. Research on Volcanic Hazard Assessment in Asia. AIST, METI*, 42-79.

Takada, A., Furukawa, R., Toshida, K., Andreastuti, S., Karatadinata, N., 2012, Geological evaluation of frequency and process of caldera-forming eruption: a compiled study of Indonesian caldera volcanoes, *G-EVER1 Abstracts Volume, Open-File Report of GSJ*, **557**, 119-121.

Takada, A., Furukawa, R., Toshida, K., and CVGHM, 2013, Can we evaluate a potentiality of caldera-forming eruption?, *G-EVER1 International Symposium Abstracts Volume, Open-File Report of GSJ*, **576**, 44-46.

Toshida, K., Takeuchi, S., Furukawa, R., Takada, A., Andreastuti, S., Kartadinata, N., Heriwaseso, A., Prambada, O., Mulyana, R., and Nururim, A., 2012, Long-term variation of pre-caldera volcanic activity in Bali and in Tengger caldera region, East Java, *G-EVER1 Abstracts Volume, Open-File Report of GSJ*, **557**, 110-113.

The analysis of efficiency, social and environmental impacts of coastal erosion protection structures in Thailand

Prasertsak Ekphisutsuntorn[1], Somsak Piriyayota[2], and Worawut Tantiwanich[2]

[1]Visuddhi Consultants Co., Ltd., Thailand
[2]Department of Marine and Coastal Resources, Ministry of Natural Resources and Environment, Thailand

Abstract

The coastline of Thailand extends for 3,148.32 km along the Gulf of Thailand and the Andaman Sea in 23 provinces. The coastal areas are the economic base of the nation as they are important sources of natural resources. Almost 600 km of coastline (accounting for 23% of the total coastline) has been eroded, especially in the Upper Gulf of Thailand and the Eastern Gulf of Thailand. Different study methods and analyses have been used to solve the coastal erosion problems through engineering structures in different areas. The eight major coastal protection structures that have been used to solve the erosion problem in the Gulf of Thailand and the Andaman Sea are Sea walls, Offshore breakwaters Revetments, Jetties, Groynes, Bamboo fencing, Concrete piles fencing and Sand sausages. These eight types of structures are analyzed for effectiveness and social, economic and environmental impacts. The analysis shows that Sea walls are suitable for all beach types (sand beach, rock beach, mud beach), Offshore breakwaters are suitable for rock beach and sand beach, Revetments for rock beaches and sand beaches but it is necessary to rehabilitate the foundations when constructing the structures, Jetties are is suitable for rock beaches and sand beaches, Groynes for rock sand sand beaches, Bamboo fencing for mud beaches, Concrete piles fencing for mud beaches and Sand sausages are suitable for mud beaches but these structure also require rehabilitated foundations when under construction.

Keywords: coastal erosion, coastal protection structures, erosion problem, beach types, Thailand

1. Introduction

The coastline of Thailand extends for 3,148.32 km, including 2,055.18 km along the Gulf of Thailand, covering 17 provinces, and 1,093.14 km along the Andaman Sea, covering 6 provinces. Almost 600 km of coastline, especially in the Upper Gulf of Thailand and the Eastern Gulf of Thailand, have been extensively eroded as shown in Fig. 1.

The problem of coastal erosion occurs in most coastal areas of Thailand. In the past, government agencies and sectors have operated on mitigating and solving coastal erosion problems through various methods and forms of protection, the efficiency of which varied from area to area. Therefore, to select optimal protection methodologies, there must be consideration of various information, e.g. engineering, economic, social, and environmental aspects (Bangkok Metropolitan Administration, 2001, 2006).

In this study, the information concerning the different methods of coastal erosion protections were collected in order to evaluate their efficiency, effectiveness, social impacts and environmental impacts and to prepare primary guidelines for the selection of measures for protection and rehabilitation of areas experiencing coastal erosion and ways to minimize their impacts.

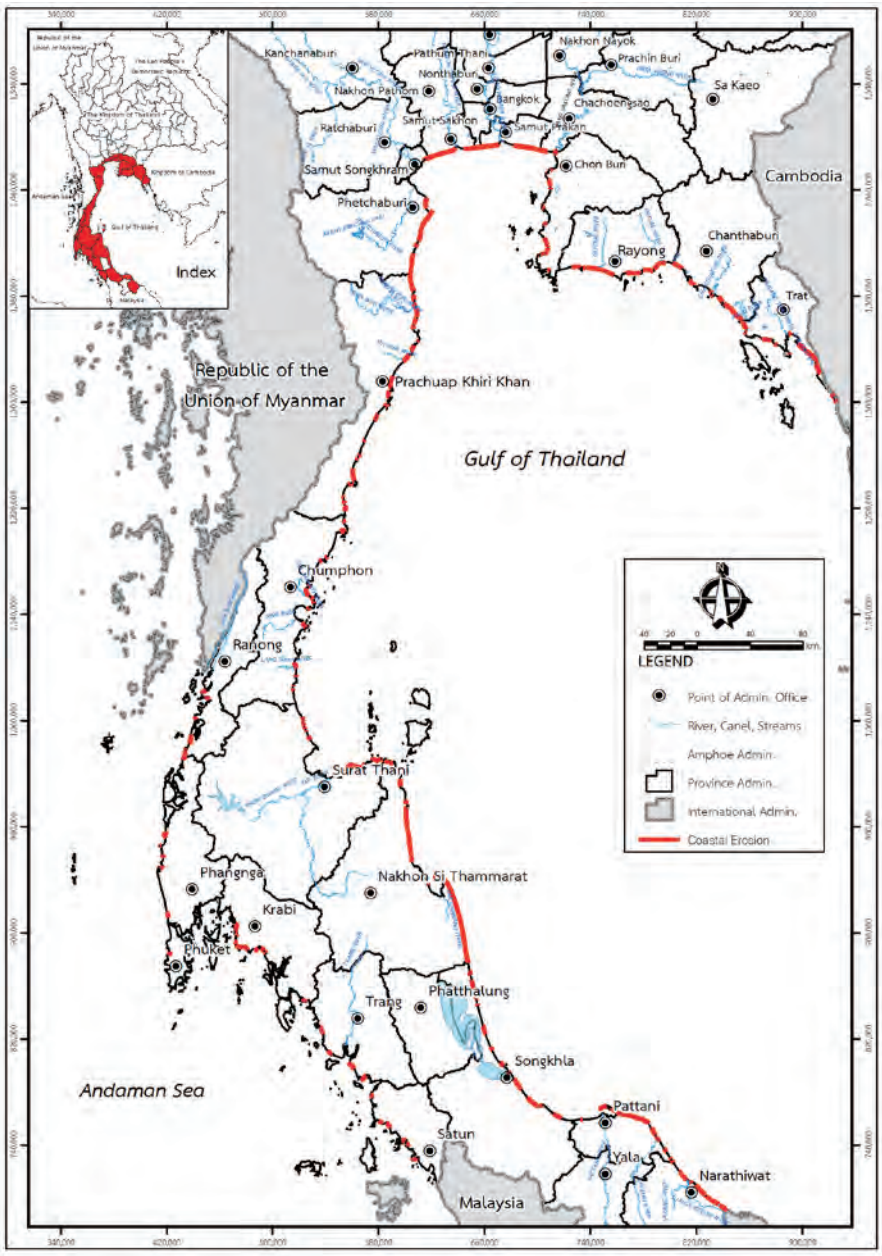

Fig. 1. The coastal erosion in the Gulf of Thailand.

2. Methodology

For the current conditions and erosion problems in the project area, aerial photographs and satellite images of the project area were collected for coastline change analysis. Coastline change was analyzed by using overlay techniques. Geographic Information System (GIS) included maps, aerial photography and satellite images which must be converted to the standard system therefore they can be compared and verified with survey data. The comparison of the coastline in years 1974, 1995, 2002 and 2011 enables analysis of the erosional and depositional areas in each period of time. The results of the coastline change analysis of the Gulf of Thailand in eight provinces from 1974-2011 in terms of the eroded and depositional areas are shown in Table 1 and Fig. 2 (Battjes et al., 1994).

Table 1. Summary of erosion and deposition area in eight provinces.

Study Area	Period	Erosion		Deposition	
		Place	Area (rai)	Place	Area (rai)
Rayong	1974-1995	33	2,221.79	12	193.6
	1995-2002	16	2,149.35	21	424.36
	2002-2011	37	288.8	20	74.44
Chachoengsao	1974-1995	13	916.05	10	172.63
	1995-2002	11	366.84	6	77.97
	2002-2011	12	230.22	6	43.2
Samut Prakan	1974-1995	16	5,285.61	15	854.53
	1995-2002	22	2,514.64	9	26.77
	2002-2011	45	1,354.33	15	66.29
Bangkok	1974-1995	1	899.97	0	0
	1995-2002	2	5,079.80	0	0
	2002-2011	1	61.65	1	14.72
Samut Sakon	1974-1995	7	1,179.18	21	22.82
	1995-2002	75	1,180.30	24	61.52
	2002-2011	84	669.59	76	126.11
Samut Songkharm	1974-1995	27	173.74	24	88.69
	1995-2002	18	296.56	4	531.38
	2002-2011	44	48.73	47	62.8
Phetchaburi	1974-1995	31	1,311.34	31	996.24
	1995-2002	46	673.43	47	493.21
	2002-2011	20	580.11	15	234.03
Songkhla	1974-1995	43	1,579.40	41	305.23
	1995-2002	36	230.57	28	80.62
	2002-2011	46	141.74	42	166.64

The study then involved the survey of the approaches used to prevent and solve the coastal erosion problems utilising eight forms of coastal erosion protection structures (total of 144 individual structures) in respective areas as shown in Table 2.

The survey of coastal erosion protection structures in eight provinces, namely Rayong, Chachoengsao, Samut Prakan, Bangkok, Samut Sakhon, Samut Songkhram, Phetchaburi and Songkhla, classified the data according to the eight forms of coastal erosion protection structures identified. The eight forms of protection structures are seawall, offshore breakwater, revetment, jetty, groyne, bamboo fencing, concrete piles fencing, sand sausage (Fig. 3). A selected case of each class of structure was studied and ranked, within their respective classes, in terms of their efficiency, effectiveness and social and environmental impacts, using the weighted-sum model for multiple-criteria analysis. The ones with the highest and lowest scores were then studied. The selection criteria for the case studies included each being a permanent structure of the government agency, having impacts on the community and being possible to operate. For the rated structures obtaining the lowest scores, additional rehabilitation measures were considered and detailed survey was conducted. The structures with the highest scores were studied for setting the preliminary guidelines for selecting coastal erosion protection measures. The parameters and weight of efficiency, effectiveness, social and environmental impacts can be summarized as shown in Table 3.

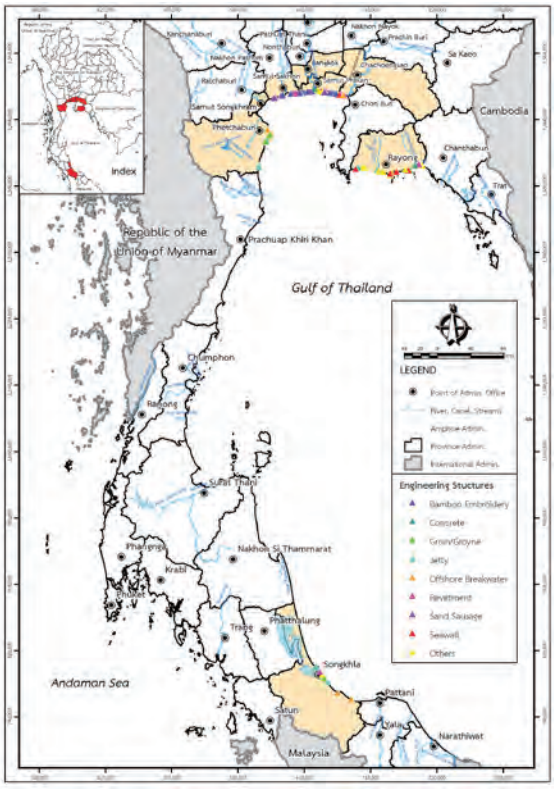

Fig. 2. The coastline change analysis of the Gulf of Thailand in eight provinces.

Table 2. Summary of erosion and deposition areas in eight provinces and respective number of protection/ mitigation structures.

Study areas	Number of structures
Rayong	24
Chachoengsao	7
Samut Prakan	15
Bangkok	3
Samut Sakhon	7
Samut Songkhram	4
Phetchaburi	40
Songkhla	14
Total	114

Table 3. Parameters and weight of efficiency, effectiveness, social and environmental impacts.

Parameter	Weight	Score
Coastal erosion protection	10	1: low, 2: moderate, 3: high
Environmental impacts	10	1: high, 2: moderate, 3: low
Slope stability and durability	8	1: low, 2: moderate, 3: high
Land use appropriateness	8	1: low, 2: moderate, 3: high
Operation period	6	1: x > 3 years, 2: 1 < x < 3 years, 3: x < 1 years
Cost-effectiveness	5	1: EIRR < 6, 2: 6 < EIRR <12, 3: EIRR> 12

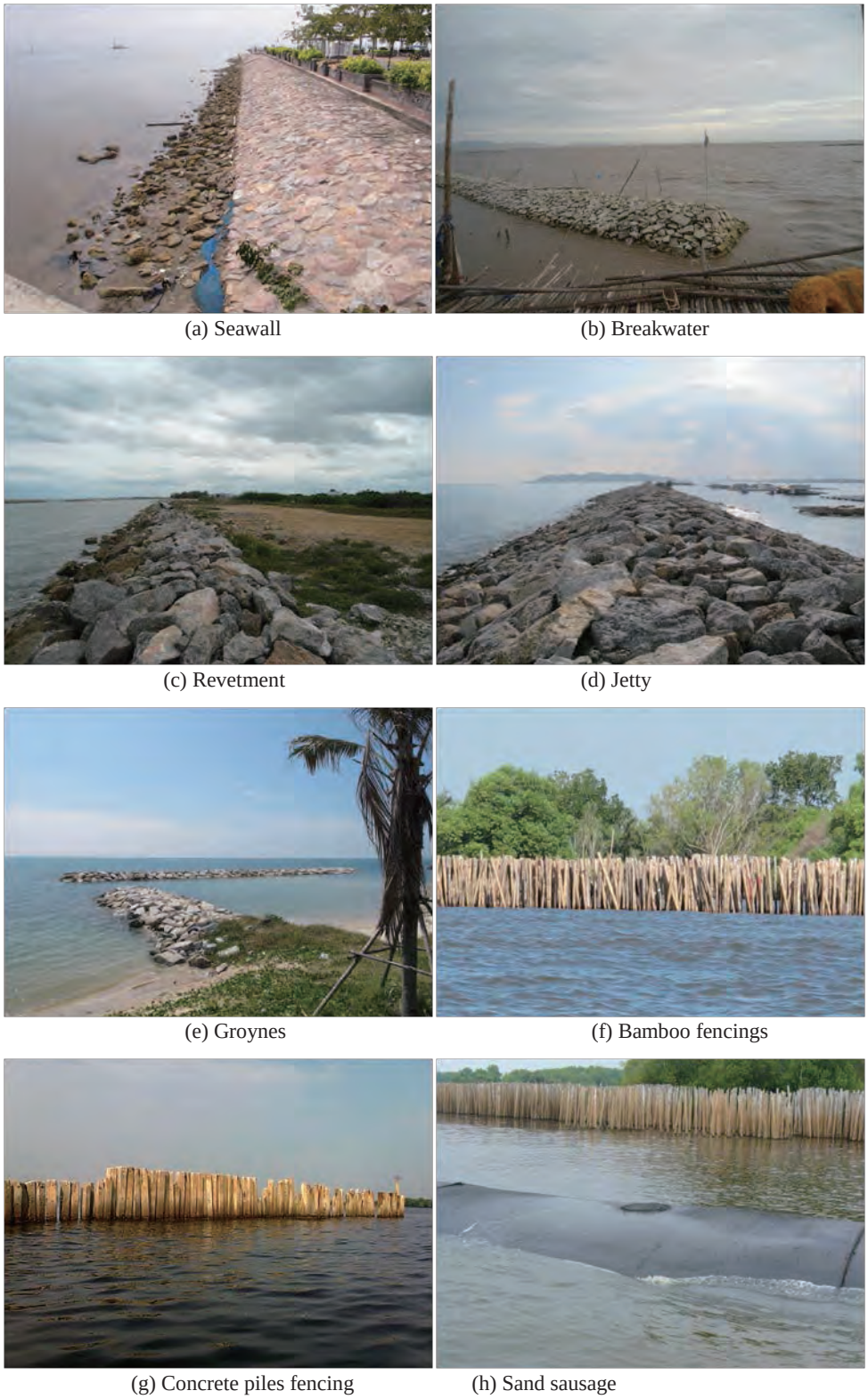

(a) Seawall (b) Breakwater

(c) Revetment (d) Jetty

(e) Groynes (f) Bamboo fencings

(g) Concrete piles fencing (h) Sand sausage

Fig. 3. The eight forms of coastal erosion protection structures.

3. Results and Discussion

The results of the analysis of the efficiency, effectiveness and social and environmental impacts of the eight models of coastal protection structures and selection of protective and rehabilitative measures for the selected cases are as follows (Hanson, 1987, 1989; Furukawa et

al., 1997; Royal Forestry Department, 2000; Department of Marine and Coastal Resources, 2013):

Sea wall

Sea wall is located parallel to the coastline, which is used for buffering wave impacts and erosion of the areas behind these. The structure chosen as the case study was the sea wall on the Puek Tian Beach in Puek Tian Sub-district, Tha Yang District, Phetchaburi as shown in Fig. 4. The Puek Tian Beach was a tourist beach, where the height of waves ranged from 0.25 to 1 m and the waves mostly moved towards the south, south-southeast and south-southwest respectively. The coastal area was composed of compact sand layers. The 20-year forecast revealed that the erosion on the Puek Tian Beach would be of 21,504 m^2 and the sedimentation would be of 1,235 m^2. The forecast of the case with or without the erosion protection under the measures in the next 10 years and 20 years suggested that the reinforcing coastal erosion control using geobags would be the most suitable. In the following 20 years, this would protect against erosion and bank failure and result in sedimentation of 7,600 m^2 maximally. The proposed structure would be stable but cause visual pollution to the beach.

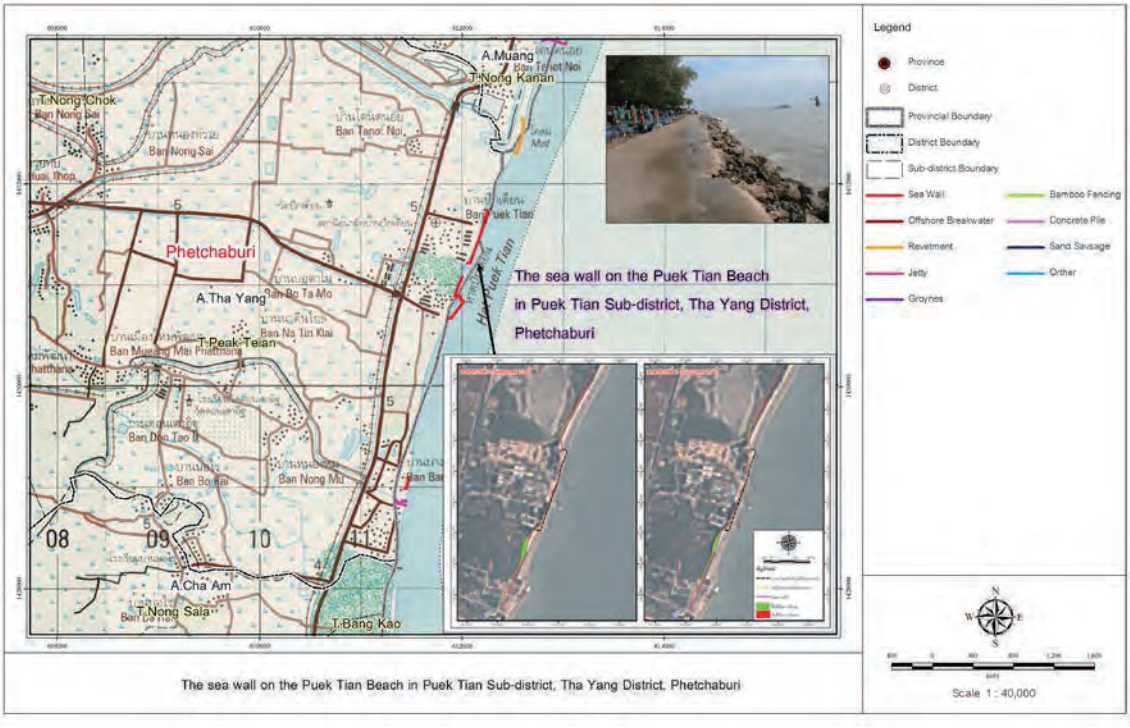

Fig. 4. The sea wall on the Puek Tian Beach in Puek Tian Sub-district, Tha Yang District, Phetchaburi Province.

Offshore breakwater

The offshore breakwater is a riprap structure located off the shore parallel with the coastline, intended to reduce the intensity of the waves towards the shore. The structure chosen as the case study was the offshore breakwater at Ban Khlong Charoen Wai in Song Khlong Sub-district, Bang Pakong District, Chachoengsao as shown in Fig. 5. The coastal community at the mouth of the Charoen Wai Canal was a fishery community, using canals as transport routes for fishing boats. Despite breakwaters, the area was still faced with erosion and shallowness at the mouth of the canal. The height of waves in the study area ranged from 0.25 to 0.75 m and the waves mostly moved towards the south-southwest, south and southwest

respectively. For the next 10 years and 20 years it was suggested that constructing jetties at the mouth of the Charoen Wai Canal with the exiting offshore breakwater as ripraps for protection of both sides would be the most suitable. This could prevent sedimentation at the canal mouth and protect against waves. The forecast of the case with or without the erosion protection under the measures in the next 20 years was that erosion would be of 16,000 m^2 and sedimentation would be of 15,200 m^2.

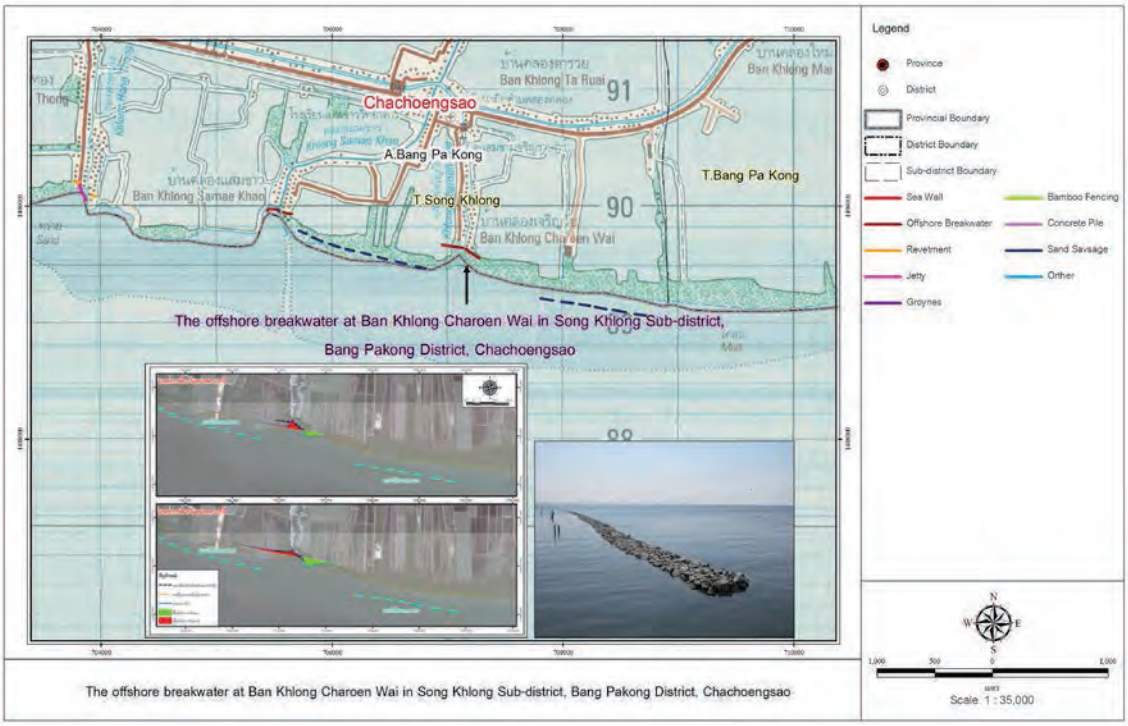

Fig. 5. The offshore breakwater at Ban Khlong Charoen Wai in Song Khlong Sub-district, Bang Pakong District, Chachoengsao.

Revetment

The revetment is a riprap structure parallel with the coast, used for buffering wave impacts and erosion behind the structure. The structure chosen as the case study was the revetment in the south from the mouth of the Bang Kula Canal in Hat Chao Samran Sub-district, Mueang Phetchaburi District as shown in Fig. 6. The study area south from the mouth of the Bang Kula Canal was open. In the area next to the jetty, there was a temporary revetment, which was dilapidated. The height of waves in the study area ranged from 0.25 to 1 m and the waves mostly moved towards the south, south-southeast and south-southwest respectively. The coastal area was composed of compact sand layers. The 20-year forecast showed that erosion in the south of the mouth of the Bang Kula Canal would be of 166,912 m^2 and the sedimentation would be of 206,203 m^2. The forecast of the case with or without the erosion protection under the measures in the next 10 years and 20 years suggested that improving the revetment next to the jetty to enable erosion protection would be the most suitable solution. It would protect against erosion and would not affect the adjacent areas. In the next 20 years, erosion would be of 1,430 m^2 and the sedimentation would be of 2,080 m^2.

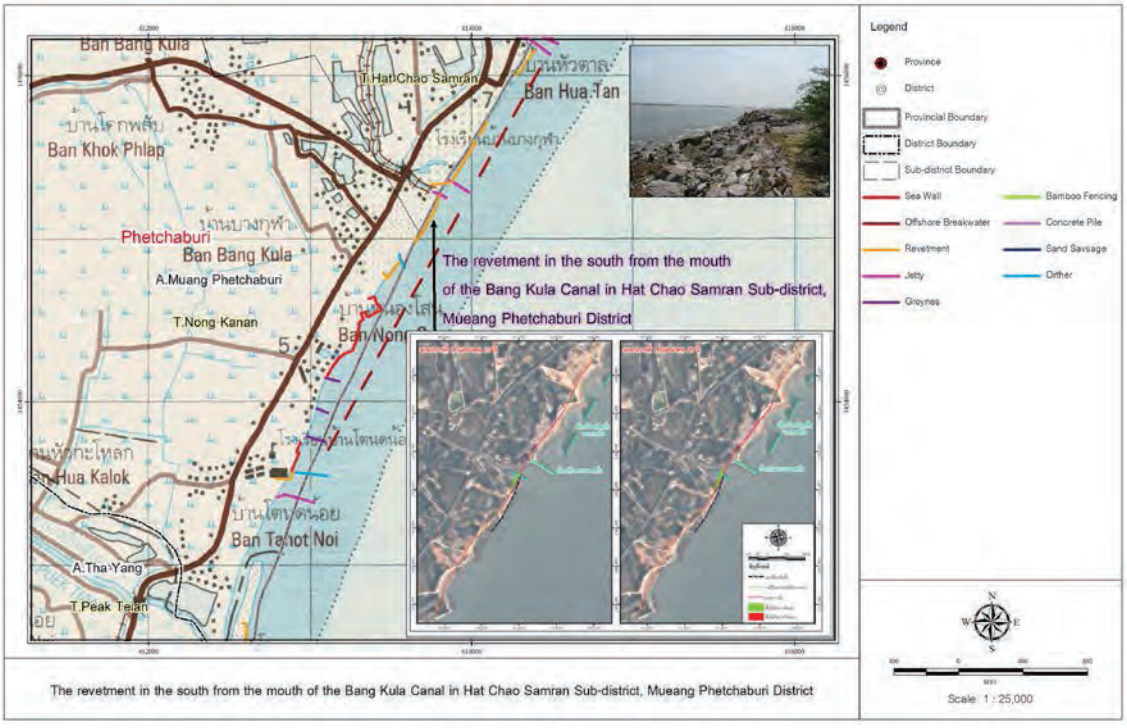

Fig. 6. The revetment in the south from the mouth of the Bang Kula Canal in Hat Chao Samran Sub-district, Mueang Phetchaburi District.

Jetty

The jetty is a parallel wall projecting from the estuary, used for preventing the deposition or blockage of sediments in the navigation channels. It does not protect against coastal erosion but may cause changes in the coastline in the adjacent areas. The structure chosen as the case study was the jetty at the mouth of the Hong Thong Canal in Song Khlong Sub-district, Bang Pakong District, Chachoengsao Province as shown in Fig. 7. The coastal community at the mouth of the Hong Thong Canal was a fishing community, using canals as transport routes for fishing boats. The exiting jetty and revetment were not very stable or strong. They were able to only partially protect against waves and protect the mouth of water channels. During the high tides, the structures could be flooded. The crest of the structures was below the mean high tide, causing low efficiency of wave and tide protection. The average height of waves in the study area was 0.86 m and the waves mostly moved towards the south-southwest, southwest, and south respectively. The coastal area was composed of clay and sandy clay layers, which were approximately 24 m thick. The 20-year forecast revealed that erosion at the mouth of the Hong Thong Canal would be of 155,522 m^2. The forecast of the case with or without the erosion protection under the measures in the next 10 years and 20 years suggested that the reinforcing of the jetty by big ripraps and constructing an offshore breakwater to reduce downstream impacts would be the most suitable as this would prevent sedimentation at the mouth of the canal and protect against sea waves without having any impacts on its adjacent areas. In the next 20 years, under the measure, the erosion would be of 34,640 m^2.

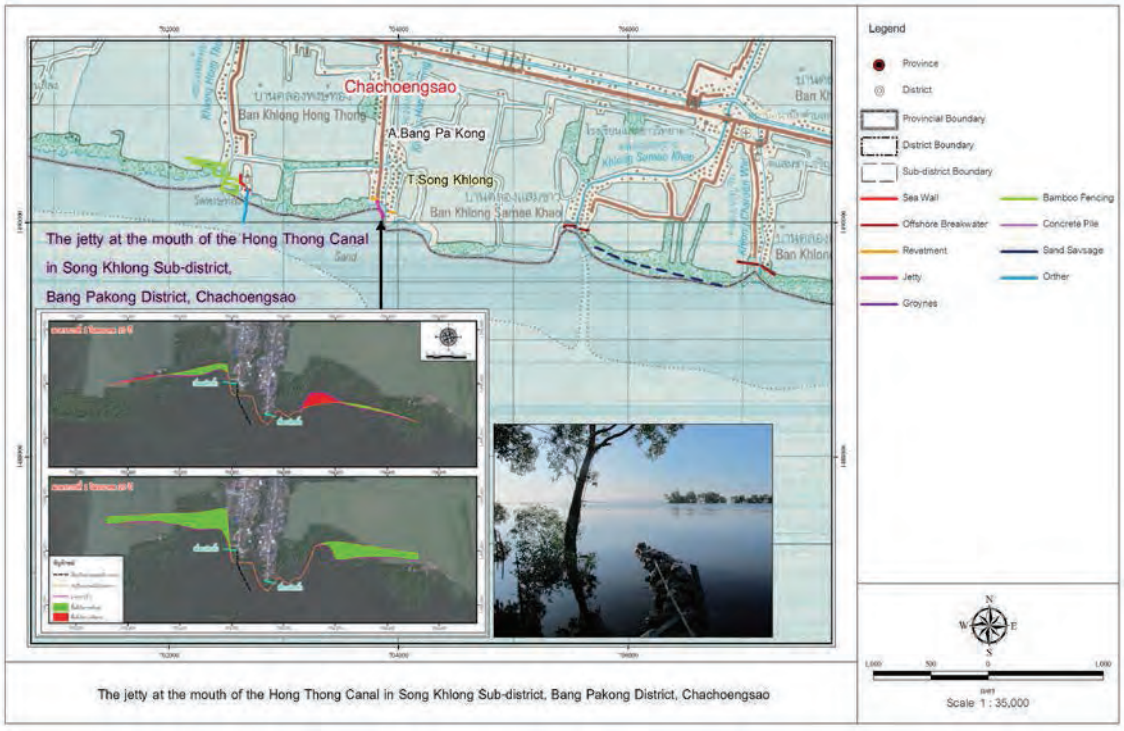

Fig. 7. Jetty at the mouth of the Hong Thong Canal in Song Khlong Sub-district, Bang Pakong District, Chachoengsao Province.

Groynes

Groyn is a structure that is perpendicular to the coastline, in order to trap sand drifting along the coastline and to stop sediment transport out of the coastline. Shapes of groynes include straight shape, T-shape, Y-shape, and fish tail shapes. The structure chosen as the case study were the groynes on the Saeng Chan Beach in Pak Nam Sub-district, Mueang Rayong District as shown in Fig.8. The Saeng Chan Beach is a tourist beach. The existing protection structures in the area included fish tail groynes and offshore breakwaters constructed between the groynes. The average height of waves in the study area equaled 1.06 m and the waves mostly moved towards the southwest, south, east southeast and west southwest respectively. The coastal area was composed of compact sand layers. The 20-year forecast revealed that the erosion at the Saeng Chan Beach would be of 1,112,296 m^2. The forecast of the case with or without the erosion protection under the measures in the next 10 years and 20 years suggested that extending the length of the onshore breakwater between groynes for sea wave dissipation by reducing the width of the open channels would protect against erosion without having any impacts on the adjacent areas and would be in harmony with the tourist beach. In the next 20 years, under the measure, the sedimentation would be of 15,550 m^2 maximally.

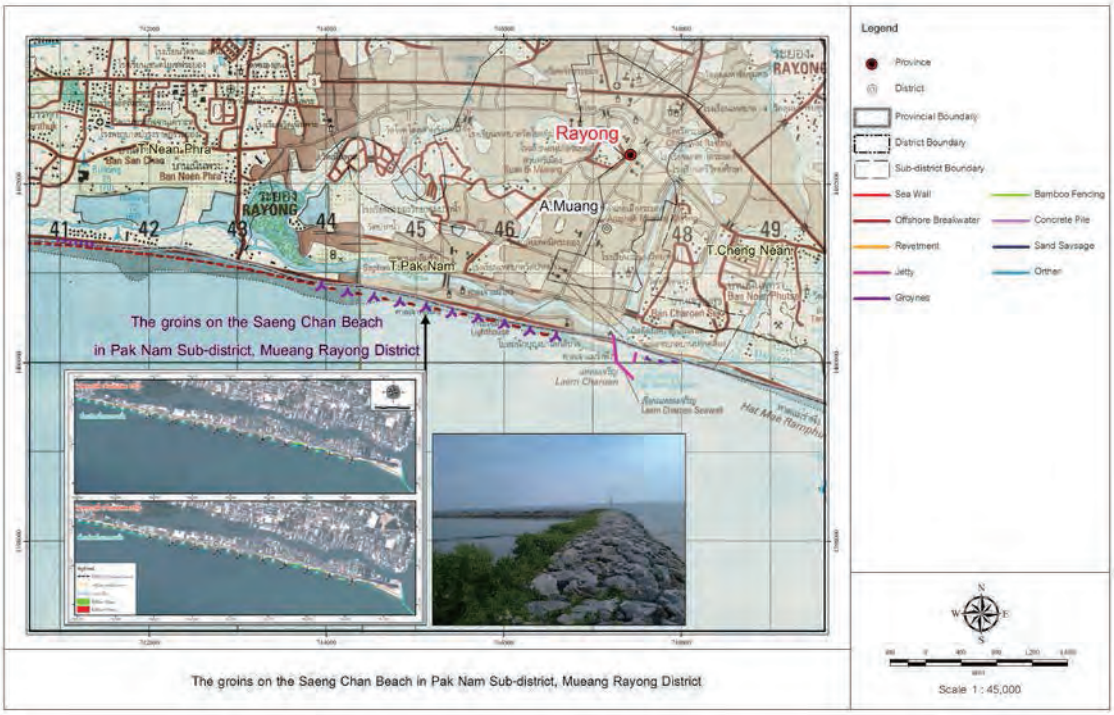

Fig. 8. Groynes on the Saeng Chan Beach in Pak Nam Sub-district, Mueang Rayong District.

Bamboo fencing

The structure is a wall made with bamboo sticking in the seabed with tips above the water surface. It is built for dissipating the energy of waves hitting the shore. The rough giant bamboos are more commonly used rather than monastery bamboos because they have a longer service life (3-4 years). Although rough giant bamboos are more expensive, they are more cost-effective. They suit the areas where winds are not strong and there are mud beaches. The structure chosen as the case study was the bamboo fencings in Laem Fa Pha Sub-district, Phra Samut Chedi District, Samut Prakan as shown in Fig. 9. The coastal community at Laem Fa Pha was a fishery community, using only one line of bamboo fencings to delay waves moving onto the coast. The bamboo fencing line was parallel with the coast, but the erosion behind the bamboo fencing line still occurred as the waves could travel through the bamboo line, and the Bamboo fencings were dilapidated. Each of the bamboo fencings had a diameter of 10 cm and all formed a line with a length of 5 km. The average height of waves in the study area was 0.86 m and the waves mostly moved towards the south-southwest, southwest, and south respectively. The coastal area was composed of soft soil layers. The thickness of the clay and sandy clay layers was approximately 24 m. The 20-year forecast revealed that the erosion at Laem Fa Pha would be of 112,311 m^2. The forecast of the case with or without the erosion protection under the measures in the next 10 years and 20 years suggested that installing more than one line of bamboo fencing (parallel with the coast) and blocks of bamboo fencing (perpendicular to the coast) would protect against erosion and reduce sediment transport on the coast. This would be in harmony with the mud beach and would not have any impacts on the adjacent areas. In the next 20 years, under the measure, the sedimentation would be of 15,550 m^2 maximally.

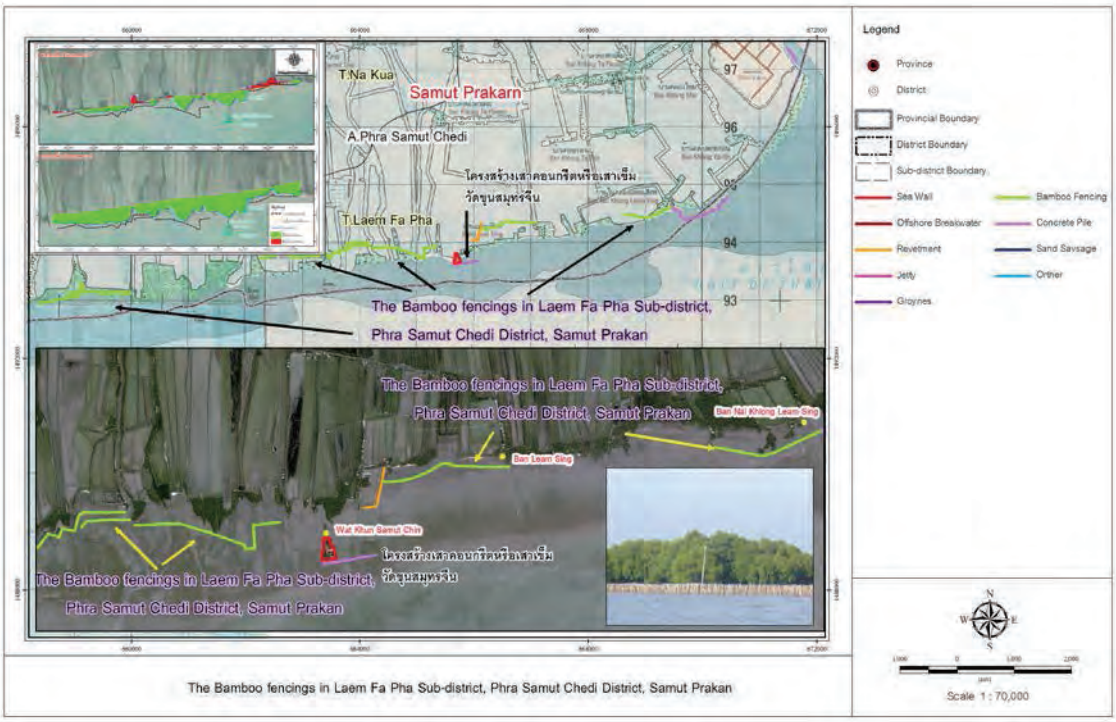

Fig. 9. Bamboo fencing in Laem Fa Pha Sub-district, Phra Samut Chedi District, Samut Prakan.

Concrete piles fencing

The structure is composed of concrete piles formed as a wall above the water surface used for dissipating the energy of the waves before they hit the coast. It was mainly operated by local communities and sub-district administrative organizations. The average length of each concrete column was 6-8 m. The structure chosen as the case study was the concrete piles fencing at the mouth of the Khun Ratphinit Chai Canal in Tha Kham Sub-district, Bang Khun Thian, Bangkok as shown in Fig. 10. The coastal community of Bang Khun Thian was a fishery community. The existing structures were concrete columns to slow waves moving onto the coast.

The concrete columns were of 0.30x0.30 m with a length of 1.50-3.00 m located at the mouth of the Phitthayalongkorn Canal parallel to the coast. The length of the protection was approximately 50 m. Other coastal erosion protection structures included Bamboo fencings and revetments along 4.7 km of coastline. However, the area was still continually eroded, and no deposition of sediments occurred. The average height of waves in the study area was 0.86 m and the waves mostly moved towards the south-southwest, southwest, and south respectively. The coastal area was comprised of clay and sandy clay layers, which were approximately 24 m thick. The 20-year forecast revealed that the erosion of the Bang Khun Thian Coast would cover 183,046 m^2, and the sedimentation in the area would be of 13,453 m^2. The forecast of the case with or without the erosion protection under the measures in the next 10 years and 20 years suggested that the installing an onshore revetment behind the concrete piles would protect against erosion without having any impacts on the adjacent areas. In the next 20 years, under the measure, the sedimentation would be of 53,030 m^2.

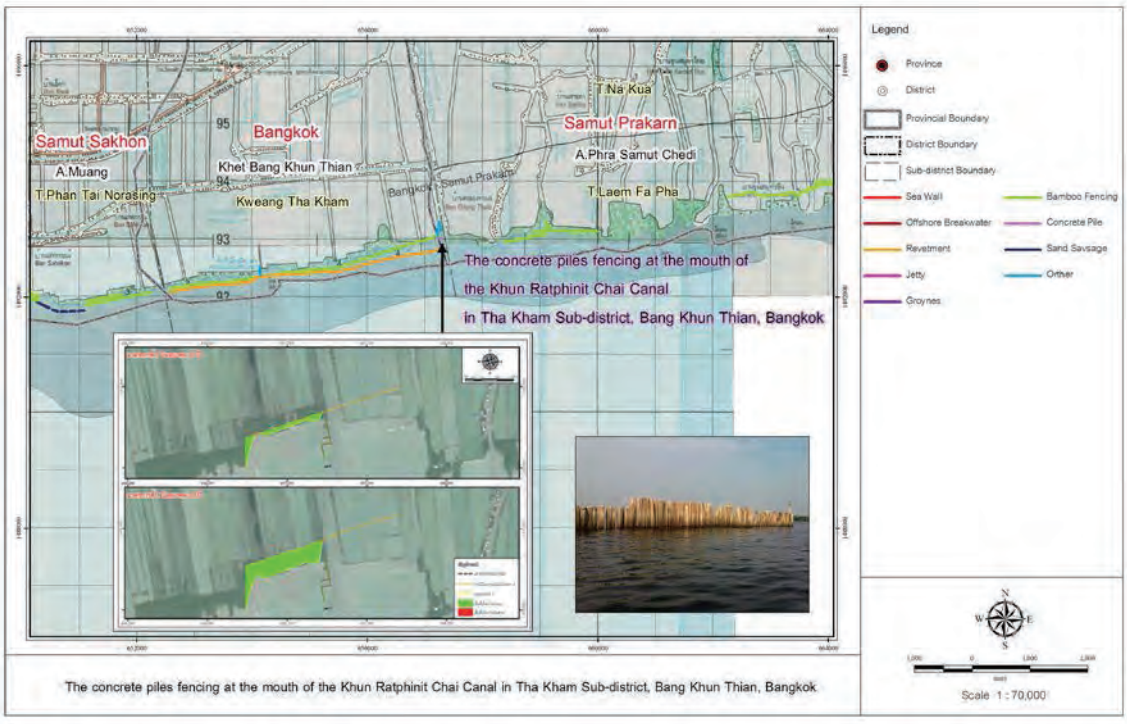

Fig. 10. Concrete piles fencing at the mouth of the Khun Ratphinit Chai Canal in Tha Kham Sub-district, Bang Khun Thian, Bangkok.

Sand sausage

Sand sausages are large sand bags, made with synthetic fibers and packed with sand by pump. They are placed parallel with the coastline, used for reducing the intensity of waves towards the coast. They have a diameter of approximately 1.8-2.1 m with a length of approximately 100 m, placed 200-400 m away from the coastline. They are located 50 m away from each other. They are suitable for mud beaches. The structure chosen as the case study was the sand sausages in Bang Krachao Sub-District, Mueang Samut Sakhon District as shown in Fig. 11. The coastal erosion protection structures in the coast of Bang Krachao consisted of sand sausages with a length of around 200 m and a width of approximately 2-3 m, constructed by the Marine Department. They had subsided and were severely damaged. The existing bamboo fencing line was constructed by the Department of Marine and Coastal Resources. The average height of waves in the study area was 0.86 m and the waves mostly moved towards the south-southwest, southwest, and south respectively. The coastal area was composed of soft soil layers. The clay and sandy clay layers were approximately 24 m thick. The 20-year forecast showed that the erosion of the Bang Krachao Coast would cover 5,059 m^2, and the sedimentation in the area would be of 26,768 m^2. The forecast of the case with or without the erosion protection under the measures in the next 10 years and 20 years suggested that elevating the crest of the sand sausages would help protect against erosion without having any impacts on the adjacent areas. In the next 20 years, under the measure, the sedimentation would be of 546,775 m^2 maximally.

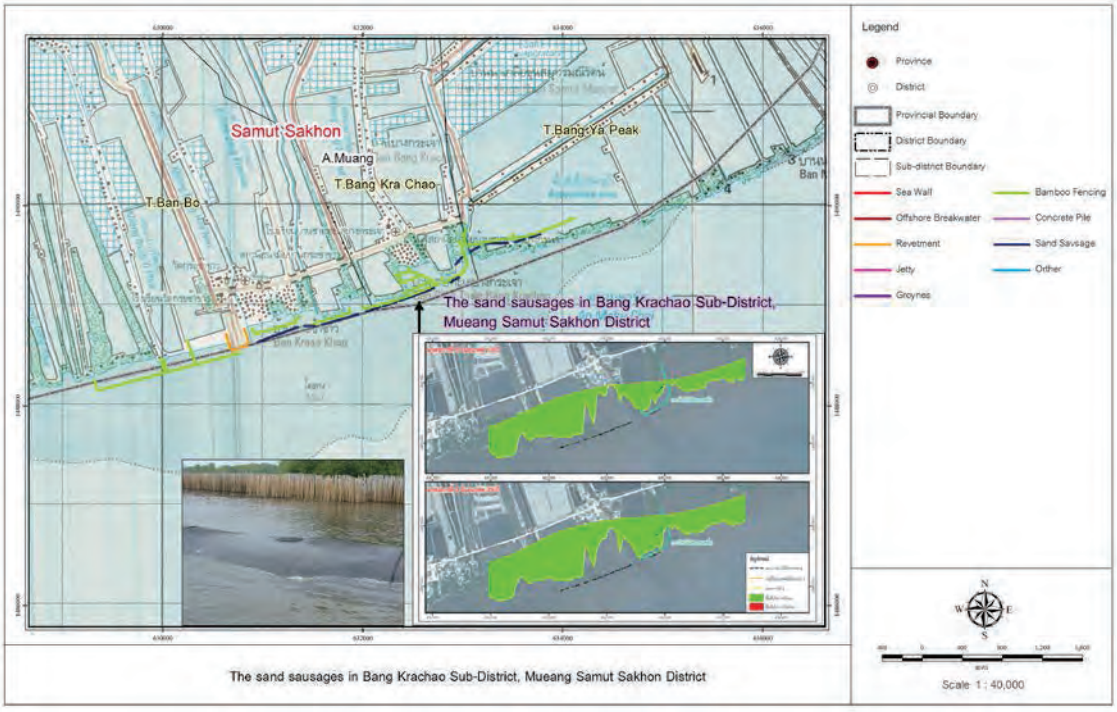

Fig. 11. Sand sausages in Bang Krachao Sub-District, Mueang Samut Sakhon District.

4. Conclusions

The primary approach to the selection of coastal erosion protection and rehabilitation measures for the areas affected by coastal erosion based on engineering, environmental, and socio-economic feasibility consists of the following two main factors as follows:

Geological conditions

This deals with the suitability of the structures and geological conditions, whereby beaches are classified into the following two groups such as 1) Rock beach and sand beach and 2) mud beach. The geological condition refers to the overall geological foundation derived from soil survey and not based merely on visual judgment.

Use of coastal land

This is related to economic, social, and environmental viability of the measures. Land use is classified into the following four groups such as 1) tourist attractions, 2) coastal communities, which are local communities, 3) mangrove forests, and 4) economically valuable areas.

Based on both factors, the primary approach to the selection of the measures for protecting and rehabilitating coastal erosion affected areas can be summarized through the diagram as shown in Fig. 12.

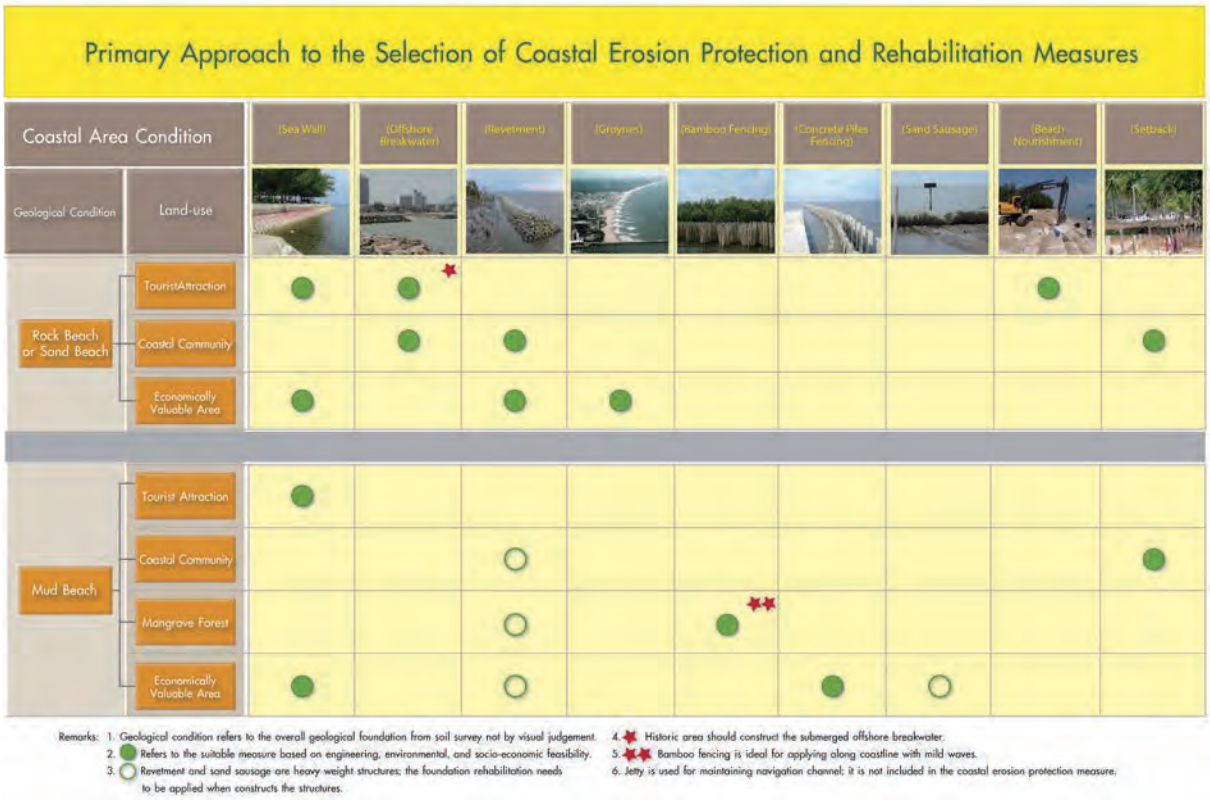

Fig. 12. Primary approach to the selection of coastal erosion and rehabilitation measures.

References

Bangkok Metropolitan Administration, 2001, Bangkhunthien pilot project coastal erosion and reclamation study, Ministry of Interior, Thailand, 75p.

Bangkok Metropolitan Administration, 2006, The Bangkhuntien shoreline protection and troubleshooting project, Bangkok, Thailand, 267p.

Battjes, J.A., Isaacson M., and Quick (Eds.), M., 1994, Shallow water wave modeling, Proceeding of Waves-Physical and Numerical Modelling, University of British Columbia, Vancouver, 1-24.

Department of Marine and Coastal Resources, 2013, Study, Survey, and Analysis of the Efficiency, Effectiveness, and Social and Environmental Impacts of Coastal Erosion Protection Structures in Thailand, Ministry of Natural Resources and Environment, Thailand, 185p.

Furukawa, K.,Wolanski, E., and Mueller H., 1997, Currents and Sediment Transport in Mangrove Forest, Estuarine, Coastal and Shelf Science, **44**, 301-310.

Hanson, H., 1987, GENESIS - A generalized shoreline change model for engineering use, Report No. 1007, Department of Water Resources Engineering, University of Lund, Lund, Sweden.

Hanson, H., 1989, GENESIS - A generalized shoreline change numerical model, Journal of Coastal Research, **5[1]**, 1-27.

Royal Forestry Department, 2000, The Feasibility Study on Mangrove Revival and Extension, Project in the Kingdom of Thailand, Draft Final Report, Sanyu Consultants (Thailand) Ltd., Panya Consultants Co., Ltd.

Coastal hazards in Indonesia with a case study in the northern coast of Java

Kumala Hardjawidjaksana

Marine Geological Research and Development Center, Ministry of Energy and Mineral Resources, Indonesia

Abstract

The major factors that affect the geological condition along the northern coastline of Java are the dynamics of discharge of rivers, the accumulation of deposited sediments, coastal processes, direction and strength of the winds, changes in coastal vegetation, changes in the shoreline caused by human activities and land subsidence. Coastal erosion is mostly caused by deforestation of mangroves, engineering projects in beach zones, hydroelectric damming of rivers (West Java), coastal hydrodynamics and subsidence. Sea level change is also a possible influence on coastal hazards in Indonesia.

The rate of coastal degradation of the Tirtamaya coastline ranges from 1 m to 10 m per year which is caused by sand mining that has reached an excavation rate of 700,000 cubic meters per year, deforestation of mangroves for coastal fisheries, and the occurrence of jetties in Balongan.

Land subsidence has occurred in Jakarta and Semarang with the rates of subsidence between 10-15 cm/year and 15 cm/year and more, respectively.

Recently, a case study in the Cipunegara Delta and its surrounding area has been undertaken in relation to geological hazards and their environments. Based on aerial photographs taken in 1946, it can be shown that further advance on the Pancer delta, and continued smoothing of the former delta lobe to the west has taken place.

There has been widespread removal of mangroves in the course of constructing tambak (brackish-water fishponds) in this area starting in the 1990s and with lack of sedimentation in places, these areas are being eroded as shown along the coast of Pondok Bali to the Muara Pancer Wetan. The others factors which influence this area are subsidence as shown in the seismic reflection profile, and sea level fluctuation with ranges between 9 and 15 mm/year (based on tide analysis and altimetry satellite data/TOPEX/Poseidon and JAS-1). Google Earth™ image in 2009 shows that the newly built northeast delta has advanced to the Java Sea by 5400 m since 1960 from the Dutch coast of 1942, indicating at least a 108 m/year advance.

Based on coastline mapping during the survey in May 2010, coastal erosion is seen to have occurred along the coast from Patimban village to Tanjungpura village from 1942 to 2010, and the coastline retreat is about 680 m in Trungtum village and 530 m in Mangsetan river mouth, therefore the average rate of erosion is 10 m/year in that area. To the west of the Cipunegara delta, coastal erosion in Pondok Bali is about 310 meter and in Legoksempring bay-Ujung Pamanukan (old distributaries channel) is about 780 m from 1942 to 2007, therefore the average rate of erosion is 4.7 m/year in Pondok Bali and 10.2 m/year in Legoksempring.

Coastal geological hazards were also induced by catastrophic events such as Krakatau's 1883 eruption that caused significant coastline changes surrounding the volcano in Sunda Strait. Other catastrophic events were Aceh's 2004 and Seram's 2006 earthquakes which were followed by tsunami that caused land subsidence, coastal landslides and inundation.

Keywords: coastal erosion, geohazards, land subsidence

1. Introduction

The major problems along the coastlines of Indonesia are caused by factors such as the dynamics of discharge of rivers, accumulation of deposited sediments, direction and strength of the winds, changes in coastal vegetation, changes in shoreline and coastal changes caused by human activities. Coastal erosion is mostly caused by deforestation of mangroves, engineering projects in beach zones, hydroelectric damming of rivers (West Java), coastal hydrodynamics and subsidence. Sea level is also a possibly influence on coastal hazards in Indonesia.

Geologically, the northern coastal area of Java is a part of the extensive coastal lowland belt of northern Java which extends eastward from the Sunda Strait to Surabaya (Fig. 1). This belt is mainly built up from unconsolidated clay and sand. This material comprising fluviatile (flood plain and channel deposits) and marine sediments (beach and beach ridges, mangrove, swamp, near shore, and shallow marine sediments) has been deposited since 6000 years ago with some beach ridges widening to form a deltaic plain. Generally the northern coast of Java is flat, especially around the coastal cities, and the shore is low lying with some parts swampy whilst the number of beach ridges increases northwards. Holocene sediments have been deposited along the old coastline of Java and are very sensitive to environmental changes such as erosion, flooding, pollution etc.

The problems and interesting phenomena on the northern coast of Java derive mainly from geological aspects and human pressure on the environment as shown in Fig. 2, illustrating how the anthropogenic aspect which might influence coastal erosion requires an integrated approach in the study area.

The coastal environments under study here are both the adjacent land and marine environments. Rapid development along the northern coast of Java currently requires integrated coastal zone management plans as the fast growth of cities in the coastal area of the northern coast of the island will require land resources. This land requirement will increase in the future and an integrated study of the coastal zone and of factors affecting the coastal environment and marine geo-hazards should be undertaken (Fig. 3).

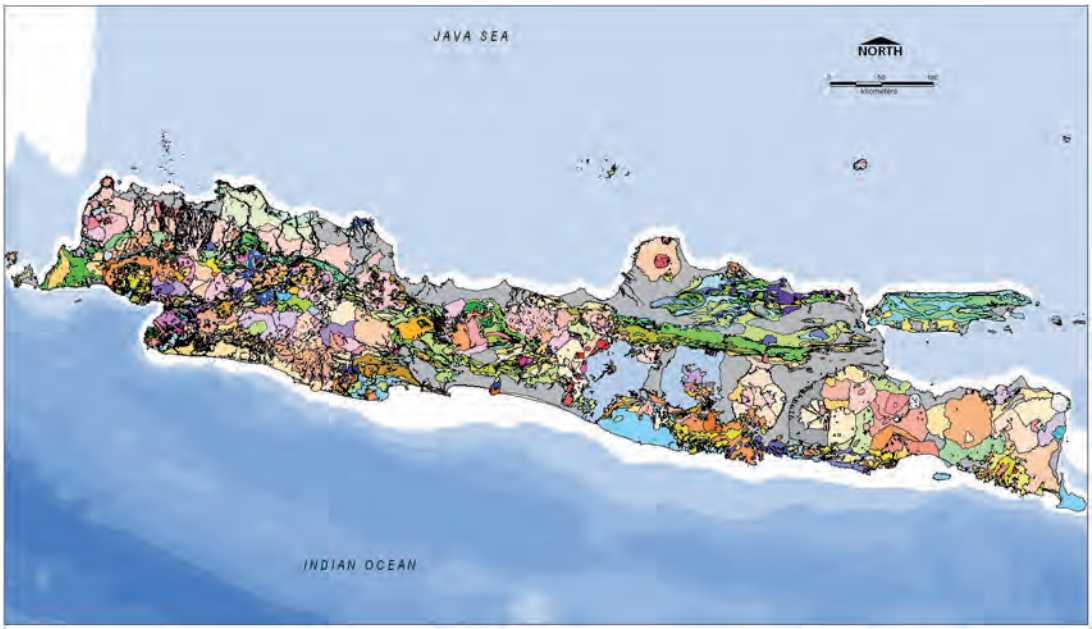

Fig. 1. Geological Map of Java Island.

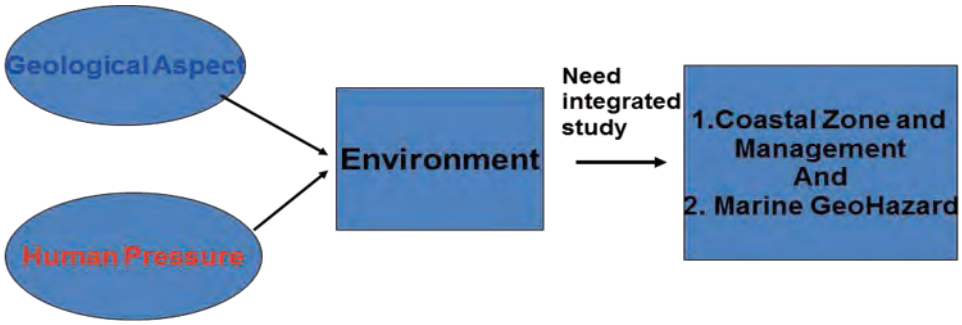

Fig. 2. Anthropogenic Aspects affecting the coastal environment requires integrated studies.

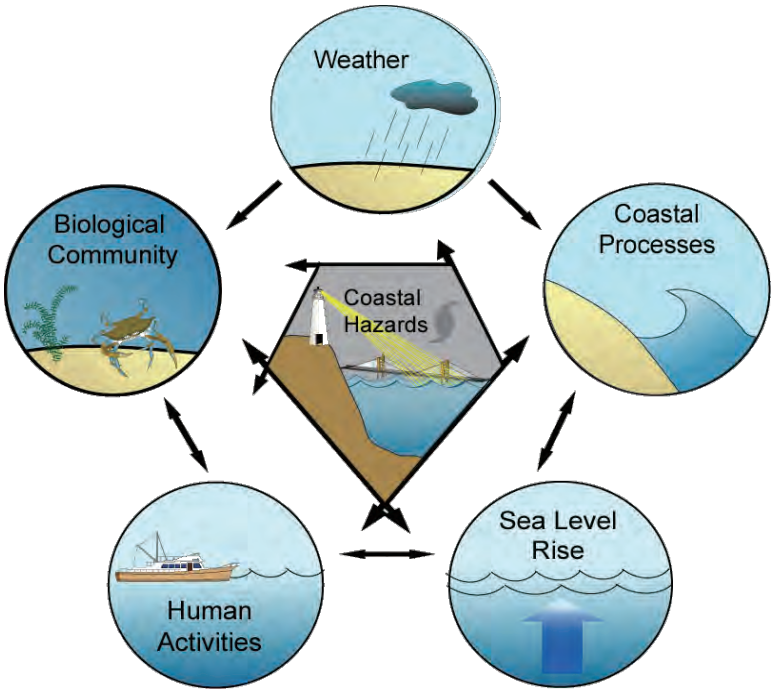

Fig. 3. Factors affecting coastal environment and coastal hazards (Pilkey et al., 1989).

Both the geological setting and the increasing population, especially in Banten Province and the cities of Jakarta, Cirebon, Semarang, and Surabaya, are responsible for the degradation and depletion of coastal resources. These problems can be attributed to the Indonesian intensive economic development plan and the high population density along the coast, as well as to the high level of poverty in the area.

Erosion of the northern Java coast is very serious, and without remedial action, a large land area will be lost to the sea. The erosion is caused mostly by mangrove deforestation, engineering work in beach zones, and the damming of rivers for hydroelectric power (West Java). Coastal hydrodynamics and land subsidence along with sea-level change are also possible causes of coastal erosion (Fig. 4).

2. Coastal erosion along the northern coast of Java

In Java Island, the most populated island, significant coastline changes are induced by dam construction in the hinterland that reduce sediment flow to the river mouths, development of harbours for the fishery industry and for boat building and also lack of sedimentation that

causes erosion in delta areas and their surroundings such as has occurred in Teluk Banten, Karawang, Pondok Bali and Cipunegara delta, Indramayu, and Tirtamaya coasts, Sidoarjo and in the north of East Java (Usman et al., 1996).

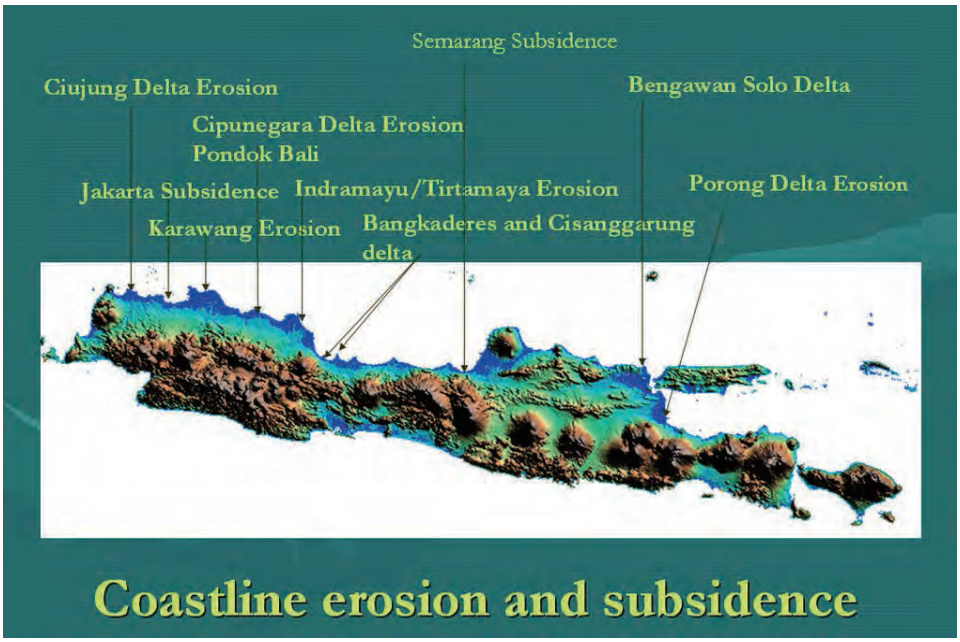

Fig. 4. Coastal erosion and subsidence along the northern coast of Java.

In Teluk Banten the Holocene sediments increase from the west to the east. The maximum thickness of Holocene sediment is found in the delta growth area from the Ciujung River. The Teluk Banten area, especially in the western part, is a very rapidly developing into an industrial and urbanised area. It is to become one of the major growth areas to the west of Jakarta, Indonesia's capital city. To support an industrial development zone an international container port is being built at Bojonegara. In the marine area, there is a marine ecosystem with sea-grass, fish, coral reefs (growing especially along the coastline and in the small islands) and also bird sanctuaries. The human activity results in environmental degradation in the bay for example by coral extraction or harvesting, by bay traffic, over-fishing, seaweed culture, mangrove clearing/cutting and increase of sediment load from land. Bathymetric data indicate the effects of some of these activities.

In some parts of the delta there is erosion from the river mouth to the east of the river. This is due to the new channel that was built to the northeastern part resulting in accretion in the front of the new channel (Fig. 5). The lack of sediment from the old channel of the river is causing abrasion along the coast of the Old Ciujung River delta.

On the north coast of Java, coastal changes are also related to the construction of dams such as in the hinterland of the Citarum River which much reduced the sediment flow and is causing coastal erosion to some parts of the delta. Coastal accretion occurred in the area of Ciparage - Sukajaya, Mekarpohaci, Cemarajaya - South Pusakajaya and East & West Tanjungpakis (Fig. 6; Usman and Yuningsih, 2007). To the east of Karawang District there are the extensive depositional plains built up by the Cipunegara River.

A case study in the Cipunegara Delta and its surroundings has been undertaken in relation to coastal erosion (Hardjawidjaksana, 2009, 2010). The Cipunegara has a catchment of about 1,450 square kilometers, with mountainous headwater regions carrying relics of a natural

deciduous rain forest and extensive tea plantations; a hilly central catchment with teak forest, rubber plantations, and cultivated land; and a broad coastal plain bearing irrigated rice fields. The river meanders across this plain, branching near Tegallurung, where the main stream runs northwards and a major distributaries of the Pancer, flow to the north-east.

Aerial photographs taken in 1946 indicate further advance of the Pancer delta, and continued smoothing of the former delta lobe to the west which is confirmed by reference to the pattern of beach ridges truncated on the eastern shores of Ciasem Bay and the 1976 Landsat images which show that a new delta has been built out to the north-east (Fig. 7).

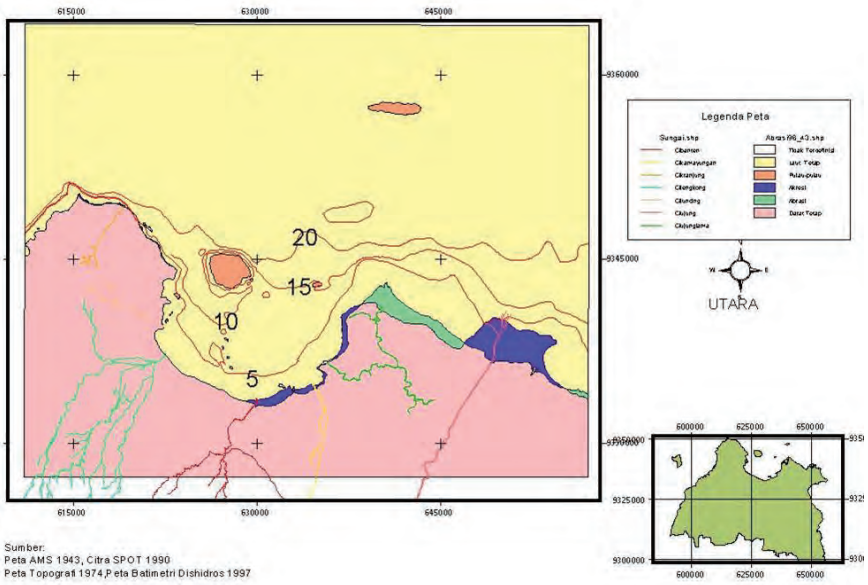

Fig. 5. Holocene sediment and coastline changes maps of Teluk Banten.

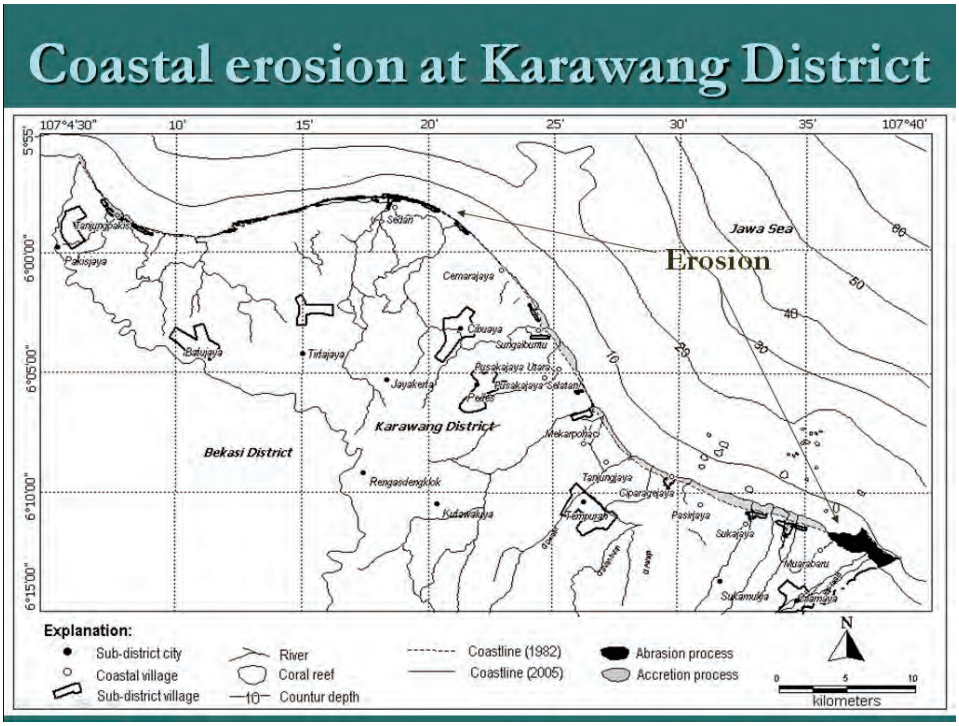

Fig. 6. Coastal erosion at Karawang District, West Java.

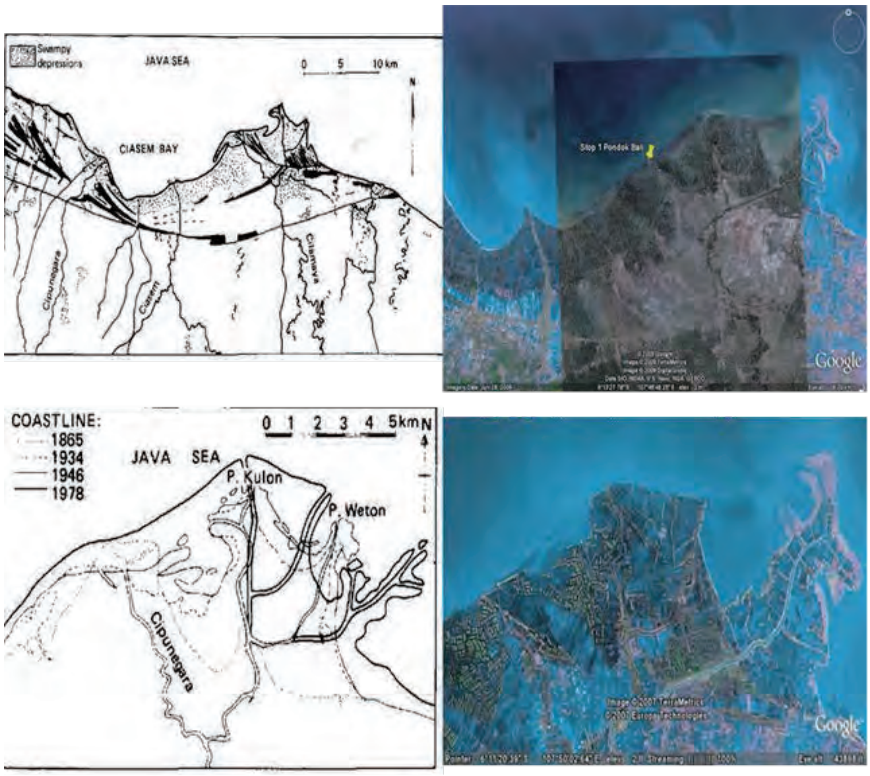

Fig. 7. Comparison of aerial photographs and Google Earth™ maps of the study area.

This delta was formed after the new northeast channel was built in 1960 to avoid flooding in the region. Along the coast of the Cipunegara delta, the mangrove fringe (mainly Rhizophora) has persisted on advancing sectors but elsewhere has been eroded or displaced by the construction of fishponds. There has been widespread removal of mangroves, in the course of constructing tambak (brackish water fishponds) in this area starting in the1990s, and with the lack of sedimentation in places these are being eroded such as shown along the coast of Pondok Bali to the Muara Pancer Wetan (Figs. 8 and 9).

Fig. 8. The widespread removal of mangrove in Pondok Bali.

Fig. 9. Coastal erosion at Pondok Bali.

The physiographic condition in the study area is generally a coastal plain which is not resistant to erosion which means that coastline change easily occurs in this area. Erosion features have been observed all along the coast on both of the two shore geo-types. Shoreline retreat is the more serious problem along the primary shorelines of the western sector on both developed and virgin areas. A survey of the distribution also shows that most of the affected coastal environments include those that evolved through the deposition of unconsolidated Quaternary sediment along the coast. Figure 10 shows the erosion that occurs along the coast of the study area.

Others factors which influence the shoreline changes in the Cipunegara Delta are: (1) Subsidence, (2) Sea level rise, (3) Sand mining, and (4) Long shore currents.

(1) Subsidence is recognized in the front of Cipunegara Delta where the structural geology is a northerly trending normal fault, identified from the seismic reflection profile as a graben in the north of Cipunegara river mouth (Fig. 11).

(2) Sea level rise in the Java Sea has affected the study area located in the northern part of Java. Thus the sea level in the Java Sea is shown to have risen by 0.5 cm/year (Ongkosongo, 2005), and Sutisna (2002) has shown that from Tanjung Priok, Semarang and Jepara the sea level rise is 0.8 cm/year. Abidin et al. (2008), based on a study in 9 coastal cities along the coast of North Java, concluded that the mean of sea level rise ranges between 9-15 mm/year (based on tide analysis and altimetry satellite data/TOPEX/Poseidon and JAS-1) as in Fig. 12.

(3) The other factor which much influences coastal erosion in the study area is sand mining along the coast as at Trungtum Village as shown in Fig. 13. The sand which is taken from the beach is at first collected at one place and then transported to the village for use in house construction.

(4) Longshore currents are also an important factor affecting erosion in the study area. Based on the results of the current study as shown in Fig. 14, the main flow of current at the time surveyed is to the northwest with a speed of 0.08 to 0.21 meter/second.

(a) **(b)**

Fig. 10. Coastal erosion at Pondok Bali and eastern study area.

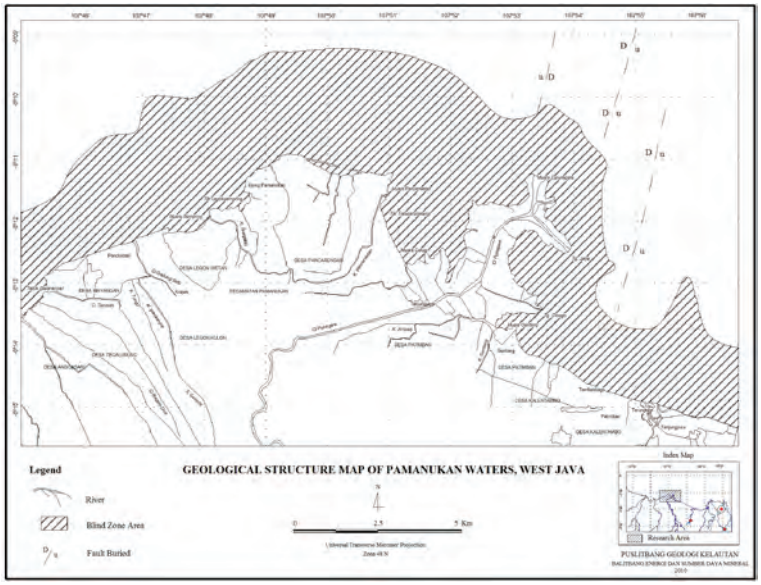

Fig. 11. Structural geology map of the study area.

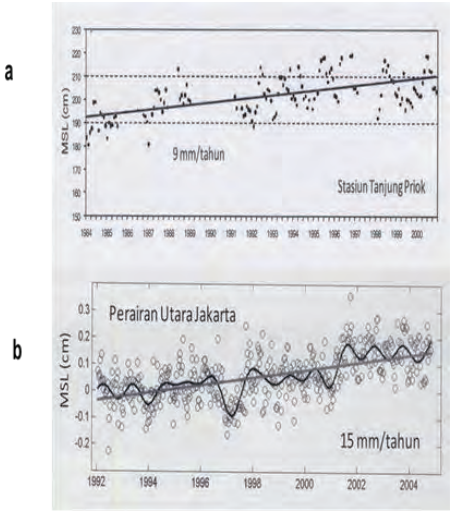

Fig. 12. Sea level rise in the Java Sea.

Fig. 13. Sand mining at Trungtum Village.

In order to reconstruct an updated shoreline migration history at an annual scale in the Cipunegara delta and its surroundings, we have recently compiled and calculated the available data which shows that it is a dynamic area where both shoreline accretion and shoreline abrasion can be found. Such effects are due to the changing of river channels and lack of sediment distributed to the sea.

Based on coastline mapping during the survey in May 2010, coastal erosion occurred along the coast from Patimban village to Tanjungpura village from 1942 to 2010, and the coastline retreat is about 680 m in Trungtum village and 530 m in the Mangsetan river mouth, therefore the average erosion is 10 m/year in that area. To the west of the Cipunegara delta, coastal erosion in Pondok Bali is about 310 meter and in Legoksempring bay-Ujung Pamanukan (old distributaries channel) it is about 780 m since 1942 up to to 2007, therefore the average erosion is 4.7 m/year in Pondok Bali and 10.2 m/year in Legoksempring. Google Earth™ image in 2009 shows that the newly built northeast delta has advanced 5400m from the Dutch coast of 1942 towards the Java Sea since 1960, an advance of at least 108 m/year (Fig. 15).

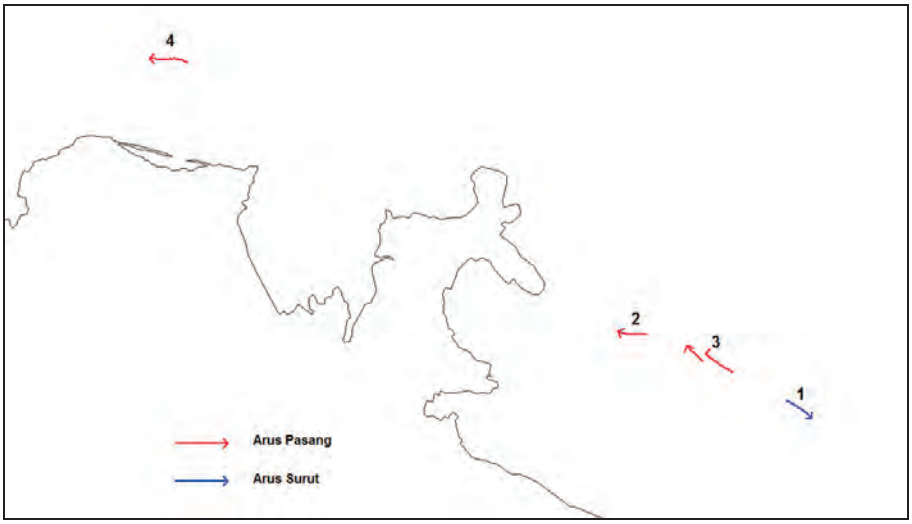

Fig. 14. Longshore currents the study area.

Fig. 15. Coastline changes in the Cipunegara Delta and its surroundings.

In Indramayu and its surroundings, the coastal erosion problem becomes more critical annually with people crowding against a retreating shoreline. Recently, the coastline of Indramayu in West Java, Indonesia, has undergone noticeable changes particularly since the development of the complex of the Cimanuk Delta. This delta was like a bird foot that was formed by accretion of three river mouths due to damage to the Pabean Udik dam in 1947 (Hehanussa, 1975, 1980). The growth of the Cimanuk delta has affected the coastal dynamics of Tirtamaya coasts including composition and distribution of sediment, coastal morphology and hydrodynamics (Fig. 16).

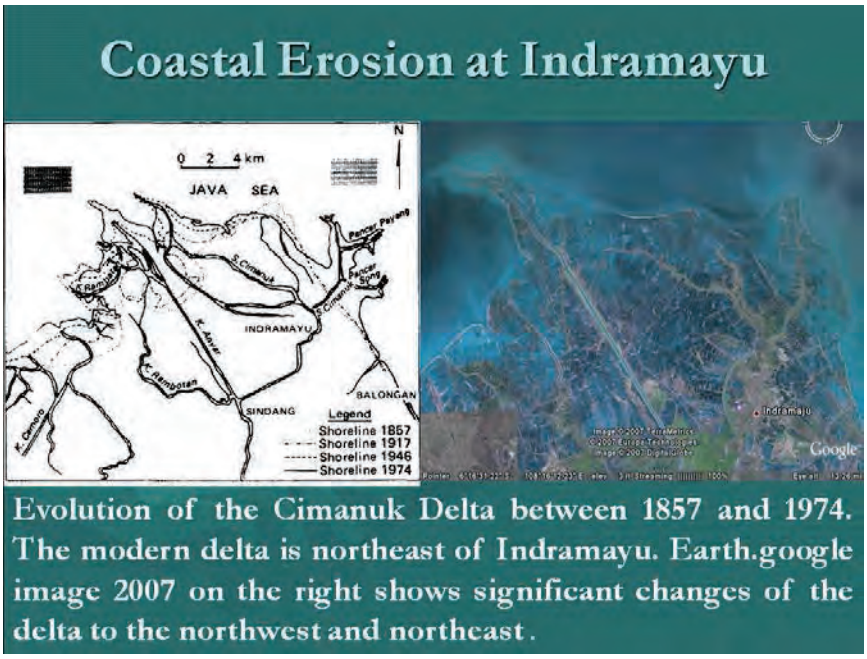

Fig. 16. Coastal Erosion at Indramayu, West Java.

In 2008 the Marine Geological Institute surveyed along the coast of Sidoarjo to study the sedimentation processes caused by the mud volcano of Sidoarjo. The results of the survey (Fig. 17) indicated that:

- The coastline changes in the Porong delta were identified from the Landsat Images of 1975 to 2008 showing that the coastline experienced accretion and abrasion, with moving direction of river flow.
- Abrasion has occurred in the northern part of the river mouth and the distance of abrasion amounting to 0.5 km (15.15 m/year) and area 24.45 Ha (6.802 Ha/year). Accretion occurs in the southern part, with the distance gained about 3.14 km or 92.647 m/year and an area of 1,124.97 Ha (59.21 Ha/year).

3. Subsidence in the northern coast of Java

Land subsidence is a severe hazard threatening people's safety and the urban infrastructure. In most cases, land subsidence may be caused by collapsing underground mines, collapsing dissolution cavities, oil and groundwater extraction, compaction of subsurface material, self-loaded consolidation and active tectonic movement.

In Jakarta and Semarang various coastal environments are severely threatened by industrialization and urban development which are the major factors accounting for environmental degradation and depletion in the area.

The evidence for land subsidence can be detected along the coastal area of Jakarta as indicated by rising of deep well construction pipes. Between 1989 tand1991 the rate of settlement in north Jakarta was 24-34 cm/year, in west Jakarta 8 cm/year, in east Jakarta 4 cm/year and in central Jakarta 3/year (Andiani et al., 1997). On the other hand, based on the results of leveling surveys, the land subsidence in the period 1982-1997 was between 1.33 to 13.33 cm/year and based on GPS survey (1997-2007), the land subsidence was between 10-15 cm/year (Abidin et al., 2008).

In Semarang city, land subsidence can be detected by Persistent Scatterer Interferometry (PSI). The rate of subsidence in 2000 was 2cm/year and it was > 8 cm/year (Figure 18; Kuehn et al., 2009; Murdohardono et al., 2009).

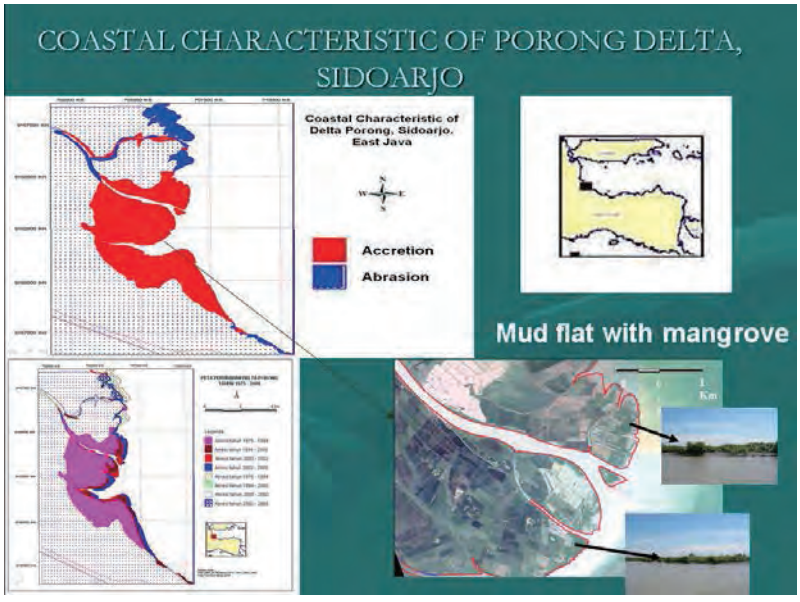

Fig. 17. Coastal characteristics of Porong, Sidoarjo.

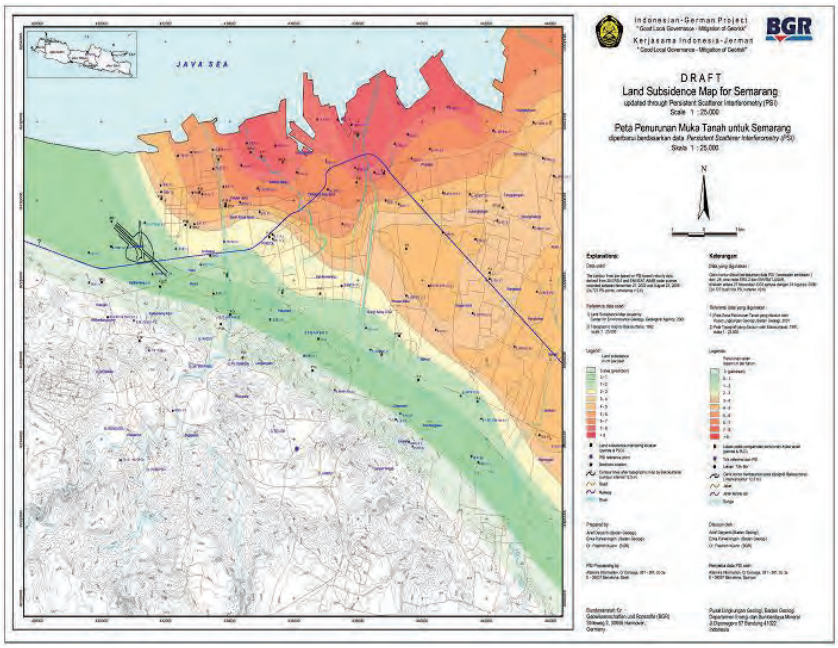

Fig. 18. Land subsidence maps of Semarang (Murdohardono et al., 2009).

On the other hand, based on the measurements of many geodetic surveys, which were carried out by local government and University of Diponegoro, the rates of subsidence varied from 1 to 9.3 cm /year. The greatest areas of subsidence, 83.04 km^2 (Fig. 19), are mostly located at or near the coastline which consists of soft and relatively unconsolidated sediment. Kuehn et al. (2009) supposed that the land subsidence in Semarang results chiefly from compaction in alluvial sediments which contain clay, from groundwater abstraction, the influence of superimposed loads by buildings (Fig. 20), effect of active tectonics or the results of self-load consolidation that together finally result in total annual land subsidence of 15 cm and more.

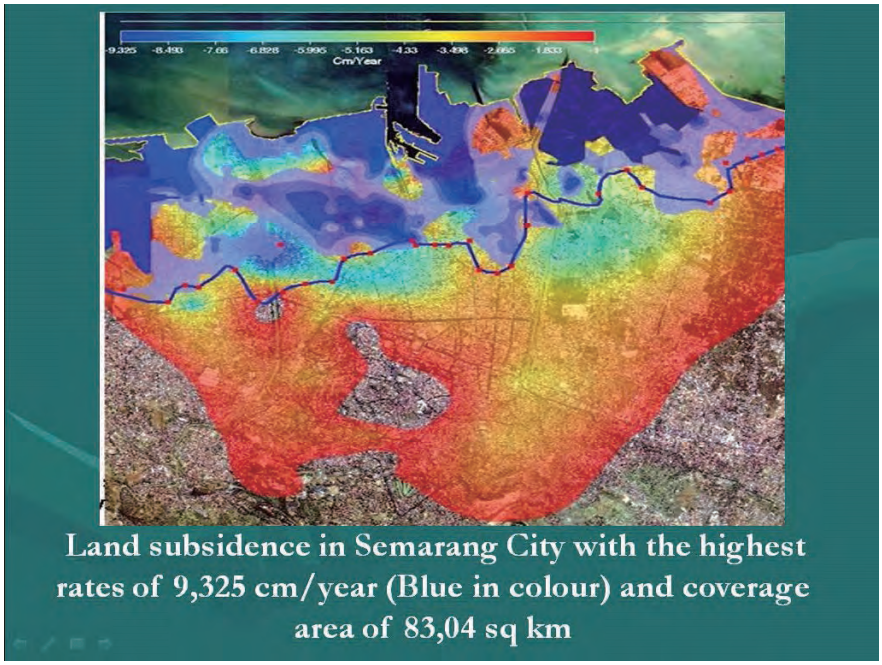

Fig. 19. Land subsidence of Semarang City based on geodetic data.

The land subsidence in Semarang has resulted in severe and costly damage to buildings, roads, railways tracks and other items of the urban infrastructure. As a further consequence, flooding occurs with increasing frequency and most severely affects living conditions especially of the poor urban population. If land subsidence continues, flooding of wide areas of the city of Semarang and progressive economic losses cannot be ruled out (Figs. 21 and 22).

4. Catastrophic events

Geologically, the Indonesian Archipelago is located at the junctions of the Indian Ocean-Australian, Pacific Ocean and Eurasian plates. This tectonic setting at a plate boundary produces a specific geodynamic evolution in Indonesia which may be responsible for some of the hazards in Indonesian coastal areas.

Coastal geological hazards have been induced by catastrophic events such as Krakatau's 1883 eruption that caused significant coastline changes surrounding the volcano in Sunda Strait. Other catastrophic events were the Aceh 2004 and Seram 2006 earthquakes which were followed by land subsidence; coastal landslides and tsunami inundation.

4.1. Krakatau (1883) eruption

The explosion of Krakatau in 1883, an island volcano in the Sunda Strait, left behind a collapsed caldera of irregular outline, up to more than 300 m deep and about 7 km in diameter (Fig. 23). The collapse caused a tsunami up to 30 m high on the shores of Sunda Strait and surges of lesser amplitude around much of Java and Sumatra (Simkin and Fiske, 1983).

Sunda Strait is bordered by volcanoes, the coast consisting of high volcanic slopes, with sectors of coral reef, some of which have developed rapidly in the century since the Krakatau explosion destroyed or displaced their predecessors. The geomorphological features of Sunda Strait need detailed investigation, with particular reference to forms that were initiated by catastrophic events generated by the Krakatau eruption more than a century ago.

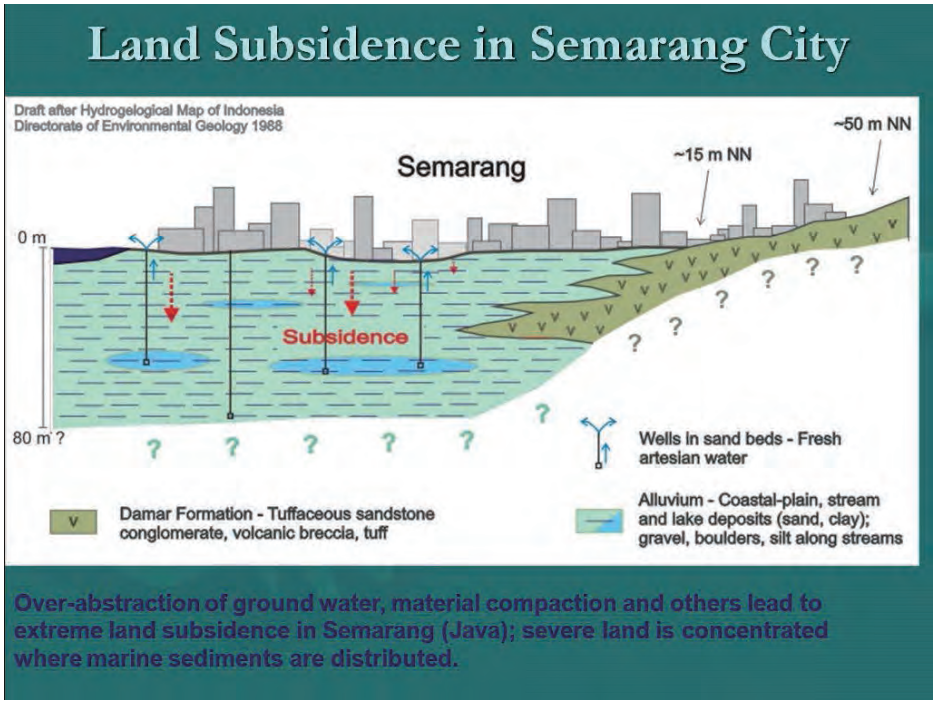

Fig. 20. Cross section of Semarang subsidence (Kuehn et al., 2009).

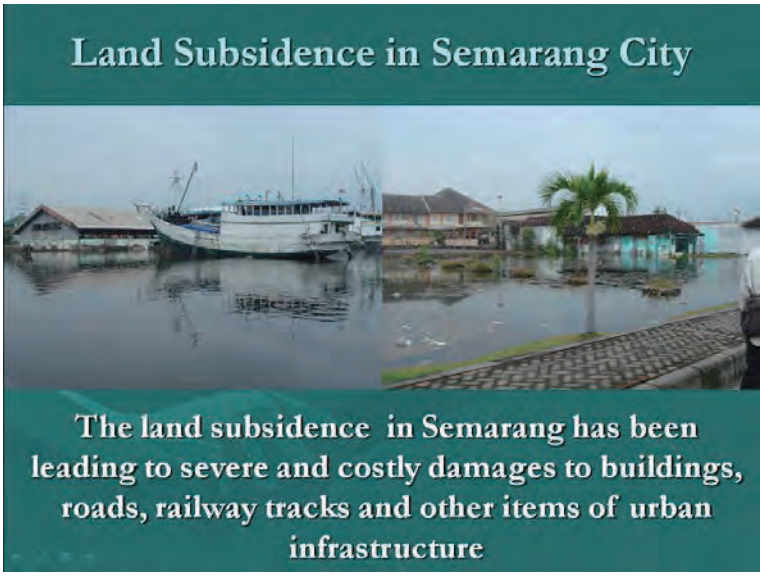

Fig. 21. Land subsidence in Semarang City.

Fig. 22. The land subsidence in Semarang has caused damage to buildings, roads, railways tracks and other items of urban infrastructure.

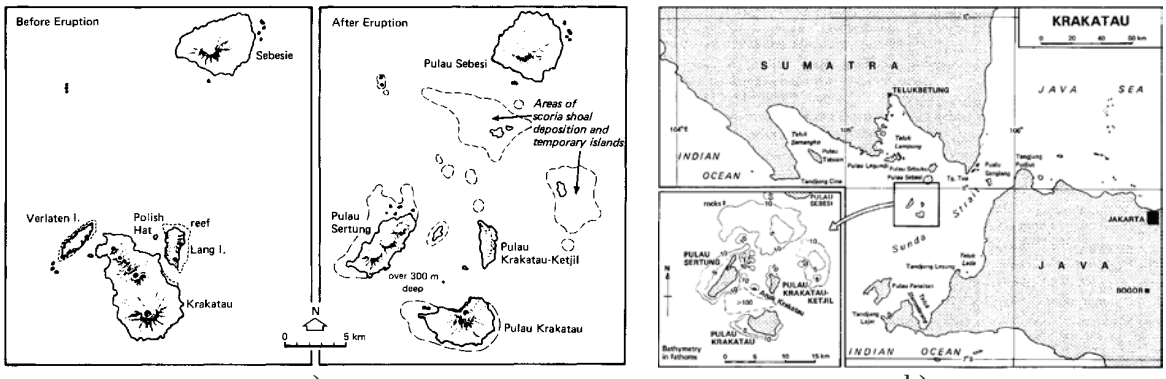

a) b)

Fig. 23. a) Krakatau Volcano before and after the catastrophic eruption of 1883, and b) Krakatau Volcano complex and the surrounding islands in Sunda Strait.

4.2. Aceh Earthquake on 26 December 2004

The 2004 Indian Ocean earthquake was an undersea megathrust that occurred on December 26, 2004, with an epicenter off the west coast of Sumatera, Indonesia. The earthquake was caused by subduction and triggered a series of devastating tsunami along the coasts of most landmasses bordering the Indian Ocean, killing more than 225,000 people in eleven countries, and inundating coastal communities with waves up to 30 meters high. The hypocentre of the main earthquake was at 3.316ºN-95.854ºE, in the Indian Ocean just north of Simeule island, off the western coast of northern Sumatra at a depth of 30 km below mean sea level. In Aceh Province, many coastal changes took place after the devastating tsunami which followed the 9.3 magnitude earthquake. The following images and figures illustrate the effects of the catastrophic disaster (Figs. 24 and 25).

Fig. 24. The red line indicates tsunami inundation boundary in northwest Aceh Province, while the yellow arrows show directions of tsunami waves.

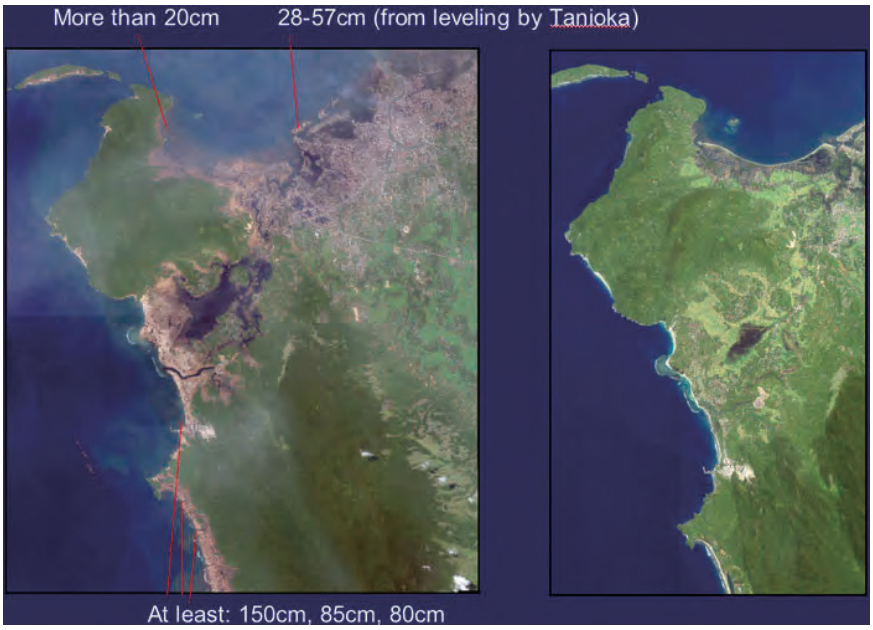

Fig. 25. Land subsidence differences in west coast and north coast of Aceh measured by USGS team shortly after the disaster (left) and previous mainland condition before tsunami inundation (right).

4. 3. The Seram Earthquake on 28 January 2006

An earthquake occurred on 28 January 2006, at 01:58':49" (local time). The epicenter was located at S5.451º and E128.075º in the Banda Sea, with magnitude of Mw7.6 and depth of 346.2 kilometers under the seafloor. The earthquake mechanism was that of a normal fault, with maximum compression east-west, showing its association with the Banda subduction zone (Fig. 26).

Earthquake effects involved damage at 13 houses with 2 houses collapsing into the sea partly because of coastal plain collapse. This phenomenon also caused damage to 12 rumpon (catching fish) at Mahu and Tehoru villages. Subsidence was observed along about 500 meters length of the beach and landslide material tumbled into the water (Fig. 27; Hardjawidjaksana et al., 2009).

Subsidence also occurred along the shoreline for ±200 m at Elpaputy village, Amahai, Central Molluca District. The same happened at the shore about ±7 m long at Weduar village, Kei Besar, Southeast Molluca District, and causing 10 houses to be destroyed.

This earthquake caused people on the southern coast of Seram Island to flee to higher places in case a tsunami should follow. People left their houses in panic because of the shaking. Other effects were cracks in house walls, and cracks on ground surface were found at some locations in southern Ceram Island.

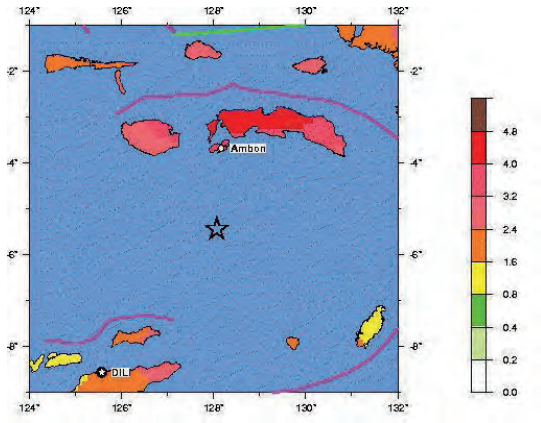

Fig. 26. Epicenter location of Ceram earthquake on 28 January 2006 .

Fig. 27. Indication of creep along the road near to the shoreline

5. Conclusions

- The coastline changes in the northern part of Java are generally caused by the dynamics of discharge of rivers, human activities, deforestation of mangroves, engineering projects in beach zones (harbours and jetties), hydroelectric damming of rivers, coastal hydrodynamics and subsidence, sea level changes and sand mining.
- Due to the sediment-deficient budget in the old channel of the river, abrasion has taken place along the coast of the Old Ciujung River delta.
- The erosion to the north-east in Pondok Bali is caused by the new channel structure of the Cipunegara River and also due to the widespread removal of mangroves in the course of constructing tambak (brackish water fishponds) starting in the1990s.
- The Cipunegara delta has been eroded, deflecting the shoreline at the old delta front by over 310 meters in Pondok Bali, about 680 m in Trungtum village and 530 m in Mangsetan river mouth, with average erosion of 10 m/year.
- Google Earth^{TM} image in 2009 shows that the newly built northeast delta has advanced more towards the Java Sea and developed by 5400 m since 1960 from the Dutch coast of 1942, meaning an advance of at least 108 m/year.
- Abrasion occurs in the northern part of the mouth of Porong river with abrasion of 0.5 km distance (15.15 m/year) or area of 224.45 Ha (6.802 Ha/year), and accretion occurs in the southern part, with accretion of about 3.14 km or 92.647 m/year or area of 1,124.97 Ha (59.21 Ha/year).
- Land subsidence in Jakarta in the period 1982 to1997 was between 1.33 to 13.33 cm/year and in the period1997 to 2007 was between 10 to15 cm/year.
- The rate of subsidence in Semarang in 2000 was 2cm/year, in 2006 it was >8 cm/year and 1up to 5 cm/year and more in 2009 over an area of about 83.04 km^2.
- The explosion of Krakatau in 1883, leaving behind a collapsed caldera up to more than 300 m deep and about 7 km in diameter, caused a tsunami up to 30 m high on the shores of Sunda Strait and surges of lesser amplitude around much of Java and Sumatra.
- The 2004 Indian Ocean earthquake (magnitude 9.3) was caused by subduction and triggered a series of devastating tsunami along the coasts of the Indian Ocean, killing more than 225,000 people in eleven countries, and inundating coastal communities with waves up to 30 meters high.
- Seram earthquake on 28 January 2006 has caused damage to 13 houses, collapse of 2 houses into the sea, damage to 12 rumpon (catching fish) at Mahu and Tehoru villages and subsidence for about 500 m length along the beach and the fall of landslide material into the water.

References

Andiani, Dandun, M., Satriyo, H., and Djaja, 1997, Coastal Management of Jakarta Bay: The Challenges of Environmental Geology on Development of Waterfront City. Proceeding COASTPLAN Workshop, Jakarta 25-28 June 1997, CCOP-DGGMR-ODA/BGS-LOCS-LIPI.

Abidin, H.Z., Andreas, H., Djaja, R., Gamal, M., Deguchi, T., and Maruyama, Y., 2008, Subsidence in Jakarta: Characteristic, caused and impacts. In relatively sea level rise and unstable coastal area and small islands in Indonesia. Report Status of DKP, LIPI, ITB, BAKOSURTANAL, ITS, ESDM AND UNPAD RESEARCH REPORTS.

Hardjawidjaksana, K., Soeprapto, T.A., Murdohardono, D., Ipranta and Yudicara, 2009, Coastal Geological Hazards in Indonesia, Workshop on Geosciences' Role on the Issues of Coastal Geohazards" Daejon, Korea.

Hardjawidjaksana, K., 2009, Coastal erosion and subsidence along the northern coast of Java. JSPS and CCOP-GSJ/AIST Joint Seminar on Coastal Erosion in Deltas, November 2009, Bangkok-Pattaya, Thailand.

Hardjawidjaksana, K., 2010, Coastal Geology of Cipunegara Delta ad Its Implication to the Geological hazards, CCOP-CGS Symposium on Muddy Coastal Geoenvironment and Climate Changes, September 2010, Tianjin, China.

Hehanussa, P.E., 1975. The development of Cimanuk Delta, Indonesia. Riset Jurnal, 1, 9-20.

Hehanussa, P.E., 1980, Excursion Guide to the Cimanuk Delta Complex, West Java, in E.C.F. Bird and A. Soegiarto (eds), Proceedings of the Jakarta Workshop on Coastal Resources Management, United Nations University Tokyo.

Kuehn, F., Albiol, D., Cooksley, G., Haas, S., Hoffman-Rothe, A., and Murdohardono, D., 2009, Detection of Land Subsidence in Semarang, Indonesia using Persistent Scatterer Interferometry. Springle Verslag Environmental Bulletin.

Murdohardono, D., Sudrajat, G.M., Wirakusumah, A.D., Kuehn, F., and Mulyasari F., 2009, Land Subsidence Analysis through Remote Sensing and Implementation on Municipality Level. BGR-GAI-CCOP Workshop on Management of Georisks "The Role of Geological Agencies in Government Practice of Risk Reduction from Natural Disaster", Yogyakarta, Indonesia

Ongkosongo, 2005, Flooding in the coastal area which caused by subsidence and involved by sea level rise. Phd Thesis in Civil Technology, Institute Technology Bandung.

Pilkey, O.H., 1989, Coastal Erosion. Episodes, vol. 14, no 1.

Simkin, T., and Fiske, R.S., 1983, Krakatau 1883: The Volcanic Eruption and Its Effects. Smithsonian Institution Press..

Sutisna, 2002, Sea surface monitoring caused by Global warming and its impact to the coastal zone and small islands. Bakosurtanal

Usman, E., Hardjawidjaksana, K., and Astjario, P., 1996, Coastal Crisis in North Coast of East Java. Marine Geological Institute, Special Publication No 2.

Usman, E., and Yuningsih, A., 2007, Inclination of Coastline Changes and Implication for Landuse Management of Karawang District, West Java Provine, 2nd Workshop on Coastal Erosion and Geological Assessment of Delta Areas in Southeast and East Asia, 4-6 December 2007, Bandung, Indonesia.

Riverbank erosion in Thailand

Somchai Rujajaruswong

Department of Mineral Resources, Ministry of Natural Resources and Environment, Thailand
e-mail: somch.ford@gmail.com

Abstract

Riverbank erosion is a serious problem in Thailand resulting in the loss of land and other property. The Department of Mineral Resources (DMR) investigated such events and found that riverbank erosion could be caused by either natural or human impacts and the latter was the primary cause of the erosion along the banks of main rivers of Thailand, especially the Chao Phraya River. Because of the low-land flood plain of central Thailand, the Chao Phraya riverbank erosion was more severe in the rainy season (May to December) due to the high energy of the current in the river course. This paper briefly reviews the main causes of riverbank erosion with special reference to Thailand.

1. Characteristics of rivers

A river is a natural watercourse usually carrying freshwater and flowing towards an ocean, a sea, a lake, or another river. In a few cases, a river may simply flow into ground or dry up completely at the end of its course without reaching another body of water. At the turn of the 20th century, Davis (1899) devised the "cycle of erosion" method of classifying rivers based on their age, as follows (Fig. 1):

1. **Young or upper river**: A river with a steep gradient that has very few tributaries and flows quickly. Its channels erode deeper rather than wider. The features of young rivers are 'v' shaped valleys, waterfalls and gorges.
2. **Mature or middle river**: A river with a gradient that is less steep than those of young rivers and flows more slowly. A mature river is fed by many tributaries and has more discharge than a youthful river. Its channels erode wider rather than deeper. The features of mature rivers are meanders, river cliffs, slip-off-slopes and sand bars.
3. **Old or lower river**: A river with a low gradient and low erosive energy. Old rivers are characterized by flood plains. The features of old rivers are oxbow-lakes, sand bars, flood plains and levees.

2. Rivers in Thailand

Rivers are very important for Thai people because Thailand is a country where agricultural products generate the main income. There are 43 rivers in Thailand with the main rivers as shown in Figs. 2 and 3.

Northern Thailand is geographically characterized by multiple mountain ranges and the river valleys which cut through them. The main rivers in northern Thailand are the Ping, Wang, Yom and Nan rivers. All of them are young or upper rivers.

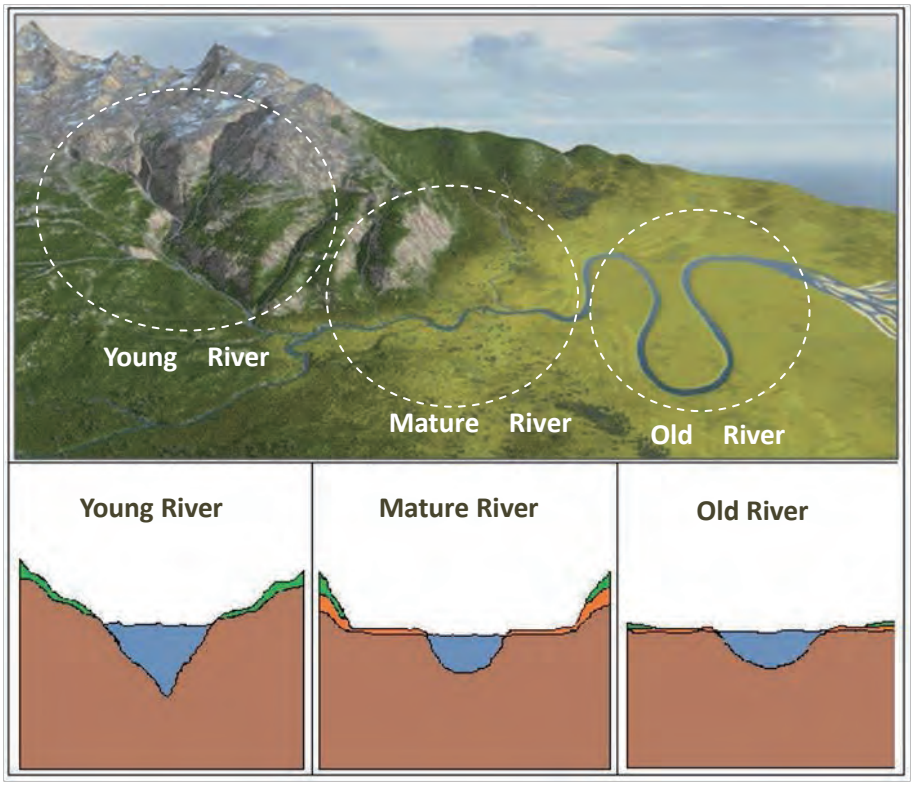

Fig. 1. Characteristics of rivers.

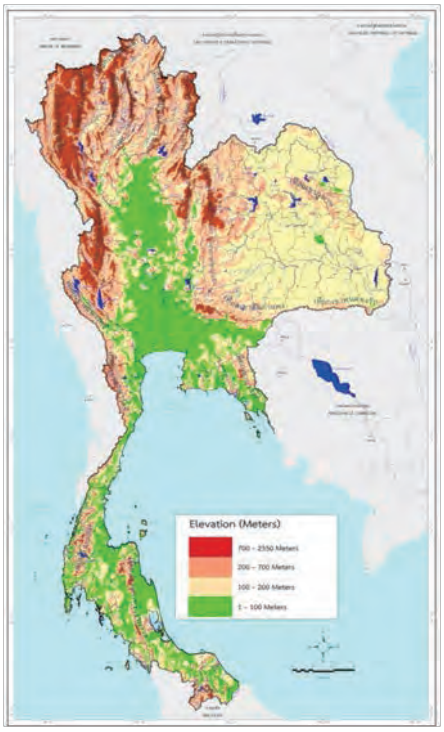

Fig. 2. Topography of Thailand.

Fig. 3. Main rivers in Thailand.

Northeastern Thailand is roughly coterminous with the Khorat Plateau. The main rivers are the Chi, Mun and Songkhram rivers. All of these are young to mature rivers.

Central Thailand (Central Plain) contains the broad alluvial plain of the Chao Phraya River. The main rivers are the Chao Phraya, Thachin, Maekhlong and Bangprakong rivers. These rivers are mature to old rivers.

Southern Thailand is located on the Malay Peninsula. The western part has steeper coasts, while on the eastern side river plains dominate. The main river is the Tapi. This river is a young to mature river.

There are 6 rivers that form boundaries between Thailand and neighboring countries. The bordering rivers of Thailand and Myanmar are the Salawin, Mei, Kraburi, Sai and Ruak, while rivers bordering Thailand and Laos is only the Mekong river. At present, Thailand and Myanmar have a dispute concerning their river boundary in which there are two issues: the first issue is the actual border due to the diversion of the rivers, and the second issue is the impact from riverbank protection on each side.

3. Causes of river bank erosion

Rivers and streams are dynamic systems which are constantly changing. Flash floods are the main cause of riverbank damage. The erosion process commonly results in the formation of river meanders and sand bars. Meanders are broad semicircular curves in a river course that develop as the river erodes the outer bank of a curve and deposits sediment against the inner bank. This natural erosion process can, over time, cause marked changes in the river's course; at present Thailand and Myanmar are in dispute over their boundary due to such a river diversion.

Riverbank erosion may be aggravated by human activities such as sand dredging, blocking by dams and water gates, over-loading or vibration from vehicles along riverbanks, groyne development and boat-generated wave impact. Groynes along the Chao Phraya riverbank cause bank erosion at downstream sites whilst sand dredging in many rivers has caused erosion due to riverbank slope failure. Over-loading by construction, vibration from vehicles along the riverbank and wave action generated by boats, mainly in urban areas, may also cause river bank erosion.

3.1 Erosion by natural process

Flash flood

Flash flooding is very rapid flooding of geomorphic low-lying areas. It is caused by heavy rain or a severe typhoon. Riverbank erosion caused by to flash floods occurs in all the main rivers of Thailand.

Sand bars

A sand bar is a ridge of sand formed in a river or along a shoreline by the action of currents. When a sand bar develops, restricting the width of the river channel, the current through the channel will flow faster and increase riverbank erosion. There are many sandbars in the Chao Phraya and Mekong rivers.

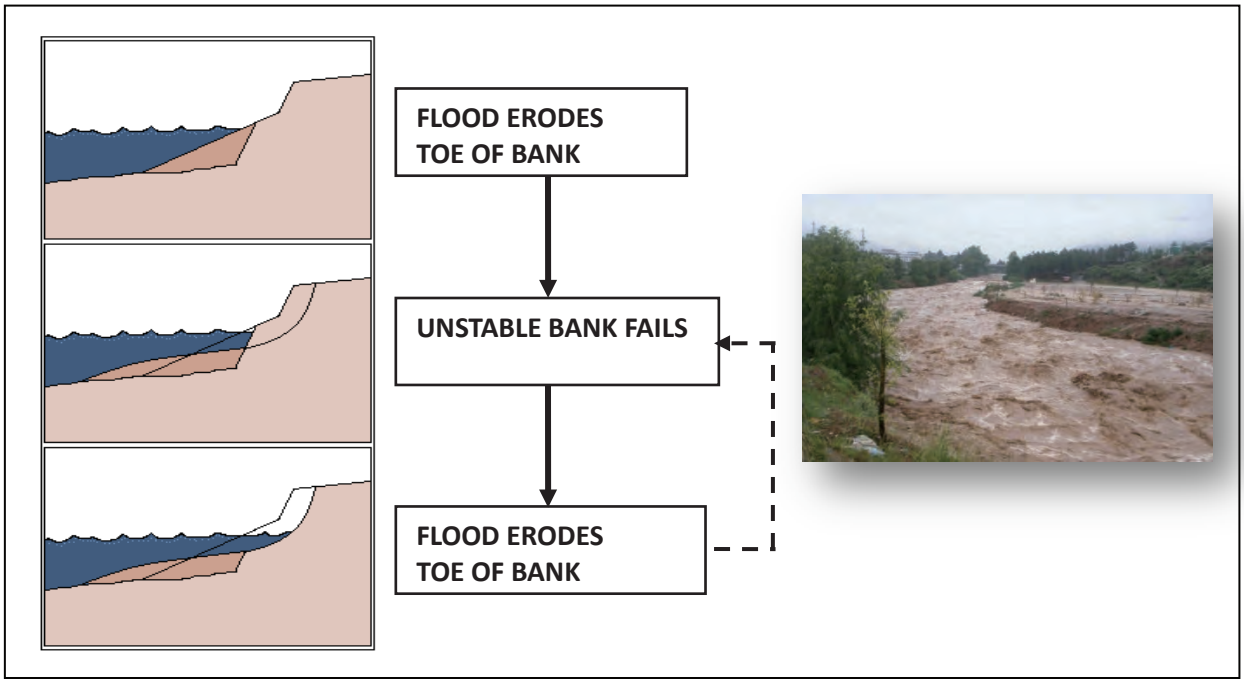

Fig. 4. Riverbank erosion by flash flooding.

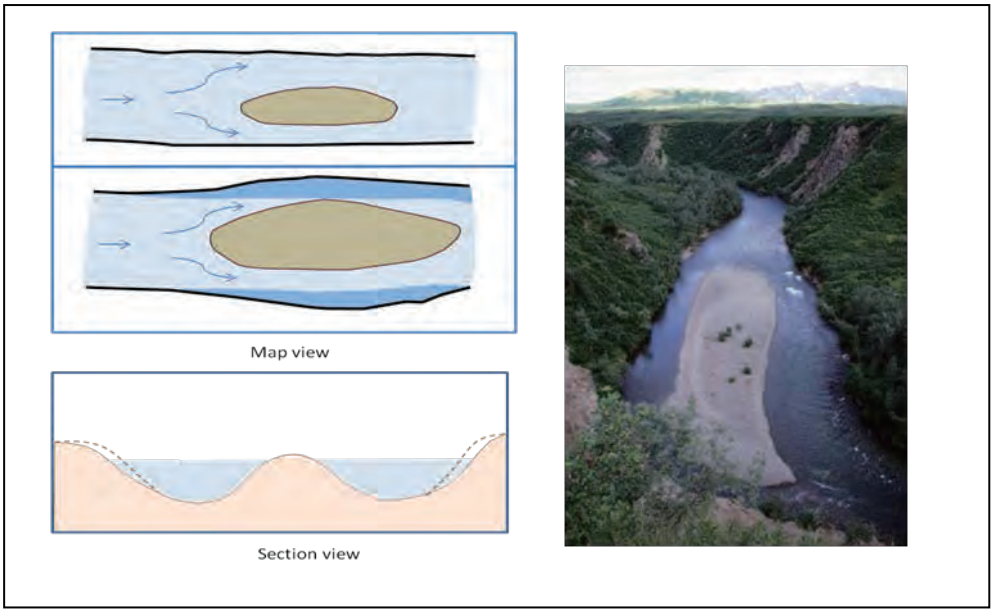

Fig. 5. Riverbank erosion in sand bar area.

Meanders

Meanders are broad, semicircular curves in a stream that develop as the stream erodes the outer bank of a curve and deposits sediment against the inner bank. Thailand and Myanmar have a current dispute over their river boundaries due to the diversion of rivers caused by meandering.

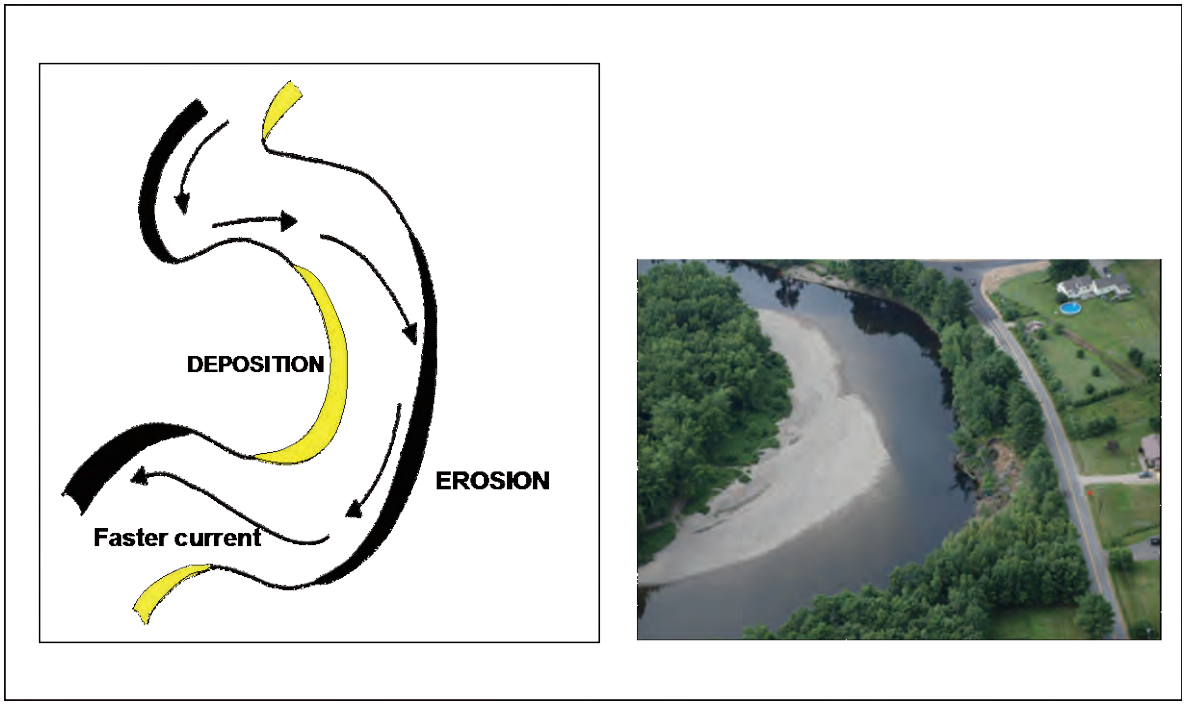

Fig. 6. Riverbank erosion in meander area.

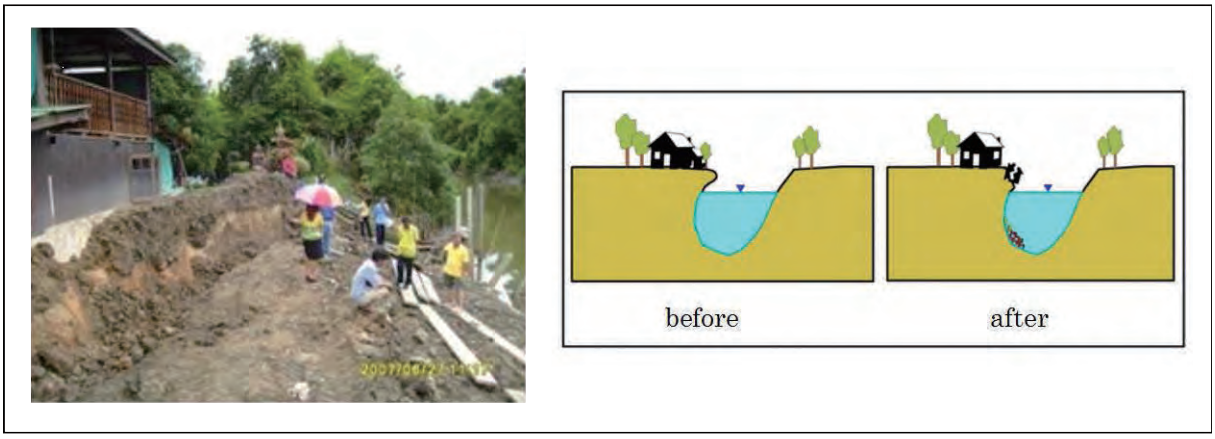

Fig. 7. Erosion in outer bank in Maeklong River.

3.2 River erosion caused by human activities

Sand dredging

Dredging is an excavation activity with the purpose of gathering up river bottom sediment and disposing of it at a different location. Dredging can change the bank-slope from a low slope to a steep slope, and cause river bank instability and erosion or collapse. There is a lot of sand dredging in rivers and canals, mostly in the northern part of Thailand.

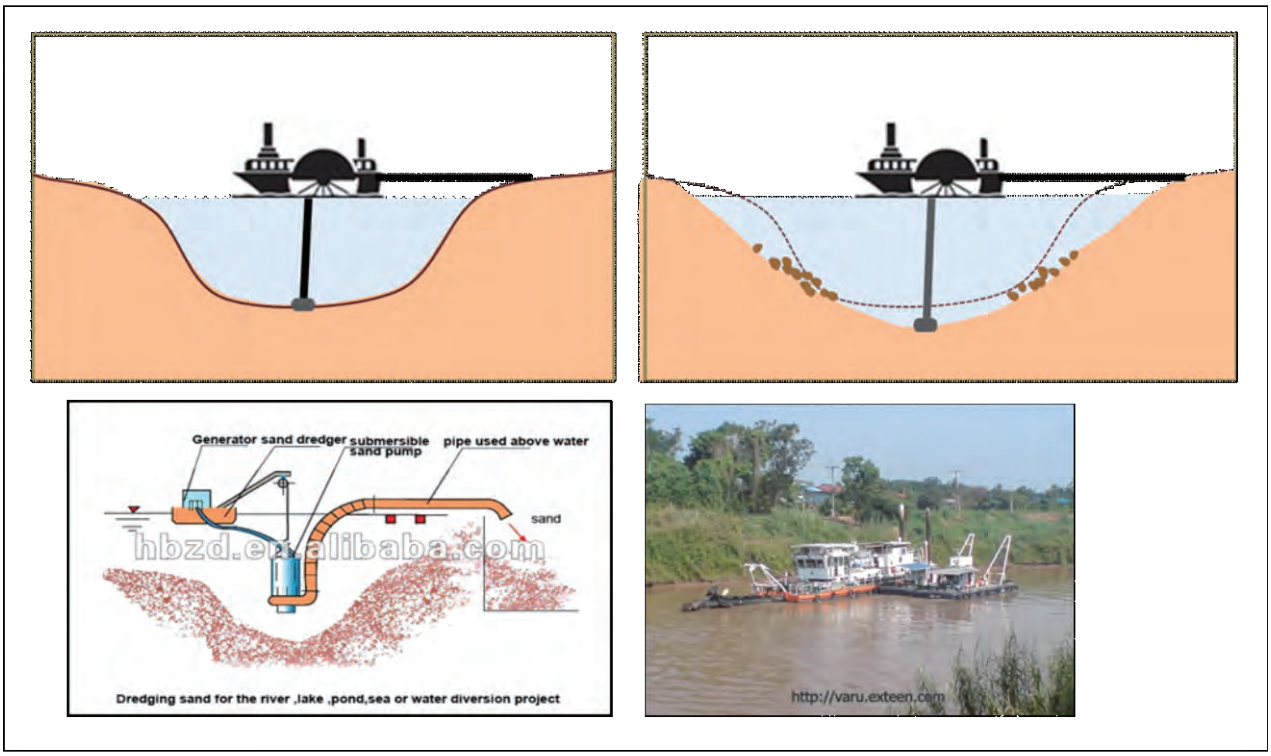

Fig. 8. Riverbank erosion by sand dredging.

Dam and water gate blockage

If the water table on land is higher than the water level of the nearby river, pressure due to the high differential head will cause riverbank to collapse.

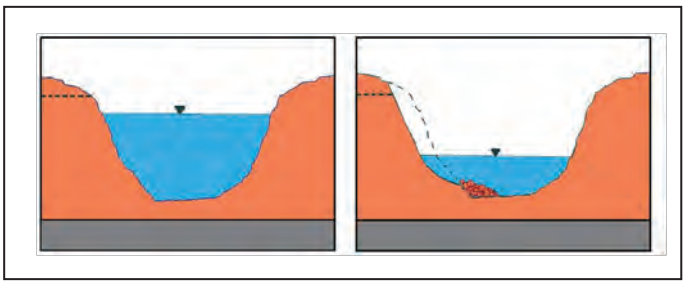

Fig. 9. Riverbank erosion by high differential head.

This can occur in 2 areas: (1) downstream from a dam and (2) at the canal connecting two rivers.

In the rainy season, the dam is almost full of water so the water level upstream is considerably higher than the water level of the river downstream.

Fig. 10. Water level in upper stream is higher than water level in downstream.

When the watergates of the canal are closed, the water levels of the river are higher than the water level of the canal and this can cause canal-bank collapse.

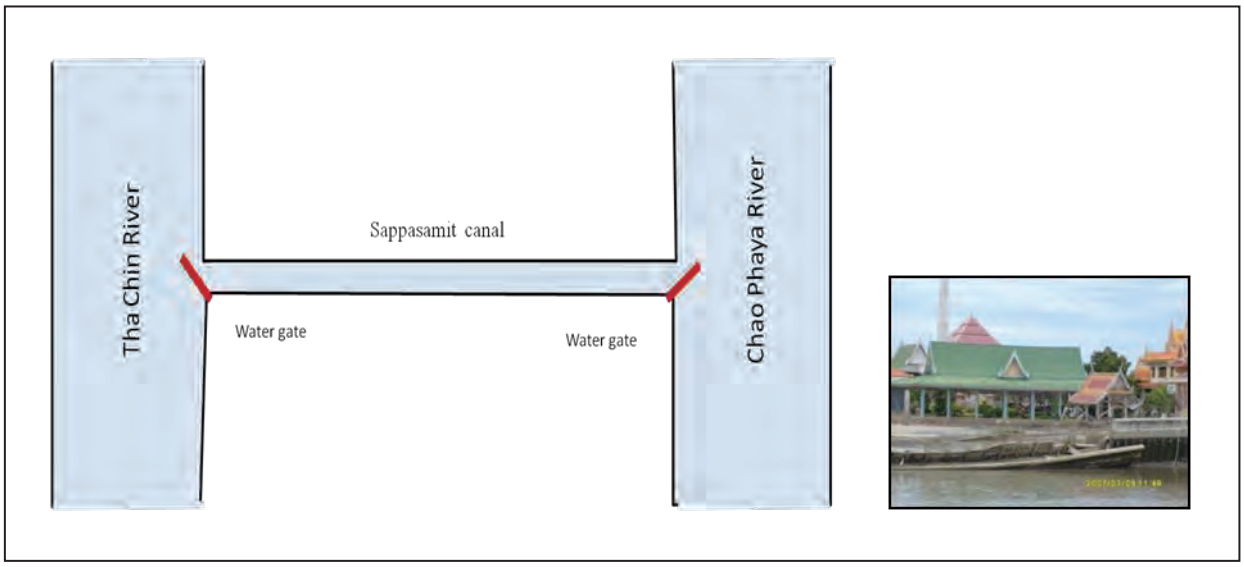

Fig. 11. Bank erosion in Sappasamit Canal which connected between Thachin River and Chao Phraya River.

Over-loading by heavy constructions or vibrations from vehicles

In Thailand there is a lot of construction close to the rivers or canals such as houses and roads. The over-loading from the construction or vibration from vehicles stimulates bank erosion.

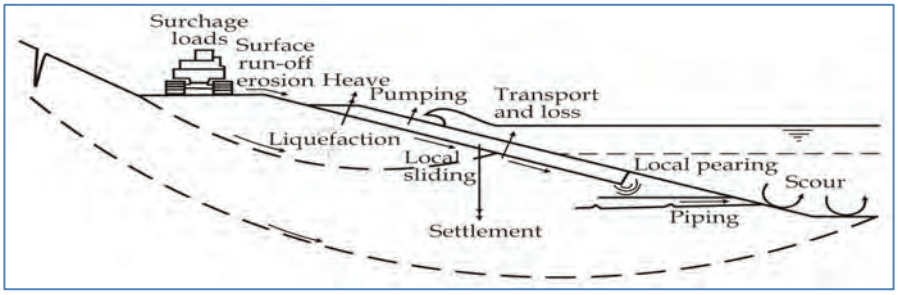

Fig. 12. Bank erosion by over-loaded construction model.

Fig. 13. Bank erosion by running vehicles.

Fig. 14. Bank erosion by overloaded construction.

Groynes

Groyn is a form of riverbank protection. They are built at right angles to a riverbank to prevent littoral drift. Positive impacts are that they trap sediments including soil being carried away by littoral drift and this creates a positive effect on the local economy. Negative impacts are that they prevent downstream areas from receiving sediment to be deposited there which can lead to increased soil erosion. This could also effect buildings and destroy private land. Four groynes in the Chao Phraya River (in Chainat Province) have had the effect of destroying the riverbank in the downstream area.

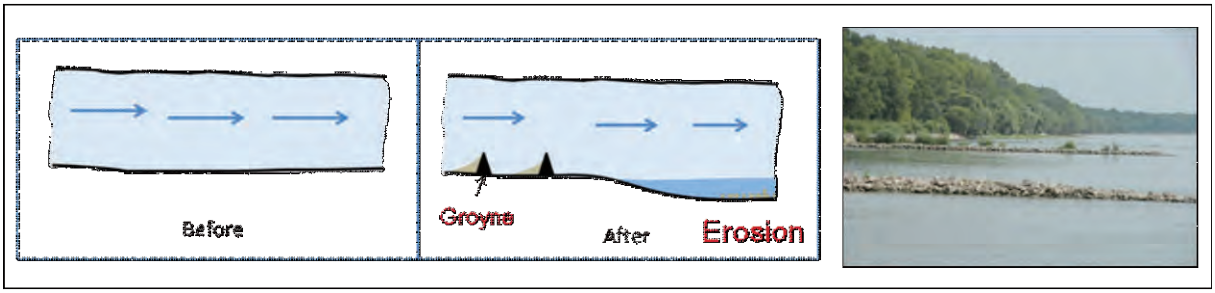

Fig. 15. Bank erosion caused by groynes.

Wave action generated by boats

All boats have the potential to generate waves. As a boat moves through the water, the water surface rises and falls, generating waves which can cause bank erosion.

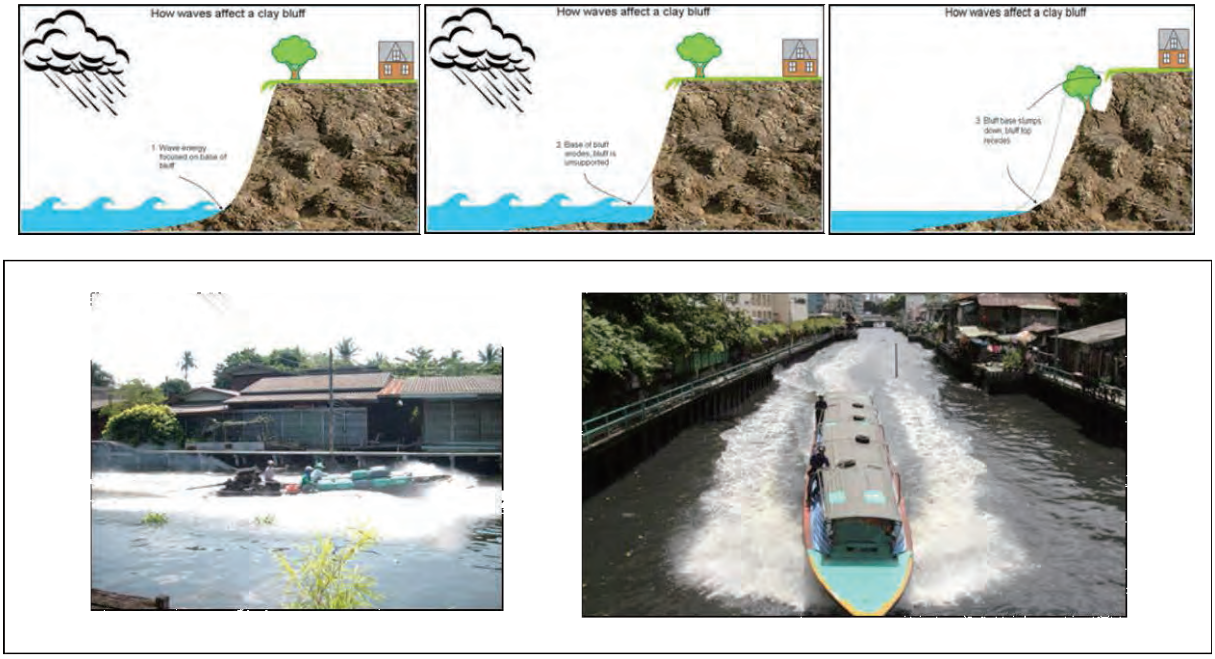

Fig. 16. Wave generated by long tail boat.

3.3 Erosion by the other factors

As mentioned above, there are several more factors causing riverbank erosion, for example:

· Removing grass at the edge of a bank; cutting down trees, or removing other vegetation.
· Permitting intense running games such as volleyball or soccer—activities that compact the soil and destroy vegetation.
· Allowing cattle to trample the banks as they seek water.
· Improper bulldozing to make a cut in the bank to provide boat access or using heavy machinery to cut steps down to the river.

Fig. 17. Impact of cattle near river bank.

4. Conclusions

Bank erosion is a natural process. without it, rivers would not meander and change course. However, land management patterns that change the hydrograph and/or vegetation cover can act to increase or decrease channel migration rates. In many places, whether or not the banks are unstable due to human activities, people try to keep a river in a single place. This can be

done for environmental reclamation or to prevent a river from changing course into land that is being used by people. One way that this is done is by placing riprap or gabions along the bank.

References

Davis, W. M., 1899. The geographic cycle, The Geographical Journal, vol. 14, no. 5, pp. 481-504.

Mapping ground surface recovery in Bangkok using persistent scatterer interferometry

Kazuya Ishitsuka[1], Yo Fukushima[2], Takeshi Tsuji[3], Yasuhiro Yamada[1], and Toshifumi Matsuoka[1]

[1]Dept. of Urban Management, Kyoto University, Japan
[2]Disaster Prevention Research Institute, Kyoto University, Japan
[3]International Institute for Carbon-Neutral Energy Research (WPI-I2CNER), Kyushu University, Japan
e-mail: Ishitsuka.kazuya.63r@st.kyoto-u.ac.jp

Abstract

In this study, we estimated recent surface displacement in Bangkok by means of persistent scatterer interferometry using SAR images obtained from November 2007 to December 2010. Previously, land subsidence due to excessive groundwater pumping has been reported, however, we detected that ground surface has uplifted during the 3 years of the observation period. We discriminated secular surface rebound from seasonal surface displacement by fitting a temporal model of each effect, and mapped the spatial distribution of natural rebound and seasonal displacement. Each spatial pattern can be interpreted as the lateral connectivity of each aquifer in a multi-aquifer system in Bangkok. Moreover, the decay coefficient non-seasonal surface recovery might show the past watershed of the Chao Phraya River.

Keywords: surface rebound, Bangkok, groundwater recovering, persistent scatterer interferometry

1. Introduction

Land subsidence due to groundwater extraction has occurred in Bangkok, leading to the damage of buildings and other infrastructure. In recent decades, in order to mitigate the over-pumping of groundwater, Bangkok has regulated groundwater pumping. This regulation successfully led to a decrease in ground water pumping rate. The history of ground subsidence and mitigation measures taken by the government are summarized in previous research publications (e.g., Phien-wej et al., 2006; Taniguchi et al., 2011; Giao et al., 2012).

Generally, the mechanism of surface rebound after groundwater pumping is described as follows: after the decrease in groundwater usage, groundwater recharge increases pressure on pore water and expands its granular skeleton. The expansion of pore volume attributed to the increase in hydraulic head induces elastic rebound of surrounding media in the aquifer. Despite such aquifer expansion, it is known that land subsidence can continue for a while, due to compaction of the aquitard, even after the cessation of groundwater extraction As a matter of fact, it has been reported that subsidence has occurred after the decrease in groundwater pumping in Bangkok. However, it can be inferred that elastic rebound of the surface is observed when the magnitude of the expansion exceeds that of the compaction.

Images acquired by synthetic aperture radar (SAR) onboard a satellite have great advantages for providing us with Earth's surface information with spatial density. Especially, SAR interferometry and persistent scatterer interferometry (PS-InSAR) have revealed and mapped a variety of surface displacement phenomena. In this study, we first detected ground displacement in Bangkok having turned to uplift, using PS-InSAR analysis of SAR images acquired by the Phased array Type L-band SAR (PALSAR) images instrument aboard the

Japanese Advanced Land Observing Satellite (ALOS). This result was compared with past ground subsidence estimated by differential SAR interferometry analysis of SAR images. Then, we interpreted the estimated pattern of natural surface rebound using a temporal model.

2. Geological background at Bangkok plain

Bangkok is situated on flat low land in the southern part of the Bangkok Plain. The Chao Phraya River flows through the city from the northern highland and discharges into the Gulf of Thailand. The Bangkok plain has an average elevation of 2 m above mean sea level (Fig. 1). It is known that the multi-aquifer system beneath the Bangkok plain consists of several interbedded aquifers and aquitards (Fig. 1). Especially, sea-level changes in the Holocene epoch play an important role in shaping the landform of the plain (Sinsakul, 2000). It is supposed that the Bangkok plain and the Gulf of Thailand was dry during the late Pleistocene. On the other hand, in the Holocene epoch until about 6000 year B.P., sea level increased and part of the present plain had been below the Holocene sea. Subsequently, the sea level has fallen and fluctuated. This variation of sea level in Holocene times possibly resulted in the present alternate layer of confined aquifers and aquitards. Confined aquifers are mainly composed of sandy and gravelly sediments, while aquitards are composed of stiff clay. About 8 aquifers are present in an interval extending to 600m below MSL, and the second and third uppermost aquifers, located about 100m and 150 m below MSL are considered as the productive aquifers called the Phra Pradang aquifer and Nakorn Luang aquifer respectively (Sinsakul, 2000).

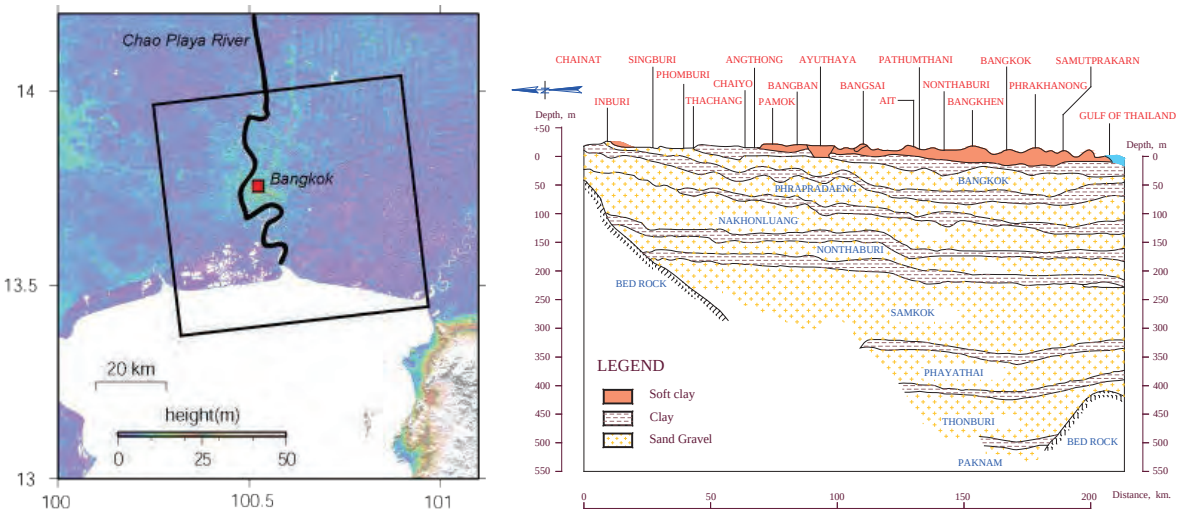

Fig. 1. Topography in Bangkok plain and the area of interest (left), and north-south cross section of the hydrogeological setting of the multi-aquifer system beneath Bangkok (right) (Piancharoen, 1997).

3. Method

3.1 Persistent scatterer interferometry

In order to measure the recent surface displacement time-series in Bangkok, we performed PS-InSAR analysis (Wegmüller et al., 2010) using 11 SAR images acquired from November 2007 to December 2010. Based on phase information of a number of SAR datasets, PS-InSAR enables us to estimate time-series surface displacement in line-of-sight direction. Since PS-InSAR analysis makes use of pixels with less phase noise, called persistent scatterers (PS), the estimated displacement is generally more accurate than that of

conventional InSAR analysis. From 11 SAR images, we selected 44 interferometric pairs with a perpendicular baseline of less than 1000 m. After selecting PS and creating differential interferograms, displacement time-series were estimated by inverting each unwrapped differential interferogram (Schmidt and Bürgmann, 2003). To mitigate atmospheric effects, we smoothed the temporal changes in phase under the assumption that the atmospheric effect would have a high temporal frequency. Because this is an over-determined problem, we could use the least-squares method to obtain a solution. Finally, we converted the estimated displacements in the line-of-sight direction to vertical direction assuming that the displacements in the horizontal direction were negligible.

3.2 Temporal model interpretation

We assumed that the estimated time-series displacements are composed of two physical processes: seasonal displacement explained by sinusoidal curve, and non-seasonal uplift described by exponential function of time.

$$U(t) = \alpha\left(\sin(\frac{2\pi}{365} t + \theta) - \sin(\theta) \right) + \beta(\exp(kt) - 1) + U_{ref} \quad (1)$$

where $U(t)$ is the observed displacement time-series with reference to the first SAR image (acquired on 25 November 2007), α and β are coefficients which describes the magnitude of each factor, and θ is the time shift of the sinusoidal function. This time shift means the starting period of uplifting for seasonal displacement with respect to the first SAR image. k is a coefficient controlling the decay rate and U_{ref} is the displacement at a reference point.

4. Results and discussions

4.1 Time-series surface displacement observed from persistent scatterer interferometry

Estimated displacement time-series show that the ground surface around the center of Bangkok has basically uplifted in the 3 years of ALOS observation periods. The west and east boundaries of the uplift area approximately correspond with the west of Chao Phraya River and the Suvarnabhumi international airport in Bangkok, respectively. The north and south boundaries roughly correspond with the extent of Bangkok city. Totally, the northwest part of the uplift area has rebounded about 1.0 to 2.0 cm during 3 years, while 2.5 cm and 1.0 cm of uplift over the 3 years were found at the southeast and the center of the uplift area, respectively. In general, the displacements at the northwest of the uplifted area tend to have been gradual, while those in the southeast of the uplift area have rather fluctuated with a seasonal trend.

Groundwater level has been measured by piezometric meter at monitoring wells in Bangkok by the Department of Ground Water Resources (Department of Groundwater Resources, 2012; Giao et al., 2012). Changes in ground water level indicate that levels increased from 1997, possibly affected by a decreasing amount of pumping. The recovery rate is almost constant over time, but the rate is different in each monitoring well. For instance, the monitoring well along the Chao Phraya River showed a recovery rate of 0.7 to 1.2 m/year. Considering the fact that the areas of the higher recovery rate correspond to the areas of greater uplift rate, we can conclude that estimated surface uplift is caused by subsurface groundwater recovery.

In order to understand the relationship between recent uplift and past subsidence, we performed DInSAR analysis from 4 datasets using 6 JERS-1/SAR images. Two datasets are referenced with a master image acquired in November 1994, and the other two datasets are

referenced with a master image acquired in April 1997. As a result of the analysis, we found a subsidence area with the rate of -2 to -4 cm/year around the center of the Bangkok, where uplift was observed by the PS-InSAR analysis of ALOS/PALSAR images. The magnitude of subsidence rate inferred from DInSAR analysis agrees with the subsidence rate previously reported (Phien-wej et al., 2006; Taniguchi et al., 2011). This result suggests that groundwater levels have mainly increased in the preceding subsidence areas where the groundwater head had been lower than the other areas.

4.2 Aquifer connectivity estimated from a temporal model

In Fig. 2, we mapped the spatial trend of the amplitude of the seasonal variation (α), the average rate of the non-seasonal uplift. For α and the average rate of the non-seasonal uplift, we plotted the values at areas where k and β are negative (uplift area) and the standard deviation of residual displacement is less than 1 cm. Non-seasonal uplift uniformly occurred in the whole area at the rate of 0.5-1.5 cm/year (Fig. 2b). On the other hand, the values of α have spatial variations (Fig. 2a).

Compared to the non-seasonal uplift (Fig. 2b), the seasonal displacement was not found in all the uplift areas (Fig. 2a). This could be attributed to the spatial connection of aquifers. As described in section 2, there is a multi-aquifer system in the Bangkok plain. Several aquifers and aquitards are interbedded and groundwater has been mainly over-extracted in the second uppermost (Phra Pradang aquifer) and third uppermost aquifers (Nakorn Luang aquifer). Seismic reflection survey in Bangkok has shown that the second aquifer is horizontally continuous and has a flat-lying structure, while the uppermost (Bangkok aquifer lying at the depth of 16-30 m) is not so continuous laterally (Whiteley et al., 1998). Although it has been reported that groundwater flows not only horizontally but also vertically (especially downward) in this aquifer system (Onodera, 2008), it is not realistic that the groundwater flows vertically with the high speed of 1.0 m/year through the clay layer. Therefore, spatially continuous non-seasonal displacements can be inferred to be caused by the lateral connection of the second and the third aquifer, and the spatial distribution of observed seasonal displacement is likely to show the horizontal connection of the uppermost aquifer.

The spatial pattern of the decay coefficient k in exponential function (Eq. 1) can be explained by the spatial distribution of the elastic coefficient. Considering if the compressibility of one aquifer can be significantly distributed, the elastic properties may differ when the depositional environment is not the same. Most parts of the Bangkok plain have been formed by tidal processes, however the fluvial processes dominated along the river (Sinsakul, 2000). Although the higher values of k are also distributed apart from the current watershed of Chao Phraya River, it is likely that the watershed has shifted due to the fluctuation of sea level.

4. Conclusions

In this study, we estimated the spatio-temporal pattern of recent surface displacement in Bangkok using PS-InSAR analysis of ALOS/PALSAR images. We detected ground surface rebound during the ALOS observation period. Since groundwater usage has decreased in Bangkok due to the regulation of groundwater pumping, and groundwater level at productive aquifers has been rising at the estimated uplift area after the regulation, this uplift can be attributed to the increase in the hydraulic head due to the preceding depression in pore pressure. We then, estimated the lateral connectivity of aquifers using a temporal model. The discrepancy in spatial distribution of seasonal and non-seasonal distribution can be the resulted of lateral hydraulic connectivity within individual aquifers of the multi-aquifer

system under the Bangkok plain. Moreover, the magnitude of the decay coefficient of the exponential function describing the secular uplift might reflect floodplain changes.

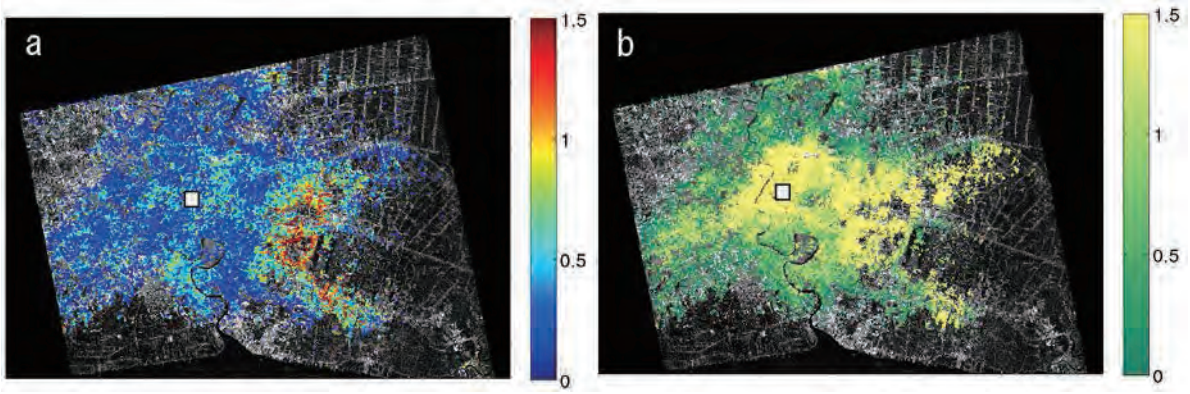

Fig. 2. The spatial distribution of a best-fit parameter for a temporal model for time-series surface displacement. A white square indicate the city center of Bangkok. (a) the magnitude of seasonal displacement in cm, and (b) the annual average of secular uplift in cm/year.

References

Department of Groundwater Resources, 2012, Investigation on the rebound of groundwater in Bangkok after excessive deep well pumping and impacts on building foundation and underground structures, Ministry of Natural Resources and the Environment of Thailand.

Giao, P. H., Paveechana, T. and Saowiang, K., 2012, Consolidation settlement analysis with reference to groundwater recovery in the Bangkok multi-aquifer system, *Proc. of the international conference on ground improvement and ground control*.

Onodera, S., Saito, M., Sawano, M., Hosono, T., Taniguchi, M., Shimada, J., Umezawa, Y., Lubis, R. F., Buapeng, S. and Delinom, R., 2008, Effects of intensive urbanization on the intrusion of shallow groundwater into deep groundwater: Examples from Bangkok and Jakarta, *Science of the total environment*, **404**, 401-410.

Piancharoen, P., 1997, Groundwater and Land subsidence in Bangkok, Thailand, IAHS. Pub., **121**, 355-364.

Phien-wej, N., Giao, P. H. and Nutalaya, P., 2006, Land subsidence in Bangkok, Thailand, *Engineering Geology*, **82**, 187-201.

Schmidt, D. A. and Bürgmann, R., 2003, Time-dependent land uplift and subsidence in the Santa Clara valley, California, from a large interferometric synthetic aperture radar data set, *Journal of Geophysical Research*, **108**, B9, 2416.

Sinsakul, S., 2000, Late Quaternary geology of the Lower Central Plain, Thailand, *Journal of Asian Earth Sciences*, **18**, 415-426.

Taniguchi, M., 2011, Groundwater and Subsurface Environments: Human Impacts in Asian Coastal Cities, Springer, New York.

Wegmüller, U., Walter, D., Spreckels, V. and Werner C., 2010, Nonuniform ground motion monitoring with TerraSAR-X persistent scatterer interferometry, *IEEE Trans. Geosci. Remote Sens.*, **48**, 2, 895-904.

Whiteley, R. J., Hunter, J. A., Pullan, S. E. and Nutalaya P., 1998, "Optimum offset" seismic reflection mapping of shallow aquifers near Bangkok, Thailand, *Geophysics*, **63**, 4, 1385-139.

Web based rapid mapping of disaster areas using satellite images, Web Processing Service, Web Mapping Service, frequency based change detection algorithm and J-iView

Joel Bandibas and Shinji Takarada

Geological Survey of Japan, AIST
Site 7, 1-1-1 Higashi, Tsukuba, Ibaraki 305-8567, Japan

Abstract

This research focuses on the development of a cost effective and efficient system of identifying areas affected by natural disasters, and the efficient distribution of the information. The developed system is composed of 3 modules which are the Web Processing Service (WPS), Web Map Service (WMS) and the user interface provided by J-iView. WPS is an online system that provides computation, storage and data access services. In this study, the WPS module provides online access to the software implementing the developed frequency based change detection algorithm to map areas affected by natural disasters. It also sends requests to WMS servers to get the remotely sensed data to be used in the computation. In this research, the WMS component provides remote access of the satellite images which are used as inputs for disaster area mapping. The 3 modules are seamlessly integrated into a single package using J-iView, which could rapidly generate a map of disaster areas that is instantaneously viewable online. The developed system was tested using PALSAR and ASTER images to map the areas damaged by the October 2010 eruptions of Mount Merapi in Indonesia and March 11, 2011 tsunami in Japan, respectively. The developed system efficiently generated maps showing the areas devastated by the disasters. Based on the initial results of the study, the developed system proved to be a useful tool to quickly identify areas affected by natural disasters.

Keywords: Web Based Disaster Mapping, Frequency Based Change Detection, WMS, WPS, J-iView

1. Introduction

Earthquakes, tsunamis and volcanic eruptions are the most destructive natural phenomena frequently occurring in most countries located along the Pacific Rim. Timely identification of areas affected by the occurrence of these phenomena is very important for successful rescue and effective emergency relief efforts. The use of remotely sensed data to delineate areas affected by natural disasters is very cost effective and efficient. Remotely sensed data can cover large areas and is relatively cheaper to obtain compared to aerial photographs and information obtained from field surveys. During natural disasters, quick acquisition and processing of remotely sensed data to identify damaged areas is very challenging. Remotely sensed data could just be obtained from a few organizations and getting the data could take time. The identification of damaged areas could further be delayed if an image processing system is not immediately available. This research focuses on the development of a cost effective and efficient system of identifying areas affected by natural disasters, and the efficient distribution of information using web services. A frequency based change detection algorithm is also developed to identify damaged areas using remotely sensed data. The web services provide web based access to remotely sensed data and the satellite image processing software. The developed rapid mapping system is composed of three modules which are the Web Processing Service (WPS), Web Map Service (WMS) and a web portal (Fig. 1). WPS implements the developed algorithm for land cover change detection and manages web based data access and storage services. The satellite images are obtained through the web based

spatial information sharing method called Web Map Service (WMS). WMS provides a simple HTTP interface for requesting geo-registered map images from one or more distributed geospatial database (OGC, 2013). Satellite images are obtained by sending GetMap requests to WMS servers. In this study, the web services are integrated using J-iView, the web based mapping system developed at the Geological Survey of Japan (GSJ) (Fig. 2).

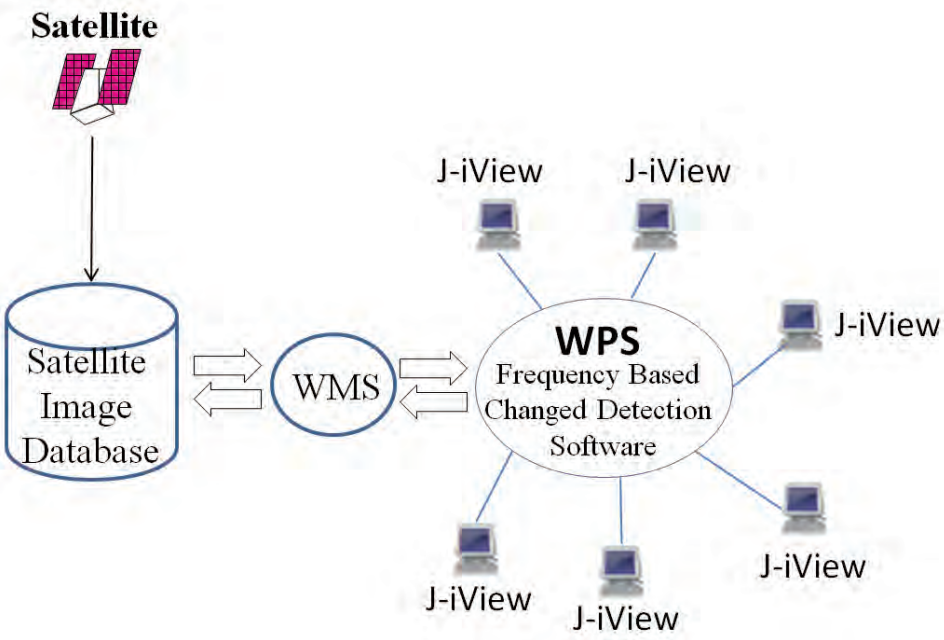

Fig. 1. Web based disaster area mapping system using Web Processing Service (WPS), Web Map Service (WMS), frequency based change detection algorithm and J-iView.

Change detection using multi-temporal remotely sensed data could be divided into two broad types: pre-classification and post-classification (Mettemicht, 1999). Post-classification methods involve the separate classification of remotely sensed data sets from individual dates. Changes could be determined by the change in land cover types between these dates. This method would indicate the areas that undergo change and how they change (e.g. from corn field to residential). Pre-classification methods on the other hand detect changes due to the variations in brightness or spectral signatures in the images compared. In this method, areas could just be labeled to have “changed” or “not changed”, not the type of change. There are several pre-classification methods for detecting land cover change using multi-temporal remote sensing data sets. Image differencing is the most common and straightforward method. It is simply the subtraction of the pixel digital values of an image recorded at one date from the corresponding pixel values of the image at the second date (Hayes and Sader, 2001). The output of image differencing indicates that values close to the mean represent areas of ‘no change’ and magnitude close to ±255 depicts areas of change (Mettemicht, 1999). Image differencing involves the processing of one band of the digital images at a time. Other methods use multiple bands of data for change detection. These include image differencing using bands ratios like vegetation indices and principal component analysis (PCA). In the temporal change detection using PCA, both the surface proportion and the magnitude of the changed area in an image determine which principal component images will contain change information. It is the relative amount of variance between the changed area and the unchanged part in an image that determine which particular PCs contain changing information (Sing,

1986).

The pre-classification method of detecting land cover change is the more appropriate procedure for mapping areas affected by natural disasters, because identifying damaged areas would not require information about the type of land cover change. Identifying damaged areas involves the determination of spectral and spatial changes in the satellite images taken before and after the occurrence of the disaster. Areas that sustained significant damage should show significant change in the spectral and spatial characteristics. The conventional pre-classification change detection algorithms described above are pixel by pixel based methods of identifying changes of land cover using multi-temporal remotely sensed data sets. However, changes in pixel values between two images are sometimes not a good indicator of land cover change. Indeed in many instances, a particular pixel's brightness covering a damaged area would not significantly change. The indications that it covers a damaged area are the changes in brightness of the surrounding pixels. In many cases, changes in texture are more important in identifying damaged areas than the absolute changes in brightness in images. Delineating damaged areas often involves identifying regions in the image whose textures significantly change in the multi-temporal data sets.

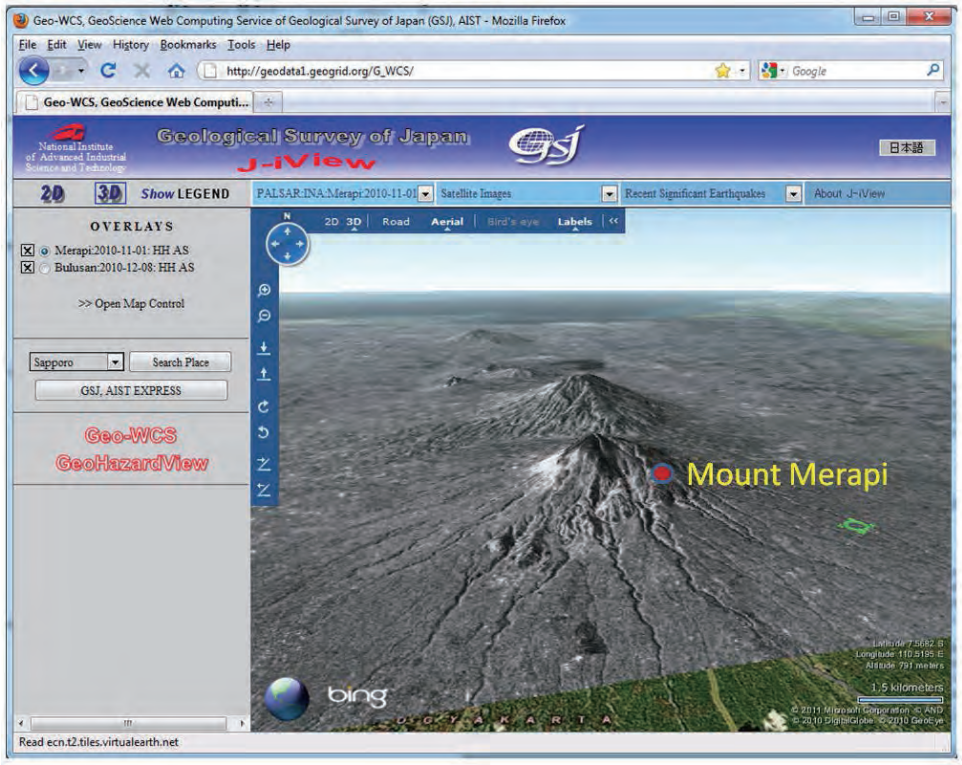

Fig. 2. J-iView WEB portal showing PALSAR image (HH As) of Merapi Volcano taken on November 1, 2010.

2. Land cover change detection algorithm

Several algorithms were developed to determine the spatial signature of pixels in satellite images. One of the earliest spatial signature based algorithms is the contextual identification of pixels or spatial correlation (Khazenie and Crawford, 1989; Alonso and Soria, 1989). A similar method developed by Peddle and Franklin (1989) termed this spatial correlation procedure as gray level-spatial dependency co-occurrence. Gong and Howarth (1992) formulated the frequency based contextual classifier wherein the identity of a pixel was

defined by the frequency of occurrence of the different spectral classes of its surrounding pixels. The land cover change detection algorithm used in this study is based on the contextual method to represent pixel's spatial signature, to detect change in multi-temporal data sets covering areas affected by natural disasters. The unsupervised frequency based changed detection algorithm developed in this study involves 3 stages: 1) the classification of the two images into 15 spectral classes, 2) spatial signature generation using the spectral class occurrence frequency method, and 3) change detection.

The first stage is the segmentation of the two satellite images into 15 spectral classes using the moving averages clustering algorithm described by Richards (1987). The first image was first segmented into 15 spectral classes. The 15 means of the cluster centers of the first image were then used to classify the second image into 15 corresponding spectral classes. If the two images are exactly the same, the aforementioned clustering sequence should generate two identical clustered images. In the second stage, the spectral class occurrence frequency is defined. The occurrence frequency ***f(i,j,c)*** is the number of times a spectral class ***c*** occurs in the window centered at ***(i,j)***. The window has a square shape with side length ***l***. Spectral classes were labeled from **1** to ***v***, where ***v*** is the total number of spectral classes.

Detecting the difference between the spectral class frequency $f_1(i,j,c)$ of the first image and the frequency $f_2(i,j,c)$ of the second image centering on the same location ***(i,j)***, was carried out by determining the Euclidean distance between the two window frequencies. The pixel window was moved pixel by pixel over the clustered images and the frequency occurrence for each spectral class within the window was computed to generate two frequency tables. The distance between the two frequency tables was computed using the formula

$$d_{(i,j)} = \sqrt{\sum_{c=1}^{v} (f_1(i,j,c) - f_2(i,j,c))^2} \quad (1)$$

where ***d(i,j)*** is the distance between the two frequencies at pixel location ***(i,j)***. If the two frequency tables are the same, the distance should be 0. The greater the distance the greater is the difference between the spatial signatures of the pixels from the two images. In this study, the distance threshold was set at 0.70 after several test runs. Distance values greater than the threshold signify change while values below the threshold means no change. The size of the pixel window used is an important factor in a frequency classifier. If the pixel window is too small, insufficient spatial information is included to characterize a specific land-cover class. If the pixel window is too large, it will result in the inclusion of too much spatial information from the other land-cover classes (Gong and Howarth, 1992). After some preliminary experiments, a 5 x 5 pixel window showed optimum change detection accuracy. This window size was used in the experiment.

3. Study area

The areas damaged by the March 11, 2011 Tohoku tsunami and the October 2010 eruptions of Merapi Volcano were chosen as test sites of the developed system. ASTER satellite images before and after the March 11, 2011 Tohoku Earthquake were used to map the areas damaged by the tsunami (Fig. 3). On the other hand, PALSAR images were used to map the areas damaged by ash falls and pyroclastic flows from the eruptions of Merapi Volcano (Fig. 4).

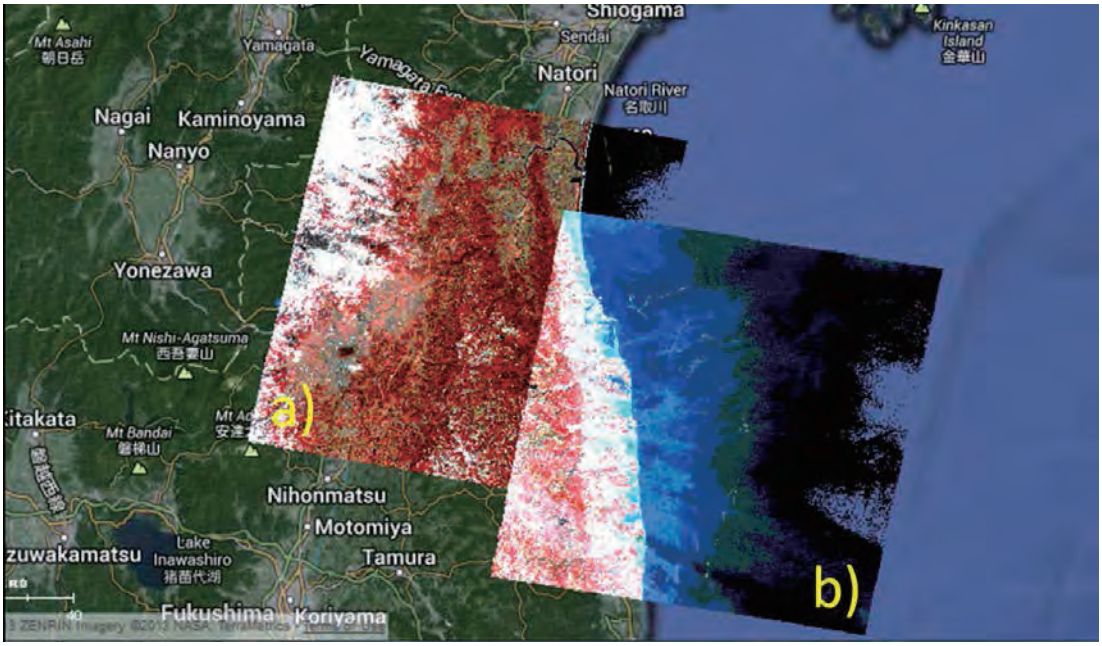

Fig. 3. ASTER images covering part of Fukushima prefecture coastline taken before and after the March 11, 2011 Tohoku Earthquake. a) ASTER image taken on Feb. 24, 2011. b) ASTER image taken on March 14, 2011.

Fig. 4. PALSAR images covering Merapi Volcano in Java Island, Indonesia before and after the October 2010 eruptions. a) PALSAR image taken on Oct. 16, 2010. b) PALSAR image taken on Nov. 1, 2010.

4. Results

This study successfully developed a cheap and efficient system of identifying areas damaged by natural disasters. The WPS and WMS make it possible to map areas affected by the disaster using a WEB browser. It also shows that satellite images obtained through WMS's GetMap requests are sufficient inputs for the developed algorithm to identify damaged areas. The frequency based change detection algorithm developed in this study successfully delineated the areas damaged by the March 11, 2011 tsunami in Honshu Island, Japan (Fig. 5). It also successfully mapped the areas damaged by ash falls and pyroclastic flows during the October 2010 eruptions of Merapi Volcano in Java, Indonesia (Fig. 6). The accuracy of the algorithm in detecting areas damaged by the tsunami is around 85 %. This was determined using aerial photographs and high resolution satellite images. The accuracy of the system in

identifying areas damaged by ash falls and pyroclastic flows was validated by comparing the results obtained using the established low level feature extraction method as shown in Fig. 6. The damaged areas identified by the developed algorithm are 86% correlated to the results obtained using the low level feature extraction method (Fig. 6a). Higher correlation could be observed in areas covered by volcanic ash shown in thin yellow shades in the maps. However, some discrepancies could be clearly observed in areas covered by pyroclastic flows which are shown in thicker yellow shades. More robust method of determining the accuracies in the identification of the areas damaged by volcanic eruptions would be done later when sufficient field data are already available.

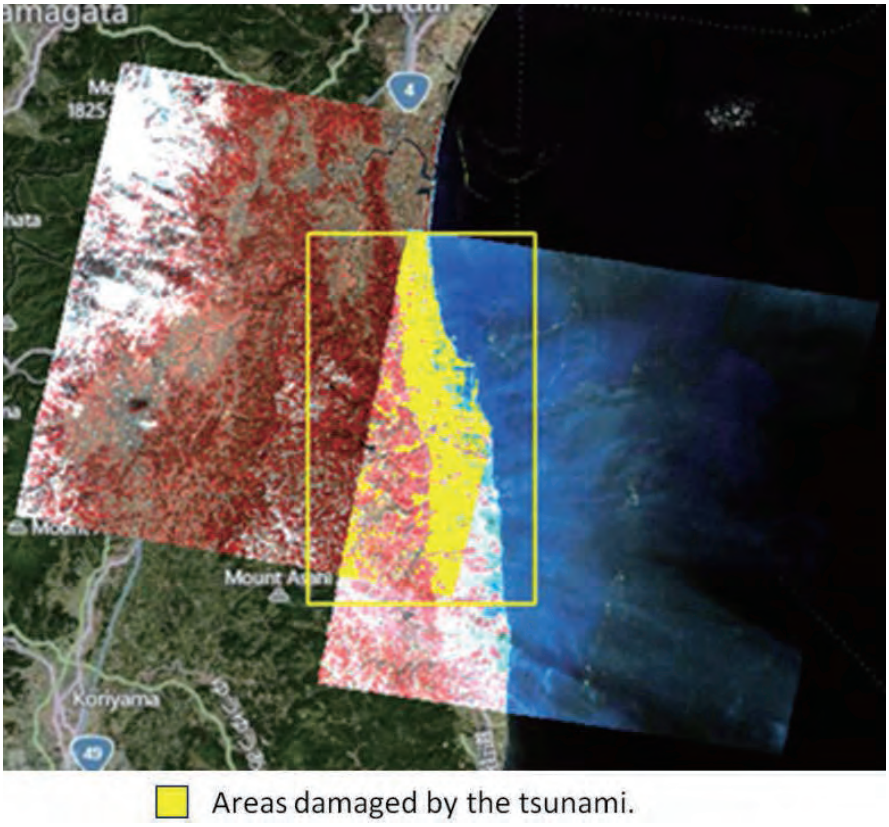

Fig. 5. Map showing areas damaged by the March 11, 2011 tsunami along Fukushima prefecture coastline in Honshu Island, Japan

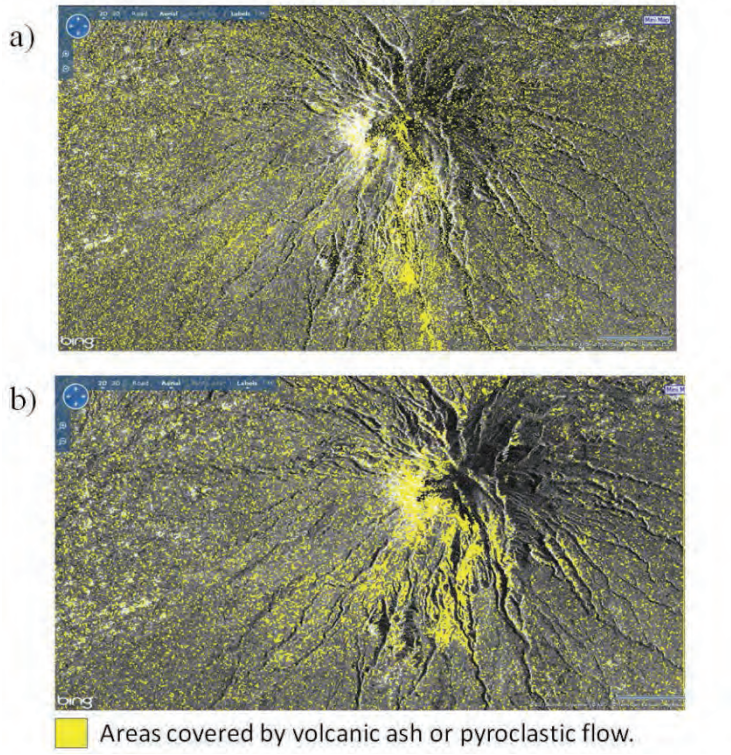

Fig. 6. Maps showing the areas affected by the October 2010 Mount Merapi eruptions. a) Map generated using low level feature extraction method. b) Map generated using the frequency based land cover change detection algorithm.

References

Alonso, F.G., Soria, S.L., 1989. Classification of satellite images using contextual classifiers. Proceedings, 12th Canadian Symposium on Remote Sensing, Vancouver, Canada, July 10-14, 1989. 2, 645-646.

Gong, P., Howarth, P.J., 1992.Frequency-based contextual classification and gray-level vector reduction for land-use identification. Photogrammetric Engineering and Remote Sensing 58(4), 423-437.

Hayes, D.J., Sader, S.A., 2001. Comparison of change-detection techniques for monitoring tropical forest clearing and vegetation regrowth in a time series. Photogrammetric Engineering and Remote Sensing 67(9), 1067-1075.

Khazenie, N., Crawford, M., 1989.Spatial-temporal autocorrelated model for contextual classification of satellite imagery. Proceedings, 12th Canadian Symposium on Remote Sensing, Vancouver, Canada, July 10-14, 1989, 2, 497-502.

Mettemicht, G., 1999. Change detection assessment using fuzzy sets and remotely sensed data: an application of topographic map revision. ISPRS Journal of Photogrammetry and Remote Sensing 54(4), 221-233.

OGC, 2013. *Making Location Count. OGC Standards and Supporting Documents.* Available online at http://www.opengeospatial.org/standards (Access: 20th September 2013).

Peddle, D.R., Franklin, S.E., 1989. High resolution satellite image texture for moderate terrain analysis. Proceedings, 12th Canadian Symposium on Remote Sensing, Vancouver, Canada, July 10-14, 1989, 2, 653-654.

Sing, A., 1986. Change detection in the tropical forest environment of northeastern India using Landsat. Remote Sensing and Tropical Land Management. John Wiley and Sons, New York, 365 pp.

Advanced technology of hazard monitoring by InSAR analysis

Shuichi Rokugawa[1], Takako Nakamura[2], Hiroki Matsuura[3], Hideaki Nakagawa[4] and Ken Tsutsui[5]

[1,2]Research into Artifacts, Center for Engineering, The University of Tokyo
[3]School of Engineering, The University of Tokyo
[4]Sankyo Material Co.
[5]NTT Data
e-mail: rokugawa@gpl.t.u-tokyo.ac.jp

Abstract

We have investigated techniques for the efficient early detection of landslides using time series analysis incorporating synthetic aperture radar (SAR) images. The study area, in the Miyazaki, Nagasaki, and Saga prefectures in Kyushu, was determined based on interference fringes detected during interference SAR (InSAR) analysis. We used ALOS/PALSAR data acquired from 2006–2011 to detect early warning signs of landslides that were poorly expressed geomorphologically by conducting time series analysis of InSAR data (Deguchi et al., 2009) acquired periodically. Moreover, in order to remove the noise caused by geographical feature stripes or phase retardation, we applied median filtering, histogram extraction processing, and enhancement of the displacement with a Laplacian filter. We evaluated the validity of each filter separately and in combination with other filters and assigned a gradient vector to each pixel value of the SAR picture using altitude data. In order to confirm the assumption that surface-of-the-earth displacement proceeds in the dip direction, we conducted direction analysis and confirmed the results of InSAR analysis by field survey. Our results prove the effectiveness of InSAR analysis in hazard monitoring over a wide area through the detection of local landslides.

Keywords: landslide, ALOS/PALSAR data, InSAR analysis, hazard monitoring

1. Introduction

The many mountainous regions in Japan are often characterised by steep topography such as valleys or cliffs, the presence of which can induce sediment disasters such as mud floods, landslides, and landslips. Recently, large-scale typhoons and abnormal weather have caused local increases in heavy rain, producing conditions that are conducive to large-scale landslides and causing extensive damage. Therefore, it is essential to develop techniques to detect such potential landslide before its occurrence in order to mitigate the effects. In the present study, we demonstrate the use of interference synthetic aperture radar (InSAR) in detecting early signs of landslides and discuss the production of a new hazard map. In the study area, the Wanitsuka Mountains in Miyazaki Prefecture (Fig. 1), a particularly noticeable large-scale collapse was induced by Typhoon 14 in 2005 (JASDiM, 2013), although collapses of varying magnitudes occur often in the region. For such areas, it should be possible to obtain information that would be useful in the prediction of landslide disasters, particularly in the detection of precursory phenomenon of large-scale landslides.

2. Methods

InSAR is the most appropriate technique for analysing changes in ground movement with time over large areas. Such monitoring can offer many advantages, particularly in the

detection of the precursory phenomena of landslide disasters. We conducted an investigation into landslide disasters occurring between 2008 and 2009 in the region around the Wanitsuka Mountains (Fig. 2), including local InSAR analysis. We used a high SAR interference pair of the coherence from a PALSAR data 10 scene acquired by December 2010 from April 2008. In the Imari area of northern Kyushu, we used 38 scenes acquired between May 2006 and January 2011 and used a high SAR interference pair of the coherence. Then, we quantitatively evaluated the precision of the InSAR data and conducted time series analysis to clarify variations in local upheaval or settlement in order to assess ground deformation. The Imari area of Saga Prefecture can be considered a real landslide disaster zone. However, the SAR imagery obtained for this area was unclear, making it an ideal location to test our newly developed detection technique. Therefore, we extracted information for a landslide that occurred on 24 April 2010 by applying filters to remove noise and clarify ground movement. As a result, for any place other than the point where landslide happened, we were able to detect the point considered that an initial change was caused. During this process, we corrected for the measurement error associated with InSAR and assessed the effectiveness of the technique. However, it proved difficult to remove all noise.

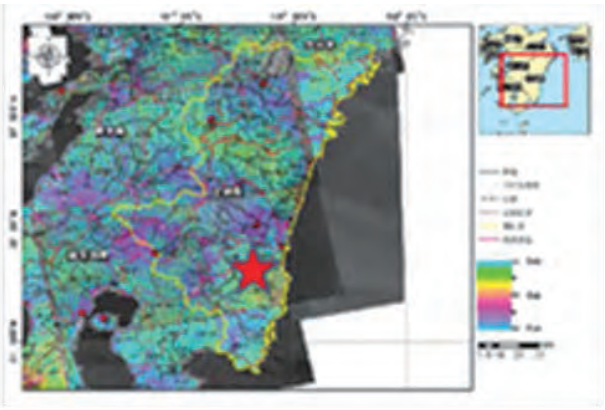

Fig. 1. The area around the Wanitsuka Mountains in Miyazaki Prefecture, indicated by the red star.

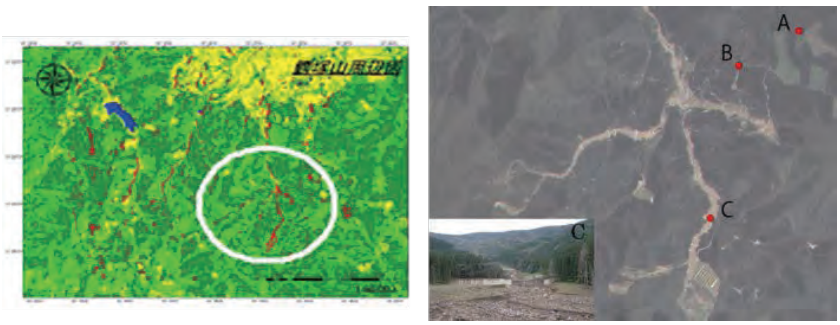

Fig. 2. Image of a disaster situation in the Mt. Wanitsuka area. The study area surrounded by white circle (left). ALOS/PRISM image and field photo of a disaster site around Mt. Wanitsuka area (right). PRISM image was acquired in 2007.

We used a composite filter incorporating three individual filtering techniques.

(1) Median filtering

We calculated a median using a 3 × 3 area comprising a target picture element and its neighbouring picture elements; the value obtained is an object pixel value. This filter was shown to be acceptable for the removal of spot-formed noise in InSAR images.

(2) Histogram extraction processing

We normalised the InSAR displacement data and removed all small displacements from the SAR image. We removed 80% of low order by the ground displacement magnitude detection of the cm unit and, in the case of mm unit, removed 60%.

(3) Laplacian filter

We used a 51 × 51 operator derived from a four-dimensional operator that radicalised the surface displacement using a standard second derivative filter to produce a weighted-mean picture element area.

3. Results and discussion

In Figure 3, the left side illustrates the results obtained for an InSAR image of the Imari area using various filter processes. Landslide detection is difficult based on the images in Fig. 3a and 3c, because big noise has not been removed from these images. Conversely, the representation of surface displacements is improved in Fig. 3b, from which big noise (but not small noise) has been removed. Fig. 3d illustrates the results obtained by radicalising displacement and noise; surface displacements can be detected in this image, indicating that it is desirable to perform Laplacian filtering after removal of noise. Fig. 3e illustrates the results achieved by applying both median filtering and histogram extraction and suggests that noise reduction is useful in the acquisition of displacement magnitude. The location of the landslide is clearly indicated in Fig. 3f, for which all filtering techniques were applied. The results presented here indicate that InSAR is effective in detecting micro-displacements that occur during the early stages of landsliding and that detection of these displacements can be improved by application of filtering processes, at least in the Imari area. The InSAR image in the right figure indicates the actually collapsed area (A) and the similar uncollapsed (B) area over the road. This area can be considered as the “risky area” for a future landslide.

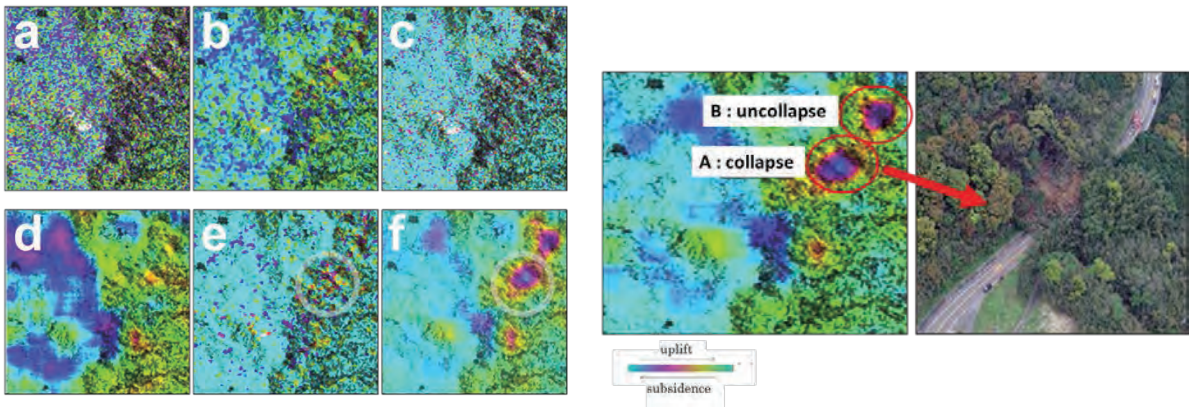

Fig. 3. Effects of filter application to InSAR imagery for the Imari area is shown in the set of left side figures. Circles indicate areas of landsliding. (a) InSAR image, (b) median filtering, (c) histogram extraction (upper 20% extract of the normalised displacement), (d) Laplacian filter, (e) median filtering and histogram extraction, (f) median filtering and histogram extraction and Laplacian filter. The right side figures are4 respectively enhanced InSAR image and landslide photo over the road.

Figures 4a and 4b illustrate the interferogram using various filter processes for the region around the Wanitsuka Mountains and an interpretation of the decay incidence area based on aerial photographs, respectively, confirming the changes in ground movement that were

suggested by previous field study. On the basis of the InSAR results, we believe that fluctuations in the ground surface continued after decay. Decay induced by the typhoon of 2005 was not detected in areas 7 and 9 (Fig. 4), although evidence suggests that subsidence continued in these areas following the typhoon. Subsidence of approximately 9 cm was found in area 4 over a period of two years and eight months; this represents the greatest fluctuation in ground level detected in the region, although subsidence of 4–6 cm was found in other areas. These results suggest that the newly developed technique is suitable for the assessment of such ground movements. However, problems remain in terms of the interpretation of the consequence of the research technique by the application to more areas and rearranging of the application limit. Therefore, the technique must be verified through further analysis.

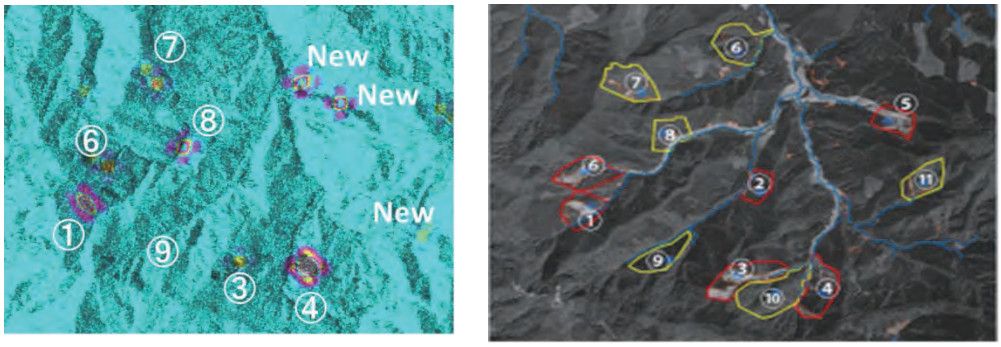

Fig. 4. The left side figure indicates the interferogram around the Wanitsuka Mountains of Miyazaki Prefecture (ALOS/PALSAR data acquired from 2006 – 2011). The right side figure shows collapsed area (red) and predicted collapse area (yellow) as was interpreted based on aerial photographs acquired from 1946 to 2005.

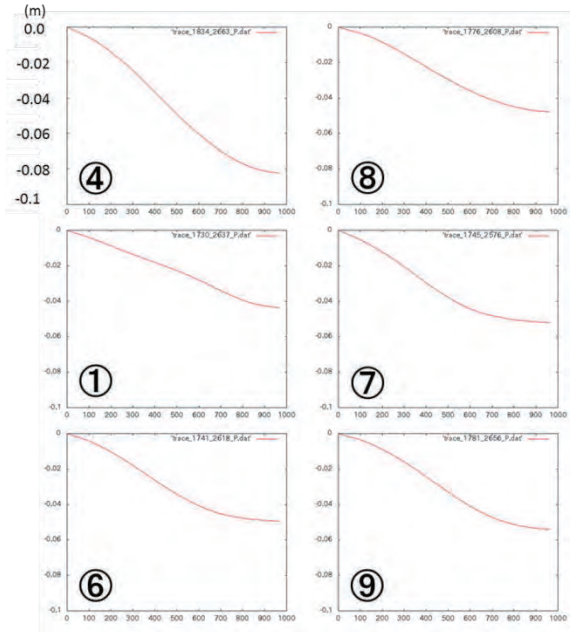

Fig. 5. The profiles of ground deformation from 2008 to 2010.

4. Conclusions

The InSAR images and time series analyses presented here enable estimation of the incidence device of the landslide and demonstrate the possibility of detecting precursory phenomena

related to the occurrence of large-scale landslides. Moreover, the results suggest that the technique evaluated here can offer information that will help the drafting of the first ground movement system of landslide measures (e.g. in deciding where monitoring components such as GPS equipment should be placed). We investigated the effectiveness of the measures described here by performing the monitor after measures sequentially. The results confirm that our techniques are effective in detecting landslide-related ground fluctuations over wide areas. Furthermore, we have demonstrated that it is possible to construct hazard maps for large areas based on the ground movements detected. In this manner, InSAR images may make a considerable contribution to disaster prevention.

Acknowledgement

The authors would like to thank ERSDAC for providing PALSAR L-band data.

References

Deguchi, T., Rokugawa, S., and Matsushima, J., 2009, Long-term ground deformation measurement by time series analysis for SAR interferometry: Journal of the Remote Sensing Society of Japan, 29, 2, 418-428.

Japan Association for Slope Disaster Management (JASDiM), 2013, http://www.jasdim.jp/kenbetu/miyazaki/miyazaki.htm.

Spatial prediction of landslide hazard along the National Road 32 of Vietnam: A comparison between Support Vector Machines, Radial Basis Function neural networks, and their ensemble

Dieu Tien Bui[1, 2], Quach Duc Tin[3], Pham Viet Ha[4], Inge Revhaug[1], Ngo Van Liem[5], Tran Thanh Ha[6], and Bui Le Hoan[7]

[1]Department of Mathematical Sciences and Technology, Norwegian University of Life Sciences, P.O. Box 5003-IMT, N-1432, Aas, Norway
[2]Faculty of Surveying and Mapping, Hanoi University of Mining and Geology, Dong Ngac commune, Tu Liem district, Hanoi, Vietnam
[3]General Department of Geology and Minerals of Vietnam, No 6 Pham Ngu Lao, Hanoi, Vietnam
[4]Department of Tectonic and Geomorphology, Vietnam Institute of Geosciences and Mineral Resources, Thanh Xuan district, Hanoi, Vietnam
[5]Vietnam Academy of Science and Technology, 84 Chua Lang Street, Hanoi, Vietnam
[6]VNU Institute of Vietnamese Studies and Development Sciences, Hanoi, Vietnam
[7]Vietnam Institute of Geodesy and Cartography, 479 Hoang Quoc Viet Street, Hanoi, Vietnam
e-mail: BuiTienDieu@gmail.com

Abstract

The objective of this study is to evaluate and compare the prediction performance of Support Vector Machines (SVM), Radial Basis Function neural networks (RBFN), and their ensemble for landslide susceptibility mapping along National Road 32 of Vietnam. First, a landslide inventory map accounting for landslides that occurred during the last twenty years was constructed from various sources. A total of 262 such landslide locations were identified. The landslide inventory was randomly split into two subsets: (i) Part 1 that contains 70% was used for building models; (ii) Part 2, a validation dataset that contains 30%, was used for the models validation. Then, ten landslide conditioning factors were prepared. These are slope, aspect, relief amplitude, topographic wetness index (TWI), toposhape, distance to roads, distance to rivers, distance to faults, lithology, and rainfall. Thirdly, using SVM, RBFN, and Bagging ensemble technique, four landslide susceptibility maps were constructed. Finally, the resultant landslide susceptibility maps were validated and compared using the validation dataset not used during the model building and the ROC method. The results show that all the models have good prediction capabilities. The SVM (AUC=0.915) and the SVM with Bagging ensemble (AUC=0.917) has the highest prediction capability, followed by the RBFN with Bagging ensemble (AUC=0.886), and RBFN (AUC=0.877). The results from this study may be useful for decision making and policy planning in areas prone to landslides.

Keywords: Support Vector Machine, neural network, ensemble technique, landslide, Road 32, Vietnam

1. Introduction

Landslides are one of the recurrent geo-hazards that are widespread in the northwest mountainous areas of Vietnam, and that have caused various types of damage variously affecting people, organizations, infrastructure, and the environment (Tien Bui et al., 2012). According to Tam (2001), the annual damage is estimated at around 100 million USD. Landslides have occurred widely on cut slopes, especially along the national highways such as the National Roads No. 2, No. 3, No. 6, and No. 32 (Duc, 2013). Therefore, the identification of areas susceptible to landslides and understanding the landslide mechanism

are an urgent task. This will help in landslide risk assessment and will contribute to public safety as well as improving land use planning and management.

Various techniques and methods for modeling landslides have been developed, and they vary from simple methods to sophisticated models (Chung and Fabbri, 2008; Tien Bui et al., 2014). Reviews of the advantages and disadvantages of these techniques and methods can be seen in Chacon et al. (2006). According to Yilmaz (2010), the prediction capability of landslide susceptibility models is influenced by the method used and sampling strategy, therefore the investigation of new techniques and the comparative studies of different methods are highly necessary.

This paper presents a comparative assessment of Support Vector Machines (SVMs), Radial Basis Function neural networks (RBFNs), and their Bagging ensemble for spatial prediction of the landslide hazard along the National Road 32 of Vietnam. The difference between this study and the aforementioned literature is that SVM and RBFN, and Bagging ensembles techniques were used. The computation process was carried out using ArcGIS^{TM}, MATLAB^{TM} and WEKA^{TM}. Finally, a comparison of the results was made in order to identify the best technique.

2. Study area and data used

2.1 Study area

The study area is situated in a northwestern region of Vietnam, along the corridor of the National Road No. 32 (Fig. 1). It covers an area of around 3,164 km^2, between the latitudes 22^{o}20$'$18$''$N and 21^{o}19$'$53$''$N, and between the longitudes 103^{o}33$'$23$''$E and 104^{o}52$'$58$''$E. The length of the road is about 250 km.

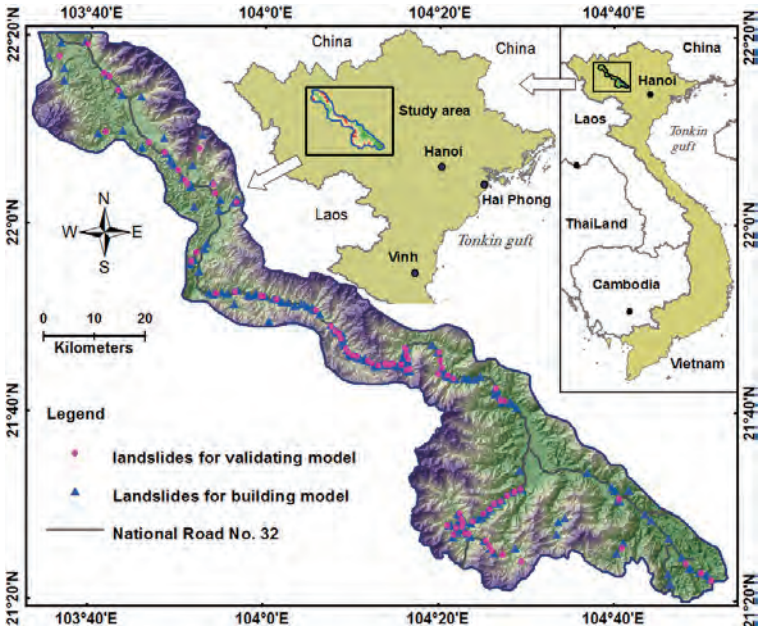

Fig. 1. Landslide inventory map of the study area.

The altitude of the study area decreases from the northwest to the southeast and ranges from 3,140 m to 120 m. The statistical analysis shows that approximately 22.3% of the total area falls within slope group 0^o-15^o, around 52.9% of the area has slope greater than 25^o, and the remaining areas are in the slope category 15^o-25^o (Tien Bui et al., 2014). Geologically, the

study area comprises sandstone, conglomerate, clay shale, clayey limestone, siltstone, limestone, and clayey limestone.

2.2 Data

In the study area, the inventory map (Fig. 1) that was prepared earlier by Ho (2008) was used for the quantitative relationship analysis between the landslide occurrences and conditioning factors. A total of 262 landslides that occurred during the last 20 years were identified and these were depicted by polygons. The largest landslide size is 37,326 m^2 and the smallest landslide size is about 476 m^2.

In the previous study, Ho (2008) investigated correlations between landslide occurrence and several landslide conditioning factors. Based on these findings, ten landslide conditioning factors were used in this study. These were slope, aspect, relief amplitude, toposhape, TWI, distance to roads, distance to rivers, lithology, distance to faults, and rainfall.

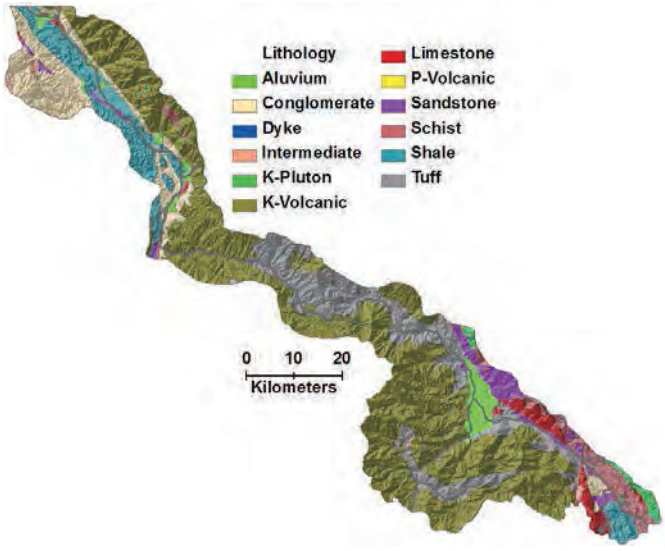

Fig. 2. Lithological map.

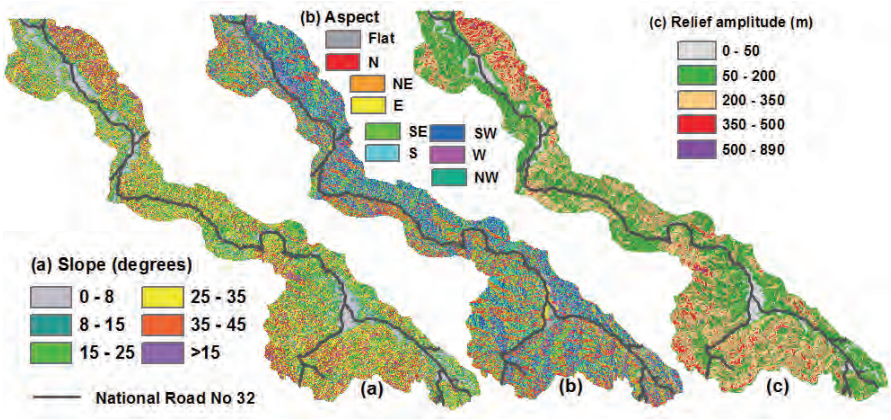

Fig. 3. (a) Slope map, (b) Aspect map, and (c) Relief amplitude map.

First, a digital elevation model (DEM) was generated using the National Topographic maps at 1:50,000 scale. The resolution of the DEM is 20 m. Using the DEM, the slope, aspect, relief amplitude, toposhape, and TWI were extracted and constructed (Figs. 3 and 4). A lithology

map (Fig. 2) and distance to faults map (Fig. 4c) were constructed from the 1:200,000 scale Geological and Mineral Resources Maps. Distance to roads and distance to rivers maps (Figs. 5a and 5b) were constructed based on the river and road networks from the 1:50.000 scale National Topographic maps. Finally, a rainfall map (Fig. 5c) was constructed and included in the analysis. The details of the classes for the ten conditioning factors are shown in Table 1.

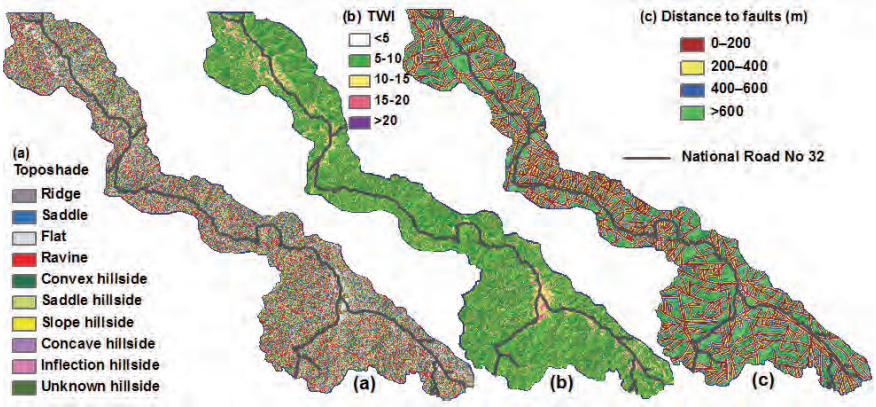

Fig. 4. (a) Toposhade map, (b) Topographic wetness index (TWI) map, and (c) Distance to faults map.

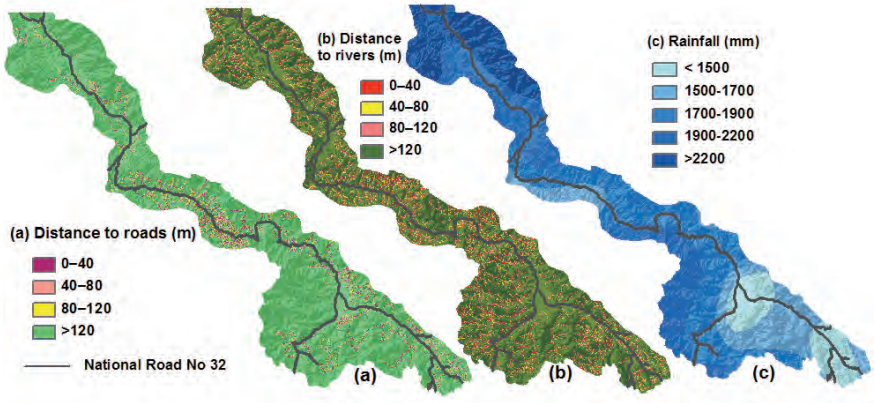

Fig. 5. (a) Distance to roads map, (b) Distance to rivers map, and (c) Rainfall map.

3. Landslide susceptibility mapping

3.1 Preparation of training and validation data

In this study, the landslide inventory and ten conditioning factor maps were converted to a grid cell format with a cell-size of 20 m. Then an attribute value for each class was assigned based on frequency ratio. Finally, the normalization process was carried out to the range 0.1 to 0.9 for each conditioning factor (Table 1) (Tien Bui et al., 2012). In this study, the landslide inventory map was randomly portioned in a 70/30 ratio for training (2781 landslide pixels) and validation (1011 pixels) of the model, respectively (Fig.1). In the next step, a total of 2,781 non-landslide pixels were randomly sampled from the landslide-free area. Finally, values for the ten landslide conditioning factors were then extracted to build a training dataset.

Table 1. Landslide conditioning factors and their classes.

Data layers	Class	Class pixel	Landslide Pixel	Frequency ratio	Attribute	Normalized classes
Slope (degree)	0-8	1050626	0	0.000	1	0.10
	8-15	707774	197	0.578	2	0.45
	15-25	1949706	1226	1.305	3	0.90
	25-35	2352056	1471	1.298	4	0.89
	35-45	1379361	748	1.126	5	0.79
	> 45	431672	150	0.721	6	0.54
Aspect	Flat	370810	0	0.000	1	0.10
	North	880893	282	0.665	2	0.39
	Northeast	954851	217	0.472	3	0.31
	East	887194	468	1.095	4	0.58
	Southeast	943832	595	1.309	5	0.68
	South	1016869	891	1.819	6	0.90
	Southwest	1061249	622	1.217	7	0.64
	West	893222	252	0.586	8	0.36
	Northwest	862275	465	1.119	9	0.59
Relief amplitude	0–50	494988	85	0.356	1	0.30
	50–200	3797449	2664	1.456	2	0.90
	200-350	3106823	994	0.664	3	0.46
	350-500	449532	49	0.226	4	0.22
	>500	27992	0	0.000	5	0.10
TWI	<5	744	0	0.000	1	0.10
	5-10	6246498	3538	1.176	2	0.90
	10-15	1328468	249	0.389	3	0.36
	15-20	233435	5	0.044	4	0.13
	>20	20661	0	0.000	5	0.11
Toposhape	Ridge	1437448	744	1.074	1	0.81
	Saddle	113672	0	0.000	2	0.10
	Flat	374668	0	0.000	3	0.11
	Ravine	1399148	546	0.810	4	0.63
	Convex hillside	1030755	517	1.041	5	0.78
	Saddle hillside	2408283	1403	1.209	6	0.89
	Slope hillside	16366	0	0.000	7	0.12
	Concave hillside	945577	555	1.218	8	0.90
	Inflection hillside	60540	27	0.926	9	0.71
	Unknown hillside	90484	0	0.000	10	0.13
Lithology	Alluvium	239956	79	0.683	1	0.10
	Conglomerate	789689	188	0.494	2	0.11
	Dyke	27674	23	1.725	3	0.21
	Intermediate	42216	0	0.000	4	0.24
	K-Pluton	87073	0	0.000	5	0.30
	K-Volcanic	4030918	1725	0.888	6	0.38
	Limestone	240162	39	0.337	7	0.43
	P-Volcanic	5770	0	0.000	8	0.46
	Sandstone	237588	192	1.677	9	0.48
	Schist	274344	125	0.946	10	0.78
	Shale	679581	269	0.822	11	0.80
	Tuff	1204892	1152	1.985	12	0.90
Distance to Faults (m)	0–200	2419662	1636	1.403	1	0.90
	200–400	2027888	989	1.012	2	0.53
	400–600	1442500	635	0.914	3	0.44

	>600	1986891	532	0.556	4	0.10
Distance to Roads (m)	0–40	273124	1139	8.656	1	0.90
	40–80	292995	958	6.787	2	0.72
	80–120	288433	582	4.188	3	0.47
	>120	7022389	1113	0.329	4	0.10
Distance to Rivers (m)	0–40	541068	467	1.792	1	0.77
	40–80	581557	518	1.849	2	0.80
	80–120	576604	555	1.998	3	0.90
	>120	6177712	2252	0.757	4	0.10
Rainfall (mm)	< 1500	892649	215	0.500	1	0.18
	1500-1700	1397443	770	1.144	2	0.64
	1700-1900	2272315	1644	1.502	3	0.90
	1900-2200	2060447	925	0.932	4	0.49
	>2200	1254071	238	0.394	5	0.10

3.2 Support Vector Machines

Assume a training dataset of instance-label pairs (x_i, y_i) with $x_i \in R^n$, and i = 1,…, n. x is a vector of input space that contains the ten landslide conditioning factors. The two classes $y_i \in \{1, -1\}$ denote landslide and no-landslide pixels. The objective of the SVM training is to find an optimal hyper-plane that separates the dataset into two classes one with landslides and one with no-landslides. The optimal hyper-plane is obtained by solving the following optimization function as follows:

$$\underset{W,b,\xi}{\text{Minimize}} : \frac{1}{2} W^T W + C \sum_{i=1}^{l} \xi_i \quad (1)$$

$$\text{Subject to } y_i (w^T j(X_i) + b) \geq 1 - \xi_i \quad (2)$$

where w is a coefficient vector that determines the orientation of the hyper-plane, b is the offset of the hyper plane from the origin, ξ_i is the positive slack variables, and C is the penalty parameter that controls the trade-off between the maximum margin and the minimum error.

The decision function that is used for the classification of new data can be written as follows:

$$f(x) = \text{sign}\left(\sum_{i=1}^{l} y_i \alpha_i K(X_i, X_j) + b\right) \quad (3)$$

where $K(X_i, X_j) = j(X_i)^T j(X_j)$ is the kernel function.

In this study, the kernel function of Radial Basis Function is selected (Tien Bui et al., 2012). The training process was carried out using 10 fold cross validation. Classification accuracy of the resulting SVM model is 89.8%. The detailed result is shown in Tables 2, 3 and 4.

3.3 Radial Basic Function Network

Radial Basic Function Network (RBFN) is defined as a supervised neural network for modeling problem in poly-dimensional space (Osanai et al., 2010). The architecture of this network is designed comprising three layers. The first one is the input layer, the second one is the hidden layer that contains m neurons, and the last one is the output layer that contains one neuron. Using the training dataset, the network is trained to find that minimize the error E as follows:

$$E = \sum_{i=1}^{n} (y_i - O(x_i)) + \sum_{j=1}^{m} \lambda_j w_j^2 \quad (4)$$

where w_i is the load coefficient; $O(x)$ is the output of the RBFN.

The output value of the output layer is calculated as

$$O(x) = \sum_{j=1}^{m} w_j h_j;\ h_j(x) = \exp\left(-\frac{\left\| x - c_j \right\|^2}{r^2}\right) \quad (5)$$

where $h_i(x)$ is output value from *j*-th hidden neuron that is the radial basis function; c_j is the center point of the basis function; r is radius of the basis function. In this study, RBFN was trained with 18 clusters. The classification accuracy of the trained model is 84.39%. The detailed result is shown in Tables 2, 3 and 4.

3.4 Bagging ensemble approaches

Bagging (short for bootstrap aggregating) is one of the earliest ensemble learning algorithms proposed by Breiman (1996). Using the training dataset, Bagging uses bootstrap sampling to generate multiple subsets. Based on each of the subsets, a classifier-based model is constructed. The final model is formed by aggregating all classifier-based models.

Using the training data set, the SVM with Bagging and RBFN with Bagging were constructed. Classification accuracy of the trained SVM with Bagging and the RBFN with Bagging models are 90.13% and 84.89% respectively. The detailed result is shown in Tables 2, 3 and 4.

3.5 Reclassification of landslide susceptibility maps

The susceptibility indexes were reclassified into five classes based on the percentage of area (Pradhan and Lee, 2010): very high (10%), high (10%), moderate (20%), low (20%), and very low (40%) (Figs. 6 and 7).

4. Validation and comparison of the landslide susceptibility models

4.1 Model evaluation

In this study, five statistical evaluation criteria were used to evaluate the performance of the four susceptibility models. They are (i) model accuracy; (ii) model sensitivity; (iii) model specificity; (iv) Cohen's kappa and (v) and the area under the success-rate curve (AUC) (Tien Bui et al., 2012). The results are shows in Tables 2, 3 and 4. It could be observed that all the models have high classification accuracy. The SVM and SVM with Bagging have the highest classification accuracy, followed by RBFN with Bagging, and RBFN.

The reliability of the four models was assessed using Cohen's kappa index. For the SVM with Bagging, Cohen's kappa index is 0.803 indicating good agreement between the susceptibility model and reality. For the SVM, RBFN with Bagging, and RBFN, Cohen's kappa indexes are 0.796, 0.698, and 0.688 respectively. They indicate that substantial agreement between the three models and reality. The detailed accuracy assessment by classes is shown in Table 3.

Table 2. Performance of the SVM, the SVM with Bagging, the RBFN, and the RBFN with Bagging models.

Parameters	SVM	SVM with Bagging	RBFN	RBFN with Bagging
Classification accuracy (%)	89.80	90.13	84.39	84.89
Cohen's Kappa index	0.796	0.803	0.688	0.698
Root mean squared error (RMSE)	0.271	0.269	0.342	0.338

Table 3. Landslide conditioning factors and their classes

Landslide model	True Positive rate (%)	False Positive rate (%)	F-measure (%)	Class
SVM	0.895	0.099	0.898	Landslide
	0.901	0.105	0.898	No-landslide
SVM with Bagging	0.901	0.098	0.901	Landslide
	0.902	0.099	0.901	No-landslide
RBFN	0.852	0.164	0.845	Landslide
	0.836	0.148	0.843	No-landslide
RBFN with Bagging	0.853	0.155	0.85	Landslide
	0.845	0.147	0.848	No-landslide

Table 4. Area under the curves (AUC) based on the validation dataset for the SVM, the SVM with Bagging, the RBFN, and the RBFN with Bagging models.

No	Landslide model	AUC	Std. Error	95% CI	
				Lower Bound	Upper Bound
1	SVM	0.915	0.00625	0.904	0.928
2	SVM with Bagging	0.917	0.00632	0.902	0.927
3	RBFN	0.877	0.00806	0.862	0.891
4	RBFN with Bagging	0.886	0.00762	0.871	0.899

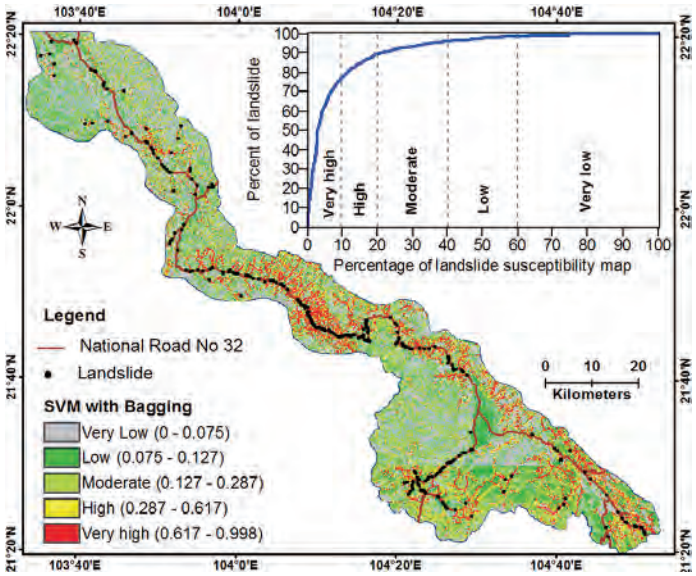

Fig. 6. Landslide susceptibility map using the SVM with Bagging.

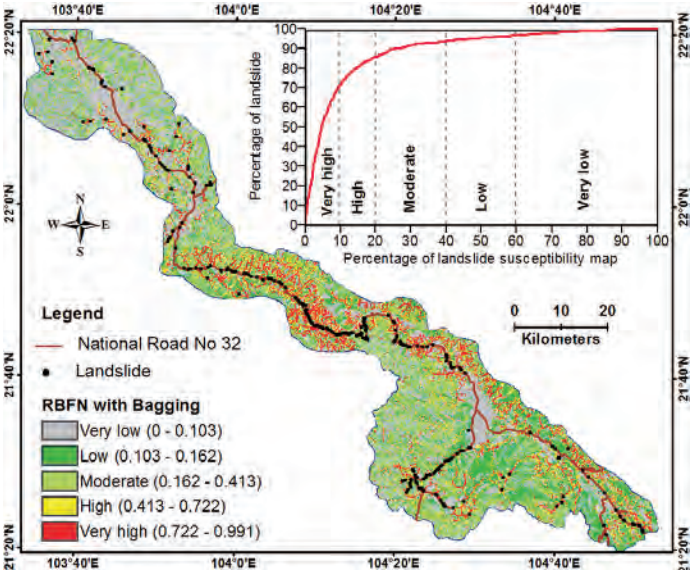

Fig. 7. Landslide susceptibility map using the RBFN with Bagging.

The degree-of-fit of the four landslide models with the training dataset were derived by comparing the 2,781 landslide grid cells with the four susceptibility maps using the ROC curve method. The areas under the ROC curves (AUC) were estimated and the result is shown Fig.8. The result shows that all the models have a good fit with the training dataset. The highest degree of fit is for the SVM (0.961) and the SVM with Bagging (0.962), they are followed by the RBFN with Bagging (0.924) and the RBFN (0.911).

By comparing the landslide grid cells in the validation dataset with the four landslide susceptibility maps, four prediction-rate curves for the landslide models were constructed. The result is shown in Fig. 9 and Table 4.

5. Discussion and conclusions

In this study, SVM, RBFN, and the Bagging ensemble techniques were used for constructing landslide susceptibility maps along National Road No 32 of Vietnam. Using ten conditioning factors and the landslide locations in the training dataset, four susceptibility models were built. These maps only show spatial predictions of future landslides.

In general, all the models have high performance. The SVM and SVM with Bagging ensemble models have higher degrees-of-fit to the training data than do the RBFN and the RBFN with Bagging models.

The prediction capability of the four landslide models were estimated using landslide location data that was not used in the training phase. The results show that the SVM with Bagging and the SVM models have the highest prediction capability. There is no significant difference between the SVM and the SVM with Bagging models. However, the prediction capability of the RBFN with Bagging model increased by about 1% as compared to the RBFN model.

The reliabilities of the landslide models were assessed using Cohen's Kappa index. The index results, from 0.688 to 0.803, show substantial agreement between the susceptibility model and reality for all the models.

As a final conclusion, the results of this study suggested that the SVM model is the most preferable. These results may be useful for policy planning and decision making in areas prone to landslides.

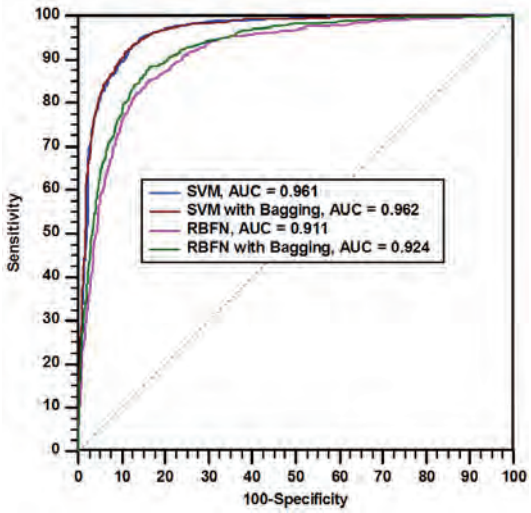

Fig. 8. ROC curves and area under the curves (AUC) for the SVM, the SVM with Bagging, the RBFN, and the RBFN with Bagging.

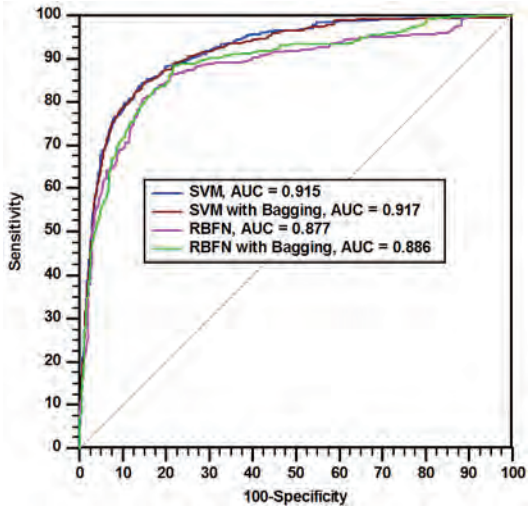

Fig. 9. Prediction-rate curves and area under the curves (AUC) for the SVM, the SVM with Bagging, the RBFN and the RBFN with Bagging.

Acknowledgements

This research was supported by the Geomatics Section, Department of Mathematical Sciences and Technology, Norwegian University of Life Sciences, Norway.

References

Breiman, L., 1996, Bagging Predictors: *Machine Learning*, **24**, 123-140.

Chacon, J., Irigaray, C., Fernandez, T., and El Hamdouni, R., 2006, Engineering geology maps: landslides and geographical information systems: *Bulletin of Engineering Geology and the Environment*, **65**, 341-411.

Chung, C.-J., and Fabbri, A.G., 2008, Predicting landslides for risk analysis - Spatial models tested by a cross-validation technique: *Geomorphology*, **94**, 438-452.

Duc, D., 2013, Rainfall-triggered large landslides on 15 December 2005 in Van Canh District, Binh Dinh Province, Vietnam: *Landslides*, **10**, 219-230.

Ho, T.C., 2008, Application of structural geology methods, remote sensing, and GIS for the

assessment and prediction of landslide and flood along the National Road 32 in the Yen Bai and Lai Chau provinces of Vietnam: Hanoi, Vietnam Institute of Geosciences and Mineral Resources, p. 118.

Osanai, N., Shimizu, T., Kuramoto, K., Kojima, S., and Noro, T., 2010, Japanese early-warning for debris flows and slope failures using rainfall indices with Radial Basis Function Network: *Landslides*, **7**, 325-338.

Pradhan, B., and Lee, S., 2010, Delineation of landslide hazard areas on Penang Island, Malaysia, by using frequency ratio, logistic regression, and artificial neural network models: *Environmental Earth Sciences*, **60**, 1037-1054.

Tam, D.M., 2001, Flooding and landslides at the highways of Vietnam, Proceedings of the International Workshop on "Saving Our Water and Protecting Our Land", 20-22 Oct. 2001, Hanoi, 18-27.

Tien Bui, D., Ho, T.C., Revhaug, I., Pradhan, B., and Nguyen, D., 2014, Landslide Susceptibility Mapping Along the National Road 32 of Vietnam Using GIS-Based J48 Decision Tree Classifier and Its Ensembles, *in* Buchroithner, M., Prechtel, N., and Burghardt, D., eds., Cartography from Pole to Pole: Lecture Notes in Geoinformation and Cartography, Springer Berlin Heidelberg, 303-317.

Tien Bui, D., Pradhan, B., Lofman, O., and Revhaug, I., 2012, Landslide susceptibility assessment in Vietnam using Support vector machines, Decision tree and Naïve Bayes models: *Mathematical Problems in Engineering*, **26**, Doi:10.1155/2012/974638

Yilmaz, I., 2010, Comparison of landslide susceptibility mapping methodologies for Koyulhisar, Turkey: conditional probability, logistic regression, artificial neural networks, and support vector machine: *Environmental Earth Sciences*, **61**, 821-836.

The importance of geological input for land-use planning - Case study in the Ranau Area, Sabah

Zamri Bin Ramli and Basharuddin Bin Ismail

Minerals and Geoscience Department of Malaysia
e-mail: basharuddin@jmg.gov.my

Abstract

Geological input is of fundamental importance during the planning of physical development and recognition of this is an essential part of sustainable land-use management. As Sabah is known for its geological complexity and active tectonics, planning should take into the upmost consideration its geological conditions. Due to its geohazard problems and its topography, the Ranau area is known as a geologically sensitive area where there is a need to recognise the geological features that could influence planning decisions. In this case study, geological terrain mapping is being employed as an effective mapping tool to identify various geological factors that will provide the geological input for land-use planning in the study area. The output of the geological terrain mapping will be the production of several derivative maps such as construction suitability map, landform map, erosion map, physical constraints map, terrain classification map and engineering geology map. In addition, for the effective interpretation of the geological input in the context of land-use planning, attention should be given to the causes and sources of the geological problems which are known to arise in the study area.

Keywords: Geology, geological terrain mapping, land-use, geohazard, derivative maps

1. Introduction

There is an increasing desire amongst those involved in the land-use planning process for the availability of adequate information on potential geological constraints to development. Basic information such as the geology, topography and landforms of the area, as well as the relevant geotechnical details are required. Effective planning requires the input of geological data at an early stage, perhaps during the formulation of the proposed development. However, for various social, political and economic reasons, there will always be development in areas prone to geohazards such as landslides or earthquakes.

For the Ranau area, which is known as a geologically sensitive area due to its vulnerability to various geohazards, there is a need to recognise the geological features that could influence planning decisions. With rapid development of the area, building platforms for resorts in hilly areas through cut and fills activities are often carried out without apparent regard to the geological factors which ultimately will influence the stability of ground condition of the particular sites. Field records show that the Ranau area has continually experienced active landslide problems. There are many signs of slope instability such as tension cracks, displacement of concrete drains, road subsidence and tilting of vegetation, fencing and electricity poles in the area. The study area is also known to have experienced tremors from earthquakes from time to time.

Earthquake records have been compiled by Lim (1985), Leyu et al. (1985) and Lim and Paulus (1992). From the above records, there are at least four previous occurrences of

earthquakes (July 27, 1911, October 18, 1965, May 18, 1966 and May-July 1991) being felt in the Ranau area. The felt intensity due to the 1991 Ranau Earthquake Swarm was VI on the Modified Mercalli Scale (Lim and Paulus, 1992). The 1992 earthquake resulted in one fatality and caused extensive damage to buildings and other man-made structures. These problems have a great impact on the community and its socio-economic development and also impose strains on the government due to the high costs of repair and maintenance of the infrastructure. Most of these misfortunes could have been avoided or at least reduced if only the role of geology has been taken into consideration during development planning.

This paper intends to highlight the importance of geological terrain mapping as a primary source of information to assist the local authorities in reviewing requests for future development in the Ranau area, as well as use by other relevant authorities, especially those involved in the town and country planning.

2. Objectives

The objective of geological terrain mapping is to collect and provide systematic geological information for land-use planning through the production of various thematic maps. The geological data and maps produced can be used to assist in the planning for future sustainable development in the Ranau area.

3. Location and Topography

The study area is located in Ranau District, encompassing JUPEM Topographical Map Sheets 7628 and 7629 at 1:10,000 scale. The mapping covers a total area of 100 km^2 as shown in Fig. 1 and is bounded as follows: latitude from 05^{o}55’25”N to 06^{o}01’10”N and longitude from 116^{o}35’45’’E to 116^{o}41’35’’E. It can be reached via the Kota Kinabalu-Sandakan Highway and is about 120 km from Kota Kinabalu.

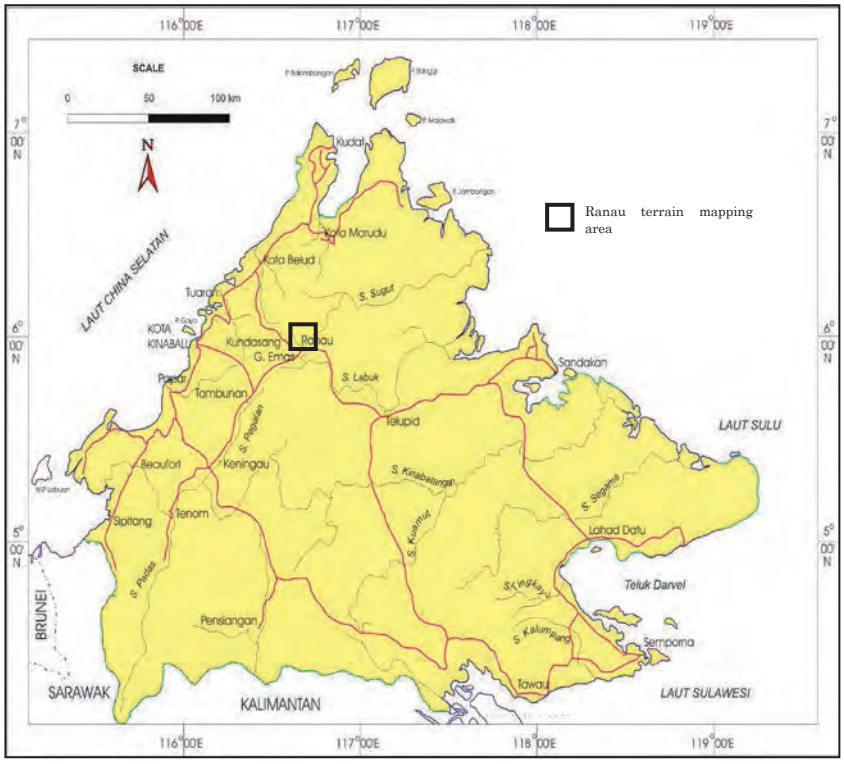

Fig. 1. Location of the study area.

The topography of the Ranau area is mountainous in the northwestern part with the highest point at 1,610m above sea level in a part of the Mount Kinabalu complex. The Elevation and Drainage Map shows that elevations of 1000-2000m occupy 32% of the mapped area, 700-1000m occupy 33%, 500-700m occupy 24%, and 300-500m occupy 11%. The mountainous terrain is covered by virgin jungle. Several parts of the hill spurs in the north western part of the study area have been cleared for the cultivation of vegetables, rice, and for grazing ground. Hill slopes are very steep in some places and landslides occur frequently in areas where the natural vegetation has been disturbed, particularly during the wet season. The lowest terrain which has an elevation of about 410m above mean sea level is found in the south eastern part of the mapped area. This latter terrain is known as the Ranau Plain (Collenete, 1958).

4. Methodology

The geological terrain mapping was conducted on the scale of 1:10,000 covering an area of 100km^2. Digital topographic maps of the area at 1:10,000 scale were acquired from Department Survey and Mapping Malaysia (JUPEM). The digital maps were processed using Triangulated Irregular Network (TIN) software to produce a Slope Gradient Map. Desktop studies, consisting of remote sensing interpretation of aerial photographs and satellite images, were carried out to acquire physical information such as geological structure and areas with erosion and landslides. Geological terrain mapping was then conducted in the field following the procedure in the Geological Terrain Mapping Manual JMGKLL (GBN) 1/2006. Four attributes, namely the slope gradient, terrain type, activity on the slope, erosion and instability, were delineated to produce polygons of geological terrain features. These polygons were subsequently coded according to the Terrain Classification Attributes (Table 1) to produce the Terrain Classification Map. The attributes in the Terrain Classification Map were analysed using JMG Map Builder (JMB) software to produce thematic maps such as the Erosion Map and the Construction Suitability Map. Subsequently auditing was carried out to verify the accuracy of the mapping information in the field before finalising the various thematic maps.

5. Geology of the study area

Studies of some aspects of the general geology have been conducted by among others, Collenette (1958), Jacobson (1970), Tjia (1974) and Henry et al., (2004). The geology of the Ranau area is generally complex. The study area is underlain by six main lithologies, namely ultrabasic rock (Middle Eocene to Oligocene age), granitic rock (Middle Eocene to Oligocene age), Trusmadi Formation (Paleocene to Eocene age), Crocker Formation (Late Eocene to Early Miocene age), Pinosuk Gravels (Pleistocene age) and alluvium (Holocene age).

The ultrabasic rock in the area is predominantly made up of serpentinite which is bluish green in colour with waxy lustre, highly sheared and brecciated. The serpentinite occupies approximately 15.5 km^2 or 13.8% of the project area particularly in the upper reaches of Sg. Luhan in the northeastern part and Sg. Mantaki in the northwest. Generally the areas occupied by serpentinite have sparse vegetation.

The Granitic rocks found in the area are adamellite and granodiorite porphyry. They occurred as dykes intruding into the Trusmadi Formation (Jacobson, 1970) in the Sg. Mantaki area at the north central part of the study area. The outcrop found in Sg. Mantaki is highly jointed and fractured and occurred as a fault contact with the ultrabasic rock.

Table 1. Terrain Classification Attributes (Geological Terrain Mapping Manual JMGKLL (GBN) 1/2006).

SLOPE GRADIENT	TERRAIN CODE		ACTIVITY CODE		EROSION AND INSTABILITY		
0° - 5° 1	Hillcrest	A	Natural Slope:		No appreciable erosion:		
			-rock	1			
6° - 15° 2	Sideslope:		-soil	2	Sheet erosion:	-minor	1
	- straight	B	-soil and rock	3		-moderate	2
	- concave	C				-severe	3
16° - 25° 3	- convex	D	Cut Slope:				
			-rock	4	Rill erosion:	-minor	4
	Footslope:		-soil	5		-moderate	5
26° - 35° 4	- straight	E	-soil and rock	6		-severe	6
	- concave	F					
	- convex	G	Fill:		Gully erosion:	-minor	7
36° - 60° 5			-rock	7		-moderate	8
	Drainage valley	H	-soil	8		-severe	9
			-soil and rock	9			
>60° 6	Flood plain	I					
			Terrace		Well defined recent		
	Coastal plain	K	-rock	a	Landslip:		
			-soil	b	(diameters)	-< 10m	a
	Littoral zone	L	-soil and rock	c		-10m – 50m	b
						- > 50m	c
	Marshy/Swampy	S					
			Reclaimation	d			
	Alluvial plain	X			Development of general		
			Mined out	e	Instability		
	Wave cut platform	W				-recent	n
			Water bodies			-relict	r
	Undulating hills	Y	-natural stream	f			
			-man-made	g	Coastal instability		w
			channel	h			
			-water storage	I			
			-pond				
				m			
			Colluvial:				
				p			
			Excavated platform				

The Trusmadi Formation consists of dark coloured argillaceous rocks, slate, phyllite, siltstone, and sandstone with rare chert horizons. The rocks are either massive, interbedded or disturbed sequences. This formation has been strongly folded and faulted and metamorphosed to the greenschist facies and meta-arenite (Tjia, 1974). The outcrops are encountered at Kg. Waang, Kg. Tambiau, Kg. Kibbas, Kg. Lipasu, Kg. Kandawayon, Kg. Badukan, Kg. Kimolohing and Taman Pasir Putih.

The Crocker Formation is generally more arenaceous than the Trusmadi Formation and consists of thicker beds of arenaceous rocks intercalated with argillite, and shale of grey and red colours. The sandstone is grey to dark grey and medium to coarse grained. The formation is also characterised by overfolded, faulted and thrusted strata. Field observation shows that the Crocker Sandstone is more resistant to weathering and erosion as compared to the sandstone of Trusmadi Formation. The Crocker Formation occupies the south western part of the mapped area and was observed on the cut slope along Kg. Koporingan, Kg. Ruhukon and BCCM Retreat Centre.

The Pinosuk Gravels unconformably overlie the Trusmadi and Crocker Formations and have a maximum thickness of about 290m (JICA and MMAJ, 1988). The beds consist of poorly consolidated gravels of various compositions. The clasts consisting of felsic igneous rock of various sizes, mainly adamellite and granodiorite in a dirty matrix of clay and sand (Henry. et al., 2004) were considered as a tilloid deposits by Jacobson (1970). It dominantly occupied approximately 20.7 km^2 or 18% of the study area in the northwestern part especially at Kg. Mesilau, Kg. Naradaw and Kg. Pinosuk.

The alluvial and terrace deposits are found throughout the study area, both as relict terraces on hillsides and as fan deposits on the Ranau Plain. Collenette (1958), described the Ranau Plain as consisting of fundamentally two types of alluvial deposits with boulders, sand and clay. These deposits form a piedmont fan in the south western end of the Plain. The north and east of the Plain is a flood plain which consists of finer detrital material consisting of boulders and cobbles in a matrix t of mainly sand, silt and clay. The western side of the Plain is a piedmont fan consisting of boulders of porphyritic granodiorite. The largest boulders are found near Ranau town and tend to become smaller to the south. The slope in the southwest of Ranau town is the original slope of the piedmont fan while the town itself is sitting on a terrace deposit.

6. Geological constraints

A geological constraint/hazard is a geological condition, process, or potential event that poses a threat to the health, safety or welfare of a group of people or to the function or economy of a community (Keng, 1992). The types of constraints faced in a particular area are controlled by the geological setting of the area. In the Ranau area, the geological constraints that may be expected to relate to planning matters are those described below.

Faults: There are several major faults trending N-S, NE-SW, NW-SE and E-W such as the Mensaban Fault, Kibbas Fault, Mamut Fault, Kihunut Fault, Kimolohing Fault, Kihunut Fault, Mantaki Fault, Tekurik, Lipasu Fault, Luhan Fault, Koporingan Fault, Marakau Fault, Waang Fault and Bambangan Fault. Some active and potentially active faults are believed to be the likely source of earthquakes in Sabah (Alexander, 2007) such as the Mesaban Fault. It was reported that the presence of the Mesaban Fault Zone might have been one of the factors that caused the damaging massive movements (landslides) in the Kundasang area.

The movement of the E-W trending Mensaban Fault which runs through Kg. Kauluan area caused damage to the preschool building in 2009. The Lipasu Fault had caused damage to a bungalow house in Kg. Lipasu and presently causes soil creep on a slope in the area and the development of cracks in the concrete house on the slope in Kg. Lipasu.

There are two identified populated areas which are intersected by the three fault lines. These areas are Kg. Kibbas and Batu 2 Rest House. The Kg. Kibbas area is intersected by the SW-NE trending Kibbas Fault, NW-SE trending Koporingan Fault and N-S trending Lipasu Fault. While the Batu 2 Rest House area is intersected by the Kibbas Fault, the NW-SE trending Tekurik Fault and the N-S trending Mamut Fault.

From the field evidence of the widespread mass movements which caused damage to man-made structures, it is believed that the Kibas Fault, Mensaban Fault, Lipasu Fault and Mamut Fault are all active. Therefore, it is suggested where possible, that construction of major structures along these faults intersection and fault zones should be avoided.

Pinasuk Gravels and Alluvium: The area underlain by these materials are not suitable foundations-rocks for high rise and major structures. Ground settlement and compaction have been consistent problems where heavy structures are built on the Pinasuk gravels and they are also prone to sliding where the land is sloping. The risk from earthquakes is caused by that the ground shaking is higher in areas underlain by these Pinasuk Gravels, alluvium and reclaimed land. On alluvial deposits, the sand layer where present, may undergo liquefaction during an earthquake.

Colluviums: The area underlain by colluviums is about 31% of the study area. This type of deposit can be observed at the foot of slopes in Sungai Luhan and along the foot of slope near Kg. Kimolohing. The colluvium which occurs in the fore grounds of steep slopes and foot of slopes generally consists of angular to sub angular rock fragments that are derived from bedrock materials from the top of the slopes. The matrix of the colluvium is made up of very loose sandy material, thus creating slope instability.

Trusmadi Formation and ultrabasic rocks: In the study area most of the unstable zones are found within the argillaceous rocks of the Trusmadi Formation and within ultrabasic rocks. Due to the deformation and the argillaceous condition of the Trusmadi Formation, the rocks are highly susceptible to weathering and eventual slope failure. These unstable zones on argillaceous rocks of the Trusmadi Formation can be observed in Kg. Kandawayon, Kg. Kibbas, Kg. Tambiau, Kg. Waang, Kg. Kimolohing, Kg. Sumaang and Kg. Lipasu. Unstable zones within the ultrabasic rock were observed at Sungai Luhan. The intrusion of the granitic rocks and ultra basic rocks into the area has caused numerous fractures and faults to transect the area. The rocks in the vicinity of these fault zones are highly fractured and faulted, where there are many relict and recent landslide and rock fall occurrences.

The concave type of landform, especially in the Trusmadi Formation, can be considered as a sign of land instability. Based on field observation, all the major relict landslides occurred within this type of morphology. Furthermore, from the soil boring investigation it was found that the groundwater table was high especially in dense vegetation areas. Special attention must be given during engineering activities such cutting and grading in these places to take steps to minimise possible landslides and rock falls.

7. Thematics maps

Several thematic maps have been prepared which should be very useful in land-use planning and development of the Ranau area: These maps include: Erosion map, Landform map, Physical Constraint Map, Engineering Geology Map and Construction Suitability Map.

Erosion Map: This map delineates the broad pattern of erosion and instability and is designed for technical and non-technical users who require information regarding the nature, degree and intensity of erosion and instability for planning and engineering purposes. The Erosion Map of the study area shows that 30% of the area has no appreciable erosion, 12% with minor sheet erosion, 2% with moderate to severe sheet erosion, 1% with minor rill erosion, 0.7% with moderate to severe rill erosion, 0.5% with minor gully erosion and 0.1% with moderate to severe gully erosion

Landform Map: This map summarises the broad pattern of attributes from the Terrain Classification Map where the slope gradient and terrain code are delineated. Based on the Landform Map, 8% of the Ranau area is gently sloping, 15% is gently to moderately sloping, 39% is moderately sloping, 29% is steeply sloping, 11% is very steeply sloping and 1% is extremely steeply sloping.

Physical Constraint Map: This map represents the major physical land constraints and is designed for technical and non-technical users who require information relating to the types of physical constraints which affect the terrain. The four main physical constraints which may affect the terrain of the study area are colluvium deposits, general instability, slope gradient (> 25^{o}) and drainage valleys. Based on the Physical Constraint Map, colluvium occupies 41% of the area, slope gradient of >25^{o} occupies 56%, drainage valleys occupy 2.4% and general instability occupies 0.6%. These four physical constraints should be taken into account in the assessment of the physical characteristic for general development planning and engineering purposes

Engineering Geology Map: The Engineering Geology Map (Fig. 2) was constructed based on geological data such as geological map and geohazard analysis of the mapped area. The occurrences of landslides, recent and relict were plotted and overlain with the geological features. From the Engineering Geology Map of the study area it can be shown that most of the landslide occurrences were found in the argillaceous facies of the Trusmadi Formation. Relict and recent landslides have also been identified in most part of the steep slope of the ultrabasic rock. The occurrences of landslides are also common in the Pinosuk Gravels areas where the loose materials become unstable when disturbed by human activities. From field evidence it was also found that most of the landslides were structurally controlled and occurred within major fault zones such as the Bambangan Fault, Kibbas Fault, Mamut Fault and Lipasu Fault.

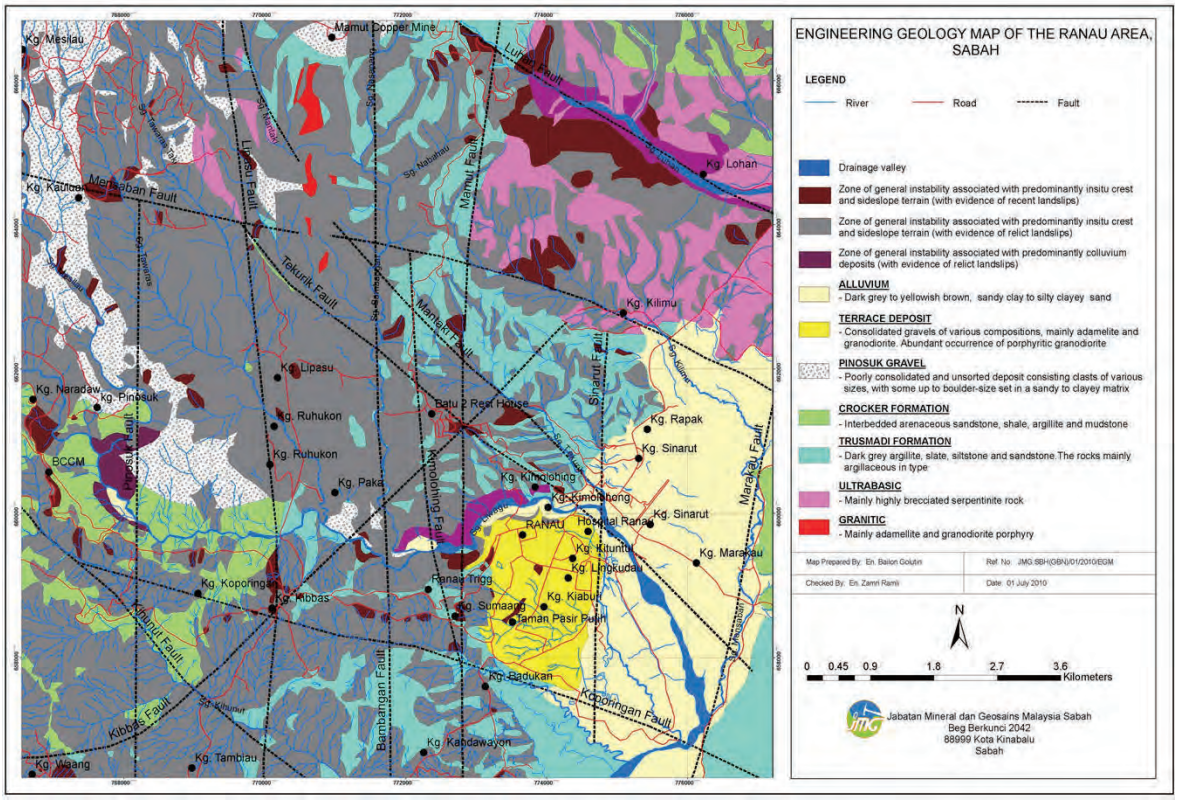

Fig. 2. Engineering Geology Map of the Ranau area.

Construction Suitability Map: This map shows four construction suitability classes:

Class I: suitable for development and would have few geotechnical constraints and low engineering costs for development.

Class II: moderate suitability for development and would incur moderate geotechnical constraints and engineering cost

Class III: areas would have high geotechnical constraint and engineering costs, Class III areas would also require intensive site investigation.

Class IV: extreme geotechnical constraints with very high engineering costs, therefore generally not suitable for development.

The Construction Suitability Map of the Ranau area (Fig. 3) shows that 13% of the mapped area is in Class I, 19% in Class II, 30% in Class III and 38% in Class IV.

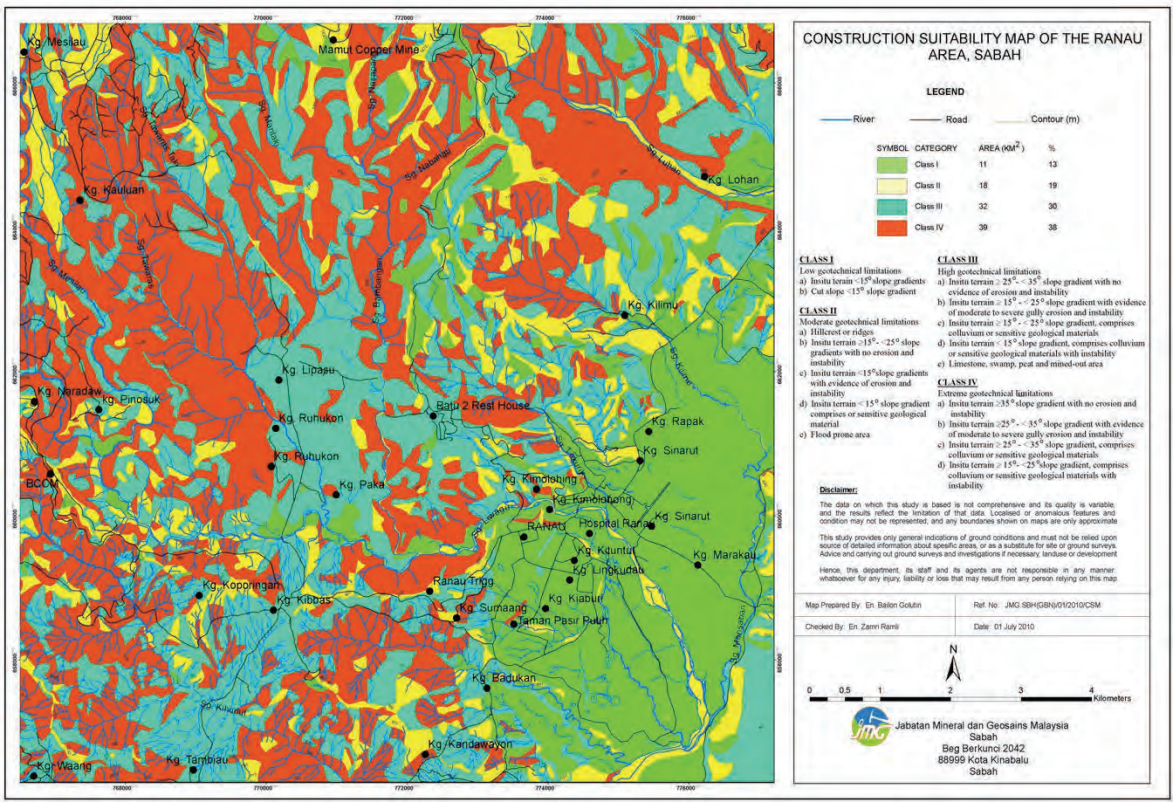

Fig. 3. Construction Suitability Map of the Ranau area.

Sixty eight percent of the mapped area is under Class III and IV. These areas are found in the western, northern, north eastern and central parts of the study area. Most of the Class I areas fall within the low-lying area in the southeastern part of the mapped area such as Kg. Marakau, Kg. Rapak and Kg. Kilimu. Class II areas are found scattered throughout the study area.

8. Recommendations

The study area is a geologically sensitive area due to the topography and its complex geology. There are various geohazard phenomena such as landslides, rock falls and earthquakes which

have occurred in the area. It is recommended that any future development plans in the Ranau area should take into account these geohazards. For any site which is earmarked for development, it is recommended that a detailed geological assessment should be made mandatory as part of the local authorities land-use regulation. For preventive measures it is recommended that the local authorities use the Construction Suitability Map in reviewing the request for future development in these areas and as well as being used other relevant authorities involved in town and country planning.

9. Conclusion

The discussion on some of the geological problems of the Ranau area are intended to highlight various important geological factors that the planners/engineer need to know for an efficient and safe development of a particular area. Aspects that should be considered include the details of any engineering geological assessment of a particular site and where possible highlight areas which are potentially prone to earthquake tremors.

References

Alexander S.W. Yan, 2007, Fault Layouts in Sabah, Proceeding of the National Seminar On Earthquakes, The Impact on Buildings and Infrastructure, 15 May 2007, Kuala Lumpur.

Collenette, P., 1958, The Geology and Mineral Resources of the Jesselton-Kinabalu Area, North Borneo. Geological Survey Department, Memoir 6.

Henry, L.A., Bailon, G., and Mohd, A.O., 2004, Geology of the Kundasang area, Seminar on Kundasang Landslide Complex: Hazard assessment and control, 25 May 2005, Promenade Hotel, Kota Kinabalu.

Jacobson, G., 1970, Gunong Kinabalu Area, Sabah, Malaysia. Geological Survey Malaysia, Report 8.

JICA and MMAJ, 1998, Consolidated report on the mineral exploration in Sabah, Malaysia.

Keng. L.S., 1992, Progress Report: Quaternary Geological Mapping of the Kuching City Area, Sarawak, Procceding of the 23rd Geological Conference, Geological Survey Malaysia No.4, 1992, 96-107.

Leyu Chong-Hua, Chang Chu-Fong, E.P. Arnold, Kho Sai Lik, Yang-The, M. Subramanian, Ong Ting-Cheong, Tan Chen-Kok, Yap Kok-Seng, Shu Yeoh Khoon and Goh Hee-Leng, 1985, Southeast Asia Association of Seismology and Earthquake Series on Seismology, Volume III-Malaysia.

Lim, P.S., 1985, History of earthquake activities in Sabah, 1897-1983, Geological Survey of Malaysia Annual Report for 1983, 350-357.

Lim, P.S. and Paulus G., 1992, The Ranau Earthquake Swarm, May-July, 1991, Sabah, Proceeding of the 23rd Geological Conference, Geological Survey Malaysia No.4, 1992. 167-193.

Tjia H.D., 1974, Sense of tectonic transport in intensely deformed trusmadi and crocker sediments, Ranau-Tenompok area, Sabah, Sains Malaysia, 3(2), 129-161.

Using weight of evidence modeling for landslide susceptibility zonation mapping in Pac Nam district, Bac Kan province, Vietnam

Nguyen Thanh Long, Le Minh Son, Nguyen Duc Ha, Nguyen Quoc Dinh, Do Minh Hien

Vietnam Institute of Geosciences and Mineral Resources
67 Chien Thang Street, Thanh Xuan District, Hanoi, Vietnam
e-mail: ntlong1974@yahoo.com

Abstract

Pac Nam district is a mountainous district in Bac Kan province located in the North Eastern part of Vietnam. Landslides occur frequently in this area and seriously affect local living conditions. Especially, three households comprising 13 persons died in 2009 due to a landslide in Khen Len village of Cong Bang commune, Pac Nam district, Bac Kan province. Hence, the spatial analysis of landslide susceptibility in this area is an important topic for both administrators and the local inhabitants. In this study, landslide causative factor maps incorporating factors such as slope angle, weathering, vegetation, maximum daily rainfall, fault density, river density, vertical dissection and distance to roads were used as input data to create a landslide susceptibility zonation (LSZ) map. A Weight of Evidence (WOE) method for landslide susceptibility mapping was applied to the study area in order to create the landslide susceptibility zonation map. The final map indicates that areas of low, moderate, high and very high landslide susceptibility zones occupy respectively 199.4 km^2 (41.9%), 185.9 km^2 (39.1%), 77.5 km^2 (16.3%) and 16.3 km^2 (2.7%) of the entire area; and most of the observed landslide areas that are best predicted, belong to the high or very high landslide susceptibility classes. Hence, the high and very high landslide susceptibility classes displayed in the final map can be considered as highly credible.

Keywords: natural hazards, landslide, susceptibility, GIS, Vietnam

1. Introduction

Many landslide occurrences happen annually and often cause serious damage to the people and properties of local communities in Pac Nam district, Bac Kan province of Vietnam.

Geologically, there is a distribution of geological entities of ages varying from Neoproterozoic to Quaternary in the study area which formed in the geological structure as the result of complicated multi-period tectonic activities together with strong weathering and deforming processes that usually have a significant effect on landslide susceptibility. Besides, in this area, high rainfall is frequently recorded and rainfall is considered to be one of the important factors causing landslides and increases the extent of the damage caused in landslide disasters in the area. In addition, the vegetation cover in the study area has been removed in recent years by burning areas of forest for cultivation which leads to an increase in soil erosion during periods of heavy rainfall and this is also an important causative factor for landsliding in the area.

In this study area, 57 landslide occurrences were identified by field investigations and collection of historic literature on landslides (Fig. 1).

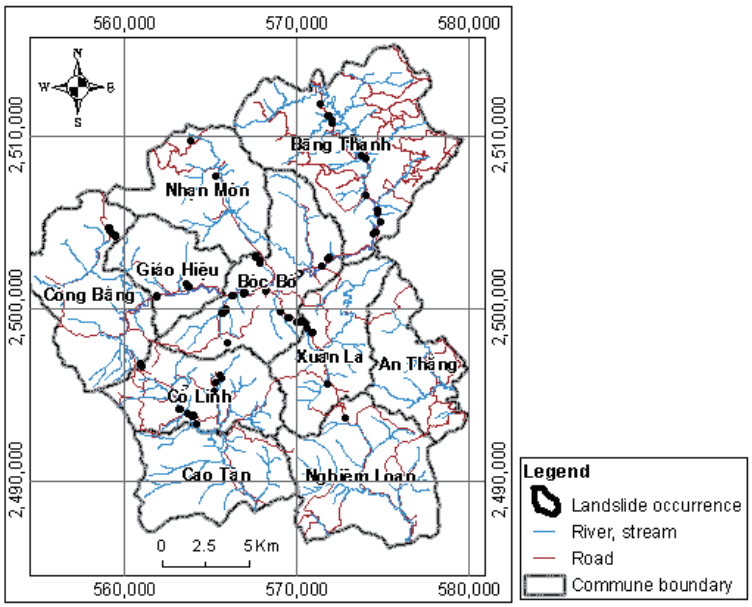

Fig. 1. Landslide occurrence map in Pac Nam district, Bac Kan province, Vietnam.

With the assistance of GIS technology, the creation of a Landslide Susceptibility Index (LSI) map was established, at a scale of 1/50,000, by using the Weight of Evidence (WOE) method. This was based on integration of multi input layers of slope angle, weathering, vegetation, maximum daily rainfall, fault density, river density, vertical dissection and distance to roads. Then, an LSI classification was undertaken to create a final map of Landslide Susceptibility Zonation (LSZ) with four landslide susceptibility categories: very high, high, moderate and low. This provides an important foundation underpinning regional socio-economic development planning, as well as provides the relevant information to the community in order to actively prevent and mitigate the consequences of landslides.

2. Landslide causative factors

The selection of causative factor maps for landslide susceptibility should be considered carefully based on considerations of their *relevance, availability and scale attributes*. The *relevance* refers to the main causative factors of landslides in the study area. The *availability* refers to relevant factors that are readily available to be used for developing a landslide susceptibility map. The *scale* attribute is an important consideration, and refers to the map scales of different causative factors of landslides that will be employed for creating a landslide susceptibility map.

Consequently, eight causative factors are selected as inputs for the models of landslide susceptibility mapping in this study, i.e., slope angle, weathering, vegetation, maximum daily rainfall, fault density, river density, vertical dissection, and distance to roads. The input parameters are used to calculate and displayed as the raster map in GIS with the grid size of 10 m x 10 m. The landslide causative factor mapping steps are described detail in next paragraphs.

- In general, topography is usually associated with landslides by virtue of such factors as slope gradient, lithology, weathering, precipitation, ground motion and soil thickness. For example, mountain areas in tropical climatic areas often experience larger volumes of precipitation, leading to greater landslide susceptibility. Hence, topography strongly affects landsliding (Guzovski et al., 1989; An et al., 1990; Thai et al., 1991; Van et al.,

2001). A digital elevation map (DEM) of the study area was obtained by digitizing the 1:10,000 scale topographic map and then using interpolation for digital contouring of the topographic map in ArcGIS™ (Fig 2).

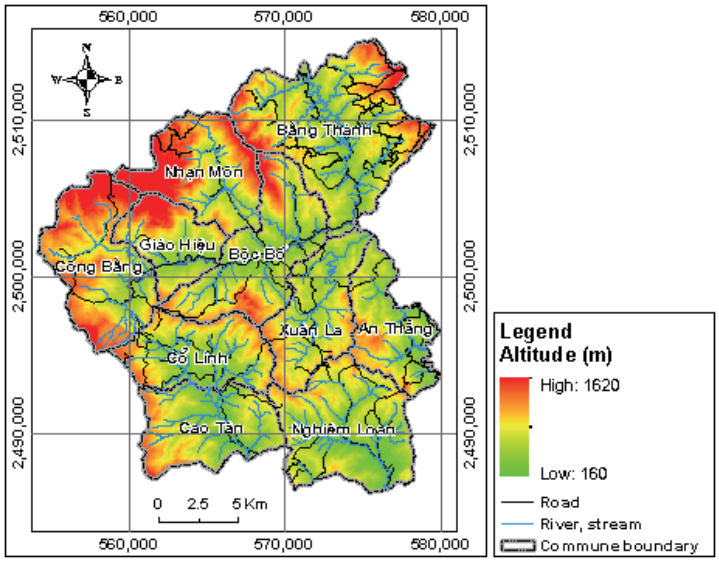

Fig. 2. DEM of Pac Nam district.

- One of important topographic indexes that is closely relevant and strongly influences landslide processes is topographic dissection in vertical direction or vertical dissection. Hence, in this study a vertical dissection map was used to present for the topographic variation (Fig. 3). There are 5 vertical dissection classes in the map: (1) <150 m/km^2, (2) 150 - 250 m/km^2, (3) 250 - 350 m/km^2, (4) 350 - 450 m/km^2, (5) >450 m/km^2.

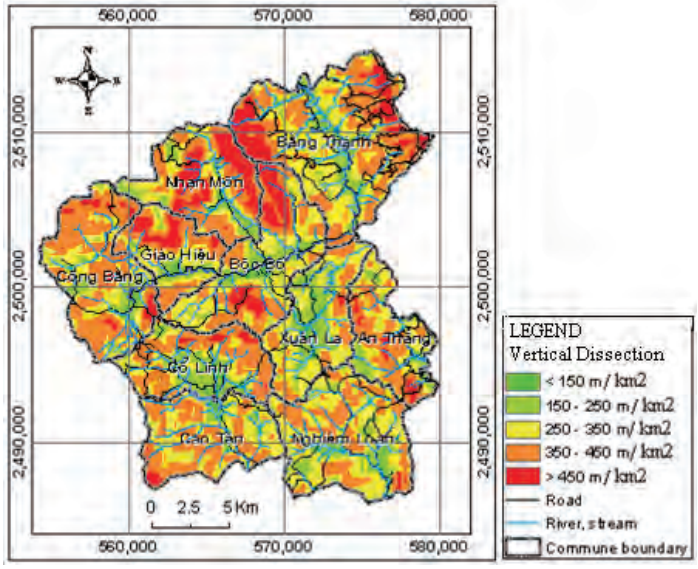

Fig. 3. Vertical dissection map of Pac Nam district.

- Slope is important with regard to landslide initiation. In most studies of landslides, the slope gradient is taken into account as a principal causative or triggering factor. The slope map of Pac Nam was derived from the DEM using the slope function of ArcGIS™ (Fig. 4). The slope map is in the form of a raster map with the same 10 m pixel size as

the DTM. A map of slope classes was generated by separating the slope angles into five different classes: (1) flat-gentle slope and fair slope (<15^0), (2) moderate slope (15-25^0), (3) fairly steep slope (25-35^0), (4) steep slope (35-45^0), and (5) very steep slope (>45^0).

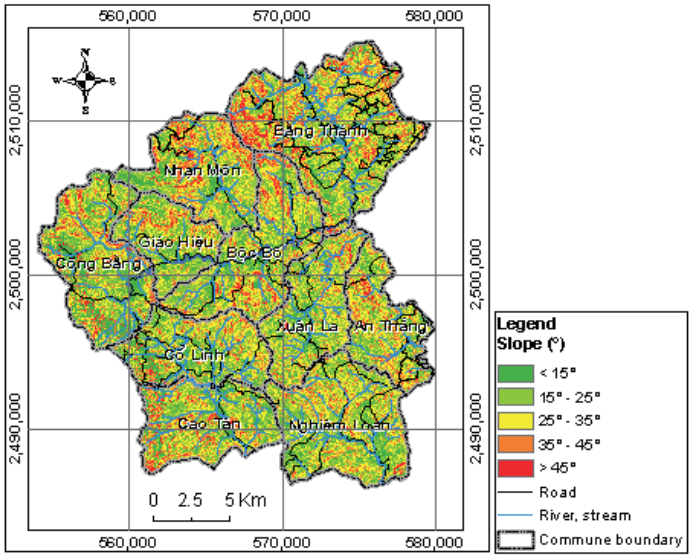

Fig. 4. Slope map of Pac Nam district.

- Weathering alters the mechanical, mineralogical and hydrologic attributes of the regolith, and hence, is an important factor of slope instability in many settings (Chigira at al., 2002; Wakatsuki et al., 2005). A map of weathering was derived from the previous work in Ha Giang, Cao Bang, Tuyen Quang, Bac Kan provinces (Khien et al., 2012) (Fig. 5) including seven different types of weathered cover: (1) bedrock and weakly weathered crust, (2) sialferite, (3) ferosialite, (4) ferosialite - sialferite, (5) sialferite - sialite, (6) sialferite - silixite, and (7) ferosialite - silixite. In addition, there exist categories 8) carbonate rocks and 9) Quaternary in the study area.

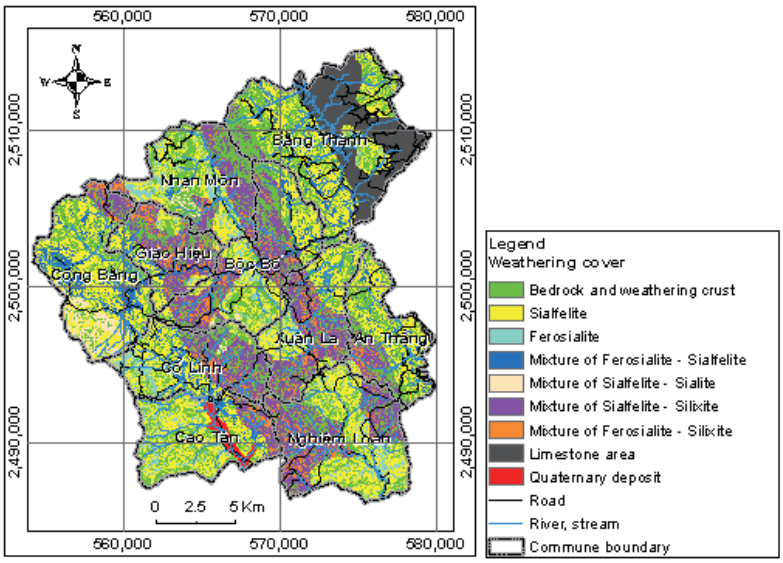

Fig. 5. Weathering map of Pac Nam district.

- The relative strength of the regolith is strongly influenced by past tectonic processes as

well as contemporary weathering (e.g., Julian and Anthony, 1996; El Khattabi and Carlier, 2004). Especially, Neotectonics contribute to slope instability by fracturing, faulting, jointing and deformation of foliation structures (Ibetsgerger, 1996; Pachauri et al., 1998). For this study, faults systems were derived from the revised geological map (1:50,000 scale) of Khien et al. (2012), and fault density was calculated as total length of faults per km^2.

- Vegetation augments slope stability in primarily two ways: (1) by removing soil moisture through evapotranspiration, and (2) by providing root cohesion to the soil mantle (Greenway, 1987). A vegetation map was derived from a Landsat TM5 image captured in 2012. The vegetation cover map was processed with the NDVI method with field check samples (Hien, 2011), resulting in eleven vegetation classes (Fig. 6): (1) rich forest, (2) mixed forest, (3) poor forest, (4) sapling forest having no reservation, (5) sapling forest having reservation, (6) bamboo forest, (7) medium forest, (8) plantation forest, (9) bare soil, (10) agriculture, soil and others, and (11) outcrop.

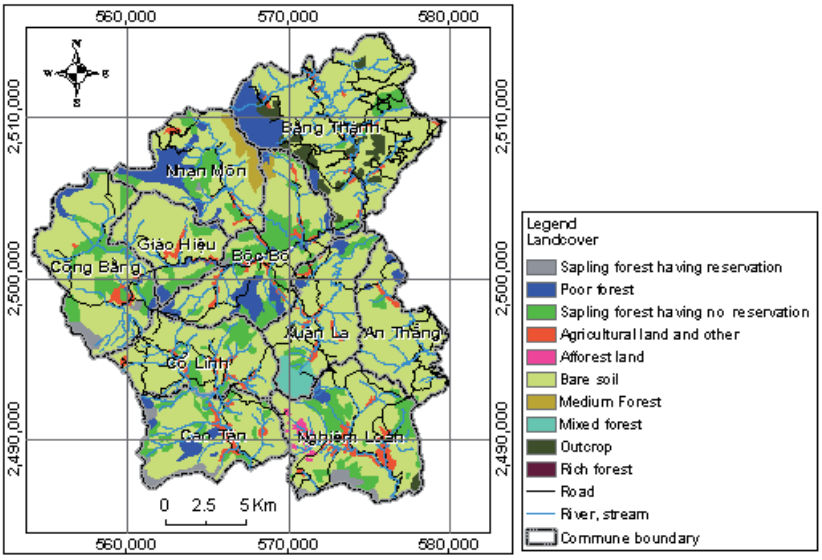

Fig. 6. Vegetation map of Pac Nam district.

- A drainage system with intensive gully erosion is an important factor controlling the occurrence of landslides. In this study, the river density map was established based on the digital elevation model and the river/stream system extracted from topographic maps at the scale of 1:10,000 through the available module, "Hydro tool", in the ArcGIS^{TM} software. River density is then classified three groups: (1) density $\leq$ 500 m/km^2, (2) 500 - 2000 m/km^2, (3) $\geq$2000 m/km^2 (Fig. 7).
- Spatial patterns of rainfall are closely associated with landslide initiation (So, 1971, Starkel, 1976) by means of their influence on the generation of pore water pressure in unstable hill slopes (Tsukamoto and Ohta, 1988). Hence, rainfall is commonly considered as the triggering factor for landsliding. The study area is strongly affected by a tropical monsoon climate with rainy seasons. For this study, the average maximum daily rainfall over a 45-year observation period from 1964 to 2009 (Fig. 8) is selected as the rainfall factor for landslide analysis. Seven rainfall stations inside and surrounding the study area: Bắc Mê, Na Hang, Chợ Rã, Ngân Sơn, Bảo Lạc, Hà Quảng, and Nguyên Bình, were selected and provide rainfall data for this study. Table 1 indicates the maximum daily rainfall measured by each rainfall station during the 1964 - 2009 period. The

average maximum daily rainfall in the study area varies from 95 mm/day to 105 mm/day. Therefore, the maximum daily rainfall map was only divided into two classes: <100 mm/day, and >100 mm/day.

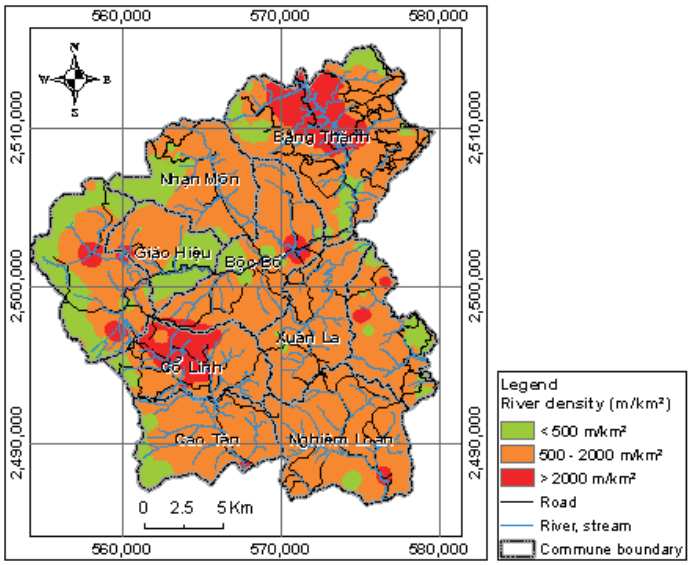

Fig. 7. River density map of Pac Nam district.

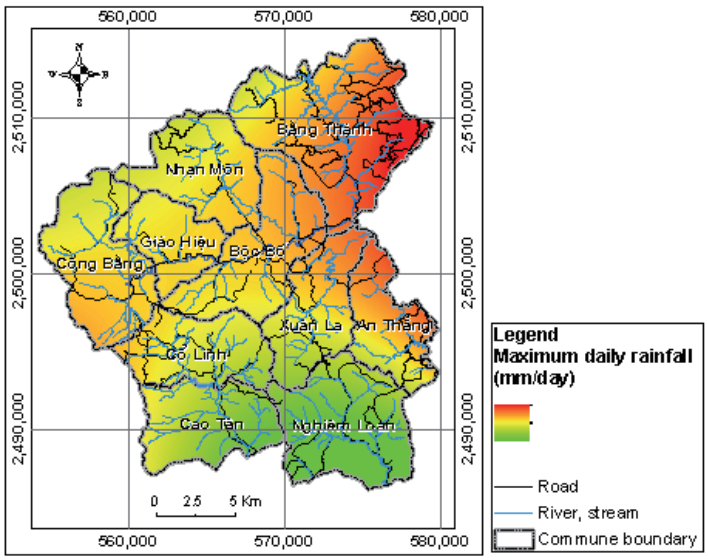

Fig. 8. Maximum daily rainfall map with 45 years of observations in Pac Nam district.

- Landslides may result directly or indirectly from the activities of people. But any attempt to address all the human activities that induce landslide occurrences will be incomplete (Long, 2008). The influence of cutting slopes along highways and railroads that increase the average slope gradients, and increase the chance of slope failure, can be seen in most of mountainous areas in Vietnam. Hence, in order to model the influence of the influence of cutting slopes along highways and railroads on landsliding, the distance from roads was taken into account in this study. The road system of the study area was taken from topographic maps (scale 1:10,000). The distances from a road were classified into three groups: <10 m, 10 – 50 m, and >50 m.

Table 1. Average maximum daily rainfall during the 1964 - 2009 period measured at 7 rainfall stations inside and surrounding the study area.

Rainfall station name	Longitude (^{o})	Latitude (^{o})	Average maximum daily rainfall with 45 year observation from 1964 to 2009 (mm)
Bac Me	105,37	22,73	95
Na Hang	105,37	22,33	126
Cho Ra	105,72	22,45	94
Ngan Son	105,98	22,43	110
Bao Lac	105,67	22,95	86
Ha Quang	106,00	22,92	105
Nguyen Binh	105,95	22,65	116

3. Weight of evidence modeling for landslide susceptibility mapping

The weight of evidence (WOE) modeling method is a quantitative 'data-driven' method used to combine datasets. The method was first applied in medicine (Spiegelhater and Kill-Jones, 1984). Afterwards, Bonham-Carter and Reddy (1990) used this approach to identify gold mineralization in the Meguma Terrane, eastern mainland Nova Scotia, Canada. The applications in geology using a Bayesian probability model to estimate the relative importance of evidence by statistical means, was developed by Bonham-Carter (1994). Since then, the WOE modeling method for landslide susceptibility mapping was applied in many case studies (Van Westen, 1993; Sentz and Ferson, 2002; Lee et al., 2002; Van Westen et al., 2003; Süzen and Doruyan, 2004; Thiery et al., 2004; Neuhäuser and Terhorst, 2007; Mathew et al., 2007; Thiery et al., 2007).

Prior probabilities and posterior probabilities are the most important concepts in the Bayesian approach. The probability P is usually determined with knowledge about the occurrence of an event E in the past under equal conditions, and as the prior probability P{E}. This probability can be modified with data B that influenced the probability, which is gained from surveys, experiments, or analyses (Malczewski, 1999). When this evidence is integrated into the calculation of the probability, a conditional or posterior probability P{E|B} is obtained. Bayes theorem gives the relationship between prior and posterior probabilities:

$$P\{E \mid B\} = \frac{P\{E\} \times P\{B \mid E\}}{P\{B\}} \quad (1)$$

By overlaying landslide locations with each possible causative factor map, the statistical relationship can be measured and assessed as to whether and how significant the particular causative factor is responsible for the occurrence of past landslides (Neuhäuser and Terhorst, 2007). Hence, starting from a prior probability P_0, which is the density of the observed landslides in the study area.

$$P_0 = f = \frac{A^*}{A} \quad (2)$$

where:

f - The landslide density within the entire map.

A* - Total area of landslides in the entire map.
A – Total area of the entire map.

Evidence maps j=1,…, n are added one after the other yielding posterior probabilities P_j given by

$$P_j = \frac{f_{ij}}{f} p_{j-1} = \left(\frac{A^*_{ij}}{A_{ij}} x \frac{A}{A^*} \right) P_{j-1} \quad (3)$$

where fij is the landslide density within the class i of parameter j. index i refers to the different classes of map j. A^*_{ij} is area of landslides in a certain class i of parameter j, and Aij is area of a certain class i of parameter j. When above equation is subsequently applied for all parameter maps, it is inherently assumed that all maps are conditionally independent from each other.

In practice, in WOE positive and negative weights (W^+ and W^-) are calculated, the magnitude of which depends on the measured association between the response variable (the landslides) and the predictor variables (causative factors). The details of the methods are given by many authors (Bonham-Carter, 1994; Porwal et al., 2003; Gary, 2006; Neuhäuser and Terhorst, 2007). The modified Bonham-Carter's definition of positive and negative weights (W^+_{ij} and W^-_{ij}) of evidence respectively of the i^{th} class of j^{th} causal factor is as follows:

$$W^+_{ij} = \ln \frac{P\{B \mid E\}}{P\{B \mid \bar{E}\}} = \ln \left(\frac{f^*_{ij}}{\bar{f}^*_{ij}} \right) \quad (4)$$

$$W^-_{ij} = \ln \frac{P\{\bar{B} \mid E\}}{P\{\bar{B} \mid \bar{E}\}} = \ln \left(\frac{1 - f^*_{ij}}{1 - \bar{f}^*_{ij}} \right) \quad (5)$$

where:

f^*_{ij} - The frequency of observed landslides in class i of parameter j.

$\bar{f}^*_{ij}$ - The frequency of non-observed landslides in class i of parameter j.

In the above expressions, the bar above the symbols means the opposite, i.e., $\bar{E}$ means not E.

In case there are no observed landslides inside of the i^{th} class of the j^{th} causal factor, the positive weight is put equal to the minimum positive weight of that causal factor (Lee et al., 2002).

Finally, the contrast C_{ij}, measures and reflects the spatial association between the evidence feature and the landslide occurrence, and is given by

$$C_{ij} = W^+_{ij} - W^-_{ij} \quad (6)$$

The contrast is positive for a positive spatial association, and negative for a negative spatial association. Hence, the contrast (C_{ij}) is the rating of each class of each factor that influences landslide occurrence.

The standard deviation of the contrast can be calculated as:

$$S(C) = \sqrt{S^2(W^+) + S^2(W^-)} \quad (7)$$

where:

S(C) – standard deviation of the contrast

$S(W^+)$ – standard deviation of the positive weight

$S(W^-)$ – standard deviation of the negative weight

The variances of the weights can be calculated by the following expressions (Bishop et al., 1975):

$$S^2(W^+) = \frac{1}{N\{B \mid E\}} + \frac{1}{N\{B \mid \bar{E}\}} \quad (8)$$

$$S^2(W^-) = \frac{1}{N\{\bar{B} \mid E\}} + \frac{1}{N\{\bar{B} \mid \bar{E}\}} \quad (9)$$

where N{X|Y} indicates the number of occurrences (pixels) of the simultaneous events X and Y.

The ratio of the contrast divided by its standard deviation provides a measure of confidence (Neuhäuser and Terhorst, 2007). In the case of a normal distribution the contrast is significantly different from zero with a confidence of 95% if |C/S(C)| is larger than 1.96. Moreover the higher the value of |C/S(C)| the higher the confidence that the associated parameter class is correlated with landslides, either positively if the value is positive or negatively if the value is negative.

The factor maps combined with the landslide occurrence map enables calculation of the positive and negative weights and the contrasts, as shown in Table 2.

Table 2. The data employed in the WOE modeling analyses for Pac Nam district.

	f_{ij}^*	$\bar{f}_{ij}^*$	W^+	W^-	C	S(C)	C/S(C)
Slope							
$< 15^0$	11.87	21.05	-0.57	0.11	-0.68	0.08	-8.39
$15\text{-}25^0$	8.47	29.39	-1.24	0.26	-1.50	0.09	-15.90
$25\text{-}35^0$	9.72	29.69	-1.12	0.25	-1.37	0.09	-15.37
$35\text{-}45^0$	26.16	14.91	0.56	-0.14	0.70	0.06	11.74
$> 45^0$	43.79	4.95	2.18	-0.53	2.70	0.05	50.93
Fault density							
< 1000 m/km^2	67.18	82.28	-0.20	0.62	-0.82	0.06	-14.61
1000-2000 m/km^2	22.48	14.66	0.43	-0.10	0.52	0.06	8.31
2000-3000 m/km^2	10.34	2.85	1.29	-0.08	1.37	0.09	15.81
> 3000 m/km^2	0.00	0.21	-0.20	0.00	-0.20	-	-
River density							
< 500 m/km^2	24.01	17.28	0.33	-0.08	0.41	0.06	6.71
500 – 2000 m/km^2	62.25	73.34	-0.16	0.35	-0.51	0.05	-9.41
> 2000 m/km^2	13.74	9.39	0.38	-0.05	0.43	0.08	5.62
Vegetation cover							
Sapling forest having reservation	0.00	1.50	-2.91	0.02	-2.92	-	-
Poor forest	0.00	7.08	-2.91	0.07	-2.98	-	-

	f_{ij}^*	$\overline{f}_{ij}^*$	W^+	W^-	C	S(C)	C/S(C)
Sapling forest having no reservation	0.76	13.96	-2.91	0.14	-3.05	0.30	-10.07
Agricultural land and others	29.29	4.65	1.84	-0.30	2.14	0.06	36.96
Afforest land	0.00	0.33	-2.91	0.00	-2.91	-	-
Bare soil	69.81	68.41	0.02	-0.05	0.07	0.06	1.15
Medium Forest	0.00	1.02	-2.91	0.01	-2.92	-	-
Mixed forest	0.00	1.05	-2.91	0.01	-2.92	-	-
Rich forest	0.00	0.00	-2.91	0.00	-2.91	-	-
Outcrop	0.14	2.00	-2.67	0.02	-2.69	0.71	-3.80
Weathering cover							
Bedrock and weathering crust	20.33	27.15	-0.29	0.09	-0.38	0.07	-5.78
Sialfelite	9.02	28.97	-1.17	0.25	-1.41	0.09	-15.38
Ferosialite	5.97	5.69	0.05	0.00	0.05	0.11	0.46
Mixture of Ferosialite - Sialfelite	2.64	6.31	-0.87	0.04	-0.91	0.16	-5.54
Mixture of Sialfelite - Sialite	0.00	1.35	-1.17	0.01	-1.18	-	-
Mixture of Sialfelite - Silixite	17.97	16.49	0.09	-0.02	0.10	0.07	1.51
Mixture of Ferosialite - Silixite	41.78	6.26	1.90	-0.48	2.37	0.05	44.43
Limestone rock	2.29	7.06	-1.13	0.05	-1.18	0.18	-6.68
Quaternary deposit	0.00	0.72	-1.17	0.01	-1.17	-	-
Maximum daily rainfall							
<100 mm/daily	35.18	47.56	-0.30	0.21	-0.51	0.06	-9.30
>100 mm/daily	64.82	52.44	0.21	-0.30	0.51	0.06	9.30
Distance from the road							
< 10 m	12.28	1.12	2.40	-0.12	2.52	0.08	31.35
10-50 m	40.39	4.44	2.21	-0.47	2.68	0.05	49.90
>50 m	47.33	94.44	-0.69	2.25	-2.94	0.05	-55.71
Vertical dissection							
<150	4.02	1.72	0.85	-0.02	0.87	0.13	6.50
150-250	40.04	14.69	1.00	-0.35	1.36	0.05	25.20
250-350	21.03	36.37	-0.55	0.22	-0.76	0.06	-11.82
350-450	34.91	37.96	-0.08	0.05	-0.13	0.06	-2.38
>450	0.00	9.25	-0.55	0.10	-0.65	-	-

Table 2 indicates that:

- Slopes lager than 35^0 have positive contrast and value C/S(C) larger than 11.74, hence, they are very highly significant for landsliding. While slopes lower than 35^0 have inverse situation with negative contrast and negative C/S(C) value, so they have no significance for landslide occurrences.
- For the vegetation factor, bare soil and agricultural land & others are significant for landslide occurrence.
- For the weathering factor, only the mixture of ferosialite - silixite crust is significant for landsliding.
- Fault densities higher than 1000 m/km^2 are very significant for landsliding.

- Maximum daily rainfall higher than 100 mm/day is very significant for landsliding.
- Distances from the road <50m are highly significant for landsliding.

The landslide susceptibility index in the study area is calculated by summing up the contrast of the factors (Lee et al., 2002; Mathew et al., 2007):

$$LSI = \sum_{i=1}^{n} C_{ij} \qquad (10)$$

The resulting LSI map is shown in Fig. 9. The classification steps in order to create a LSZ map are as follows: the observed landslide map was overlaid on the landslide susceptibility index map, the accumulation percent values of observed landslide respectively with landslide susceptibility index values are determined. In this study, classification method is used to divide landslide susceptibility index into four different susceptibility classes based on the LSI classification method which was proposed by Galang (2004).

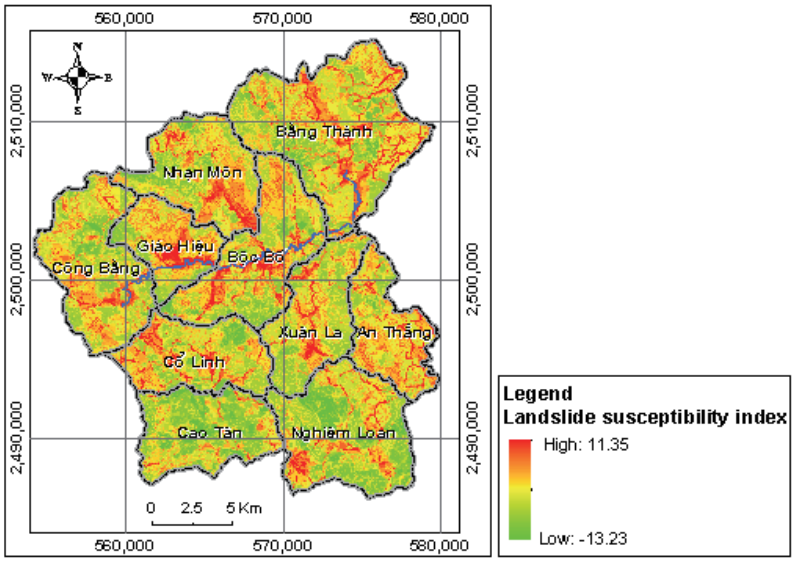

Fig. 9. Landslide susceptibility index map of Pac Nam district.

The accumulation graph of observed landslide percentage against LSI value of the study area is shown in Fig. 10. Three thresholds of observed landslide accumulation value to classify LSI range value into 4 groups were defined. Those are 6.7% as the dividing value between low and medium classes of landslide susceptibility, 20% between medium and high classes, and 46.7% between high and very high classes.

Base on the classification mentioned above, LSZ map (Fig. 11) were created from LSI map. The LSZ map, indicates that areas of low, moderate, high and very high landslide susceptibility zones occupy respectively 199.4 km^2 (41.9%), 185.9 km^2 (39.1%), 77.5 km^2 (16.3%) and 16.3 km^2 (2.7%) of the entire area.

The result of overlaying of the observed landslide inventory on the LSZ map shows 4 landslides (7.02%) in the low landslide susceptibility class, 7 landslides (12.28%) in moderate landslide susceptibility class, 16 landslides (28.07%) in high landslide susceptibility class, and 30 landslides (52.63%) in very high landslide susceptibility class. Hence, if it can be said that the observed landslides in high and very high susceptibility classes represent valid

prediction as more than 80% of observed landslide areas and 80.7% of observed landslides are predicted correctly in the LSZ map.

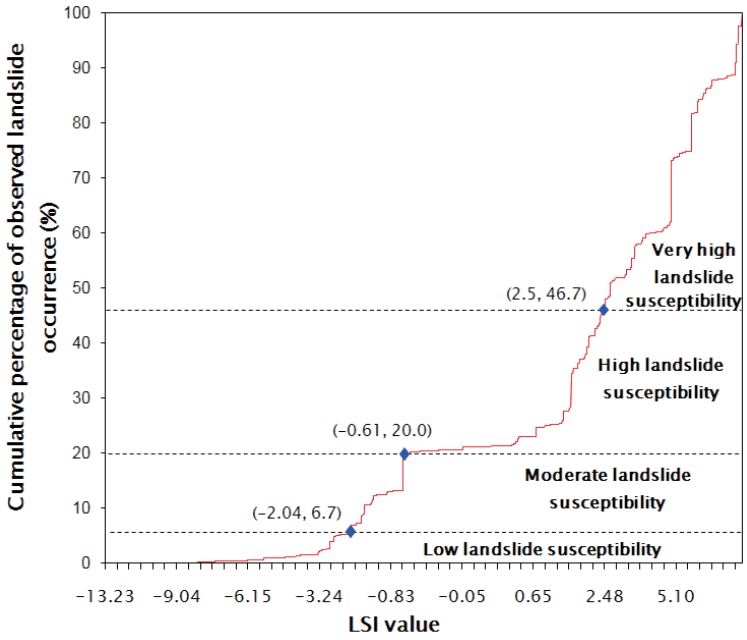

Fig. 10. Cumulative percentage of observed landslide occurrence against with LSI values using the probability method for Pac Nam district.

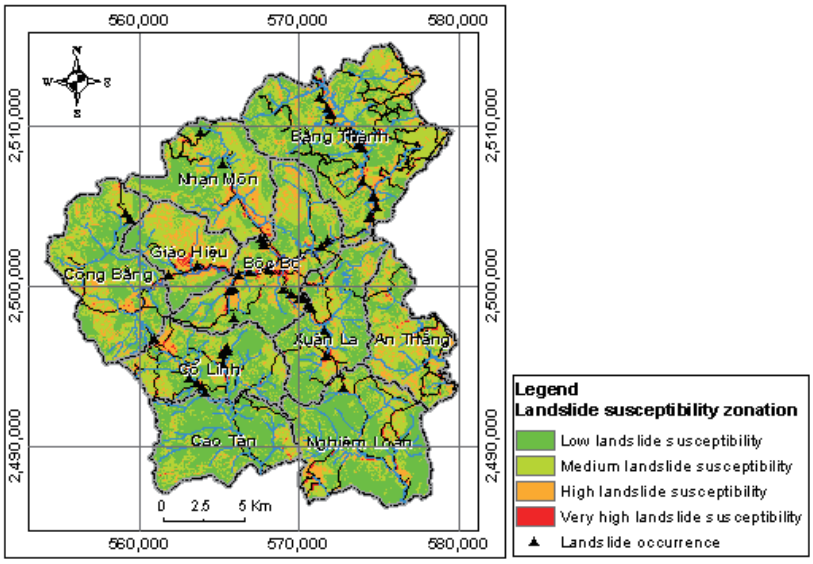

Fig. 11. Landslide susceptibility zonation map of Pac Nam district.

4. Conclusions

In this research, the assessment and the identification of the current observed landslide have been implemented mainly through the field survey. Besides, the landslide inventory is also supplemented through data collection from previous recorded work. As the result, the landslide inventory map in the study area with 57 observed landslides was established. This is the important scientific basis to evaluate the distribution and the susceptibility of landslide hazard in Pac Nam district, Bac Kan province.

The landslide susceptibility zonation was established from eight landslide causative factors i.e. slope angle, weathering, vegetation, maximum daily rainfall, fault density, river density, vertical dissection, and distance to roads. The LSZ map had high accuracy with reality >80%. The LSZ map indicated that 19% of study area has high and very high landslide susceptibility. Hence, the measurements for prevention, protection and preparedness for these areas need to be improved in order to mitigate damage that can potentially be caused by landslides.

References

An, P.V., Binh, H.V., Hien, L.V., Phu, D.X., Dung, N.T., 1990. Geochemical characteristics of the tropical humid weathering crust in Vietnam. Geology and Mineral Resources Journal, Hanoi, Vietnam, 3, 95-104.

Bishop, T., Frienberg, S., Holland, P., 1975. Discrete multivariate analysis. Cambridge, MA: M.I.T. Press.

Bonham-Carter, G.F., Reddy, R.K.T., 1990. Preliminary results using a forward-chaining inference net with a GIS to map base-metal potential: Application to Snow Lake Greenstone Belt, Manitoba, Canada. In Proceedings of International Workshop on Statistical Prediction of Mineral Resources, Wuhan, China, Oct. 20-25, 1990, Vol. 1.

Bonham-Carter, G.F., 1994. Geographic information systems for geoscientists: Modelling with GIS. In: Bonham-Carter, F. (ed), Computer Methods in the Geosciences, Pergamon, 13, 398 pp.

Chigira, M., Nakamoto, M., and Nakata, E., 2002. Weathering mechanisms and their effects on the landsliding of ignimbrite subject to vapor-phase crystallization in the Shirakawa pyroclastic flow, northern Japan. Engineering Geology, 66(1-2), 111-125.

El Khattabi, J., and Carlier, E., 2004. Tectonic and hydrodynamic control of landslides in the northern area of the Central Rif, Morocco. Engineering Geology, 71(3-4), 255-264.

Galang, J.S., 2004. Master thesis "A Comparison of GIS Approaches to slope instability zonation in the central Blue Ridge mountains of Virginia". Faculty of Virginia Polytechnic Institute and State University, Blacksburg, Virginia. 99 pp.

Gary, L.R., 2006. MI-SDM v2.51.0 tutorial (based on USGS Open-File Report 01-221) available at http://www.avantra.com.au.

Greenway, D.R., 1987. Vegetation and slope stability. In: Anderson, M.G., and Richards K.S. (eds), Slope stability, geotechnical engineering and geomorphology, John Wiley & Sons, Chichester, UK. 187-230 pp.

Guzovski, L.A., Toan, T.X., Hien, P.D., 1989. Some problems of study on the weathering crust in South Vietnam. Geology and Mineral Resources, Geological section 6, Ho Chi Minh city, Vietnam, 2, 29-36.

Hien, D.M., 2011. Vegetation mapping for Ha Giang - Cao Bang - Tuyen Quang - Bac Kan provinces (in Project “Evaluating geohazard occurrences, determining causes, predicting high geohazard risk areas and proposing the methods for reducing effects in Ha Giang - Cao Bang - Tuyen Quang - Bac Kan provinces”). VIGMR Archives, Hanoi, Vietnam. 31pp.

Ibetsberger, H.J., 1996. The TsergoRi landslide: an uncommon area of high morphological activity in the Langthang valley, Nepal. Tectonophysics, 260, 85-93.

Julian, M., and Anthony, E., 1996. Aspects of landslide activity in the Mercantour Massif and the French Riviera, southeastern France.Geomorphology, 15(3/4), 275-289.

Khien, N.X., Hung, L.Q., Long, N.T., Hien, D.M., 2012. Project report “Evaluating geohazard occurrences, determining causes, predicting high geohazard risk areas and proposing the methods for reducing effects in Ha Giang - Cao Bang - Tuyen Quang - Bac Kan provinces”. VIGMR Archives, Hanoi, Vietnam. 110pp.

Lee, S., Choi, J., and Min, K., 2002.Landslide susceptibility analysis and verification using a Bayesian probability model. Environmental Geology, 43, 120-131.

Long, N.T., 2008. Landslide susceptibility mapping of the mountainous area in A Luoi district, Thua Thien Hue province, Vietnam. Dissertation Vrije Universiteit Brussels. 231pp.

Malczewski, J., 1999. GIS and multicriteria decision analysis. John Wiley and Sons, New York, 392pp.

Mathew, J., Jha, V. K., Rawat, G. S., 2007. Weights of evidence modelling for landslide hazard zonation mapping in part of Bhagirathi valley, Uttarakhand. Current Science, Vol. 92, No. 5, 628-638.

Neuhäuser, B., and Terhorst, B., 2007. Landslide susceptibility assessment using “weights-of-evidence” applied to a study area at the Jurassic escarpment (SW-Germany). Geomorphology, 86, 12-24.

Pachauri, A.K., Gupta, P.V., and Chander, R., 1998. Landslide zoning in a part of the Garhwal Himalayas. Environmental Geology, 36(3-4), 325-334.

Porwal, A.K., Carranza, E.J.M., and Hale, M., 2003. Knowledge - driven and data - drive fuzzy models for predictive mineral potential mapping. In: Natural resources research, 12(1), 1-25.

Sentz, K., and Ferson, S., 2002. Combination of evidence in Dempster-Shafer theory. Report SAND2002-0835, Sandia National Laboratories, Albuquerque, New Mexico, 96pp.

So, C.L., 1971. Mass movements associated with the rainstorm of June 1966 in Hong Kong. Inst. British Geographers Trans, 53, 55-65.

Spiegelhater, D., and Kill-Jones, R.P., 1984. Statistical and knowledge approaches to clinical decision-support systems, with an application in gastroenterology. Journal of the Royal Statistical Society, 147(1), 35-77.

Starkel, L., 1976. The role of extreme (catastrophic) meteorological events in the contemporary evolution of slopes. In: Derbyshire, E. (ed), Geomorphology and Climate, John Wiley & Sons, New York. 203-246 pp.

Süzen, M.L., and Doyuran, V., 2004. A comparison of the GIS based landslide susceptibility assessment methods: multivariate versus bivariate. Environmental Geology, 45, 665–679.

Thai, T.N., Di, T.Q., Tien, L.B., Quan, T.N., Duc, K.C., 1991. Mineral composition of some kaolin weathering crust types in Vietnam and method of mineral quantification in weathering kaolin formations. Proc. 2nd Conf. Geological Indochina, Hanoi, 2, 201-209.

Thiery, Y., Sterlacchini, S., Malet, J.P., Puissant, A., Maquaire, O., 2004. Strategy to reduce subjectivity in landslide susceptibility zonation by GIS in complex mountainous environments. In: Toppen, F., Prastacos, P. (eds), Proceedings of AGILE 2004: 7th AGILE Conference on Geographic Information Science. 29th April – 1st May 2004, Heraklion, Greece, 623-634.

Thiery, Y., Malet, J.P., Sterlacchini, S., Puissant, A., Maquaire, O., 2007. Landslide susceptibility assessment by bivariate methods at large scales: Application to a complex mountainous environment. Geomorphology, 92(1), 18pp.

Tsukamoto, Y., and Ohta, T., 1988. Runoff processes on a steep forested slope. Journal of Hydrology, 102, 165-178.

Van Westen, C.J., 1993. Application of Geographic Information System to landslide hazard zonation.ITC-Publication No. 15, ITC, Enschede, 245.

Van Westen, C.J., and LulieGetahun, F., 2003. Analyzing the evolution of the Tessina landslide using aerial photographs and digital elevation models. Geomorphology, 54(1-2), 77-89.

Van, T.T., Tuy, P.K., Giap, N.X., Ke, TD.,Thai, T.N., Giang, N.T., Tho, H.M., Tuat, L.T., San, D.N., Hung, L.Q., Chung, H.T., Hoan, N.T., 2001. Project report "Assessment and prediction of geohazards in the 8 coastal provinces of Central Vietnam from QuangBinh to Phu Yen - present situation, causes, prediction and recommendation of remedial measures". Research Institute of Geology and Mineral Resources, Hanoi, Vietnam, 215pp.

Wakatsuki, T., Tanaka, Y., and Matsukura, Y., 2005. Soil slips on weathering-limited slopes underlain by coarse-grained granite or fine-grained gneiss near Seoul, Republic of Korea. Catena, 60(2), 181-203.

Engineering geological investigation and landslides hazard zonation of Mount Batur Geopark, Bali, Indonesia

Muhammad Wafid Agung

Geological Agency of Indonesia

Abstract

Following the landslide on the 13th of March 2012, an engineering geological investigation was conducted along the Caldera of Mount Batur, a part of the Mount Batur Geopark. Several types of landslides triggered by rainfall were identified during the investigation, e.g., earth slides, rock flows, rock falls and debris flows. In general, the factors influencing landslide events are: a) natural factors, including lithology, loose and uncompacted volcanic materials, heavy rainfall, steep slopes, and b) anthropogenic factors, including land use and building construction.

Especially debris flow events indicated that the human involvement had caused mass movement in the upper part of the outer Caldera where the debris materials were sourced, i.e., the failure of a retaining wall of the slope foundation of a school building. The detached material (debris) was carried away by rain water through the path (channel) existing within the inner Caldera to be deposited in the lower valley.

Another factor identified in the field was the existence of an ideal path for debris flows along the stream of Balingkang River in which the river wall was composed of massive ignimbrite and a natural levee (dam) was formed by debris material during the event. This natural dam was finally destroyed by headflow accumulation when mixed material consisting of debris-mud-water was ejected and severely damaged houses downstream.

For the future protection of Mount Batur Geopark, a landslide hazard zonation map has been made. Landslide Hazard Zones were differentiated into three types: a) Type I is dominated by earth, rock and debris slides and some places show surficial exfoliation sliding and fall phenomena, b) Type II is dominated by debris flows and river bank slides and debris material could form natural dams during flow especially along the Balingkang River and its tributary, and c) Type III is dominated by rock fall and flow of rock materials.

Based on the collected data and engineering geological information together with the newly established landslide hazard zones, some recommendations for spatial planning purposes are proposed for protecting the vicinity of the geopark.

Keywords: engineering geology, landslides, caldera wall, landslides hazard zonation, spatial planning

1. Background

Mount Batur is the first geopark in Indonesia which is part of the UNESCO Global Geopark Network since 2013. Consequently it should be conserved to protect important geological sites and phenomena. Potential hazards that threaten the Batur Geopark sites must be identified and future risk reduced. One of the vulnerabilities that threaten this site is landslides around the caldera, as occurred on 13-14 of March 2012. This paper deals with an engineering geological investigation of that incident.

A landslide susceptibility map that explains the tendency for landslides to occur in Bangli Regency has already made by the Geological Agency of Indonesia. Unfortunately, the map

does not describe landslide types that could potentially occur. Therefore, to enhance the utility of the existing map, a landslide hazard map is proposed with the aim of identifying preventive efforts that could mitigate the effects of the future incidence of various types of landslides.

Furthermore, since human activities can increase the hazard, land use regulation is an essential issue in dealing with potential landslide hazards within the Batur Geopark.

2. Landslide occurrences in March 2012

Several types of landslides were triggered by intense and heavy rainfall that occurred between 13 and 14 March 2012 and resulted in fatalities and damage to properties in Pingan, Blandingan, Songan, and Yeh Mampeh villages, Kintamani District, Bali Province. Amongst others, the most damaging types were debris flows along the Balingkang River and in the North Batur village area.

Data from field surveys revealed that the driving factors for the debris flows were: morphology of steep slopes, lithology of unconsolidated volcanic material and embankment failure at the top of the caldera slopes (in the village of Pura Dalem) caused by inappropriate engineering work. The main triggering factor was the high intensity rainfall. Meteorological data shows that on 11 - 14 of March 2012, Bangli and Badung regencies and the vicinity in Bali province suffered severe storms (heavy rain and very strong wind). This situation made the water volume increase in almost all rivers and increased flow downstream. Erosion and landslides on the upper slopes and the fall of large trees in the strong winds contributed to erosion and the increasingly muddy flow in the rivers.

2.1 Landslide in the Pura Dalem village

One of the landslides on the upper slope in Pura Dalem village was a major source of material for the subsequent flow-type landslide event (debris flow) on the lower slope in Yeh Mampeh on January 13 and March 14, 2012. Landfill materials mixed with rain water were mobilized downstream from the top of the outer caldera to the inner caldera through the existing channel, eventually reached and deposited in North Batur village.

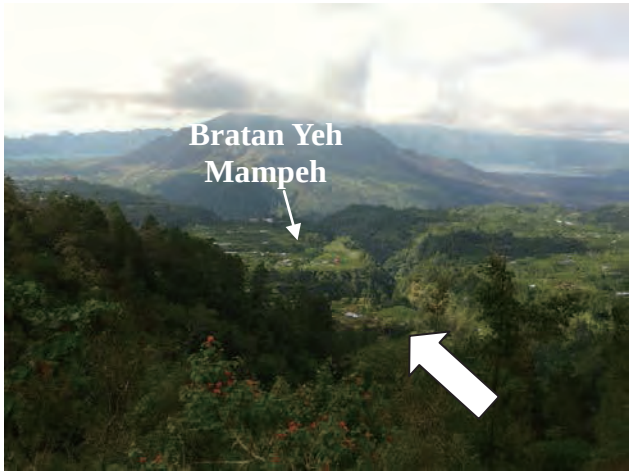

Fig. 1. Morphology showing streams lead to caldera wall II and discharge into the North Batur and Bratan Yeh Mampeh villages.

Fig. 2. Condition of school building in Pura Dalem which is still threatened by landslide.

2.2 Mechanism

An illustration of the debris flow event in North Batur village in March 2012, which can be separated into three stages, is given in Fig. 3. The main factor in the incidence of the debris flow is the collapse of the soil foundation of the school building in Pura Dalem village at the top of the caldera wall I. This collapse happened due to disproportionate technical construction, i.e., compaction and gabions set up. Triggered by heavy rainfall the soil foundation collapsed and, in the water-saturated conditions, mixed materials flowed down along an existing intermittent channel. Due to the fairly steep slope coupled with the saturated conditions, mixed materials slid rapidly to the bottom of the slope through the inner caldera wall and finally hit villages in low-lying areas. During the flow, the mobilized materials could reach the distant depositional area because pore water pressure increased at the interface. As shown in the circle sketch in Fig. 3 the pore water pressure at the failure plane was only generated within the mobile soil mass with no dissipation and with excess pore water pressure in the bedrock.

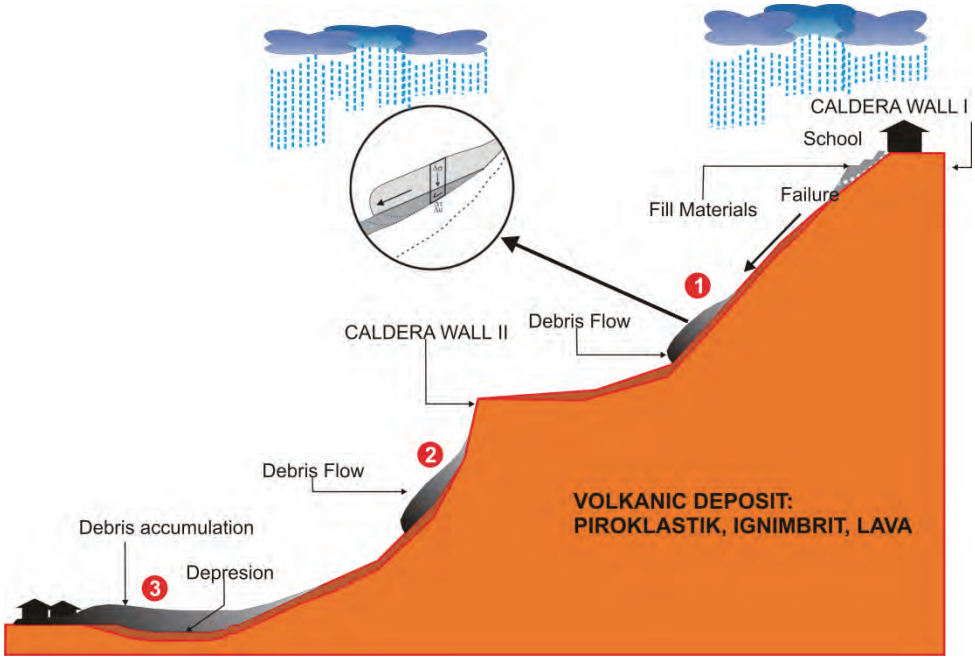

Fig. 3. Mechanism of debris flow deposits derived from materials that were not managed well technically in saturated conditions (image without scaling).

3. Engineering geology of caldera walls

The Mount Batur Caldera can be separated into two parts (Fig. 4), i.e., an outer part (caldera 1) and inner part (caldera 2) which formed in separate episodes during its eruption history.

The outer part (caldera 1) was more resistant to landslide occurrence than was the inner part. The outer part has a quite gentle morphology with the thickness of its weathering products more than 5 m (around Kintamani and Sukawana villages). On the other hand, the inner part has a very steep morphology (steepness >70%), unconsolidated younger volcanic materials and weathering products with the thinnest soil cover. These geological and geomorphological settings make the inner part of caldera more vulnerable to landslide whilst the outer part is more stable unless human activities are a factor involved within this region (Fig. 5).

Fig. 4. Bird-eye view of Mount Batur's calderas (source: Google Map, 2013).

Fig. 5. Illustration of some flow types of March 2012 landslides between the inner and outer parts of caldera.

There are at least two zones of depression around North Batur village especially around a Bratan Yeh Mampeh. These depressions are the lowest morphological terrain and form accumulating places or recharge areas of the intermittent river flows from both inner and outer parts of caldera.

4. Landslide hazard zonation

From the initial survey supported by other data, three landslide hazard zones were defined, based on the predominant landslide types.

4.1 Type I landslides hazard zone

This zone is dominated by flow type landslides which can be initiated by slide and fall. Materials involved in this hazard zone consists of fine to coarse grained materials (soil and debris) up to boulder sizes (Varnes, 1978). This zone contains some villages, i.e., Culali, Bratan Bugbugan-Kintamani to Bratan Kuta Dalem-Sukawana within caldera 1; and Bratan Yeh Mampeh-North Batur in the vicinity of caldera 2. Weathering products around caldera 1 at the above locations are relatively thicker (> 4 m), but relatively thin (< 2 m) for caldera 2.

Within North Batur village, the track of the March 2012 debris flow could be clearly seen. Lithological composition at caldera 2 consists of lahar, volcanic breccia, pumice, and welded tuff with a fairly thin weathering zone. The area still has the potential for rock-fall and debris flow occurrences. Laboratory analysis of the "disturbed" pumice shows that soils are easily crushed during friction and their aggregation tends to display adhesive phenomena. These properties make it easier for the material to travel long distances.

In Bratan Yeh Mampeh village there is an ideal channel for the flow path of a debris flow. Soils around this location seem to be unstable and easily dredged by mobile flows (Figs. 6, 7 and 8).

4.2 Type II landslides hazard zone

This hazard zone is dominated by debris flows especially along the Balingkang River and its

tributary, including several seasonal streams on the slopes of the inner caldera wall in Sukawana village.

Fig. 6. Intermittent channel as an ideal path for debris flow in Bratan Yeh Mampeh village.

Fig. 7. One of the locations of the debris flow in March 2012 in North Batur village.

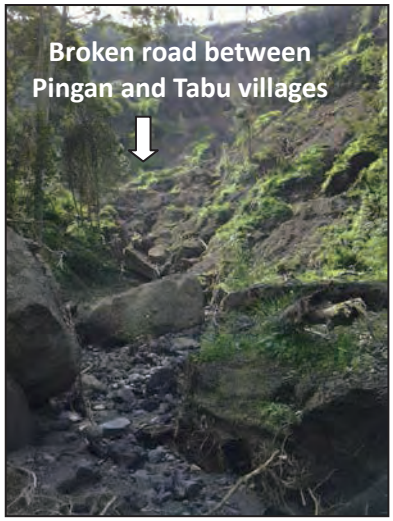

Fig. 8. Material debris of various sizes in the village of Tabu village.

The results of field surveys revealed that there were ideal conditions favouring the occurrence of debris flows along the Balingkang River. Narrow branched tributaries of orders either 2 or 3 with the river banks in some places are formed by hard and strong ignimbrite (Fig. 9), while at the certain parts of the channel there is quite thick soil in which several landslides have occurred (Fig. 10). This condition suggests that natural dams may be formed during a debris flow. In the field the remains of plants such as grass and tree roots are still attached to rock debris on the riverbed. This zone includes Sukawana, Pinggan, Belandingan, and Songan villages.

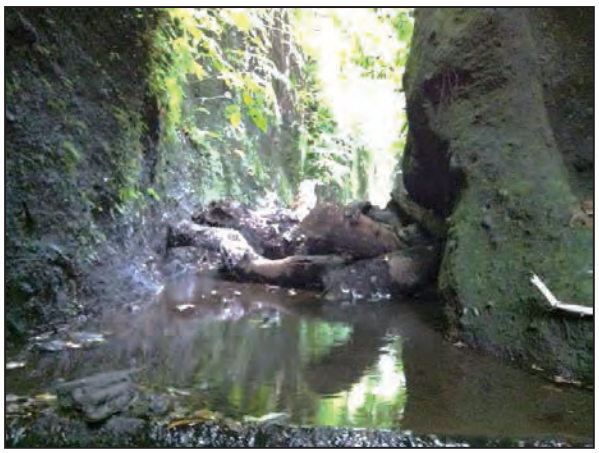

Fig. 9. Wall of Balingkang tributary formed by ignimbrite on the right and left sides. Logs are stuck to the wall that illustrates the process of forming natural dams by debris.

Fig. 10. Landslide that has occurred on the open walls of tributaries of Belingkang River which supposedly contributed to the formation of natural levees.

The conditions above clearly record a debris flow event along Balingkang River and its tributaries on March 13-14, 2012 where a natural levee was formed by debris material mixed with plants and bushes from the river bank.

This mixed materials then stemmed the flow, as is supported by the presence of rocks on the riverbed and solid river walls. Furthermore, because the natural dam eventually could not restrain the upstream debris flow, the dam was ruptured and a huge mass of mobile material flowed down stream.

If all the tributaries that flow into the Balingkang River experienced such events then the subsequent volume of water flowing in the Balingkang River must have become very large and invaded villages around the river mouth. In addition, the flow of debris into Kintamani Lake would have raised its level such that it overflowed and inundated Songan village.

4.3 Type III landslides hazard zone

This type of landslide hazard zone is dominated by the falls and flows of rock types which occur in the eastern part of the caldera wall up to the southern ridge of the relatively stable area of Mount Abang. It is observed that there is still the potential for rock falls in some locations, whilst along the Sapujagad River there is also the potential for rock flows.

Fig. 11. Sapujagad riverbed material formed by gravels.

Fig. 12. Rock falls from the wall or cliffs of Hulundanu Pura Batur.

5. Recommendations

Land use planning within caldera 1 should be managed proportionally, either for residents, construction as well as for agriculture and cultivation.

Establishment of new buildings should only be allowed on the upper slopes of Caldera 1 within very strict engineering regulations. Further, all existing buildings should be obliged to undertake foundation stability monitoring and evaluation of slope stability around the building, and be required to take immediate technical action if cracks or damage to buildings is found. Especially in the case of schools in Pura Dalem, reinforcement by retaining walls on the upper and lower slopes with detailed engineering design should be constructed according to carful calculation and high quality design.

Spatial planning and land use management within the upstream areas of the Balingkang River and Belingkang Sub-Basin should include retrofitting the river walls in some places. The river walls at the mouth of the Balingkang River (Inlet of Kintamani Lake) need to be strengthened

and drainage to be modified in order to protect the residential area during a debris flow or increased volume of water flow and height of water level during floods.

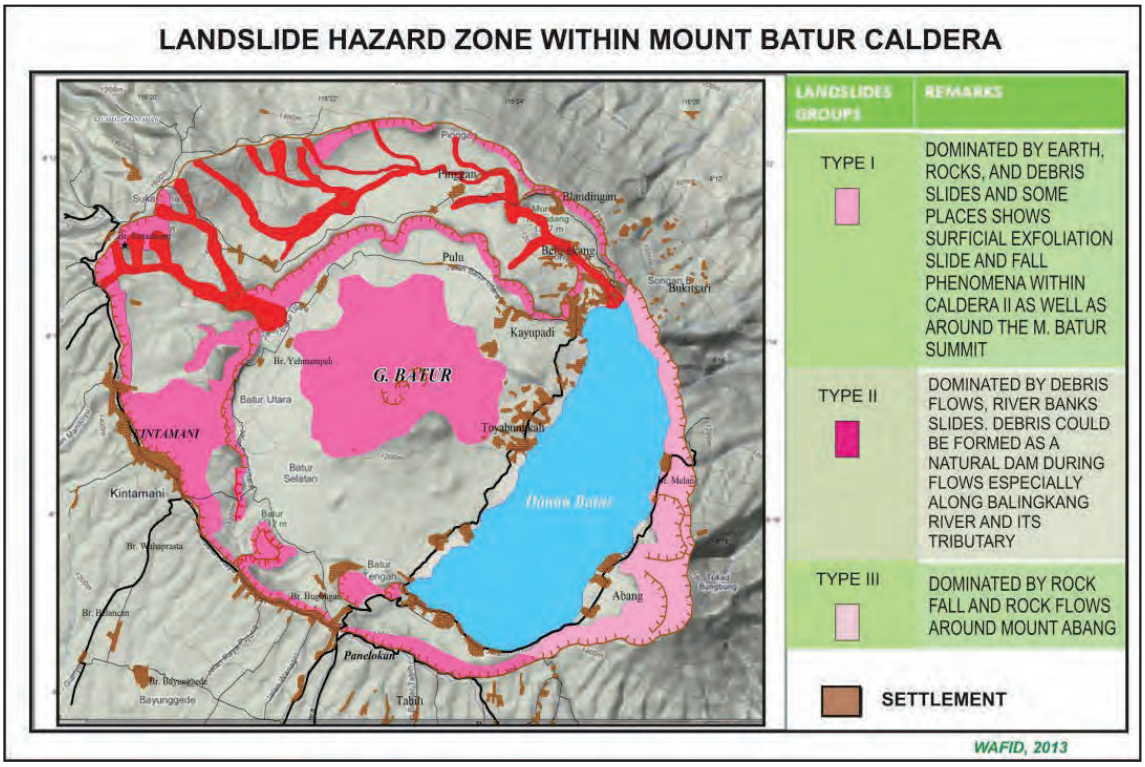

Fig. 13. Map Hazard Zones based on dominant types of landslides within the Mt. Batur calderas.

The caldera 2 (inner Caldera) was, actually, an inappropriate area for settlement and the construction of permanent buildings not only because it is a high risk area for landslides but also because this is part of a high risk zone for volcanic hazards (direct impact) due to the volcanic activity of Mt. Batur.

Especially for Pura Tirta Mas, there needs to be protection against the possibility of landslides through retrofitting walls by shotcrete and lightweight wiremesh. For this purpose, exfoliating and cleansing the weathered soil layers that are still hanging should be undertaken. At the bottom edge of the slope a trench or ditch should be emplaced in order to accommodate and direct any rock material and mud arriving by landslide.

References

Vernes, D.J., 1978, Slope Movement Types and Processes, in Schuster R.L., and Krizek, R.J. eds, Landslides Analysis and Control, Transportation Research Board, Special Report 176, National Academy of Sciences, USA.

Google, 2013, https://www.google.com/maps/preview, accessed in March 2013.

Landslide in Indonesia, case study: Malausma landslide in Majalengka region, West Java

Wawan Irawan

Geological Agency of Indonesia

Abstract

Indonesia is often hit by violent geological events such as volcanic eruptions, earthquakes, tsunamis, and landslides. Landslides happen every year in Indonesia and data recorded in the Geological Agency of Indonesia suggested that landslide increases during the rainy season. In the period from 2009 to 2012 more than 100 landslides occurred each year and in 2013, up to August, there have been already 112 landslides occurred.

Geological conditions, climate, and human activities may cause landslides, however in Indonesia landslides are most commonly triggered by heavy rainfall. Geological conditions that control landslide in Indonesia include the presence of porous rocks, lithological contacts such as slip surfaces, steep morphology, and tectonic activity.

An interesting landslide, which took place in the Malausma district, Majalengka region, West Java province on 15 April 2013, causing extensive damage, is the subject of this study. The type of the movement was slide and creep and this mechanism was influenced by heavy rainfall as well as the geological conditions of the area. The main recommendation for this disaster area is that it is not habitable and residents who lived around the area need to be relocated to a safer area.

1. Introduction

The Republic of Indonesia is located at the confluence of three active tectonic plates, causing the Indonesian region to be the site of frequent geological disasters (Fig. 1).

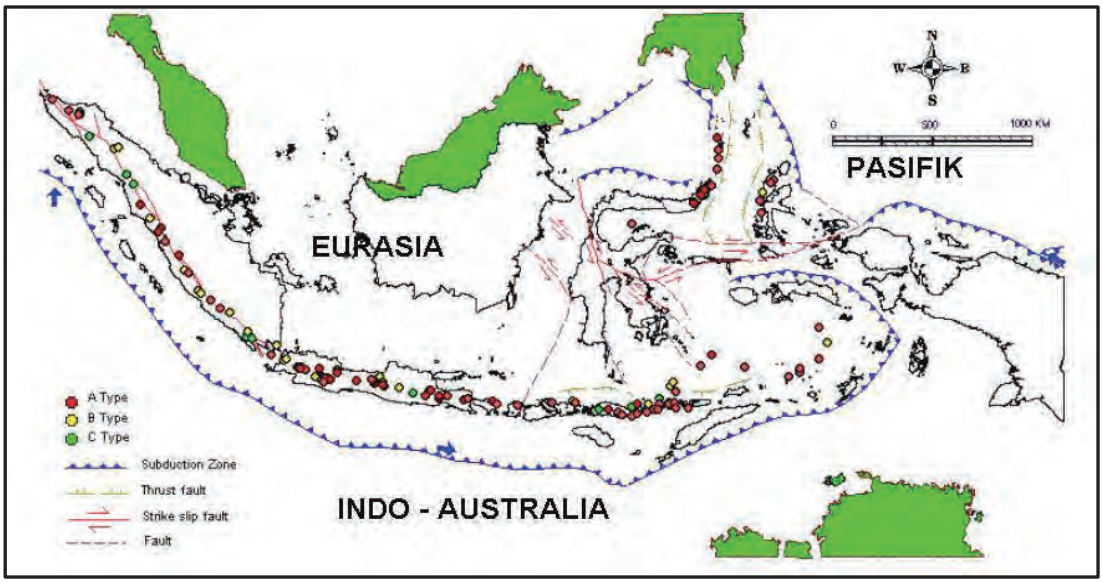

Fig.1. Indonesia: location among three active plates in the world.

Geological disasters that strike Indonesia include volcanic eruptions, earthquakes, tsunamis, and landslides. Landslides occur every year in Indonesia and may cause fatalities.

Data recorded in the Geological Agency of Indonesia suggests that landslides increased during the rainy season (Fig. 2). In the 2009 to 2012 period, there were more than 100 landslides each year, except in 2011. In 2010, a year of particularly high rainfall, 199 landslides were recorded, higher than in 2009 (161), 2008 (139) and 2007 (101) as well as in 2011 (82) and 2012 (124). In 2013, 112 landslides had already been recorded by August (Table 1). One such landslide that caused extensive damage occurred on 15 April 2013 in Malausma, Majalengka Region, West Java.

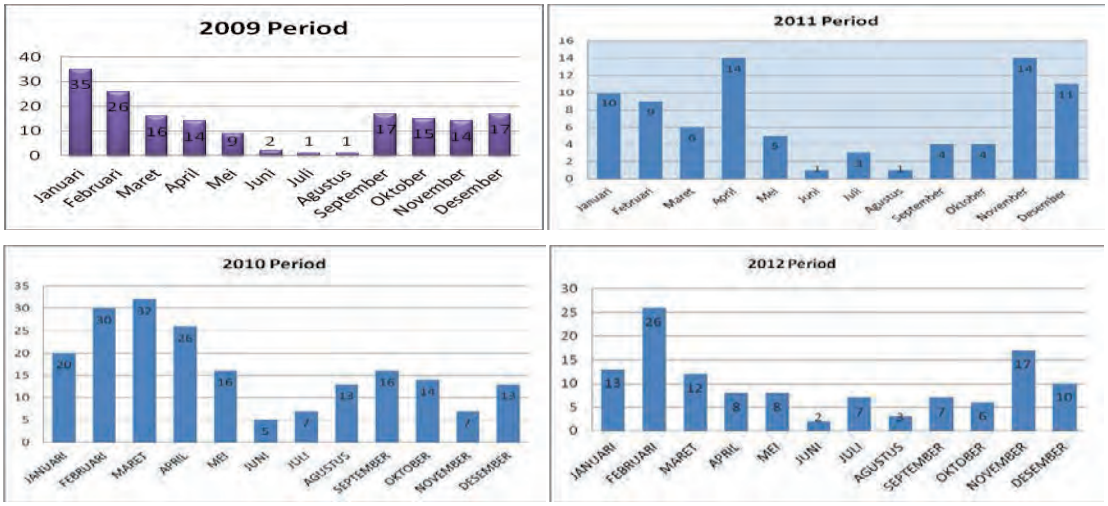

Fig. 2. Monthly statistics of landslides in Indonesia (2009-2012 period).

Table 1. Landslide events in Indonesia (up to 20 August 2013).

PROVINCE	EVENTS	PEOPLE KILLED	INJURED	DAMAGED HOUSES	DESTROYED HOUSES	THREATENEDHOUSES
West Java	65	47	16	868	55	269
Central Java	12	13	12	55		46
East Java	6					13
D.I. Yogyakarta	1		1			
Banten	2	1	3	13	4	
Bali	2					
NTB	1			14		
NTT	1					
West Sumatera	1	20	4		12	
North Sumatera	3	1	2			
South Sumatera	4	9	3	3		2
North Sulawesi	2	14		4500	12	
South East Sulawesi	1					
West Sulawesi						
Jambi	1	5	4			
Aceh	5					
Papua	3	32	12	10		
Lampung						
Maluku	2	13	10	30	9	
TOTAL	112	155	67	5493	92	330

2. Landslide controlling factors in Indonesia

Geological conditions, climate, and human activities may cause landslides, however the common landslides in Indonesia are triggered by heavy rainfall. Geological conditions that control landslide in Indonesia are generally the presence porous rock, lithological contacts that act as slip surfaces, steep morphology, and tectonic activity (Figs. 3 and 4).

The high rainfall in Indonesia can cause the soil mass and pore water pressure to increase and also reduces cohesion so that soil or rock strength decreases. When such soil is on a slope it is easily mobilized when affected by a triggering mechanism such as an earthquake.

Fig. 3. Landslides triggered by 30 September 2009 earthquake in West Sumatera (left). Rockfall triggered by 2 September 2009 earthquake in West Java (right).

Fig. 4. Landslides triggered by earthquake in Aceh Province on 2 July 2013.

Human activities such as the development of residential and other facilities may also affect the slope stability. Slopes excavated whilst ignoring the basic rules of slope stability can trigger a landslide.

3. Case Study: Malausma landslide in Majalengka Region, West Java

A landslide took place in the Malausma district, Majalengka region, West Java province on 17 April 2013. The type of movement was slide and creep under influence by heavy rainfall.

Impacts of the landslide were 6 hectares of paddy fields buried, 110 houses damaged, more than1km road damage and dropped by 3-5 meters depth and 1842 people were evacuated to a refuge. Two weeks after the landslide, the damage was still wide spread. More than 100 hectares of residential area, paddy fields, gardens, and roads have been damaged (Fig. 5.).

Fig. 5. Houses and road damaged.

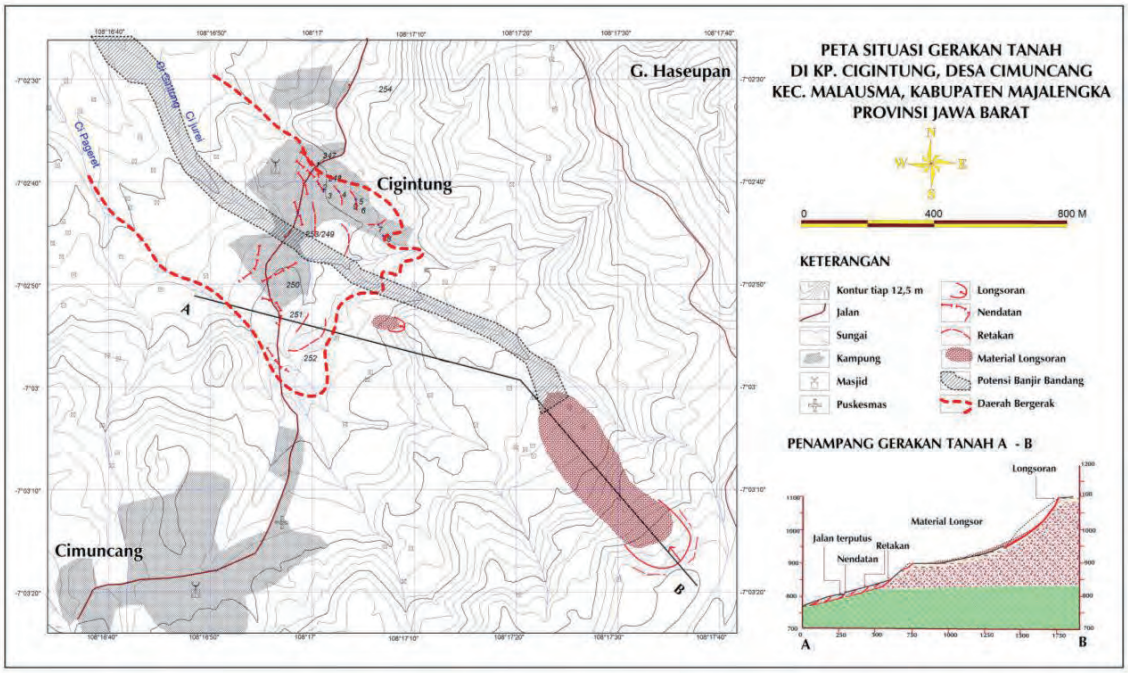

Fig. 6. Landslide situation map.

3.1 General condition

The morphology around the Cimuncang village is hilly with 5 - 45° slopes. The altitude is between 750 - 1100 m above sea level. The Cijurei River and other small rivers occupy the valleys.

Based on the Geologic Map of Tasikmalaya, Java (Budhitrisna, 1986), the geology around the movement area is seen to comprise: an upper part composed of breccia, tuff and lava (old volcanic deposits of Sawal, Qtvs) and an underlying part composed of Kaliwangu Formation claystone (Tpkw). On the upper slopes, groundwater was found at 1-5 meters depth but in the lower part, composed of claystone, groundwater is hard to be found. Land on the upper slopes has a cover of scrub and pine forest. Paddy fields, gardens, settlements and fish ponds occupy the lower slopes in the valley.

3.2 Mechanism

The Malausma landslide was caused by the interaction of high rainfall and geological conditions. According to the information of residents, the landslide occurred after a period of prolonged and high intensity rainfall. Geological conditions that controlled the slide were porous soil lying on claystone with the slip-surface located at the soil/claystone contact. Sliding happened on upper slopes over an area 200m long and 100 m wide, materials moving down slope towards the paddy fields.

Creep occurred at the bottom of the slope, followed by slumping and cracking. Slumping took place in several locations over 5-50 meters length and a drop from 30 centimeters up to 6 meters. Cracks and slumps had the same movement direction and struck the settlements in Cigintung. Creep type motion was controlled by light blue claystone which is suspected of having expanding properties. This claystone has a wide distribution around the location of the movement, thus led to such a wide spread impact.

3.3 Post-disaster mitigation

The main recommendation was that the disaster area is not habitable. Residents who live around the disaster area should be relocated to a safe area. The problem then to be addressed is to determine the area for relocation. Local governments proposed two sites as relocation areas: Block Cibeber in Cimuncang Village and Block Cipicung in Werasari village.

After observation and field studies, it was concluded that the area in Block Cipicung in Werasari village was safe as a relocation area with its relatively gentle slopes and stable land, clean water availability, and electricity line all within a low to medium landslide susceptibility zone.

When building on the relocation area the following matters must be considered:
- Settlements to be built on the ramp area,
- Terracing system for structuring the slopes,
- Surface water should be laid out well through watertight channels,
- Preservation of the vegetation on the upper slopes,
- No pools to be established at the bottom and top of the slope.

4. Conclusion

Landslides happen every year in Indonesia, and may cause fatalities. Geological conditions, climate, and human activities may cause landslide. Commonly landslides in Indonesia are triggered by heavy rainfall.

The mechanism of the Malausma landslides was influenced by heavy rainfall and geological conditions of the surrounding areas. Creep type motion was controlled by light blue claystone that has a wide distribution around the location of the movement. A field survey concluded that the disaster area was no longer habitable. Residents who live around the area should be relocated to a safe area.

References

Budhitrisna, T., 1986: *Geologic Map of Tasikmalaya Quadrangle, West Java*. Geological Research and Development Centre, Bandung.

Photo on the back cover:
A group photo at the Arahama coast, Sendai City, during the field excursion on 24 October 2013. The Arahama area was hit by the tsunami of the 2011 off the Pacific coast of Tohoku Earthquake on 11 March 2011.

Geological Survey of Japan (GSJ),
National Institute of Advanced Industrial Science and Technology (AIST)